1-1-1970

Strain dependence of dynamic birefringence and dynamic x-ray diffraction in low density polyethylene.

Eng Pi Chang
University of Massachusetts Amherst

STRAIN DEPENDENCE OF DYNAMIC BIREFRINGENCE AND DYNAMIC X-RAY DIFFRACTION IN LOW DENSITY POLYETHYLENE

A Dissertation Presented

By

ENG PI CHANG

Submitted to the Graduate School of the
University of Massachusetts in
partial fulfillment of the requirements for the degree of

DOCTOR OF PHILOSOPHY

August 1970

Major Subject: Polymer Science and Engineering

STRAIN DEPENDENCE OF DYNAMIC BIREFRINGENCE AND DYNAMIC X-RAY DIFFRACTION IN LOW DENSITY POLYETHYLENE

A Dissertation

By

ENG PI CHANG

Approved as to style and content by:

Richard S. Stein
(Chairman of Committee)

Roger S. Porter
(Head of Department)

F. E. Karasz
(Member)

Jacques Wesemann
(Member)

W. J. MacKnight
(Member)

(Month) (Year)

TABLE OF CONTENT

ACKNOWLEDGMENT

The author wishes to express his sincere thanks to Dr. R. S. Stein, thesis director, for his invaluable guidance, his magnificent inspiration and encouragement during the course of this work.

The author also wishes to extend his gratitude to the following persons for their help in making this thesis a reality.

Dr. Seymour Newman, Professors F. E. Karasz and W. J. Macknight served as members of the Thesis Committee.

Messrs. Daniel Keedy, Roland LaBonte for their kind and coorperative technical assistance.

Members of the Polymer Research Institute made the author's stay at the University of Massachusetts a pleasant and memorable one.

Dr. E. Drott of Monsanto Company, Texas city for the GPC characterization of samples.

The author is grateful to the office of the Petroleum Research and the Naval Research for the financial support of the research assistanceship held by him during his course of study.

DEDICATED

TO

MY PARENTS

who teach me hope and fidelity.

ABSTRACT

The dynamic birefringence technique has been used to study the total orientation of low density polyethylene, and the dynamic x-ray diffraction technique is augmented to single out and evaluate the crystalline orientation. Swelling studies on the same type of samples were made using the dynamic birefringence apparatus to assess the form contribution due to orientation of boundaries between two regions of different refractive index. Samples having different internal structure were obtained by imposing different static strain on the samples, and their morphology was varied by the processes of quenching and annealing. The dynamic birefringence results are explained in terms of molecular mechanisms and the crystalline orientation is explained with respect to the orientation of the a, b and c axes of the unit cell of polyethylene.

It has been found that at low elongations of about 10%, for quenched sample the amorphous and the crystalline contributions to the total dynamic birefringence are comparable and amount to about 40% each. With annealing, the amorphous contribution increases with lower crystalline contribution. At high elongations beyond 50%, the crystalline contribution has been found to be 70-80% of the total in both types of samples. Form contribution is about 5-15% in both cases depending on the static strain of the sample.

Additional dynamic birefringence results are reported on the

quenched sample of substituted polyethylenes and the substituent effects on the dynamic mechanical and optical quantities are assessed and discussed.

II. INTRODUCTION

Polycrystalline polymers such as polyethylene, polypropylene, nylon and "Telfon" owe their unique mechanical properties to their being multi-phase systems in which a more rigid phase; the crystalline region, is interconnected by the more flexible amorphous or disordered region. The mechanical behaviour of these material is dependent upon both the internal structure and interaction between these regions. Factors which are important are the fraction of crystalline material, the morphology and perfection within these crystalline regions, the chain connectivity of the amorphous chains between the ordered regions, and the orientation of both the crystalline and amorphous regions. The distribution of applied stress between these regions and the mechanisms by which these regions may deform and change to relieve stress concentration is dependent upon morphology and structure and may be affected by the thermal and mechanical treatment to which the polymer is subjected during preparation and processing.

While the study of the dynamic mechanical properties has long been used as a method for characterizing the deformation mechanism, optical techniques may augment there for the specification of the rates of such changes. Dynamic x-ray diffraction and dynamic infra-red dichroism serve to define the rate of crystal orientation. Dynamic light scattering characterizes changes in the crystalline super-structure, while dynamic birefringence measures the total orientation rate. In general, each of these dynamic observables may be resolved into a real and imaginary part representing the components of the

response which are in- and out-of-phase with the strain.

STRUCTURAL CONCEPT

Two divergent views exist concerning the structure of crystalline polymers. The older classical picture of the fringed micelle model advocated by Gerngross, Horrman and Abitz and Kratky and Mark[1-2] is illustrated in Figure (1). The crystals were considered as being dispersed in an amorphous matrix. The crystals were believed to behave as inert filler particles binding the amorphous chains together and which merely change their orientation upon stretching while preserving their size integrity. The amorphous chains were believed to pass mostly from one crystal to the other. The structure is fairly well described in terms of two phases in which the crystalline regions are fairly perfect and the amorphous regions are completely disordered and have a structure similar to that of a completely amorphous polymer such as a rubber. The boundary regions between the phases must be in a state of intermediate order but these represent a small fraction of the total.

While this picture qualitatively accounted for the properties of crystalline materials, it suffered several deficiencies, such as the following: (1) It did not account for the specific orientation of particular planes of crystals upon stretching. (2) It did not account for the accompanying change in crystal size and perfection. (3) It did not take into account the microscopically observed superstructure such as spherulites. (4) The model effectively involved having crystalline

and amorphous regions acting in series with each other and predicted a lower modulus than experimentally found. (5) The origin of the stress according to this model was of rubber elasticity origin and resulted from the entropy decrease of the amorphous chain upon stretching. This does not account for the appreciable internal energy contribution to stress determined from thermo- chemical studies and (6) The model could not account for the experimentally determined relaxation spectra.

A more recent thinking, influenced by the studies of the morphology of simple polymer crystals grown from dilute solution by Keller[3] and Fisher and Stuart[4], involves a different model (Figure 2.) in which the chain zig-zags back and forth within a single crystal and does not pass from one crystal to the next. The chain may be perpendicular to or tilted at angle to the larger face of the crystal. On the basis of observations of the pyrimadal structure of these solution grown crystals, and from deductions of electron microscope studies, it is believed by some that the chain folding is regular and the emergent chain re-enters the crystal immediately adjacent to itself and in the same relative position within any sector of the crystal (Figure 3). Only a relatively small number of chain atoms are involved in this turn-around and these are arranged in a fixed conformation and cannot be considered as truly amorphous.

Perhaps with the existing knowledge of properties of crystalline polymers, it is best to advocate a compromise model (Figure 4). Chain folding of varying perfection or regularity is included with some

connectivity between crystalline regions. Some chain ends, stacking-faults, short side groups, and loops are included within the crystal but there is a tendency toward exclusion of these imperfections in intercrystalline regions as demonstrated by kinetic and morphological studies by Keith and Padden[5]. Such a structure is, however, not an equilibrium one but is an accident of the growth kinetics and may be modified by variation of crystallization conditions. Structural modification occurs upon annealing, resulting in a greater degree of crystal perfection and of exclusion of less perfect structure into intercrystal region. Also, there is probably a decrease in connectivity between crystals giving rise to embrittlement of the polymer with heat treatment.

SPHERULITE STRUCTURE

Spherulite crystallization is typical in polymers where the crystals are not uniformly and randomly distributed throughout the polymer but grow in spherically symmetrical aggregates of a type well described by Keith and Padden[6]. These result from crystallization initiating from primary nuclei and growing primarily in the immediate vicinity of the previously grown crystals. The primary nuclei are often foreign matter (sometimes intentionally added) or may be incompletely melted crystalline material remaining from previous crystallization.

The spherulite is believed to grow through low-angle non crystallographic branching of radial crystalline fibrils. This results

in a preferred crystal orientation with respect to the spherulite radius. Quite often, the polymer chain axis is oriented perpendicularly to the radial fibril, resulting in the association of this fibril with the folded-chain lamella, with the polymer chain zig-zagging back and forth perpendicular to the fibrillar lamella and tangential with respect to the spherulite.

This usually gives rise to a negatively birefringent spherulite where the refractive index along the radius is less than that perpendicularly to the radius. However, the crystal orientation with respect to the radius may be variable and depend upon the crystallization temperature as with nylon[7] and "Teflon"[8]. This may be partly consequence of the variation of crystal branching angle and frequency.

Lamellae, often observed to twist as they radiate outward from the spherulite center give rise to banded appearance when viewed in polarized light associated with the periodicity of orientation of the refractive index ellipsoid[9,10,11]. The twist period decreases with increasing growth temperature.

The size of spherulites is governed by the number of primary nuclei from which their growth starts, which is a function of growth temperature, maximum temperature and time of melting and impurity concentration. Generally, large spherulites are formed from melts which had been heated to a high temperature where traces of previous crystallinity is lost, and from samples crystallized at low degrees of

supercooling where spontaneous nucleation rates are low. In polyethylene, spherulites may fill the volume of the sample but if (a) the crystal malt is quenched (not possible for polyethylene) before the spherulite growth is complete or (b) there is sufficient non-crystallizable material excluded during spherulite growth so that the remaining non-spherulitic material becomes difficultly crystallizable, the volume of the sample will be incompletely filled with spherulites. In the former case, the space between spherulite is often filled with crystalline material which grew in state of low order during the rapid cooling of the sample.

Spherulites generally contain both crystalline and amorphous material. The crystalline material is believed to be contained within the lamella whereas the more disordered regions occupy the interlamellar spaces. The internal texture has been characterized by Keith and Padden by a parameter, δ which is the ratio of the rate constant of growth to that of diffusion where δ expresses the characteristic size for which the impurities have time to diffuse out of the crystalline regions during the time of growth. By varying this parameter, the coarseness of internal structure may be affected. Slower crystallization may sometimes occur for this inter-lamella material giving rise to "secondary crystallization" in which there is an increase of the degree of crystallinity of the spherulite which follows its growth. Such interlamellar crystallization often binds lamella together and may greatly restrict the internal mobility within the spherulite. These amorphous chains will generally not be random in their disposition but will have an orientation relative

to the crystalline material within the spherulite. As discussed earlier, annealing or slow crystallization tends to reduce connectivity between lamella and will result in spherulites which tend to crack along the radial lines when subjected to mechanical stress or the swelling or capillary pressure of active solvents. Similarly, the presence of excludable non-crystallizable material results in its concentration between lamella and between spherulites leading to a tendency toward failure in these regions.

DEFORMATION MECHANISMS AND RATES

As a result of the growth mechanism, it is apparent that a crystalline polymer possesses organized structure which determines its mechanisms for yielding to applied strain. Such a material possessing interconnected "soft" and "hard" structural units and may be formally represented by a network of springs and dashpots connected in series and parallel[12]. For rapid deformation or at low temperature (below T_g), the material behaves as an elastic glassy solid where each structural unit deforms by an amount inversely proportional to its modulus. Thus, if the polymer consists of "hard" spherulites or crystals suspended in a less rigid amorphous matrix, most of the deformations occurs in this matrix. For a material in which the spherulite structure fills the volume, deformation must result in either a separation of the spherulites (probably resulting in a failure) or their deformation or transformation (Figure 5) as may be inferred from distortion of the light scattering pattern[8,13]. This

process occurs very rapidly as may be shown using the laser low angle photographic light scattering technique[14,15].

The deformation of the spherulites produces internal changes which are time-dependent, if the deformation is faster than the time period for these internal transformations, the internal structure of the spherulite will be subjected to approximately an affine-like transformation, and crystals will be oriented accordingly. For spherulites which are negatively birefringent, this results in an initial negative birefringence of the polymer (Figure 6) and a tendency for the c-axis to initially orient perpendicularly to the stretching direction as has been experimentally demonstrated by Sasaguri, Hoshino and Stein[16]. At longer times or with greater strain, the internal stresses within the spherulites will be relieved by structural rearrangement which may include (a) extension of amorphous chains, (b) physical rotation of crystals, (c) unfolding of folded chain crystals (d) recrystallization (e) dislocation migration, slip and twinning within the crystals (f) formation of "tilted chain" type crystals (g) crystal structure transition (h) deformation of the crystal lattice and (i) change in the crystallinity.

BACKGROUND OF RHEO - OPTICAL STUDIES OF POLYETHYLENE

The morphology of polyethylene samples is usually spherulitic as a consequence of their heterogenous nucleation and preferred

growth along a particular (the b) crystal axes[17]. The size and perfection of these spherulites is dependent upon the linearity and molecular weight of the polyethylene, the thermal history of the melt and the crystallization temperature. While quenched low-density polyethylene show no obvious spherulitic morphology under the microscope, spherulitic-type correlation among crystals may be demonstrated by light scattering[18]. In such spherulites, the b-axis is directed along the radius with the a-and c-axes helicodally oriented perpendicularly to the b-axis with more-or-less radial order[17]. The b-axis is believed to be the direction of the extension of the lamellae which are branched and twisted. Three types of imperfections may occur. These are (a) those within the crystals which may be chain ends, short branches, or chain links; (b) those on the surface of the crystals, which may be large loops, longer branches or chain ends; and (c) inter-lamellae material, which may be tie chains or non-crystallizable material that may be low molecular weight or highly branched. These imperfections are important in our understanding of the loss processes.

The stretching of polyethylene is accompanied by deformation of the spherulites[19,20]. This may be directly observed by light or electron microscopy or may be indirectly concluded from the changes in light scattering patterns. As has been demonstrated with high speed motion pictures[21], the spherulite deformation is extremely rapid, being able to follow sample deformations occuring in times of the order of a millisecond[22]. The deformation is not affine, however,

as has been demonstrated by selected area electron diffraction studies[19,20]. This may be also indirectly concluded from observations of birefringence changes during the deformation. A simple affine deformation in which the b-axis continues to be radially directed within the spherulite should lead to a birefringence which becomes increasingly negative with elongation. While this is not usually observed with polyethylene (except in vibration of high-density polyethylene at low temperatures), a negative birefringence is found on deforming aged samples of polypropylene and polybutene-1 at low temperatures. The positive birefringence found for polyethylene and for these higher poly-olefins at higher temperatures is explained on the basis of reorientation within the deformed spherulites. The orientation process is not the same throughout the spherulite. The principal mechanism at small deformation in the equatorial part of the spherulite has been postulated to be a twisting of the lamellae about their b axes so as to turn the c-axis (the chain direction) toward the stretching direction (Figure 7)[23-26]. In the 45° to polar parts of the spherulite, shearing of the lamellae leads to chain tilt with repect to the lamellae plane. Both of these processes result in the birefringence becoming more positive. Quantitative theories attempting to account for the experimentally observed crystal orientation function in terms of these mechanisms have been proposed[17-29].

The observation that the birefringence of polyethylene continues to increase with time following stretching[30] indicates that the reorientation of crystals within the spherulite takes place in times

several orders of magnitude longer than that required for spherulite deformation. The birefringence increase occurs in shorter times at higher temperatures and may be superposed by a horizontal shift along the time axis with an activation energy of about 25 Kcal./mole[31]. Similarly, dynamic birefringence studies, observed using a vibrational strain, show a decrease in the strain-optical coefficient with increasing frequency, exhibiting frequency-temperature superposition, with a similar activation energy[32].

DYNAMIC BIREFRINGENCE TECHNIQUE

A. GENERAL BACKGROUND

Birefringence or double refraction is associated with the anisotropy of refractive index. In general for light polarized along the x, y and z axes, an object has three perpendicular refractive indices n_x, n_y and n_z respectively. The three birefringence values are equal to the difference between these principal refractive indices.

where $$\Delta_x = n_y - n_z \qquad (1)$$

$$\Delta_y = n_z - n_x \qquad (2)$$

$$\Delta_z = n_x - n_y \qquad (3)$$

For cylindrically symmetrical objects, there is only one birefringence value which is needed to characterize the sample since two of the other pricipal refractive indices are equal.

By the Lorenz-Lorentz equation, the refractive index, n, can be related to the specific polarizability P.

$$\frac{n^2-1}{n^2+2} = (4/3)\pi P \qquad (4)$$

If the difference between the principal refractive indices is sufficiently small, the differential expression may be applied to the finite difference giving, for example, the expression

$$\Delta_x = n_y - n_z = (2/9)\,\pi \frac{(n^2+2)^2}{n} (P_y - P_z) \qquad (5)$$

relating the birefringence to the specific polarizability difference. n is the average refractive index in this equation.

In the case of a polymer, this anisotropy of polarizability is related to the anisotropic distribution of chemical bonds which are themselves anisotropic. The polarizability essentially measures the mobility of the electrons, and in general, it is found that electron moves easier along the bond than perpendicular to it.

B. BIREFRINGENCE OF AMORPHOUS POLYMERS

For an undrawn film of crystalline polymer such as polyethylene, the chains are arranged with an average random orientation, and the difference in polarizability averages to zero giving zero birefringence. However, when a polymer is deformed, the chains orient along the stretching direction (z-direction) leading to birefringence. In the case of uniaxial deformation, the refractive indices in the x- and y-directions are equivalent, and only one birefringence value is necessary to optically characterize the medium.

$$\Delta = n_{\parallel} - n_{\perp} \qquad (6)$$

where $n_{\parallel}$ and $n_{\perp}$ are the refractive indices along and perpendicular to the stretching direction.

For such a system, the birefringence can be given to a good approximation by

$$\Delta = f_i^o \Delta_i^o \qquad (7)$$

where f_i^o is the orientation function of the amorphous chains and Δ_i^o is the intrinsic birefringence value of the perfectly oriented chain.

C. BIREFRINGENCE OF CRYSTALLINE POLYMERS

In accordance with the approximation of the two-phase model of polymer morphology, by considering the relative orientation of the crystalline and amorphous region, the birefringence of an uniaxially-oriented crystalline polymer may be written as [33]

$$\Delta = X_c f_c \Delta_c^o + (1-X_c) f_a \Delta_a^o + \Delta_f \qquad (8)$$

where X_c is the volume fraction of crystalline material, f_c is the orientation function of the crystalline part, and f_a is the orientation function of the amorphous part. Δ_c^o and Δ_a^o are the intrinsic birefringence

values of the pure, perfectly oriented crystalline and amorphous phases. Δ_f is the form birefringence which arises as a result of the refractive index of oriented boundaries between two regions of different refractive index[34].

In the static case, the crystal contribution to the birefringence can be calculated by multiplying the optical anisotropy of the crystals by the orientation function for the crystals obtained from azimuthal x-ray diffraction scans and the degree of crystallinity[35]. With an assumed value of the crystal birefringence[36], the crystalline contribution to the birefringence has been found to vary from 60-90% of the total birefringence from the low to high density sample[37].

Rewriting Equation (8)

$$\Delta = X_c[(n_a - n_c)f_a + (n_b - n_c)f_b] + (1-X_c)f_{am}\,\Delta^o_{am} + \Delta_F \qquad (9)$$

and assuming that X_c and X^o_{am} are independent of strain during vibration, the strain-optical coefficient is given by

$$\begin{aligned} K' = \left(\frac{d\Delta}{d\varepsilon}\right) &= X_c\,(n_a - n_c)\left(\frac{\partial f_a}{\partial \varepsilon}\right) + (n_b - n_c)\left(\frac{\partial f_b}{\partial \varepsilon}\right) \\ &\quad + (1-X_c)\,\Delta^o_{am}\left(\frac{\partial f_{am}}{\partial \varepsilon}\right) + \left(\frac{\partial \Delta_F}{\partial \varepsilon}\right) \\ &= X_c K'_{cr} + (1- X_c)\,K'_{am} + K'_F \end{aligned} \qquad (10)$$

The third factor K_F' which is the contribution due to form birefringence was neglected in most of the previous work. For a multiple system where the light wave encounters several regions of differing birefringence, the retardations are additive if the regions are large as compared to the wavelength of light, neglecting distortion of the electric field at phase boundaries, so that

$$R = \sum_i R_i = \frac{2\pi}{\lambda_o} \sum_i d_i \Delta_i \qquad (11)$$

so that

$$\Delta = \sum_i \left(\frac{d_i}{d}\right) \Delta_i \qquad (12)$$

where (d_i/d) is the fraction of the path of the light wave occupied by phase i. Since $\Delta_i = \Delta_i^\circ f_i$, therefore,

$$= \sum_i \left(\frac{d_i}{d} \Delta_i^\circ f_i\right) + \Delta_F \qquad (13)$$

The term Δ_F is the form birefringence which is added to represent the lack of additivity of retardations of the phases and includes the effect of distortion of the field at phase boundaries. It is a function of the shapes and sizes of the different regions and of the average refractive index difference between the phases. An analytical expression for this term is not available, except for some very idealized cases described by Weiner[34].

MEASUREMENT OF BIREFRINGENCE

Birefringence can be measured by measuring directly the refractive index with polarized light by one of the classical refractometer methods, but the more sensitive intensity method or the Babinet compensator methods are usually used for the measurement of the birefringence of polymers.

For a non-scattering non-absorbing birefringent film, the fractional transmission of a sample for monochromatic light between crossed polarizers with their polarization axes at 45° to the optic axes of the film is

$$T = \sin^2\left(\frac{\delta}{2}\right) \qquad (14)$$

where δ is the retardation given by

$$\delta = \frac{2\pi\Delta d}{\lambda} \qquad (15)$$

Δ is the birefringence, d is the thickness of the film and λ the wavelength of the light used. The transmission passes through a maximum and minimum for each order of retardation.

In the Babinet compensator method, the birefringence of the polymer film is balanced by inserting an object of known retardation

(a quartz wedge in this case) where birefringence is opposite to the direction of the sample birefringence. The motion of the quartz wedge with retardation which is linear with position is used to compensate the birefringence of the sample. At the position where the retardation balance, a dark "zero order fringe" appears as predicted by Equation (14).

When the sample is removed, the number of turns required to move a micrometer screw on the quartz wedge to return the "zero order fringe" to its original position is calibrated to read the retardation of the sample in units of fractions of a wavelength.

In the dynamic birefringence experiment, where the dynamic strain amplitude are less than 1%, the more sensitive intensity method is used to follow the birefringence change of the polymer as it is deformed by the sinusoidal varying stress.

INTRODUCTION TO DYNAMIC BIREFRINGENCE

The time dependence of birefringence characterizes the rate of change of total orientation of a polymer and, when combined with the results of other dynamic measurements, characterizes the rate of response of crystalline and amorphous media. The birefringence may increase or decrease depending upon the anisotropy of the structural unit involved, and whether a process takes place with an increase

or decrease in orientation. Measurements in a dynamic experiment are capable of yielding more informations since molecular mechanisms having relaxation time too short to contribute to static experiment are accessible.

The dynamic birefringence technique was first introduced and developed by Onogi, Keedy, Sasaguri and Stein[38,39] and by Legrand and Erhardt[40], Yamada[41-42], Read[43-44] and Rudd[45]. Simultaneous measurement of the real part of the strain-optical coefficient K', the real part of the modulus E', the birefringence-strain phase angle α , and the stress-strain phase angle δ are obtained.

DYNAMIC BIREFRINGENCE THEORY

When a polymer is subjected to sinusoidal strain

$$\varepsilon = \varepsilon_o + (\Delta\varepsilon)\cos\omega t \qquad (16)$$

where $\omega = 2\pi\nu$, and ν is the measured frequency in hertz, ε_o is the static strain, and $(\Delta\varepsilon)$ is the dynamic strain amplitude.

Then during such an experiment, the stress also varies sinusoidally so that the complex modulus can be represented as

$$\sigma = \sigma_o + (\Delta\sigma)^*_e{}^{(i\omega - \delta)t} \qquad (17)$$

$$E^* = \left(\frac{d\sigma}{d\varepsilon}\right)^* = \left(\frac{\Delta\sigma^*}{d\varepsilon}\right) = E' + E''$$
$$= |E| \cos\delta + i|E| \sin\delta \qquad (18)$$

where E' and E'' are the real and imaginary parts of the modulus respectively. The in-phase portion of the modulus E', can be represented as

$$E' = |E^*| \cos\delta \qquad (19)$$

where δ is the phase angle between the stress and strain. Similarly, the out-of-phase or the loss modulus is given by

$$E'' = |E^*| \sin\delta \qquad (20)$$

Thus

$$|E^*|^2 = (E')^2 + (E'')^2 \qquad (21)$$

and

$$E''/E' = \tan\delta \qquad (22)$$

In analogy to the complex modulus and the loss tangent in the viscoelastic system, the birefringence is[46]

$$\Delta = \Delta_o + \left[\Delta(\Delta)\right]^* \cos\omega t$$
$$= \Delta_o + \left[\Delta(\Delta)\right] \cos(\omega t - \alpha) \qquad (23)$$

and the strain-optical coefficient is

$$K^* = \frac{d\Delta}{d\varepsilon} = \frac{\Delta(\Delta)}{\Delta\varepsilon}$$
$$= K' + K''$$
$$= |K| \cos\delta + i|K| \sin\delta \qquad (24)$$

Various derived quantities may then be obtained such as the stress-optical coefficient

$$M^* = \frac{d\Delta}{d\sigma} = \frac{\Delta(\Delta)^*}{\Delta\sigma^*} = \frac{|\Delta(\Delta)|}{|\Delta\sigma|} \frac{\cos\alpha + i\sin\alpha}{\cos\delta + i\sin\delta}$$
$$= |M| (\cos\beta + i\sin\beta)$$
$$= M' + iM'' \qquad (25)$$

where

$$|M| = \frac{|\Delta(\Delta)|}{|\Delta\sigma|} \qquad (26)$$

and

$$\beta = \alpha - \delta \qquad (27)$$

In all of these relationships, it is assumed that the phenomena are linear, so that for example $K' = (\frac{\Delta(\Delta)}{\Delta\varepsilon})$, is independent of $\Delta\varepsilon$.

In the mechanical case, the stress always leads the strain, but the birefringence can lead or lag the strain in phase depending on whether K'' is neagative or positive.

Just as E' and E'' can be related to the relaxation function

$$E' = \int_{-\infty}^{\infty} \frac{\omega^2\tau^2}{1+\omega^2\tau^2} H(\ln\tau)\, d\ln\tau \qquad (28)$$

and

$$E'' = \int_{-\infty}^{\infty} \frac{\omega\tau}{1+\omega^2\tau^2} H(\ln\tau)\, d\ln\tau \qquad (29)$$

Stein; et. al.[39,42] have proposed a phenomenological linear theory in which the birefringence functions may be described by

$$K' = \int_{-\infty}^{\infty} \frac{A\omega^2\tau^2+B}{1+\omega^2\tau^2}\, d\ln\tau$$
$$= \int_{-\infty}^{\infty} \frac{(A-B)\omega^2\tau^2}{1+\omega^2\tau^2}\, d\ln\tau + \int_{-\infty}^{\infty} B\, d\ln\tau \qquad (30)$$

and

$$K'' = \int_{-\infty}^{\infty} \frac{(A-B)\omega\tau}{1+\omega^2\tau^2}\, d\ln\tau \qquad (31)$$

where A and B are the birefringence spectra terms associated with the elastic and viscous processes[39,42]. By using methods similar to those used to obtain relaxation spectra from mechanical data[47,48], birefringence spectra function may be obtained by inversion of the experimetnal data[42]. Only a combination of function (A-B) can be obtained. A method for separating this into the individual function has not been developed.

Read, in an extension of the molecular theory of viscoelasticity, has proposed a somewhat different formulation

$$K' = \int_{-\infty}^{\infty} \Phi_k(\ln\tau) \frac{\omega^2\tau^2}{1+\omega^2\tau^2}\, d\ln\tau \qquad (32)$$

and

$$K'' = \int_{-\infty}^{\infty} \phi_k(\ln\tau)\frac{\omega\tau}{1+\omega^2\tau^2}\,d\ln\tau \qquad (33)$$

but it can be shown that Stein's (A-B) is equivalent to Read's ϕ_k. Dispersions in K' and K'' and tanα can be described in terms of these birefringence spectrum functions which are related to molecular mechanisms.

Yamada et. al. [42] have postulated that K' is composed of three types of contributions, that is

$$K' = K'_A + K'_D + K'_0 \qquad (34)$$

where K'_A is the contribution from orientation of molecules in amorphous domains, K'_D the contribution from the deformation of shperulites and K'_0 the contribution from the orientation of crystallites.

DYNAMIC X-RAY DIFFRACTION

INTRODUCTION

The dynamic x-ray diffraction has been described by previous workers[49-51]. The orientation of a particular plane i, is described in terms of a Hermans-type orientation[52,53], f_i as

$$f_i = \frac{3\langle \cos\alpha_i \rangle_{av} - 1}{2} \qquad (35)$$

where α_i is the angle that the normal to the i^{th} crystal plane makes with respect to the stretching direction. For static measurements, this function may be determined from a numerical integration of a function of the diffracted intensities over the azimuthal diffraction angle. This is a number having a value which characterizes the degree of uniaxial orientation of the i^{th} crystal plane. A value of zero indicates random orientation, and it becomes increasingly positive as the plane normal tends to orient parallel to the stretching direction, and negative as it tends to orient perpendicular to this direction.

A quantity called the orientation function of a particular crystal plane i is defined as

$$\begin{aligned} f_i &= f_{oi} + (\Delta f_i)^* \\ &= f_{oi} + |\Delta f_i| \cos(\omega t - \gamma_i) \end{aligned} \qquad (36)$$

where the dynamic orientation function amplitude $(\Delta f_i)^*$ is a complex number

$$(\Delta f_i)^* = (\Delta f_i)' + i(\Delta f_i)'' \qquad (37)$$

where the real part

$$(\Delta f_i)' = |\Delta f_i| \cos \chi_i \qquad (38)$$

is the part varying in phase with the strain, while the imaginary part

$$(\Delta f_i)'' = - |\Delta f_i| \sin \chi_i \qquad (39)$$

is the part varying 90° out of phase. The loss tangent for orientation is then

$$\tan \chi_i = - \frac{(\Delta f_i)''}{(\Delta f_i)'} \qquad (40)$$

The orientational compliance C_i^* may then be defined as

$$\begin{aligned} C_i^* &= \left(\frac{\partial f_i}{\partial \varepsilon}\right) \cong \left(\frac{\partial f_i}{\Delta \varepsilon}\right) \\ &= C_i' + iC_i'' \\ &= |C_i| \cos \chi + i |C_i| \sin \chi \end{aligned} \qquad (41)$$

where

$$C_i' = |C_i| \cos \chi \qquad (42)$$

$$C_i'' = |C_i| \sin \chi \qquad (43)$$

The dynamic x-ray technique determines the strain dependency of the intensity of x-ray diffraction of the (h,k,l) plane; $I_{hkl}(\theta, \phi)$ at a particular Bragg angle, θ , and azimuthal angle ϕ , as a function of static strain. In the case of polyethylene, the a-axis orientation can be obtained from diffraction of the (h00) plane.

The b-axis orientation, however, cannot be determined directly because of the lack of a sufficient strong (0k0) reflection. Nevertheless, by using the Wilchinsky relationship[54], and from the orientation function for the a-axis and from the orientation function of the 110 normal

$$f_b = \sec^2 \rho_{110} f_{110} - \tan^2 \rho_{110} f_a \qquad (44)$$

(where ρ is the angle between the b-axis and the normal to the 110 plane) the b-axis orientation can be obtained. Further by the use of the orthogonality relationship of the a, b, c axes

$$f_a + f_b + f_c = 0 \qquad (45)$$

it is possible to characterize all the three axis orientation.

A PHENOMOLOGICAL TREATMENT FOR DYNAMIC ORIENTATION FUNCTIONS

Recalling that the strain-optical coefficient in a relaxation experiment can be given by[39,42]

$$K(t) = \int_{-\infty}^{\infty} \phi_k(\ln\tau)\, e^{-t/\tau} d\ln\tau + \int_{-\infty}^{\infty} B(\ln\tau)\, d\ln\tau \qquad (30)$$

A similar formalism may be carried out for the crystalline (and amorphous) orientation functions. In terms of a Maxwell element (Figure 21), having a total strain, ε, composed of components ε_s and ε_d from the spring and the dashpot, such that

$$\varepsilon = \varepsilon_s + \varepsilon_d \qquad (46)$$

The orientation function of the i^{th} crystal plane is

$$f_i = L_i \varepsilon_s + V_i \varepsilon_d \qquad (47)$$

where L_i and V_i are the elastic and viscous components of the orientation-strain coefficient for the i^{th} plane. The stress on the element, σ, is proportional to the strain on the spring

$$\sigma = E \varepsilon_s \qquad (48)$$

where E is the elastic modulus of the spring

$$f_i = \frac{L_i}{E} + V_i \left(\varepsilon - \frac{\sigma}{E} \right)$$

$$= \frac{L_i - V_i}{E} \sigma + V_i \varepsilon \qquad (49)$$

Thus the orientation function can be divided into two parts, one of which is proportional to the stress and the other proportional to the strain. The orientation function-strain coefficient for the Maxwell element is then

$$C_i = \frac{f_i}{\varepsilon} = \left(\frac{L_i - V_i}{E} \right) \frac{\sigma}{\varepsilon} + V_i \qquad (50)$$

In a relaxation experiment at constant length = ε_o, the stress on the Maxwell element decays according to the equation

$$\sigma = \varepsilon_o E e^{-t/\tau} \qquad (51)$$

where τ is the relaxation time of the element

$$\tau = \eta/E \qquad (52)$$

and η is the viscosity of the dashpot. Thus

$$C_i(t) = (L_i - V_i) e^{-t/\tau} + V_i \qquad (53)$$

For a distribution of Maxwell elements, this may be then generalized to give

$$C_i(t) = \int_{-\infty}^{\infty} \psi_i(\ln\tau)\, e^{-t/\tau}\, d\ln\tau + \int_{-\infty}^{\infty} V_i(\ln\tau)\, d\ln\tau \qquad (54)$$

an equation analogous to the strain-optical coefficient equation (30) where $\psi_i(\ln\tau)$ is the orientational compliance relaxation function defined by

$$\Psi_i(\ln\tau) = L_i(\ln\tau) - V_i(\ln\tau) \qquad (55)$$

This equation can be applied in the same way as Equation (30) for describing linear rheo-optical phenomena.

It should be emphasized that equations (30) and (54) may be interrelated, since if we consider that the total birefringence is due to the sum of the contributions arising from the orientations of the various crystal planes and other structural elements (such as amorphous chains), then the total birefringence is

$$\Delta = \sum_i X_i \Delta_i^o f_i \qquad (56)$$

where the sum is over all of the orientationally independent structural elements. X_i is the volume fraction of each element and Δ_i^o is the intrinsic birefringence of each element. Thus the strain-optical coefficient can be written as

$$K = \frac{\partial\Delta}{\partial\varepsilon} = \sum_i X_i \Delta_i^o C_i \qquad (57)$$

where $C_i = \left(\frac{\partial f_i}{\partial \varepsilon} \right)$, assuming that X_i and Δ_i^o are independent of strain.

If one combines equations (30), (54) and (57), it follows that

$$\int_{-\infty}^{\infty} \phi_k(\ln\tau) e^{-t/\tau} \, d\ln\tau + \int_{-\infty}^{\infty} B(\ln\tau) \, d\ln\tau$$
$$= \sum \left\{ X_i \Delta_i^o \left[\int_{-\infty}^{\infty} \psi_i(\ln\tau) \, e^{-t/\tau} \, d\ln\tau + \int_{-\infty}^{\infty} V_i(\ln\tau) d\ln\tau \right] \right\} \quad (58)$$

so that

$$\phi_k(\ln\tau) = \sum X_i \Delta_i^o \psi_i(\ln\tau) \quad (59)$$

and

$$B(\ln\tau) = \sum X_i \Delta_i^o V_i(\ln\tau) \quad (60)$$

so that the birefringence relaxation functions are related to the orientation compliance functions.

While the phenomological description is rigorous for linear rheo-optical behavior in terms of a distribution of Maxwell elements, it is easier to interrelate a model involving Voigt elements to a molecular description. Iwayanagi et. al. [68,81] have represented the mechanical properties in terms of a six parameter Voigt model shown in Figure (8). The Voigt element α represents the retarded viscoelastic response of the crystalline lamellae while β represents the viscoelastic deformation of the interlamellae amorphous material. These

elements are associated with moduli E_α and E_β , viscosities η_α and η_β and retardation times $\tau_\alpha = \eta_\alpha/E_\alpha$ and $\tau_\beta = \eta_\beta/E_\beta$. (The Iwayanagi equations are formulated in terms of shear moduli ϵ_i, as our experiment are carried out in tension, we substituted tensile moduli E_i.)
In accordance with our previous discussion, we associate compliance parameter with each of the elements. In general we may write that

$$f_{ij} = L_{ij}\,\varepsilon_{sj} + V_{ij}\,\varepsilon_{dj} \qquad (61)$$

where f_{ij} is the orientation function of the i^{th} crystal plane resulting from the j^{th} viscoelastic mechanism.

PART II

EXPERIMENTAL

A. INTRODUCTION

The dynamic birefringence apparatus used in this work is the one described by Yamada and Stein[55], with some modifications which will be described accordingly in the later part of this section. By varying the combination of the belts and pullies, the mechanical driving system can sinusoidally deform a polymer specimen with an upper frequency limit of approximately 10 cycles per second. The lowest frequency available, is determined solely by the patience of the experimenter and stability of the apparatus.

The birefringence is determined by measuring the transmitted intensity between crossed 45° polariods. The stress and strain signals were obtained using standard transducers. α and δ were measured by the Lissajous figure technique with a simultaneous display on the oscilloscope of the stress-strain and the birefringence strain Lissajous figures[41,42,46,55].

B. VIBRATION SYSTEM

The sample is subjected to a forced tensile vibration by the

sinusoidal motion of the upper and lower clamps which are connected to an eccentric cam device rotating with a constant speed. It is felt that such a vibration system will enable us to focus the optics at one constant spot of the sample during vibration. The static strain on the sample could be varied by the operation of a screw mechanism or the lowering of the lower clamp by the loosening and retightening of the hex-nut. A dial gauge was used to monitor the positions of the upper and lower clamps. The static strain was necessary to prevent the sample from slackening during the vibration cycle.

C. STRAIN DETECTION

A core of a Schaevitz linear variable differential transformer (Type 100 MS-LT) fastened to the moving rod of the vibration generator serves to monitor the strain of the sample. The voltage output of the LVDT is powered by a low-noise audio-frequency oscillator (10,000 cps) where output is amplified by aTektronix Type 122 low level preamplifier. The output of the LVDT is amplified by a Ballantine Model 300 electronic voltmeter before it is fed into the half-wave rectifier. The rectified signal is applied to the horizontal plates of a Tektronix Model 502 Dual-Beam Oscilloscope.

D. STRESS DETECTION

The displacement of a TDC-4M miniature dynanometer purchased from

Schavitz Engineering was used to measure the stress in the sample. It consists of a precisely-machined proving ring with two integral threaded bosses at opposite sides for easy mounting. A small shielded linear variable differential transformer (LVDT) is mounted on one boss, and a magnetic core on the opposite boss. When a tensile or compressive force is applied to the bosses of the ring, the core is displaced from its normal null position. This displacement induces an output voltage proportional to the applied force. A simple manual zero adjustment is provided for cancellation of tare loads.

E. OPTICAL SYSTEM

Two different light sources were used for the birefringence measurement. The first which is shown in Figure (9) is an H100-A4/T General Electric mercury vapour lamp operated by 100 volt D.C. from a motor-generator which is filtered using a condenser choke system. The lamp is started by momentarily applying 200 volt A.C. from an auto-transformer, after which it is changed to a D.C. source. By adjusting a 200 ohm variable resistance, the D.C. current is kept constant at 0.8 ampere. D.C. operation is used rather than conventional A.C. operation for which the lamp was designed because the A.C. operation resulted in a 120 hertz modulation of the intensity which would beat against the modulation by the sample vibration. The light beam, rendered parallel by a condensing lens is made monochromatic by a 5461 Å interference filter. The light is polarized at 45° to the stretching

direction by a polaroid, passes through the sample and analyzer (polaroid) which is crossed to the polarizer. Retardation plates which are used to maximize sensitivity and linearity of response are inserted between the sample and the analyzer. The beam then strikes a 1P 21 photomultiplier tube. The linear region of the photomultiplier is checked and may be adjusted by using a (Kodak) neutral density filter.

In the second light source system, a He-Ne laser of 6328 Å wavelength was used instead of the mercury lamp. This is a more handy and more collimated light source in which no D.C. voltage and polarizer is needed as the laser is self-rectified and polarized. The polarization direction can be adjusted by the use of a Polarization Rotator (Spectra Physics Model 310) and an alignment Mount (Spectra Physics Model 304).

The signal for the 1P21 is traced on the remaining channel of the Tektronix Dual-Beam Oscilloscope. The electrical output of the photomultiplier is a function of birefringence and is calibrated by inserting a retardation plate of known retardation.

F. PHASE DETECTION

The optical- and mechanical-loss tangent were measured by the hysteresis loop method. Simultaneous display of the stress-strain and birefringence-strain Lissajous figures was achieved by using the dual-beam Tektronix Model 502 Oscilloscope. The two alternating stress and birefringence signals were fed into the Y deflecting

plates. The method of determining tanα , tanδ , E' and K' are discussed in detail in the later section.

G. ENVIRONMENTAL CONDITIONING

In order to enable the studies of the dynamical mechanical and optical properties to carry out over a wide range of temperature, the sample chamber was sufficently insulated and the temperature in the chamber could be controlled from -140° to 200°C. This was rendered possible by the use of the arrangement shown in Figure (10). A slab of copper with four copper coils soldered on the inner side was constructed to mount perfectly to the temperature chamber. Liquid nitrogen can be directed through a Y-shaped common inlet leading to the copper coil whereby the vaporized liquid nitrogen is sprayed onto the sample. Temperature can be varied by the proper adjustment of the inflow liquid nitrogen which has been dried by passing through dessicator and concentrated sulphuric acid to ensure complete removal of moisture. For the high temperature operation, air was circulated through the environmental chamber as indicated in Figure (10). A fixed heater which could be set from 0 to 1500 watts was used in conjunction with the 0 to 750 watt heater controlled by the thermostat.

The two slits which are furnished on the opposite sides of the sample chamber to permit light to pass through the sample were made as small as possible to keep heat loss to a minimum. Temperature was

measured both by placing a thermometer near the sample as well as by a thermocouple detection device. Asbestos was used to clamp the sample ends in order to avoid thermal gradients in the sample due to rapid heat transfer at the metal clamps.

H. EXPERIMENTAL PROCEDURE

To ensure stability of the light source and electronics, a warm-up period of at least 30 minutes was necessary before performing the measurements. Sample sizes of 4-6 cm. length, 1-1.2 cm.width and 3-5 mils thick were used in the experiments. The sample was subjected to an initial static strain to prevent buckling of the specimen during the vibration cycles. Before applying the dynamic strain, the sample was allowed to relax to equilibrium. The amplitude of vibration was about 1%. Measurements were made after vibrating the sample for 10-15 minutes to reach a steady state.

In the temperature variation experiment, the desirable temperature was first obtained by adjusting the Variac setting after which it is kept steady with the sample in this environment for $\frac{1}{2}$ hour. Measurements were made at 5-10^{o} temperature intervals. In the strain variation experiment, twenty minutes was allowed for every new strain imposed in order for the sample to relax to equilibrium.

DYNAMIC X-RAY DIFFRACTION

A. INTRODUCTION

The dynamic x-ray diffraction technique for following the responses of polymer crystals to mechanical excitation of sinusoidal strain has been described by previous workers[49-51]. The intensity change may be resolved into a real part $\Delta I'$, varying in-phase with the strain and an imaginary out of phase component $\Delta I''$. From these one may obtain the change in orientation of the reciprocal lattice vector and deformation of lattice spacing of specific crystal planes with the change in the external periodic strain.

B. PRINCIPLE OF METHOD

Figure (11) shows the general picture of the dynamic x-ray diffractometer where a modification in the detection system has been made; The Geiger counter was replaced by a scintillation counter (Model DM 228) purchased from the Harshaw Chemical Company. Such modification increases the sensitivity of detection and eliminates the error due to dead time correction. Also the mechanical commutator was replaced by an optical commutator in which a rotating sector sychronized with the sample stretching intercepted the light beam falling on a bank of four photocells which drove gating circuits such that when light falls on a photocell, the corresponding counting circuit was activated. The program of activation of scalers was

determined by the pattern cut out on the rotating sector, which is shown in Figure (12) where $0 \rightarrow \pi$, $\pi/2 \rightarrow 3\pi/2$, $-\pi/2 \rightarrow \pi/2$ and $\pi - 2\pi$, correspond to channels 1, 2, 3 and 4 respectively.

Figure (13) shows the optical arrangement of the dynamic x-ray diffractometer in an application of the transmission technique. A film specimen S in a vertical plane V is subjected to tensile sinusoidal deformation. An incident x-ray beam impinges in the horizontal plane H and falls on the specimen at a Bragg angle θ to the film normal. The axes of a detector is fixed horizontally and is tilted to the film normal by the same angle . The film specimen can be rotated about its normal axis (x-axis) to give any desired azimuthal angle ϕ where the value is taken to be zero when the tensile stress direction of the film specimen is vertical. In practice, the tensile stress is applied in the longitudinal direction of the film specimen which has a ribbon shape, and it follows the ϕ rotation of the specimen.

C. DESCRIPTION OF APPARATUS

A pinhole collimated x-ray beam (General Electric XRD-675 K.V.P. generator powers a G.E. Type EA-75 tube.) (0.4 cm wide x 1.4 cm high in dimensions at the sample with a horizontal angular divergence of $\pm 1^{\circ}$ and a vertical divergence of $\pm 2^{\circ}$). The x-ray tube is mounted on a plate which may slide horizontally on a base plate and which may be rotated with respect to the sample axis in order to adjust the angle of incidence for the x-ray.

The sample is mounted in a vibrator (Figure 14) which permits one to vary the azimuthal angle while the sample is subjected to tensile vibration*. This is powered by a 1 H.P. D.C. motor and Ratiotrol** electronic variable speed control. Through the use of this and an arrangement of gears and timing belts, continously variable speeds between 0.01 and 20 revolutions per second can be provided. By rotation of pairs of eccentric cams, the vibrator produces linear vibrations of the both sample jaws at strain amplitudes of 0.08, 0.1, 0.4, and 0.8 cm. The circular plate holding the cam and jaw assembly may be rotated through 360° of azimuthal angle while the sample is vibrating by manually rotating a drive shaft and worm gear which engages with gear teeth on the periphery of this plate. Provision is made so that a motor drive for this azimuthal angular adjustment may be provided for automatic scaning.

The sample, usually of 2 cm. x 4 cm. x 0.05 cm. dimension, is mounted between clamps which can be adjusted by means of a screw, with respect to the drive rod from the cam assembly so as to provide a static strain. The application of such a static strain is necessary in order to prevent slackening of the sample during the minimum strain part of the vibration. By adjusting lengths and replacing cams of different sizes, it is possible to achieve vibrational strains of 0-40% amplitude superimposed on static strains of 0-100%. Samples having static strains higher than 100% can also be obtained by prestretching the sample to the desirable elongation on an extentometer after which it is left

*Manufactured by Iwamoto Scisakushi Inc. Kyoto, Japan.
** Boston Gear Co. Boston, Mass.

there for two weeks to allow relaxation to reach equilibrium. A sample of the above mentioned dimension is then cut out and mounted on the clamps where a further small strain is added in order to prevent slacking.

The diffracted radiation is detected by a crystal solid state scintillation detector which is mounted on an arm whereby a selected Bragg angle corresponding to diffraction from the crystal plane under study can be manually adjusted.

While the specimen is sinusoidally deformed, the detected and preamplified (Baird-Atomic Inc. preamplifier Model 231) x-ray signals are continously fed through a non-loading amplifier (Model 215)* and a single channel pulse height analyzer (Model 510)*, and finally fed to the four channels of an automatic digital counter**. These channels are activated respectively at a particular strain phase intervals for each channel by means of a gating circuit activated by signals received from a photoswitch commutator rotating in synchronism with the sample vibration.

D. THE PHOTOSWITCH COMMUTATOR

Details of the "photo-switch" are shown in Figure (15). The light from the bulb (an automobile headlamp) is collimated into a vertically elongated rectangle focused on the chopper disc by a

* Baird-Atomic Inc., Cambridge Mass.
** Digital Automation Co.

cylindrical lens and mirror. The chopper disc contains four sector windows of angular width corresponding to the fraction of the time a given channel is to be activated and are located at an angular position corresponding to the phase angle between the strain and the time that the corresponding counting channel is to be activated.

The "photoswitch commutator" may be calibrated by feeding a constant frequency signal (Eico Audio generator of square waves) through the gating circuit (instead of the scintillation detector signal) and determining the "sector constant" s_k which is the fraction of the entire vibration period that a given counting channel is activated. When making an actual measurement, the scaler reading would then be divided by its s_k in order to determine the counting rate. Examination of the signals with a dual beam oscilloscope has verified that no phase difference are introduced by the electronics.

The entire diffractometer is enclosed in a lead-lined wooden box to protect the operator from stray radiation. Temperature control for the sample can be adjusted by circulating heated air (temperature being varied by the Variac setting) about the sample. Temperature could be maintained to $\pm$ 1°C in the range of 25° to 100° C, prior to measurements the sample was thermally conditioned for half an hour after which it was further mechanically conditioned by vibrating at the desired frequency for $\frac{1}{2}$ hour.

E. AUTOMATIC PRINT-OUT AND STORAGE OF DATA

The duration of counts in seconds and the number of counts will be printed out by a teletype* which is connected to the TTY terminal of the digital counter. An example of the print out is shown as below:-

30,1

200120	674257	673300	674022	678131

where the first line indicates the azimuthal angle 30°, followed by the number of trials which in this case has been chosen for simplicity to be 1. The first column of the second line indicates the time of counts in thousandth of a second (which in this case is equivalent to 200.120 seconds). The next four columns indicate the counting of the 1,2,3 and 4 channels respectively. These data which would be carried out for all the azimuthal angles (from 0 to 90° at intervals of 10°)and for both the 110 and 200 planes (the two most intense reflection planes of polyethylene) would be stored in the form of punched tape which could be fed directly into the CDC 3600 computer for processing. A computer program by the name of XMOD 7 has been written for such computation, and is listed in Appendix II together with a sample calculation for the quenched sample at 20% static strain (Appendix III).

* Teletype Corporation, Skokie, Illinois.

METHOD OF CALIBRATION AND CALCULATION OF DYNAMIC BIREFRINGENCE

A. INTRODUCTION

The measurement of the dynamic birefringence is based upon the observation of the change in transmitted light when the sample is vibrated between $\pm 45^{\circ}$ crossed polaroids. In practice, the method is calibrated against some absolute method of measuring birefringence such as with a Babinet compensator. Corrections must be made for transmission changes resulting from the reflection absorption and scattering by a sample. It is the purpose of this section to discuss the details of this calibration and the calculation procedure.

B. METHOD

It has been pointed out earlier that when a purely birefringent object is placed between polaroids crossed at +45 and -45° to the optic axis of the object, the fraction of the incident intensity which is transmitted is [46,56]

$$T = \sin^2 (\delta/2) \qquad (62)$$

where $T = I_{trans}/ I_o$, I_{trans} is the transmitted intensity, I_o is the incident intensity, δ is the retardation defined as

$$\delta = (2\pi \Delta d)/\lambda \qquad (63)$$

where Δ is the birefringence of the object, d is its thickness in the direction of the incident beam and λ is the wavelength of the light in air. If the object reflects, absorbs or scatters light, this equation may be modified to give

$$T = F \sin^2(\delta/2) + T_s \qquad (64)$$

where F is the attenuation of the light beam resulting from reflection, absorption and scattering which is given by

$$F = e^{-(\kappa + \tau)d} (1-r) \qquad (65)$$

where κ is the absorption coefficient, τ the turbidity and r the reflectivity of the sample. The quantity T_s is the transmittance of the sample arising from (a) depolarization of the transmitted light resulting from the presence of locally birefringent structures such as spherulites, and (b) the low angle scattered light which can reach the photometer and which is measured along with I_{trans} because of its admitting light diverging up to some finite angle. This term gives rise to transmission even if there is no macroscopic birefringence and may change with elongation and consequently will vary during a dynamic birefringence experiment.

The quantity F may be estimated by measuring the transmittance of the sample with the analyzing polaroid removed, in which case

$$T_F = F_o - T'_s \qquad (66)$$

where F_o is the true attenuation and T'_s is the part of the scattered light measured in the absence of the analyzer. Assuming that this varies with elongation in the same manner as F_o we shall define an effective attenuation as $F = F_o - T''_s = T_F$ which we shall use in Equation (64). The effect of including T''_s in F is to make the attenuation a bit less than F_o because of the inclusion of the low angle scattering in the transmitted beam. The T_s term in Equation (64) is then the residual scattered and transmitted intensity which is depolarized and which is included in the T'_s term.

The only rigorous way to resolve the scattered intensity into T_s and T'_s contribution is to accompany the dynamic birefringence experiment with a dynamic light scattering experiment[56]. An approximate way is to relate T_s to FT_+, the transmitted intensity for polarizer and analyzer at 0^o and 90^o to the optic axis. Under these conditions, macroscopic birefringence will not result in transmission and the light measured by the photometer will be that which is scattered at small angles. (This will not necessarily be the same as T_s in the oriented state since T_+ measures the scattering for 0^o- 90^o polarization whereas T_s requires the scattering for $\pm 45^o$ polarization. At low orientations, the two are the same.)

As has been shown, when the strain ε is changed by a small amount, differentiation of Equation (64) gives

$$\frac{\partial T}{\partial \mathcal{E}} = F \sin\left(\frac{\delta}{2}\right)\cos\left(\frac{\delta}{2}\right)\left(\frac{\partial \delta}{\partial \mathcal{E}}\right) + \sin^2\left(\frac{\delta}{2}\right)\left(\frac{\partial F}{\partial \mathcal{E}}\right) + \left(\frac{\partial F T_+}{\partial \mathcal{E}}\right) \qquad (67)$$

A plot of the variation of T with δ is given in Figure (16) assuming F and T_s to be constant. It is noted that the slope $\left(\frac{\partial T}{\partial \delta}\right)$, and hence $\left(\frac{\partial T}{\partial \mathcal{E}}\right)$ is most constant and greatest at $\delta = \pi/2$, when $\sin(\delta/2)\cos(\delta/2) = \frac{1}{2}$ and $\sin^2(\delta/2) = \frac{1}{2}$. In practice, to meet this condition, a retardation plate of calibrated retardation δ_R is placed in the light path between the crossed polarizers so that the total retardation is

$$\delta = \delta_R + \delta_S \qquad (68)$$

where δ_S is the retardation of the sample. Since a continous range of retardations δ_R is not available, it is not always possible to achieve $\delta = \pi/2$, in which case $\sin(\delta/2)\cos(\delta/2) = a$, a constant close to but not necessairly equal to $\frac{1}{2}$. Then $\sin^2(\delta/2) = \frac{1}{2} \pm (\frac{1}{2} - a)^{\frac{1}{2}}$. Since this second term in Equation (67) is a correction term which is small as compared with the first term, it is sufficiently accurate to allow $\sin^2(\delta/2)$ to be $\frac{1}{2}$ even though a differs slightly from $\frac{1}{2}$. Under these conditions, Equation (67) becomes

$$\left(\frac{\partial T}{\partial \mathcal{E}}\right) = aF\left(\frac{\partial \delta}{\partial \mathcal{E}}\right) + \frac{1}{2}\left(\frac{\partial F}{\partial \mathcal{E}}\right) + \left(\frac{\partial [F T_+]}{\partial \mathcal{E}}\right) \qquad (67a)$$

In practice, the transmitted intensity is measured using a photomultiplier tube, the amplified signal from which is displayed as the vertical displacement of the oscilloscope trace h. Assuming

that the response is linear, we may write

$$h = K\,T$$

where K is a proportionality constant. (In fact, K is proportional to the incident intensity, I_o, and the assumption of a constant K presumes that I_o remains constant in the course of measurements. A better practice would be to monitor I_o and correct K for its variation during the experiment.)

If the displacement is small, the change in oscilloscope displacement during the sample vibration is

$$h_B = \Delta h = \left[aKF \left(\frac{\partial \delta}{\partial \varepsilon}\right) + \tfrac{1}{2} \left(\frac{\partial [KF]}{\partial \varepsilon}\right) + \left(\frac{\partial [KFT_t]}{\partial \varepsilon}\right)\right] \Delta \varepsilon \qquad (69)$$

where the displacement h_B is indicated in Figure (17).

To determine the proportionality constant K, one changes the retardation by a known amount using a calibrating retardation plate of known small retardation δ_c and observing the displacement of the cathode ray trace. In the absence of the plate δ_c, a plot of Δh against $\Delta \varepsilon$ has the appearance of the central plot of Figure (17) which is elliptical and called a Lissajous figure. The ellipticity arises from the phase difference between birefringence and strain (to be discussed later). If there were no phase difference, the ellipse would collapse to a straight line.

When the calibrating plate is inserted, the entire Lissajous figure is displaced upward as indicated in the figure. If the calibrating plate is rotated through 90° about its normal so that its retardation is $-\delta_c$, the figure is displaced downward. If the response is linear, so that h is proportional to δ, the upward and downward displacements are equal and no distortion of the shape of the figure occurs. As indicated in Figure 17, we will designate the displacements at the two ends of the figure h_1 and h_2 (which should be equal in the linear case.). We shall call the average value h_c where $h_c = (h_1 + h_2)/2$.

If equation (64) is differentiated with respect to δ, one obtains

$$\left(\frac{\partial T}{\partial \delta}\right) = F \sin(\delta/2)\cos(\delta/2) + \sin^2(\delta/2)\left(\frac{\partial F}{\partial \delta}\right) + \frac{\partial [F T_r]}{\partial \delta} \qquad (70)$$

If δ_R is chosen such that $\delta \simeq \pi/2$, and $\sin(\delta/2)\cos(\delta/2) = a$, and is in the linear region, the change in transmission in a calibration experiment in which a calibrating plate of known retardation is inserted is

$$\left(\frac{\partial T_c}{\partial \delta}\right) = a F \qquad (71)$$

so

$$(\Delta T_c)_1 = a F \Delta \delta \qquad (72)$$

If the calibrating plate is rotated through 90° so the sign of its retardation is reversed, then $(\Delta T_c)_2 = - a F \Delta \delta$. The total change

in transmission is

$$\Delta T_c = (\Delta T_c)_1 - (\Delta T_c)_2 = 2\, a\, F \Delta \delta \qquad (73)$$

and the total displacement of the oscilloscope is h_c where

$$h_c = K \Delta T_c = 2\, a\, K\, F \delta_c \qquad (74)$$

The value of δ_c may be determined using a Babinet compensator. If R_o is the distance between two successive fringes of the compensator and R_c is the displacement of the zero order black fringe when the calibrating plate is inserted, it follows that from the principle of operation of the compensator that

$$\delta_c = 2\pi (R_c / R_o) \qquad (75)$$

so that

$$KF = h_c \,/\, 4\pi a (R_c / R_o) \qquad (76)$$

The derivative $(\frac{\partial \delta}{\partial \varepsilon})$ appearing in Equation (67a) is equal to $(\frac{\partial \delta_s}{\partial \varepsilon})$ since δ_R does not vary with strain. Now δ_s is related to the sample birefringence and thickness by

$$\delta_s = 2\pi d \Delta_s / \lambda \qquad (77)$$

so it follows that

$$\left(\frac{\partial \delta}{\partial \varepsilon}\right) = (2\pi/\lambda)\left[d\left(\frac{\partial \Delta_s}{\partial \varepsilon}\right) + \Delta_s\left(\frac{\partial d}{\partial \varepsilon}\right)\right] \qquad (78)$$

The derivative $$K = \left(\frac{\partial \Delta_s}{\partial \varepsilon}\right) \qquad (79)$$

is the strain-optcial coefficient of the sample which is the quantity sought.

The derivative $\left(\frac{\partial d}{\partial \varepsilon}\right)$ is related to Poisson's ratio ρ of the sample by the equation

$$\rho = -(1/d)\left(\frac{\partial d}{\partial \varepsilon}\right) \qquad (80)$$

which is $\frac{1}{2}$ if deformation occurs with conservation of volume (as is usually the case above the glass temperature). The average retardation of the sample may be determined using a Babinet compensator where

$$\delta_s = 2\pi\,(R_S/R_o) \qquad (81)$$

where R_S is the displacement of the zero order fringe when the sample is inserted.

Thus

$$\left(\frac{\partial \delta}{\partial \varepsilon}\right) = (2\pi\, d/\lambda)\, K - 2\pi(R_s/R_o)\rho \qquad (82)$$

The second term in Equation (67a) is obtained by carrying out the vibration of the sample with the analyzing polaroid removed.

Under these conditions, an oscilloscope trace of the sort of Figure (18) is obtained which is shown here as a straight line indicating that the transmission is varying in phase with the applied strain. While this is usually found to be the case experimentally, it is possible for there to be a phase difference between the transmission and strain in which case an elliptical Lissajous figure will be obtained. The method for treatment of data in this case will be discussed later.

The change in transmission of the sample in the course of vibration is obtained from Equation (66) since

$$\left(\frac{\partial F}{\partial \varepsilon}\right) = \left(\frac{\partial T_F}{\partial \varepsilon}\right) = \frac{1}{K}\left(\frac{\partial h_F}{\partial \varepsilon}\right) \qquad (83)$$

where h_F is the oscilloscope displacement during the experiment where the sample is vibrated with the analyzer removed as defined in Figure (18) where $h_F = h_4 - h_3$, thus it follows that

$$\left(\frac{\partial (KF)}{\partial \varepsilon}\right) = \frac{\partial h_F}{\partial \varepsilon} \simeq (h_F)/\Delta\varepsilon \qquad (84)$$

Similarly, the third term in Equation (69) is evaluated by carrying out a vibrational experiment under 0-90°crossed polarization conditions in which case, the oscilloscope displacement during vibration is indicated as h_s and

$$\left(\frac{\partial(KFT_+)}{\partial\varepsilon}\right) = (h_s/\Delta\varepsilon) \qquad (85)$$

Uon substituting Equations(76), (82), (84) and (85) into Equation (69) , one obtains

$$h_B = \tfrac{1}{2}\left(h_c/2\pi(R_c/R_o)\left[\frac{2\pi d}{\lambda}K - 2\pi\left(\frac{R_s}{R_o}\right)\rho\right]\Delta\varepsilon + \tfrac{1}{2}h_F + h_s \qquad (86)$$

If one uses $\Delta\varepsilon = 2A/L$, where A is the amplitude of the vibration of the sample and L is the length of the sample where $L = L_o + \Delta L$, L_o being the original length and ΔL being the static deformation of the sample, then one may rearranges Equation (86) to give

$$K = \frac{\lambda L\left(\frac{R_c}{R_o}\right)}{h_c d A}\left(h_B - \tfrac{1}{2}h_F - h_S\right) + (\lambda/d)(R_S/R_o) \qquad (87)$$

All of the quantities required by this equation are experimentally measurable.

C. EFFECT OF PHASE DIFFERENCES

It is well known that the birefringence change may differ in phase from that of the applied strain so that if

$$\varepsilon = \varepsilon_o + A\cos\omega t \qquad (88)$$

then

$$\Delta = \Delta_o + B \cos(\omega t + \alpha) \tag{89}$$

This may be readily represented by using an exponential form of Equations (88) and (89)

$$\mathcal{E} = \mathcal{E}_o + A\, e^{i\omega t} \tag{90}$$

$$\Delta = \Delta_o + B\, e^{i(\omega t + \alpha)} \tag{91}$$

Then it follows that

$$d\mathcal{E} = A\, i\omega e^{i\omega t}\, dt \tag{92}$$

$$d\Delta = B\, i\omega e^{i\omega t}\, e^{i\alpha}\, dt \tag{93}$$

so that one obtains

$$\begin{aligned} K^* = \left(\frac{\partial \Delta}{\partial \mathcal{E}}\right) &= (B/A)(\cos\alpha + i \sin\alpha) \\ &= K(\cos\alpha + i \sin\alpha) \\ &= K' + K'' \end{aligned} \tag{94}$$

where $K = B/A$, $K' = K\cos\alpha$, and $K'' = K\sin\alpha$.

A consequence of the phase difference is that h_B will also differ in phase from $\mathcal{E}$ with a phase angle β , and can be represented in complex exponential form

$$h_B^* = h_B(\cos\beta + i \sin\beta) = h_B' + i\, h_B'' \qquad (95)$$

Similarly h_F^* and h_S^* may differ in phase from $\mathcal{E}$ and are similarly represented as

$$h_F^* = h_F (\cos\phi + i \sin\phi) = h_F' + h_F'' \qquad (96)$$

and

$$h_S^* = h_S (\cos\alpha + i \sin\alpha) = h_S' + i\, h_S'' \qquad (97)$$

While the change of thickness of the sample will probably not differ in phase from the strain, this eventually may be formally treated by allowing Poisson's ratio to be a complex number

$$\rho^* = \rho(\cos\mu + i \sin\mu) = \rho' + i\rho'' \qquad (98)$$

Experimentally, through use of the Lissajous figure technique, one determines the absolute value of each of the quantities h_B, h_F

and h_s and the respective phase angles β , ϕ , and σ . There are no reported values of the Poisson ratio phase angle and will take this as zero in our work.

It is then necessary to write Equation (87) in terms of complex quantities

$$K^* = \frac{\lambda L\left(\frac{R_c}{R_o}\right)}{R_c\, dA}\left(h_B^* - \tfrac{1}{2} h_F^* - h_S^*\right) + (\lambda/d)\,(R_S/R_o)\rho^* \qquad (99)$$

Then by equating real and imaginary parts, one obtains

$$K' = \frac{\lambda L\left(\frac{R_c}{R_o}\right)}{R_c\, dA}\left(h_B \cos\beta - \tfrac{1}{2} h_F \cos\phi - h_s \cos\sigma\right) + (\lambda/d)(R_S/R_o)\,\rho\cos\mu \qquad (100)$$

and

$$K'' = \frac{\lambda L\left(\frac{R_c}{R_o}\right)}{R_c\, dA}\left(h_B \sin\beta - \tfrac{1}{2} h_F \sin\phi - h_s \sin\sigma\right) + (\lambda/d)(R_S/R_o)\,\rho\sin\mu \qquad (101)$$

from which one may obtain the birefringence-strain phase angle as

$$\tan\alpha = K''/K'$$

It is noted that the usual approximation that $\alpha = \beta$, is only valid when the correction terms are negligible.

THE DETERMINATION OF THE PHASE ANGLE OF A DYNAMICALLY VARYING QUANTITY FROM THE LISSAJOUS FIGURE

Suppose some quantity like the transmission of the sample is proportional to the vertical displacement of an oscilloscope trace, h, as shown in Figure (19)

$$h = K\,T \tag{103}$$

where K is a constant of proportionality. The horizontal displacement, q, is proportional to the strain

$$q = m\varepsilon \tag{104}$$

where m is another proportionality constant. If q varies sinusoidally with time

$$q = q_o + Q\cos\omega t \tag{105}$$

then h may also vary sinusoidally with a phase angle θ

$$\begin{aligned} h &= h_o + H\cos(\omega t + \theta) \\ &= h_o + H(\cos\omega t\cos\theta - \sin\omega t\sin\theta) \end{aligned} \tag{106}$$

At $\omega t = 0$, it follows from Equations (105) and (106) that

$q_1 = q_o + Q$ and $h_1 = h_o + H \cos\theta$. This corresponds to the point labelled (1) on Figure (19). At $\omega t = \pi/2$, point (2) corresponds to $q_2 = q_o$ and $h_2 = h_o - H \sin\theta$. Similarly at $\omega t = \pi$, point (3) corresponds to $q_3 = q_o - Q$, and $h_3 = h_o - H \cos\theta$, whereas point (4) at $\omega t = 3\pi/2$ represents $q_4 = q_o$ and $h_4 = h_o + H \sin\theta$. It is apparent that the point moves around the figure in a clockwise direction as indicated in Figure (19). The experimental observation of such a clockwise motion of a point indicates a positive phase angle as is assumed in the equation. For a negative phase angle, the point migrates in a counter-clockwise fashion.

It is apparent that the distance BC indicated in Figure (19) is given by

$$BC = h_4 - h_2 = 2H \sin\theta \qquad (107)$$

Also it is evident that the distance AD is equal to 2H, thus it follows that

$$\sin\theta = BC/AD \qquad (108)$$

from which the phase angle may be calculated. The absolute value of the change in h (equal to 2H) may be obtained by comparing AD with the vertical displacement of the oscilloscope trace h_c occuring in a calibration experiment as discussed in the text.

When BC =0, the ellipse degenerates to a line which corresponds to zero phase angle.

PROCESSING OF DATA AND THE CORRECTIONS INVOLVED IN DYNAMIC X-RAY TECHNIQUE

A. STATIC SITUATION

This section concerns mainly with the resolution of overlapping of diffracted peaks from each crystallographic plane in the radial diffracted intensity distribution curve. This can be obtained by using the dynamic x-ray diffractometer for the usual purpose of intensity scanning along twice the Bragg angle 2θ . Several corrections will be considered here.

Consider the case where there are N diffraction peaks overlapping in a linear manner. Let each of the peaks be represented by Lorentzian or Gaussian functions or by other functions such that the peaks are expressed as functions of $(2\theta - 2\theta_{B_j})/\beta_j^o$ to give a symmetric functional form with respect to $2\theta_{B_j}$ [57], where $2\theta_{B_j}^o$ is twice the Bragg angle of diffraction giving the maximum intensity and β_j^o is the half width of the j^{th} peak with $\lambda = \lambda_o$. Then the total diffracted intensity at an angle of diffraction $2\theta_i$ is given by

$$I_i = \sum_{j=1}^{N} C_{ij} I_{mj}^o \qquad (109)$$

where $I_{m,j}^o$ is the individual (not overlapped) maximum intensity of the j^{th} peak with $\lambda = \lambda_o$,and C_{ij} is given by

$$C_{ij} = \chi\left[(2\theta - 2\theta^{\circ}_{B_j}) / \beta^{\circ}_{j}\right] = \chi(u) \qquad (110)$$

where

$$u = (2\theta - 2\theta^{\circ}_{B,j})/\beta^{\circ}_{j} \qquad (111)$$

and χ is a function of u, to give best agreement between the calculated (by Equation 109) and observed diffraction curves. Each peak must be symmetric as

$$\chi(u) = \chi(-u) \qquad (112)$$

Resolution of the overlapping curves may be made by roughly evaluating at first the value of $2\theta^{\circ}_{B,j}$ and β°_{j} from the observed diffraction curve and by solving the simultaneous equations represented by Equation (109) to give T°_{mj}. A desmearing program titled "Multi Fit" (See Appendix IV) written by Desper[58] was used, whereby the intensities of the three main peaks (namely the amorphous, 110 and 200) are fixed, and by suitable adjustment of the half width β°_{j}, a best agreement between the observed and the calculated intensity curve is obtained, in the range of 14-28° 2θ. From the parameters which give the best calculated curve we are able to split the observed profile into 3 components I_{am}, I_{110} and I_{200} (corrected).

The parameters obtained from the calculation curve are only applicable to one profile and when this profile is altered, in particular by changing ϕ, static strain or temperature, the parameters should

be redetermined, and this involves a determination of the angular distribution over all the values of ϕ for each value of static strain or temperature, at which measurements are required.

B. DYNAMIC SITUATION

In the dynamic situation, the specimen is sinusoidally deformed, while the tilting angle of the incident x-ray beam and the detector axis is held constant at θ. The azimuthal angle ϕ is also held constant. The problem will be treated stepwise in the following paragraphs.

(a) DYNAMIC SINUSOIDAL STRAIN

The specimen is subjected to a forced, periodic strain,

$$\lambda(t) = \lambda_o + \Delta\lambda\, e^{i\omega t} \qquad (113)$$

where λ_o is the static strain as shown before, $\Delta\lambda$ the amplitude of the dynamic strain, and ω the angular frequency of vibration.

(b) ASSUMPTION OF THE SINUSOIDAL VARIATION OF THE MAXIMUM INTENSITY $I_{m,j}$ AS WELL AS THE ANGLE OF DIFFRACTION GIVING THE MAXIMUM INTENSITY $2\theta_{B,j}$.

The sinusoidal strain is assumed to produce a sinusoidal

variation of $I_{m,j}$ and $2\theta_{B,j}$ as expressed by the complex numbers

$$I_{m,j} = I_{m,j^o} + (\Delta I'_{m,j} + i\Delta I''_{m,j})\, e^{i\omega t} \qquad (114)$$

$$2\theta_{B_j} = 2\theta_{B_j^o} + (\Delta 2\theta'_{B,j} + i\Delta 2''_{B,j})\, e^{i\omega t} \qquad (115)$$

where $\Delta I'_{m,j}$ and $\Delta I''_{m,j}$ are the components of the variation of $I_{m,j}$ which are in-phase and out of phase, and similarly, $\Delta 2\theta'_{B,j}$ and $\Delta 2\theta''_{B,j}$ are the in-phase and out-of-phase components of the variation of $2\theta_{B,j}$ on an experimental basis, β_j may be assumed to be constant during the vibration.

A computer program XMOD 7 was written which are briefly outlined as follows:- (See Appendix II for a complete list out)

Readings at each ϕ value (0 to 90^o) (total number = 10) are taken, and the four sector constants are determined and denoted as α_1, α_2, α_3 and α_4. Also background counts which are determined by measuring the count in the absence of sample at the corresponding 110 and 200 peak positions are read in.

SAMPLE CALCULATION $\phi = 0$.

The two desmeared constants k_1 and k_2 at the 110 and 200 peaks were obtained from the " Multi-Fit " program and read. Counts of

intensity ΣI_1, ΣI_2, ΣI_3 and ΣI_4 at an accumulated time (T =200 or 300 seconds) were read in both for the 110 and 200 peaks, this is repeated for all the ϕ angles. These data are stored in the form of punched tapes in the order of 110 peak (ϕ=0, 10,--------,90°) followed by 200 peak (ϕ= 0, 10, ---------,90°).

Corrections for background intensity and absorption are then made by the following equation.

$$I^{\circ}_{backg.} = I^{\circ}_{exp.backg.}\, e^{-\mu d_o \sec\theta} \qquad (116)$$

$$I^{\circ}_{exp.scatt} = I^{\circ}_{exp} - I^{\circ}_{backg} \qquad (117)$$

$$I^{\circ}_{scatt} = I^{\circ}_{exp.scatt}\; h(\Theta)\; K^{\circ}_{abs} \qquad (118)$$

where $I_{exp.backg.}$ is the observed intensity with the specimen removed from the beam. μ the linear absorption coefficient of the specimen which can be obtained by the equation.

$$(I_2 - I_4) = (I_1 - I_3)\, e^{-\mu t} \qquad (119)$$

where I_1 = Intensity at the peak with no absorption of sample.

I_2 = Intensity at the peak with sample absorbing.

I_3 = Intensity at background with no absorption of sample.

I_4 = Intensity at background with sample absorbing

d_o = thickness of specimen with $L = L_o$ (i.e. undeformed state)

I_{expo} = experimentally observed intensity for the specimen.

$h(\theta)$, I_{abs}^{o} = Polarization and absorption correction factors respectively

$$h(\theta) = 2/(1 + \cos^2 2\theta) \qquad (120)$$

$$K_{abs}^{o} = (e^{\mu d_o \sec\theta})/\sec\theta \qquad (121)$$

A correction for the incoherent scattering intensity I_{incoh} was made by using the method of Krimm and Tobolsky[59] where it is assumed that at large scattering angles the observed coherently scattering is of the same intensity as would be produced by an entirely random assembly of atoms scattering independently of one another with no interference effect. Thus the corrected diffracted intensity I^o is given by

$$I^o = I_{scatt}^{o} - I_{incoh}^{o} \qquad (122)$$

DYNAMIC SITUATION

When the sample is subjected to a periodic strain, $\lambda(t)$

is given by

$$\lambda(t) = \lambda_o - \Delta\lambda \cos \omega t \qquad (123)$$

where λ_o is the static tensile strain

$\Delta\lambda$ is the dynamic strain amplitude

ω angular frequency of vibration

The vibrating sample also gives a vibrating intensity given by

$$I_{diff.} = I^o - I_{diff.} \cos(\omega t - \chi) \qquad (124)$$

where I^o is the static diffracted intensity at strain $\lambda = \lambda_o$

$I_{diff.}$ is the amplitude of the periodic vibration in intensity which lags the strain by phase angle χ

Expressed in the complex notation

$$I_{diff.} = I^o - \Delta I'_{diff.} \cos\omega t - I''_{diff.} \sin\omega t \qquad (125)$$

where

$$\Delta I'_{diff.} = \Delta I_{diff.} \cos\chi \qquad (126)$$

is the component of $I_{diff.}$ which is in-phase with the strain, and

$$I''_{diff.} = I_{diff.} \sin\chi \qquad (127)$$

When the sample is vibrated, its thickness d will also vary periodically with amplitude Δd.

$$d(t) = d_o + \Delta d \cos(\omega t - \delta d) \qquad (128)$$

It is assumed that the thickness changes in phase with the length ($\delta d = 0$), and the volume is assumed conserved and the strain is uniaxial.

Then

$$\Delta d = -(\Delta\lambda/2)\, d_o \qquad (129)$$

Corrections for background intensity and incoherent scattering may be made in such a manner such that their effects upon the dynamic data arise only from their intensity variation due to thickness change of specimen during vibration. This is because the intensities of background and incoherent scattering are not affected by the molecular orientation of the specimen. Furthermore, the phase angle between the thickness variation and the external strain was neglected as described previously, so the problem can be treated in the static situation rather than the dynamic one. The change in intensity of the background resulting from the thickness change is $[-(d_o/2)\Delta\lambda]$, and this was substracted from the real components of the dynamic data for the total intensity as is described in the following section.

The change in the background intensity arising from the thickness change of δd from the static value d_o at $\lambda = \lambda_o$ is given by

$$\begin{aligned} \delta I_{backg^o} &= -I_{exp.back}^{\ o}\ \mu \sec\theta\ e^{-\mu d_o \sec\theta}\delta d \\ &= -I_{backg}^{\ o}\ \mu \sec\theta\ \delta d \end{aligned} \qquad (130)$$

substitution of $\delta d = -\frac{1}{2} d_o \Delta\lambda$ into Equation (130) leads to the following dynamic correction factors; The dynamic correction for the background intensity is

$$\tfrac{1}{2}\, d_o \Delta\lambda \mu \sec\theta\ I_{backg}^{\ o} = \varepsilon_{dyn.backg.}\ I_{backg}^{\ o} \qquad (131)$$

where

$$\varepsilon_{dyn.backg.} = \tfrac{1}{2}\, d_o \Delta\lambda \mu \sec\theta \qquad (132)$$

On the other hand, the thickness dependence of the intensity of the incoherent scattering will be given by

$$I_{incoh.} = K\, I_o\, d\, \sec\theta\, e^{-\mu d \sec\theta} \qquad (133)$$

where K is a constant, and I_o is the intensity of the incident x-ray beam. Thus

$$\begin{aligned} \delta I_{incoh^o} &= K I_o\, d_o\, \sec\theta\, e^{-\mu d_o \sec\theta} \left(\frac{1}{d_o} - \mu \sec\theta \right) \delta d \\ &= I_{incoh^o} \left(\frac{1}{d_o} - \mu \sec\theta \right) \delta d \end{aligned} \qquad (134)$$

From equation (134), we have the dynamic correction for the incoherent scattering

$$-(\Delta\lambda/2)(1-\mu d_o \sec\theta)\, I^{o}_{incoh} = \varepsilon_{dyn.incoh.}\, I^{o}_{incoh} \qquad (135)$$

where

$$\varepsilon_{dyn.incoh.} = -(\Delta\lambda/2)\,(1-\mu d_o \sec\theta) \qquad (136)$$

(c) The diffracted intensity is also affected by the variation of the thickness during vibration, the effect of which upon the dynamic data can be treated just as for the incoherent scattering. The dynamic correction for the diffracted intensity is $\varepsilon_{dyn.diff.} I^{o}$

$$\varepsilon_{dyn.diff.} = \varepsilon_{dyn.incoh.} \qquad (137)$$

(d) The total dynamic correction are given by the following :-

$$I_{dyn.corr.} = \varepsilon_{dyn.backg.}\, I^{o}_{backg.} + \varepsilon_{dyn.incoh.}\, I^{o}_{incoh} + \varepsilon_{dyn.diff.} I^{o} \qquad (138)$$

where I^{c}_{backg}, I^{o}_{incoh}, and I^{o} are the static values as appeared in Equations (116) and (122). $\Delta I_{dyn.corr.}$ is to be substracted from the real component of the dynamic data $I'_{exp.}$ which was experimentally obtained by the semicircular technique which will be described in the next page.

(4) Finally, $\Delta I_{i\ exp}'$ and $\Delta I_{i,exp}''$ should be corrected for the absorption by the specimen according to

$$\Delta I_i' = (\Delta I_i'_{exp} - \Delta I_{i\ dyn.corr.}) \frac{e^{\mu d_o \sec\theta_i}}{h(\theta_i)\sec\theta_i} \qquad (139)$$

$$\Delta I_i'' = \Delta I_i''_{exp} \frac{e^{\mu d_o \sec\theta_i}}{h(\theta_i)\sec\theta_i} \qquad (140)$$

SEMI-CIRCULAR SECTOR TECHNIQUE

The rotating sector of the photo-switch is constructed so that the counting channel is activated during π or 180° of the straining cycle. These periods are staggered in phase so that the first is activated between 0 and π, the second between $\pi/2$ and $3\pi/2$, the third from $-\pi/2$ to $\pi/2$, and the fourth from π to 2π. By comparing the accumulated counts over many cycles of vibration (200 to 300 cycles) during these intervals, it is possible to obtain $\Delta I'$ and $\Delta I''$.

$$N_{0-\pi}(\tau) = n\int_o^{T/2} I(2\theta,\phi)\,dt = n\int_o^{T/2}\left[I^o + \Delta I \sin(\omega t + \chi)\right] dt$$

$$= (nT/2)\left[I^o - (2/\pi)\Delta I\cos\chi\right] \qquad (141)$$

The average intensity (measured in units of counts per second) is then

$$I_{0-\pi} = \frac{N_{0-\pi}(\tau)}{\tau/2} = I^o - (2/\pi)\Delta I\cos\chi \qquad (142)$$

Similarly, for the other counting channels

$$I_{\pi \to 2\pi} = I^{o} + (2/\pi)\,\Delta I \cos\chi \qquad (143)$$

$$I_{\pi/2 \to 3\pi/2} = I^{o} + (2/\pi)\,\Delta I \sin\chi \qquad (144)$$

$$I_{-\pi/2 \to \pi/2} = I^{o} - (2/\pi)\,\Delta I \sin\chi \qquad (145)$$

Combining Equations (142) to (145)

$$I^{o} = \frac{(N_{0 \to \pi} - N_{\pi \to 2\pi})}{\tau} = \frac{(N_{\pi/2 \to 3\pi/2} - N_{-\pi/2 \to \pi/2})}{\tau} \qquad (146)$$

$$\Delta I' = \Delta I \cos\chi$$

$$= \pi (N_{\pi \to 2\pi} - N_{-\pi/2 \to \pi/2}) / 2\tau \qquad (147)$$

$$\Delta I'' = \Delta I \sin\chi$$

$$= \pi (N_{\pi/2 \to 3\pi/2} - N_{-\pi/2 \to \pi/2}) / 2\tau \qquad (148)$$

Thus from measurements of the counts of the four channels; $N_{0-\pi}$ $N_{\pi-2\pi}$, $N_{\pi/2-3\pi/2}$, and $N_{-\pi/2-\pi/2}$, it is possible to obtain I_o, $\Delta I'$ and $\Delta I''$.

It has to be understood that the actual count of each channel has to be multiplied by its corresponding sector constant, so as to obtain the corrected values.

Having obtained I°, it has to be multiplied by two correction factors, the first one being the static desmearing constant at the particular peak, and the second one is that due to the polarization, background and absorption.

$$I^{\circ}_{corr.} = I^{\circ} \cdot x_1 \cdot 2/(1 + \cos^2 2\theta) \cdot (e^{\mu d_o \sec\theta} / \sec\theta) \qquad (149)$$

Similarly for the dynamic $\Delta I'$ and $\Delta I''$, a correction factor C.F. is needed.

where

$$(\Delta I')_{corr.} = I' - C.F.$$

$$C.F. = -(\Delta\lambda/2)(1 - \mu d_o \sec\theta)(I^{\circ} + I_{incoh.}) + I^{\circ}_{exp.back} \exp^{-\mu d_o \sec\theta} \cdot \mu \sec\theta \cdot (d\Delta\lambda/2) \cdot (e^{\mu d_o \sec\theta} / \sec\theta) \cdot 2/(1 + \cos^2 2\theta) \qquad (150)$$

As it is understandable that desmearing for all azimuthal angles will be different, so a complete azimuthal desmearing correction is performed.

From the calculated profile, the intensity of the 110 peak at the 200 peak position I_1' and the intensity of the 200 peak at the 110 peak position I_2'' were determined. If the change in I_1 at

the 110 peak position is ΔI_1, then the change in 110 intensity at the 200 peak position is $\Delta I_1 .(I_1''/I_1)$. Similarly the change in 200 peak intensity at the 110 peak position is $\Delta I_2 .(I_2''/I_2)$.

Hence

$$\Delta I_1' = \Delta I_1 + \Delta I_2 .(I_2''/I_2) \qquad (151)$$

and

$$\Delta I_2' = \Delta I_2 + \Delta I_1 . (I_1''/I_1) \qquad (152)$$

Thus from the two simultaneous equations, corrected values of ΔI_1 and ΔI_2 can be calculated. It has been found that the differences between ΔI_1 and $\Delta I_1'$ are generally small for the 110 peak, but in the 200 case, the effect can be appreciable.

In the analysis, negligible change in the intensity of the amorphous peak has been assumed which to our knowledge is justifiable, as the experiments are carried out in room temperature. If the temperature has been very close to the melting point of the sample, a similar analysis with three simultaneous equations has to be used.

The same desmearing procedure has been carried out for the out of phase $\Delta I''$.

CALCULATION OF DYNAMIC ORIENTATION FUNCTIONS

The following integrals are carried out by computer based

on the Simpson's rule summation.

$$X_o = \int_o^{\pi/2} \cos\phi\, I_o \, d\phi \tag{153}$$

$$X_1 = \int_o^{\pi/2} \cos\phi \sin^2\phi\, I_o \, d\phi \tag{154}$$

$$Y_o = \int_o^{\pi/2} \cos\phi \Delta I'_{corr.} \, d\phi \tag{155}$$

$$Y_1 = \int_o^{\pi/2} \cos\phi \sin^2\phi\, \Delta I'_{corr.} \, d\phi \tag{156}$$

$$Z_o = \int_o^{\pi/2} \cos\phi \Delta I''_{corr.} \, d\phi \tag{157}$$

$$Z_1 = \int_o^{\pi/2} \cos\phi \sin^2\phi\, \Delta I''_{corr.} \, d\phi \tag{158}$$

Then the orientation function f_o is given by

$$f_o = \frac{3(X_1/X_o) - 1}{2} \tag{159}$$

Similarly for the dynamic orientation function

$$f' = (3/2)\left\{(Y_1/X_o) - (Y_o/X_o)(X_1/X_o)\right\} \tag{160}$$

$$f'' = (3/2)\left\{(Z_1/X_o) - (Z_o/X_o)(X_1/X_o)\right\} \tag{161}$$

In terms of orientation compliance C' and C''

$$C' = (3/2)\left\{(Y_1/X_o) - (Y_o/X_o)(X_1/X_o)\right\}L_o/\Delta\lambda \quad (162)$$

$$C'' = (3/2)\left\{(Z_1/X_o) - (Z_o/X_o)(X_1/X_o)\right\}L_o/\Delta\lambda \quad (163)$$

where L_o = extended length of the sample

$\Delta\lambda$ = dynamic amplitdue of vibration

In polyethylene, as it has been mentioned earlier, the a-axis orientation function can be obtained directly from (h00) plane diffraction. Since diffraction is weak for the (0k0) plane, the b-axis orientation can be found by combining the a-axis and the 110 plane results, and using the equation

$$f_b = \sec^2\rho_{110}\, f_{110} - \tan^2\rho_{110}\, f_a \quad (164)$$

and substituting values of ρ in the case of an orthorhombic unit cell of polyethylene. (ρ is the angle between the b-axis and the normal to 110 plane).

$$f_{ob} = 1.447\ (f_o)_{110} - 0.447\ (f_o)_{200} \quad (165)$$

$$C'_b = 1.447\ (C')_{110} - 0.447\ (C')_{200} \quad (166)$$

$$C''_b = 1.447\ (C'')_{110} - o.447\ (C'')_{200} \quad (167)$$

and making use of the orthogonality relationship of the a, b and c axes, orientation of the three crystal axes can be determined.

Also the crystalline contribution to the strain-optical coefficient K' can be obtained by substituting Equation (164) to Equation (9) and inserting the values for the refractive indices and for ρ_{110}.

$$K'_{cr} = (-0.0361\ C'_a - 0.0809\ C'_{110}) \qquad (168)$$

PREPARATION OF SAMPLES

Samples were prepared from an experimental Monsanto Low Density Polyethylene (P.E. Grade 910, Research Serial No. AA-1933) $\rho = 0.918$ Melt Index = 7. The results of the Gel Permeation Chromatography analysis has been shown in Appendix I. For the x-ray samples, films were molded with a laboratory press at 155°C using a 25 mil. copper spacer between aluminum foil and stainless steel plates. After remaining 15 minutes in the press, a pressure of 10,000 p.s.i. was applied to ensure homogenous pressing, after which they were quenched in a dry-ice ethanol bath. For the dynamic birefringence samples, no spacer was used, and by varying the pressure applied after complete melting, a sample thicknesses of 3-5 mils could be obtained. X- ray examination of samples prepared in this manner revealed no orientation. Also the two types of samples were ensured to have the same degree of quenching and morphology by carrying out the determinations of their static and dynamic orientation functions by stacking layers of the thin dynamic birefringence samples to a comparable thickness like the molded x-ray samples, the results indicate negligible difference.

For the annealed samples, the quenched samples were heat treated at 90-95°C for 2 hours, with a pressure of 5000 p.s.i. applied, after which they were then allowed to cool to room temperature in about 3 hours.

The percentage of crystallinity of the resulting samples was determined by x-ray diffraction to be 54% and 64% by volume respectively for the quenched and annealed samples.

VIII. DYNAMIC BIREFRINGENCE OF LOW DENSITY POLYETHYLENE

A. INTRODUCTION

The technique of dynamic birefringence has emerged as a new tool for investigating the molecular mechanism of mechanical relaxation in polymers. One of the most important results obtained by Stein, Onogi and Keedy[30,38,49] has been that the strain-optical coefficient that is--the birefringence per unit strain, is dependent upon the frequency. Also later work by Yamada et. al.[32,42] and Read[60] has led to interesting frequency and temperature dependence results on crosslinked rubber, polyethylenes, polypropylene, nylon -6, polyethylene terephthalate and polyacetaldehyde.

Studies of static birefringence on a series of poly-α olefins have indicated that the birefringence first becomes negative and then becomes positive with increasing strain[16] . These curves were theoretically explained on the basis of a spherulite deformation model[61]. The affine deformation of a negatively birefringence spherulite contributes negatively to the macroscopic sample birefringence. At higher elongations, crystals must reorient with their chain axes becoming parallel to the stretching direction. The two contributions and their different time dependence are made apparent if the strain on a stretched polypropylene film is relieved[16]. The positive birefringence initially becomes more positive upon initial decrease

of strain after which it decreases with further release of strain. The rapid increase in positive birefringence with decrease in strain arises from a decrease in negative birefringence assoicated with a decrease in spherulite deformation. This negative birefringence component is superposed on the large positive birefringence of these deformed spherulites.

The longer relaxation time assoicated with the crystal reorientation within the deformed spherulite may be observed from the birefringence change of polyethylene during relaxation at constant length[30]. Upon rapid extension of polyethylene at room temperature, the birefringence is found to increase. Further increase occurs with time at constant length, again with a relaxation time of the order of 1 second for medium density polyethylene at room temperature.

As it has been shown by previous workers mentioned above that the static birefringence is strongly dependent upon strain and the strain-optical coefficient is dependent on time, morphology and internal structure of polymers, the main aim of this thesis work has been to investigate the effect of internal structure (lamellar orientation) on the strain-optical coefficient. This has been done by stretching low density polyethylene samples to different elongations, and having allowed the relaxation to reach equilibrium, a dynamic vibrational strain of about 1%, at a frequency of 1 hertz was superimposed on the resulting samples. The crystal morphology was also varied by quenching

and annealing, and the dynamic optical and mechanical quantities (namely the strain-optical coefficient K', optical loss tangent tand , storage modulus E' and mechanical loss tangent tan δ were simultaneously measured.

From the measurement of K' which gives the total orientation of the crystalline, amorphous phases and their phase boundaries, our next objective will be to evaluate these corresponding contributions separately. This will be treated in this and the following sections.

B. STRAIN DEPENDENCE OF QUENCHED SAMPLE

Figure (20) shows the effect of static strain on K'. It is seen that a slight increase in K' is observed at low elongation of about 10%, after which the strain-optical coefficient falls off gradually approaching a value of 2.9×10^{-2} at 50% elongation. Such results can be understood and explained by means of the spherulite deformation model[61]. Within the undeformed spherulite, lamellae are in close contact and are separated by chain folds, tie-chains and non-crystallizable polymer (chain-ends, branches). With an introduction of small strain, the originally spherically symmetrical spherulites are transformed into ellipsoidally symmetrical ones, with maximum strain occuring in the equatorial region, resulting in the splaying apart of the lamellae, together with a slight twisting and tilting of the optic axis (Figure 7) which might be the contributing deformation mechanism as pointed by Stein et. al.[62]. It is postulated that

this separation of lamellae from each other renders the mobility of lamellae greater. This explanation is supported by dynamic x-ray diffraction results which will be described in a later section.

At higher strains (>15%), it was shown (Figure 60) that there is a decrease in K'_{am} which indicates a decrease in the change of amorphous orientation with strain which is presumably assoicated with the tightening of tie-chains between crystals (Figure 37). This not only leads to a decrease in the amorphous chain mobility but also to a decrease in the mobility of the crystals interconnected by these chains, and this is borne out by the falling off of the K' value after 15% elongation in Figure (20).

The black solid curve in Figure (20) shows the values of $(d\Delta_s/d\varepsilon)$, obtained from the slopes of the plot of static birefringence with strain in irreversible and reversible processes, the strain-optical coefficient K' measures only the reversible processes such as the elastic stretching of tie-chains in the amorphous phase and rotational motion occuring in the crystalline phase. The comparable values in $(d\Delta_s/d\varepsilon)$ and K' at low elongation (< 10%) and high elongation (> 40%) indicate the dominating contribution of the reversible processes to $(d\Delta_s/d\varepsilon)$ in these regions. To explain in terms of a Maxwell Model (Figure 21) where two strain-optical coefficients are introduced, one of those, $A(\tau)$ characterizes the

spring,

$$\Delta_s(\tau) = A(\tau)\mathcal{E}_s(\tau)$$

While the other, $B(\tau)$ characterizes the dashpot

$$\Delta_d(\tau) = B(\tau)\mathcal{E}_d(\tau)$$

$\mathcal{E}_s(\tau)$ and $\mathcal{E}_d(\tau)$ are the strain on the spring and dashpot respectively, and $\Delta_s(\tau)$ and $\Delta_d(\tau)$ are the contributions to the birefringence of this Maxwell element by the spring and dashpot respectively. The total birefringence contributed by this element is assumed to be the sum of these contributions giving

$$\Delta(\tau) = \Delta_s(\tau) + \Delta_d(\tau)$$

Thus, the birefringence relaxation of such a polymer may be interpreted in terms of two distribution factors $A(\tau)$ and $B(\tau)$. Where the motion of spring represents the orientation of the amorphous region, and the motion of the dashpot is analogous to the slipping of crystal.

At very small strain ($\sim$10%), the spring will be slightly displaced and will recover to its original equilibrium position after the removal of strain. Thus at this region, the dashpot is assumed to be stationary, since the strain is very small, and the tension imposed on

the spring causes only negligible slipping of the dashpot, and $(d\Delta_s/d\varepsilon)$ which measures the irreversible and reversible processes at long time and K' which measures reversible processes at a time scale of 1 hertz (such frequency will understandably be too fast for any response from the dashpot) will both observe the reversible motion of the spring. (Figure 21a). It is thus, understood that at this region of strain, the two values will be very comparable.

At medium elongation of 10% to 40%, the spring will be stretched considerably, and in a relaxation experiment at constant length, the tension of the spring causes a slight slippage of the dashpot (Figure 21b), at this stage, the $(d\Delta_s/d\varepsilon)$ sees both the effects from the spring and the dashpot, and it is understandable that its value would be slightly higher than that at lower strains due to the contribution of the irreversible dashpot slippage. The K', however observes only the reversible motion of the spring during the vibrational experiment, and this explains the bigger value of the $(d\Delta_s/d\varepsilon)$ as compared with K' at this region.

At high elongations (>50%), the spring has been highly extended, and almost all the response to further external strain is borne out by the slipping of the dashpot (Figure 21c). It is in this region, that $(d\Delta_s/d\varepsilon)$ represents almost only the irreversible process of this dashpot slippage, Δ_s might still be increasing with strain, but a much lower $(d\Delta_s/d\varepsilon)$ is expected due to viscous contribution of the dashpot. K', however measures again, the elastic response of the spring

during the 1 hertz vibration, and it is understandable that its value is fairly constant, since for an idealized spring, the stress-strain plot should be linear and recoverable at all elongations. The deviation of this constant K' at all elongations based on the Maxwell Model from the experimentally observed K' versus static strain plot indicates the oversimplification of such a model and the idealized behavior assumption of the spring, which in reality, would become stiffer and stiffer as it is more highly elongated.

The diagrammatic representation of the Maxwell Model behavior at different strains has been shown in Figure (21a,b and c). Figure 22, shows a sketch of the different processes observed respectively by $(d\Delta_s)/d\varepsilon$ and K'.

Variation of the optical loss tangent is found to be negative at all elongations indicating that the strain leads the birefringence in phase. This is understandable for a crystalline polymer like polyethylene where one would not expect the response of the crystalline phase to be instantaneous.

Figure (23) shows the variation of the dynamic moduli E' and E'' (measured on the dynamic birefringence apparatus) with static strain. It is interesting to observe that E' decreases gradually up to 40% of strain, beyond which the E' increases significantly due most probably to the onset of fibrillar morphology. The results are in

agreement with those obtained by Raumann and Saunders [63] and Ward[64] in which a similar decrease in modulus was observed. Hillier and Kolsky[65] have also previously reported a minimum in the curve of dynamic modulus (at 3000 hertzs) against extension for polyethylene. The minimum was less pronounced and occured at a slightly smaller strain than that reported here. The initial decrease in modulus is not caused by a reduction in crystallinity with strain since it has been pointed out by Raumann and Saunders[63] that on drawing low density polyethylene, there is a continous increase of density with draw ratio, and this amounts to about 0.3% over a range of draw ratio of 1.0 to 4.65. In isotropic polyethylene, such an increase in density would correspond to an increase in crystallinity of only about 1.7%. Ward has compared experimental results for the uniaxially oriented polyethylene film with those expected on the basis of a very simple aggregate model[66] in which the distinction between crystalline and non-crystalline region is ignored. The elastic properties of the film with intermediate degree of molecular orientation are determined by regarding as an aggregate of elastic units, where elastic properties are those of the fully oriented film. A basic assumption is that the distribution of molecular orientation for the intermediate degrees of orientation can be found in terms of the stretch or draw ratio. He found that for polyethylene, the theoretical curves reproduce the approximate form of the modulus curve with a minimum occured at about 40% elongation. This arises in his model due to the very large value of the torsional compliance as compared with the extensional and transverse compliances; and the

torsional compliance makes its greatest contribution to the extensional modulus at low draw ratio.

Plots of static birefringence Δ_s, strain-optical coefficient K' and optical-loss tangent; tanδ are shown in Figure (24) for quenched samples at high elongations up to 300%. While the static birefringence first increases sharply with strain, then more gradually at higher elongations, the K' , however levels off to a constant value of 2.8×10^{-2} at 100% elongation and thereafter. This can be accounted by looking at the contributing terms of $(\partial T / \partial \varepsilon)$ in Equation (67) of page (47). Neglecting effect due to the factors $(\partial F / \partial \varepsilon)$ and $(\partial F_T / \partial \varepsilon)$ (which has been shown to be so in our experiment.), the term $(\partial \delta / \partial \varepsilon)$ can be written as

$$\frac{\partial \delta}{\partial \varepsilon} = \frac{\partial (\delta_R + \delta_S)}{\partial \varepsilon} = \frac{\partial \delta_S}{\partial \varepsilon}$$

$$\text{and} \quad \frac{\partial \delta_S}{\partial \varepsilon} = (2\pi/\lambda)\left[\Delta_s (\partial d / \partial \varepsilon) + d(\partial \Delta_s / \partial \varepsilon)\right]$$

The second term $(\partial \Delta_s / \partial \varepsilon)$ is gradually decreasing as the sample becomes more highly stretched, but the first term $\Delta_s \frac{\partial d}{\partial \varepsilon}$ is steadily increasing as shown by the plots of Δ_s with strain (Figure 24). The compensating nature of these two terms thus gives a constant value at high elongations. It has been observed at 300% elongation, almost all of the K' contribution comes from the correction term $\Delta_s (\partial d / \partial \varepsilon)$ (i.e. $\partial \Delta_s / \partial \varepsilon \to 0$), which corrects for the thickness change of the sample during the vibration.

Figure (25) shows plots of E' and tanδ for a quenched sample at high elongations. The former having reached a minimum value at about 40% elongation, increases sharply to give a value of E' which is more than three times the value at 5% elongation. This large value of modulus has been attributed by Ward[64] to the high degree of orientation in highly drawn polyethylene.

TEMPERATURE DEPENDENCE

The customary means for studying the α , β or γ loss processes in bulk semi-crystalline polymers has been to measure the dielectric or mechanical loss at a constant frequency. Plots of the loss at constant frequency against temperature then reveal loss maxima, the highest temperature relaxation process being called α , the next β , and so on. In the case of high density polyethylene, the three relaxation processes have been observed by previous workers. These are the α peak at about -120°C, the residual β peak at 0°C, and the γ relaxation at about 60°C. There has been much recent speculation about the nature of the alpha mechanical loss mechanism[67-81]. The prevalent opinion[82] appears to be that the α process consists of two components. The low temperature part, designated α_1 (or α by McCrum and Morris and α_1 by Takayanagi) occurs when the stress of the elastic shear deformation of the crystalline lamella decays through the viscous flow (or slip) at boundary layers[77,68,81], while the other (α_2 or α by McCrum and Morris and α_c' by Takayanagi) is

concerned with the twisting oscillation of molecular chains constituting the crystalline lamella[77]. The α_1 mechanism is found to have an activation energy of about 25 kcal/mole on the basis of time-temperature superposition of dynamic mechanical spectra and of stress relaxation data, while the α_2 mechanism has a higher activation energy of the order of 45 Kcal. per mole[76]. For single crystals which are not annealed only the α_2 mechanism is found which is dependent upon the thickness and thermal history of the crystal but independent of the state of compaction of the crystal matte[79-80] indicating its intracrystalline nature. Studies by Sinnot[75], Hoffman, et. al.[76] and Takayanagi[79] indicate that this α_2 peak may have more than one component and may partly result from internal motion within the crystal and partly from motion of the chain folds on the surface. Recent studies by Hidashima[72] showing the effect of solvent on this peak indicate the probability of a surface contribution. The recent studies of Takayanagi, et. al.[83] showing that the variation of the temperature of this peak with crystal thickness parallels the variation of the temperature at which the a-axis expansion coefficient of the crystal changes slope demonstrates the connection between at least a part of the α_2 loss upon the internal motion within the crystal. The success of a theory[84] involving torsional motion of the chains in the crystal lattice in accounting for the crystal expansion coefficient indicates that this same motion must also be assoicated with the α_2 loss.

The α_1 viscoelastic loss is much affected by irradiation[79],

again indicating its intercrystalline nature. It is markedly affected by crystalline and spherulitic morphology and is different in samples having distinctive lamella orientation.

No evidence of a β effect is found in (linear) polyethylene single crystals, and only a very small β effect is found in linear bulk polyethylene. Highly branched low density polyethylene exhibits a peak between the α_c and the γ regions that is usually called β and commonly attributed to the " amorphous phase"- its true origin is in the opinion of the authors by no means settled-but it has been shown to be related to the part of the amorphous phase containing the branched points[85-87] and has a high activation energy corresponding to that of a glass transition. The γ process was originally considered to be due to motion of long-CH_2 sequences in the amorphous region[88]. Recent work[76,89] has suggested that the γ relaxation is also a composite relaxation process with contribution from both the crystalline and amorphous phases.

As previous optical measurements for these three transitions have been scarce and only carried out at temperatures down to the peak region[46], the effort of this work was to make measurements at temperatures as low as those of the γ relaxation region to get some insight about this relaxation process. Figure (26) shows the changes of K' with temperature for both quenched and annealed low density polyethylene (the annealed data were taken from Yamada[46] for comparison)

It is observed that the quenched sample shows a higher maximum at about 40°C, as compared to that of the annealed sample which occured at a higher temperature of 60° and has a K' value about three-quarters that of the quenched. These results may be interpreted as being due to the quenched sample, having less ordered spherulite structure permitting the interlamellar slipping process to occur more readily (i.e. at a lower disordering temperature T_d). The sharper fall off of K' with temperature of the quenched sample near the melting point further supports such reasoning.

As Yamada[46] only cooled the annealed sample to about -40°C, no comparison is possible for the two types of samples at lower temperatures. However, a very prominent feature is evident in the case of the quenched sample where no negative K' value was observed even at a very low temperature, while high density polyethylene exhibited a negative K' at low temperature as seen in Figure (27). This absence of negative K' in quenched low density polyethylene can be attributed to two reasons (1) the contribution of the β relaxation process related to motion of some type occuring in the amorphous phase (2) the absence of deformational birefringence of negative spherulites because of the very poorly developed spherulitic structure in the quenched low density polyethylene. From dynamic mechanical data, a temperature around -120°C has been assigned to the γ relaxation region for high density polyethylene, and the sharp rise observed in K' below -100°C may be attributed to this relaxation process.

This sharp K' increase can possibly be due to the stiffening of the amorphous chain near the glass transition temperature T_g, where a high value of distortional birefringence could occur as described previously in the birefringence ralaxation studies of poly-ethyl acrylate by Stein and coworkers[90].

Figure (27) shows a similar study of the variation of K' with temperature for high density polyethylene. The quenched sample was prepared by heating to 175°C and was quenched in an ice-salt mixture. Data of the annealed sample by Yamada[46] were also drawn on the same figure for comparison. As expected, the quenched sample showed a much higher K' value, over most of the range of temperature until near the melting point, when the quenched and annealed samples showed similar values of K'. At higher temperatures, K' for the quenched sample decreases more sharply than that for the annealed sample. The maximum in K' occurs at a higher temperature of 100°C rather than at 60°C as for the low density polyethylene. Thus the higher melting, more perfectly crystalline sample must be heated to a higher temperature than that for low density polyethylene to permit a corresponding amount of crystal orientation to occur during the period of vibration. At temperatures lower than that of the minimum, K' of the annealed high density polyethylene sample rapidly drops passing through zero to negative values. These negative K' values are not seen for the quenched sample until very low temperatures of about -50°C are reached indicating that a positive contribution

from the β relaxation occurs in the amorphous phase of the quenched sample. The reversal in sign of K' implies a dominating negatively birefringent low-temperature mechanism not encountered with low density polyethylene because of its poorly developed structure. Also the lower temperature of -50° C when the quenched high density polyethylene sample begins to have negative K' values can be attributed to the less perfect spherulite structure for which a lower temperature is required for the deformation of negatively birefringent spherulites. Similar negative K' values have been found to be important for annealed polypropylene and polybutene[23].

Plots of E' and tan δ for the two types of samples have been shown in Figure (28). The quenched sample, as expected from its less perfect structure shows a lower E' value than that of the annealed, also at low temperature below -30°C, the mechanical loss tangent of the annealed sample is about zero, while that of the quenched sample is still finite and increasing, indicating the onset of another process, most probably the γ relaxation.

EFFECT OF ANNEALING ON STRAIN DEPENDENCE

With annealing, it is generally true that the internal structure are made more perfect, and the spherulits more orderly. This will inevitably lower the mobility of the structural entity so that a lower K' value is expected, and this is indeed found to be the case. Figure (29) shows the variation of K' with static strain up to 50% elongation, the

plot shows an unmistakeable lower K' value at low elongations. As compared to the quenched sample in Figure (20). The data also show less dependence of K' on static strain than for the quenched sample.

The solid black curve in Figure (29) shown in the upper side of the figure gives the plot of the $(d\Delta_s/d\varepsilon)$ obtained from the slopes of the static birefringence versus static strain plot. It is noted that the $(d\Delta_s/d\varepsilon)$ curves for both the quenched (Figure 20) and annealed samples are almost idential to each other, indicative of the same dependence of the samples for static birefringence. The same general type of Maxwell Model picture (Figure 21) can be given for the annealed case except the dashpot (whose slippage is analogous to the lamella slippage) has a higher viscosity or a longer relaxation time. At low elongations before the slippage of the dashpot, the model predicts a similar values of static birefringence and $(d\Delta_s/d\varepsilon)$ for both the quenched and annealed samples. At high elongations when the dashpot is slipping at a high rate, the increase of static birefringence with strain would be expected to be less than that found in the quenched case, since the dashpot slippage would be less in consideration of its higher viscosity. The K' values would be very similar in this region as compared with those at lower elongations since they account for the same type of reversible vibrational motion of the spring. As shown in Figure (22) for the quenched sample, the $(d\Delta_s/d\varepsilon)$ measures mostly reversible processes (response of the spring only) at low elongations, both reversible and irreversible

processes (stretching of spring and slipping of dashpot) at medium elongations, and only irreversible processes (the spring has highly been extended, and additional strain is mostly borne out by the dashpot) at high elongations. The K' , however measures only the reversible process (the vibration of the spring) which would be expected to be fairly constant at high elongations.

Figure (30) shows plots of E' and E'' versus static strain for the annealed sample. It is understandable that E' is much higher than that for the quenched sample as expected from the effect of decreasing the structural mobility by annealing. Also a minimum in E' is observed at about 30% elongation which is lower than the 40% minimum observed in the quenched case. It has also been found for quenched high density polyethylene that there is a minimum in modulus at even a lower elongation of 10%. (Figure 31). Ward[91] , however has found no minimum in modulus with strain for high density polyethylene. Combining all the modulus minimum results, one may generalize that as the percentage of crystallinity and perfection of crystals become greater in polyethylene, the minimum will become smaller and occur at a smaller elongation, and will ultimately disappear as the structure become so perfect that (in terms of Ward's explanation) the torsional compliance resulted from mechanical twinning becomes very small as compared with the extensional and torsional compliances, and such absence of modulus minimum (e.g. in nylon) has been found and explained on the same bases by Ward[64].

D. DISCUSSION

Several generalizations of results can be made from this section. The strain-optical coefficient K', which is a measure of the total orientation in the crystalline, amorphous phases and their phase boundaries (i.e. $X_{cr}K'_{cr} + (1-X_{cr})K'_{am} + K'_F$) is sensitive not only to morphology but also to the internal structure of the sample. Quenched low density polyethylene which has the most disordered and imperfect spherulites among all the samples investigated, has the highest orientability. Comparing values of $(d\Delta_s/d\varepsilon)$ with K', at low elongation (< 10%) for the quenched sample, the two values are very similar showing the dominating deformation mechanism is of a reversible nature. At slightly higher strains (10-15%), irreversible changes starts to appear (like the splaying apart of lamellae), and this has some pronounced effect on $(d\Delta_s/d\varepsilon)$ which because of the irreversible process contribution, is higher than K'. At this stage, a slight increase of K' is also observed (though not as markedly as $(d\Delta_s/d\varepsilon)$), due to the splaying apart of the lamellae which makes the rotation around the b-axis easier.

At still higher strains (15-40%), further breaking-up of the spherulite with some chain tilt and slip will occur (which are irreversible), thus rendering the $(d\Delta_s/d\varepsilon)$ even higher. On the other hand, the onset of tie-chain tightening between the lamellae makes the reversible process in the crystalline phase (e.g. rotation around b-axis)

and in the amorphous phase (stretching of tie-chains) less easy, and this results in a sharp drop in K', thus making the difference between $(d\Delta_s/d\varepsilon)$ and K' even greater. At very high elongations (> 50%), the original spherulites have completely been destroyed. Every crystal may be broken down into small blocks of tilted folded chains which together with a great many unfolded tie-molecules are incoporated in the highly oriented drawn sample. It is expected at this stage, almost all of the $(d\Delta_s/d\varepsilon)$ contributions comes from irreversible processes (as explained by the slippage of the dashpot in the Maxwell Model) of chain unfolding, and the $(d\Delta_s/d\varepsilon)$ value drops very sharply. The K', however measures reversible stretching of the unfolded tie-molecules and rotations of the new fibrils which would be expected to be fairly constant even at a much higher elongations.

Comparing the quenched versus the annealed sample, the latter is less orientable, and has a lower K' value which is also less dependent upon strain. The modulus is understandably higher and there is a much smaller decrease in modulus and a lower elongation modulus minimum when plotted against static strain. The temperature variation of K' indicates that the quenched sample is likely to exhibit a β relaxation contribution to K' which is due to motion of branches in the amorphous phase. The distortional birefringence of negative spherulites is not important because of the poorly developed structure. These two effects combine so that K' remains positive at low temperatures.

Comparing low density polyethylene with high density polyethylene samples, the latter has higher modulus, less orientability, and exhibits a negative value of K' at low temperatures which is caused by deforming the negatively birefringent spherulites. The inversion of sign in K' occurs at a much lower temperature for the quenched sample as compared to the annealed high density polyethylene, which is related to the relaxation process being present only in the quenched sample.

IX. DYNAMIC X-RAY DIFFRACTION OF LOW DENSITY POLYETHYLENE

STRAIN DEPENDENCE OF THE QUENCHED SAMPLE

In order to assess the term $X_{cr} K'_{cr}$ in Equation (10) (Page 15) the technique of dynamic x-ray diffraction is used. The same type of sample as employed in the case of dynamic birefringence but with a much greater thickness was prepared. To ensure that the thin sample for dynamic birefringence and the thick sample for dynamic x-ray diffraction have the same degree of quenching and morphology, only regions surrounding the edges of the quenched thick sample were used. It is thought that when the thick sample is plunged into the dry-ice-ethanol mixture, the most efficiently quenched regions are those near the edges; the central portion of the sample would inevitably be less quenched because of the poor conductivity of the polymer. To further check that the two kinds of samples were comparable, the static and dynamic orientation functions of this selected thick sample was compared with those layers of thin dynamic birefringence samples stacked together to give comparable thickness. The results are tabulated as follows:-

	Thick sample (20 mils)	Thin samples (4 layers of the 5 mil sample stacked on one another)
f_{oa}	-.08	-.08
f_{ob}	-.04	-.02

	-Thick sample-	-Thin samples-
f_{oc}	.12	-.10
C'_a	-.35	-.26
C'_b	-.10	-.10
C'_c	.45	.36
$X_{cr} K'_{cr}$	1.4×10^{-2}	1.2×10^{-2}

The results indicate that the two types of sample are of a very similar nature, and can be considered as having the same morphology and internal structure.

STRAIN DEPENDENCE OF THE QUENCHED SAMPLE

Figure (32) shows the mean static orientation (f_{oi}) of the a, b and c axes. They all increase in magnitude with static strain though with different slopes. It is evident from the figure that the a-axis orientation is much greater than that of the b-axis and they are both negative indicative of a perpendicular orientation of these axes to the stretching direction. The c-axis orientation function which is the sum of those for a and b axis with the sign reversed, is positive and indicates that it is orienting along the stretching direction. It is to be noted that these are the mean orientation f_{oi} and they

represent the average f_i of a sample subjected to a dynamic strain about an average strain ε_o. They may differ from the orientation functions measured at the same strain ε_o in a static experiment as reported, for example, by Hoshino, et. al.[33] and by (ONK)[24] because of the possible vibrational effect imposed on the sample. However our results indicate that such difference is negligible at high elongations, and only become appreciable at very low elongations ($\leqslant 10\%$). It can be seen that during the first 10% elongation, there is little change in f_{ob} consistent with a rotation about b-axis type of orientation. Figure (33 a) shows similar orientation function plots for quenched samples at high elongations. It is noted that at 200% elongation and higher, the orientation functions level off to constant values. The value of 0.8 for the c-axis orientation function at 300% elongation is in agreement with that found by Fujino et.al.[24].

Figure (34) gives the plots of the orientational compliances C_i' versus static strain. At very low elongation of ~5% (i.e. at the initial stage of the deformation of the spherulite), C_b' is very small, showing again that the orientation response is essentially rotation about the b-axis. In the range of strain up to $\varepsilon_o = 0.10$, the magnitudes of C_a' and C_b' increase with static strain indicating a greater ease of rotation about the b-axis while at strains greater than 0.15, there is a decrease. Such observation is in good agreement with the data found by previous workers[92].

The incresing C_i' value can be explained in terms of the spherulite deformation model as shown in Figure (35). At low strains, the rotation of the lamellae about the b-axis is opposed by the boundary layer viscosity which depends on the nature of the interlamellar material; the distance between the lamellae and the viscosity of the interlamellar material. Since static strain produces spherulite deformation, the separation of the lamellae in the equatorial region of the spherulite must increase.This should lead to a decrease in the effective boundary layer viscosity and should therefore lead to an increasing C_a' as twisting of the lamellae become more easy.

The decrease in the magnitude of C_a' and C_c' beyond $\varepsilon_o = 0.15$ may be accounted for in terms of the tightening of the chains between lamellae as shown in Figure (36). These tie chains contribute to the effective modulus opposing the process of lamellae slip. This tightening of the tie-chains results also in a decrease in amorphous mobility which is supported by the fall off of K' at higher strains (Figure 20) as explained in the previous section.

As shown in Figure (34), at higher strains, there is again an increase in $|C_a'|$ followed by a decrease at still higher strains. The increase in $|C_a'|$ is assoicated with an increase in mobility of crystallites assoicated with the disruption of the spherulitic structure. It is known that upon drawing to about 60%, the spherulitic morphology transform to fibrillar morphology. The lamellae do not preserve their

integrity during this transformation. According to Peterlin[93], " Every crystal is broken down into small blocks of tilted folded chains".

The effective viscosity opposing the lamella slip process not only depends upon the properties of the interlamellar layer but also upon the size of the moving crystalline units. The reduction in size accompanying the break-up of the lamellae should lead to a decrease in the effective viscosity and hence an increasing C_a'. The increasing strain should lead to a continued increase in orientation of the tie-chains with a consequent increase in effective modulus. This should ultimately lead to a further decrease in C_a' at higher elongations as is observed.

When "break-up" of the lamellae occurs, rotation about the a-axis as well as the b-axis should become possible. This may in part, account for the increasing value of C_b' with elongation. Two other reasons for the increase in C_b' may be (1) With increasing elongation, the chain axis tilts with respect to the plane of the lamellae. This is probably not a reversible process. However when such tilting occurs, the b-axis will no loner be restricted to the axis of the lamella but will be at an angle to it. In this case, the process of lamella twist about its axis will lead to a change in the orientation of the b-axis as well as that of the a-axis.

Figure (37) shows plots of the slopes taken from Figure (32) which give orientational compliances ($df_i/d\varepsilon$) at long times and include

contributions from both reversible and irreversible processes. While data at low elongations ($\leq 10\%$) are not accurate enough (since they are obtained from the slopes of another curve) to be meaningful, the general trend of the three axis orientational compliances shows a sharp decrease with static strain. Comparing the $(df_i/d\varepsilon)$ with C_i's, two interesting observations can be made. (1) the $(df_i/d\varepsilon)$s are in most cases ($<60\%$ elongation) much greater than the experimentally determined C_i', indicating the important irreversible contribution to $(df_i/d\varepsilon)$. At low strains, such irreversible process would understandably be the initial deformation of the spherulites. C_i', however measures reversible processes like the rotation around the b-axis. It is recalled in the $(d\Delta_s/d\varepsilon)$ and K' comparision, we have also indicated that the former is much bigger in magnitude than the latter at elongations of 10-40%. It has been inferred then and there as the onset of chain tilt and slip in the course of the spherulite deformation, which contribute importantly to the value of $(d\Delta_s/d\varepsilon)$, thus making it higher than K'. In the present case, $(df_i/d\varepsilon)$ has been found to be about two to three times bigger than C_i' owing to the fact that the irreversible processes occur mainly in the crystalline phase which is focused and magnified by the x-ray diffraction study.(2) Beyond 60% elongation, the calculated $(df_i/d\varepsilon)$ includes irreversible processes like chain unfolding in the formation of drawn fiber structure; the C_i' at this region of strain however, accounts for the twisting of the new fibrillar lamellae causing the chain axis and the lamellae axis to orient parallel to the stretching direction. This explains the higher values of C_i than $(df_i/d\varepsilon)$.

The effect of static strain on the imaginary part of the orientational compliances is shown in Figure (38). It is noted that all the C_i'' values have opposite sign to those of the C_i's, indicating that $\tan\gamma_i$ (where γ_i is the phase angle between orientation and strain) is negative. This means that the strain leads the orientation in phase which is reasonable in polyethylene since the response of the crystalline region to a vibrational strain would not be instantaneous, but takes a finite time in the order of seconds.

It is difficult to interpret the maxima observed in the C_1'', since the precision in such determination is comparatively poor, and the conventional way of assigning an optical loss peak on either side of the C_1' maximum cannot be applied like in the case of temperature variation experiment since experiments on strain dependence are usually irreversible.

B. EFFECT OF ANNEALING

The plot of the orientation functions (f_{oi}) versus static strain for the annealed sample are shown in Figure (39). As compared to the data of the quenched sample in Figure (32), f_{ob} is very similar at all elongation for the two types of samples, but f_{oa} for the quenched sample is somewhat lower (especially at low elongations) than that for the annealed case showing that the effect of annealing is to increase the orientability of the a-axis at least for irreversible process. At elongations bigger than 20%, there is very little difference in the

orientation functions between the two types of samples, showing that after the "break-up" of the spherulitic structure, the structure of the two types of samples are very similar to each other.

Plots of the orientation functions at high elongations are shown in Figure (33b). The similar values indicate the common resulting oriented fibrils in both cases.

The much greater effect of annealing on the orientational compliances is shown in Figure (40). At very low elongation ($\leqslant 10\%$), drastic differences occur between the two types of samples. A positive value of C_b' is observed upon increasing the extension, together with a negative but sharply decreasing C_a'. It is recalled that in the quenched case, C_b' is small but never becomes positive indicative of rotation around the b-axis. Here the finite value of C_b' and the large negative value of C_a' could mean that several processes are occuring in different regions of the sample (Figure 7). The most probable ones are (1) chain tilting in the polar region of the sample which gives rise to a large $|C_a'|$ (2) lamella bending in the equatorial regions which gives rise to a positive C_b' value. It is suggested that in the course of the above two processes, the more orderly annealed spherulites are broken down into less perfect ones just like those in a quenched sample, and at static strains beyond about 10%, the annealed sample behaves very similarly to the initially unstrained quenched sample, and the maximum in the C_i' observed at 20% of the quenched sample can be explained by the similar explanations of rotation about the b-axis given in the quenched case. At higher

strains, the similarity of these orientational compliances reflects a similarity of structure of the two types of samples and indicates that after the "break-up" of the spherulitic structure (in the annealed case this refers to the second break-up of the less perfect spherulites resulted from the first break-up of ordered structures within the more perfect ones), the structure of the resultant oriented mosiacs is not so sensitive to the original structure.

Plots of slopes of curves for the variation of the orientation function with static strain are shown in Figure (41). Excluding again the discussion of the calculated results at elongations lower than 15%, the similarity of the two sets of $(df_i/d\varepsilon)$ curves of the quenched and annealed samples reflects the very little dependence of $(df_i/d\varepsilon)$ on whether the samples are quenched or annealed. This can be inferred to as the occurence of irreversible processes is rather insensitive to to the morphology of the samples.

Plots of the imaginary part of the orientational compliances are shown in Figure (42), here again all the $\tan\delta_i$s show negative values and are bigger in magnitude as compared with the values obtained in the quenched case. This shows that the orientation in the annealed samples lags the strain even more in phase. This is understandable from the fact that the annealed crystalline phase is more orderly and better developed and thus less mobile and this will result in a bigger phase difference between the orientation and strain.

DISCUSSION

The contribution due to the orientation in the crystalline region has been determined. By the set of Equations from (165) to (168) (Pages 74 and 75). $X_{cr}K_{cr}$ and $X_{cr}K'_{cr}$ have been evaluated for the quenched (where X_{cr} =0.54 by volume) and the annealed samples (where X_{cr}= 0.64 by volume using x-ray diffraction method). These samples have different internal structures in the stretched state resulting from different static strains imposed. In the static case for the quenched sample, the crystalline contribution to the total birefringence is much larger than the amorphous contribution at low and medium elongations. At elongations greater than 50%, the fractional contribution of $X_{cr}K_{cr}$ decreases gradually but still contributes about 50-60%. In the annealed sample, the crystalline contribution is an even greater fraction of the total, over 100% is observed from very low elongation up to 50% of elongation, beyond which it tapers off to about 70-80%. A summary of the results is given diagrammatically in Figure (59) and the calculated fractional contributions are tabulated in Table III (Page 212 and 153 respectively.). Similar negative contributions of the amorphous phase in polyethylene[33,37] and polypropylene [94] have also been previously reported by other workers.

In the dynamic case, the orientation of the crystalline and amorphous phases are very different from those in the static case. This is a consequence of the difference between the two types of experiments, the static experiment measures both the irreversible and

reversible processes occuring in the crystalline phase, while the dynamic experiment accounts only for the reversible processes. For the quenched sample, the crystalline contribution ($X_{cr}K'_{cr}$) to the total K' has been evaluated to 40-50% at low elongations (~10%). This occurs mostly by rotation around the b-axis. At elongations higher than 10%, $X_{cr}K'_{cr}$ increases markedly to make the major contribution. At this stage after the splaying apart of the lamellae, rotation about the b-axis is much easier, also some twinning motions as pointed out by Peterlin[93] could be possible reasons for the increase in $X_{cr}K'_{cr}$. The much higher ($df_i/d\varepsilon$) as compared with the latter is probably due to the mechanism of chain tilting around the {310 axis}[95-97] which proceeds by successive chain slip along the c-axis by one repeat unit at a time. As a consequence, the chains are progressively shifted toward the draw direction. The slip is made particularly easy by axial crystal defects such as sequences of lattice vancancies along the c-axis. This occurs by the incoporation of a free end of the macromolecule. At still higher elongations (> 60%), the crystalline contribution is about 70-80% of the total, indicating there is a great increase in the ease of orientability of the crystalline phase. We attribute this to the structural transformation from broken spherulites to drawn fiber structure.

For the annealed sample, we started with a more orderly and better developed spherulites. The initial 10% of strain deforms and virtually transforms the original spherulites to less ordered ones just like those found in the initial unstrained quenched samples.

Several processes are occuring; for example chain-tilting in the polar region and lamella bending in the equatorial region, this accounts for the positive C_b' and sharp drop in C_a' . The crystalline contribution at this stage is about 10-30%. As the sample becomes more highly elongated, we are virtually starting to strain a quenched sample, and the similarities between the two sets of results (with the difference in the shifting of the maxima at a higher elongation for the annealed sample) can be explained on the same bases of reasonings and interpretations as given previously in the quenched case.

The dynamic x-ray diffraction results indicate that the major contribution of the strain-optical coefficient K' still comes from the crystalline phase, although in some cases the amorphous contribution $(1-X_{cr})K'_{am}$ could be appreciable. If we examine the two contributing factors K'_{cr} and K'_{am}:-

where $K'_{cr} = C'_{cr} \Delta^{o}_{c}$

and $K'_{am} = C'_{am} \Delta^{o}_{am}$

and substitute values of $\Delta^{o}_{am} = 261 \times 10^{-3}$ [98] and $\Delta^{o}_{cr} = 58.5 \times 10^{-3}$ (Bunn and Daubeny[99]), similar values in K'_{cr} and K'_{am} would mean that C'_{cr} is about four times as large as C'_{am} would mean that C'_{cr} is about four times as large as C'_{am}. This means that the crystalline phase would orient four times more than the amorphous phase for a given

change in strain. Thus, even at the extreme case of the 10% annealed sample where we have observed that K'_{cr} is only one-tenth that of K'_{am}, the C'_{cr} in fact is about half the value of the C'_{am}. Thus the importance of the crystalline contribution to both the static birefringence as well as the strain-optical coefficient cannot be over emphasized. It is perhaps enough for us to say that the crystalline contribution is slightly less important in a dynamic experiment than in a static experiment owing to the fact that only reversible processes are observed in the former type of experiment. At high elongations, however, the crystalline contribution in a dynamic experiment is as important or perhaps more so than in a static experiments. Such results have indeed been observed as shown by Figures (60) and (61) together with Table III, and these we attribute to the importance of the reversible processes occuring in the crystalline phase, the most probable ones are the easier rotation about the a- and b-axis after the complete break-up of the spherulites.

Comparing the results of the annealed sample with those of the quenched, there is an appreciable difference in the crystalline contributions at low elongation (up to 20%). The $X_{cr}K'_{cr}$ of the former is lower in magnitude, and is decreasing from an unstrained to a 10% strained sample. Judging from the values of X_{cr}, the annealed sample has a slightly higher value, and has found to be fairly constant during this range of elongation. The observed lower value in $X_{cr}K'_{cr}$ and the minimum at 10% have therefore been attributed to the breaking down of the more perfect annealed spherulites

to less orderly ones with possibly reversible processes like tilting, lamella bending and twinning. From dynamic mechanical data in Figure (30), the annealed sample has a modulus about twice as great as does the quenched sample. Such high modulus has usually been explained by the observation that the crystalline phase of the annealed sample is more perfect and does not respond much to an external strain, and this ties in with the lower value of $X_{cr}K'_{cr}$ in the annealed sample than in the quenched.

In order to evaluate precisely the actual contribution due to the amorphous phase, it is essential to carry out experiments where the third contribution due to the oriented boundary regions between the crystalline and the amorphous phase (i.e. K'_F) can be assessed, and this we resort to swelling studies of dynamic birefringence which will be discussed in the next section.

XII. SWELLING STUDIES OF DYNAMIC BIREFRINGENCE

INTRODUCTION

By the approximation of a two-phase model, the crystalline phase of a crystalline polymer like polyethylene can be imagined as particles inter-dispersed in a continuum of amorphous phase. In this case, the oriented particles are optically isotropic but assymmetric in shape, and their average refractive index is different from that of the amorphous phase. Such a difference in refractive indices gives rise to the so-called form birefringence[34]. This birefringence is a function not only of the shape and concentration of the crystallites, but also of the square of the difference between the refractive indices of the two phases.

It has been calculated by Bullough[100] that the most general form birefringence in a two-component anisotropic system consists of four terms which need not necessarily depend on $(n_a - n_b)^2$, the square of the difference of the refractive indices of the two components. However, when point-to-point fluctuations in composition greatly exceed fluctuations in the volume fraction of the crystallites, the four form terms reduce to a single "excess" term which does depend on $(n_a - n_b)^2$.

It is possible to vary the refractive index of the amorphous phase . This can be done by swelling it with a solvent which produces a change in the refractive index which will be proportional to the

volume fraction of the solvent incorporated. When the refractive index of the swollen amorphous phase equals numerically to that of the crystalline phase, this would correspond to the minimum point in a birefringence versus solvent refractive index plot[34,102], and the form birefringence vanishes. In the static birefringence experiment, the fraction of the total birefringence arising from the form birefringence was estimated by such swelling studies to be 5-10% of the total for annealed low density polyethylene[102]. It is conceivable that the form birefringence contribution to the strain-optical coefficient may be much greater than in the static case since the vibrational strain may produce deformation of voids which are of the same order in size as the wavelength of light, and this would contribute appreciably to the form birefringence. Also form birefringence determination is important since the amorphous birefringence contribution is calculated from the difference between the total birefringence and the sum of the crystalline and form contribution. The experiment described in this section concerns with the determination of the form birefringence Δ_F and the form contribution $(d\Delta_F/d\varepsilon)$ to the strain-optical coefficient.

Samples of low density polyethylene were stretched to the desirable static strains, and allowed to relax to equilibrium. Measurements on static and dynamic birefringence were carried out, and the subsequent stretched samples were swollen in solvents with varying refractive index for about two weeks. The thickness of the swollen samples was corrected in every case.

With the assumptions that the swelling solvents only enters the amorphous phase and the degree of crystallinity is not affected, the following procedures for the calculation of swelling ratio and the refractive index of the swollen amorphous phase were adapted.

Let ϕ_c = initial volume fraction of crystallinity

= volume of crystals/ volume of dry polymer

ϕ_s = volume fraction of solvent based upon weight of dry polymer

= volume of solvent absorbed/ volume of dry polymer

Then $\frac{\phi_s}{1-\phi_c} = \frac{\text{(volume of solvent / volume of dry polymer)}}{\text{(volume of dry amorphous phase/ volume of dry polymer)}}$

= volume of solvent absorbed/ volume of dry amorphous phase

If we assume volume of swollen amorphous phase = volume of dry amorphous phase + volume of solvent

Then

$$1 + \frac{\phi_s}{1-\phi_c} = \frac{\text{volume of dry amorphous phase + volume of solvent}}{\text{volume of dry amorphous phase}}$$

$$= \frac{\text{volume of swollen amorphous phase}}{\text{volume of dry amorphous phase}}$$

$$= 1/\phi'_{am}$$

$$= (1-\phi_c+\phi_s)/(1-\phi_c)$$

ϕ'_{am} = Volume fraction of amorphous polymer in swollen amorphous phase

$= (1-\phi_c)/(1-\phi_c+\phi_s)$

ϕ'_s = Volume fraction of solvent in swollen amorphous phase

$= 1 - (1-\phi_c)/(1-\phi_c+\phi_s) = (1-\phi_c+\phi_s-1+\phi_c)/(1-\phi_c+\phi_s)$

$= \phi_s/(1-\phi_c+\phi_s)$

If n_{sa} = refractive index of the swollen amorphous polymer

n_s = refractive index of solvent

n_a = refractive index of dry amorphous polymer

Assume

$$n_{sa} = \phi'_{am}\, n_a + \phi'_s\, n_s$$

$$= \frac{(1-\phi_c)\, n_a + \phi_s\, n_s}{1-\phi_c+\phi_s} \qquad (169)$$

The refractive index of the amorphous phase can be calculated by the following assumptions

$$\frac{1}{\rho_c}\,\frac{n_c^2-1}{n_c^2+2} = \frac{1}{\rho_A}\,\frac{n_A^2-1}{n_A^2+2} \qquad (170)$$

and substituting that $n_c = (n_a + n_b + n_c)/3$

where n_a, n_b and n_c are the refractive indices (1.514, 1.519, 1.575 respecively)[36] along the a, b and c axes of the polyethylene unit cell.

we have

$$n_c = 1.536$$

assuming $$\rho_c = 1^{103}$$

$$\rho_A = 0.852^{103}$$

Equation (170) after simplification, gives

$$n_A = 1.44$$

Substituting values of n_A, ϕ_c, ϕ_s and n_s in Equation (169) for all the cases, the results for the swelling ratios and the refractive index of the swollen amorphous phase were tabulated in Tables I and II respectively. The reason for first studying the annealed samples is that they are expected to contribute more form birefringence owing to their probably having more discrete and oriented phase boundaries.

Figure (43) shows the plot of the static birefringence versus the refractive index of the swollen amorphous phase. An equation given by Weiner[34] predicts the parabolic curvature of the plot when the static birefringence is plotted against the refractive index of solvent. Since we have modified the method of our plot (i.e. the abscissa is the refractive index of the swollen amorphous phase instead), the difference in the shape of the curves from that of Bettelheim[102] is understandable. Further the curvature of our plot also increases with increasing static strain (except the 30% elongation case) indicative of a higher elongated and /or oriented particle with stretching the sample.

According to the Weiner theory[34], there is no contribution from the birefringence at the minimum of these curves, indicating that the refractive indices of the crystalline and the swollen amorphous phase are equal numerically, and the birefringence at the minimum point is given by

$$\Delta = X_c f_c (n_{\parallel} - n_{\perp}) + X_a \Delta_a$$

Where X_c and X_a are the volume fractions of crystalline and amorphous material in the swollen sample respectively. f_c is the orientation factor for the crystals. $n_{\parallel}$ and $n_{\perp}$ are the refractive indices of the crystals parallel and perpendicular to their c axis, and Δ_a is the birefringence of the amorphous phase.

It is to be noted that swelling the samples imparts three effects on the sample: (1) The solvent enters and swells the amorphous phase producing a change of the latter's refractive index which will be proportional to the volume fraction of the solvent incorporated. When the resulted refractive index of the swollen amorphous phase equals to that of the crystalline phase, the form birefringence vanishes. (2) Irreversible structural change occurs due to the swelling of the amorphous phase. Such an effect can be appreciable, and is best observed by comparing the birefringence values of the bulk and swollen sample. An effort is made to assess this irreversible effect by first swelling the bulk sample and then drying the swollen sample in a vacuum dessicator (until the weight of the dried sample is the same as that of the bulk), the first

step will affect or eliminate the form contribution while the drying process brings back the form contribution but retains the irreversible structural change effect. The difference between the bulk and the dried sample serves as an indication of the amount of structural change that has been imparted by swelling. (3) In the presence of a solvent in the amorphous phase, some mobility change will inevitably be observed during the vibration of the sample, this is difficult to assess since the removal of the solvent will result in the reappearance of the form birefringence. Perhaps a way of doing this would be to select a solvent such that in the presence or absence of this solvent, the refractive index difference between the crystalline and amorphous phase is the same in magnitude but different in sign. Thus the difference in K' between the swollen and dried sample gives only the mobility effect, but such solvent is very difficult to find because of the complication of the swelling ratio which determines the refractive index of the swollen amorphous phase. Further, the mobility change created by this solvent would not necessarily be the same as that created by the solvent which eliminates the form birefringence. In view of these difficulties, the form contribution has been assessed together with the accompanying mobility change effect.

Also in order to assure that the swelling change is an equilibrium and reversible one, dried samples have been reswollen and its dynamic and static birefringence has been compared with that of the originally swollen sample.

Figure (44) shows the strain-optical coefficient variation with the refractive index of the swollen amorphous phase. Again a small curvature is observed in all cases indicating that at some particular refractive index, $K'_F = 0$ (This has been found to be lower value of refractive index of the swollen amorphous phase than that in the static case.). If we compare the shape and behavior of curves of K' and $\triangle_s$, the position of the minimum and the curvature of curves are fairly different in the two cases. This can be understood by the different mechanisms operating in the two types of experiments.

Although the minima in K' may vary slightly with different static strain, they generally fall in the range of 1.45 to 1.46. A convenient solvent; xylene, with refractive index (1.4980) has been selected for the swelling studies in the quenched case.

Figures (45) and (46) show plots of the variation of static birefringence and strain-optical coefficient with static strain when using xylene as the solvent. Four types of samples were studied namely; the bulk, swollen, dried and reswollen. It was found that the swollen and reswollen samples behave very similarly indicating that the swelling process is very reversible after the first swelling. The bulk and the dried sample however, are not the same, the former always has a higher birefringence and K' value than that of the latter and this is indicative of some permanent change during the swelling process, which cannot be removed on drying. The reversible change is small as compared to the irreversible change. If we assume the drying and

reswelling processes result in the bringing back and the redisappearance of K_F' without the interference of any significant mobility effect, then the difference between these curves will furnish us the contribution of K_F', and this is indeed what we have assumed in our calculation.

It has been estimated in this work that in the static case, at a low elongation of about 10%, form birefringence amounts to about 20% of the total. At medium elongation of 30-40%, this decreases to about 10-15%, due most probably to the breaking up of the phase boundaries. On further elongation (up to 50%), it drops down to about 10% of the total.

In the dynamic experiment, it was originally supposed that if there were changes in the shape of voids of size in the order of the wavelength of light, this would contribute importantly to the form birefringence during the vibration. However, the obtained results showed that this is not the case, as only 10-15% of the total has been found to be due to the form contribution together with the mobility effect involved during the vibration in the presence of a solvent.

EFFECT OF QUENCHING

Since the form contribution is not as large as expected, and judging from the supposition that the phase boundaries would be less discrete and oriented in the quenched case than the annealed, a much more simplified swelling studies has been undertaken to assess the Δ_F

and K'_F for the quenched sample. Xylene is chosen to be the solvent which most nearly eliminates the form birefringence (that is based on the understanding that the refractive index of the crystal and amorphous phase is not very different for both the annealed and quenched samples). Figure (47) shows the static birefringence plotted versus static strain for the same four types of samples (bulk, swollen, dried and reswollen). The swelling or the irreversible effect is again large as compared with the form or the reversible effect, and the observation that swollen and reswollen samples behave similarly, while bulk and dried samples are different, is again found here.

Figure (48) shows similar plots of the variation of K' with static strain. If we examine the four curves obtained, the following inferences can be made.

(1) The shape of curves for the swollen, dried and reswollen samples are very similar to each other, but are slightly different from that of the bulk sample in that the maximum has been shifted to a higher elongation of 25% as compared to 15% in the quenched case. The K' values are also substantially lower, especially at low elongations. It is recalled that in the annealed case, the same type of maximum and very similar K' values are observed just as for these three types of samples. Thus it can be inferred that with swelling, structural changes similar to those caused by annealing are being imparted to the quenched sample.

(2) Also it is found that there is a fair difference between K' values for the swollen and reswollen samples at low elongations. This can be due to the incomplete annealing effect during the first swelling, and

with reswelling, the annealing effect continues to occur, thus making K' values even smaller,reaching almost values similar to those for the annealed bulk sample (ref. Figure 32). At high elongations, no such effect is observed, indicating that for oriented samples, after the break-up of spherulites, there is little sensitivity to swelling, and the four types of samples behave very similarly.

It is our aim to assess the amount of form contribution to both the static and dynamic birefringence. The static birefringence presents a lesser problem because it does not involve any complication due to the mobility effect which would occur in a vibrational experiment, hence, the difference between the dried and swollen or reswollen samples will furnish us with the value of Δ_F.

In the dynamic case, as we have found there is some difference between the swollen and the reswollen samples, our method has been to estimate the maximum limit of the K'_F contribution, and we have taken the difference between the dried and reswollen samples for our calculation. Actually the value which is calculated from this method will include the effect of mobility change in the swollen sample. Further, to be exact, the process of swelling and drying has to be repeated many times until two successive swellings give similar results, thus ensuring complete equilibrium of structure. In this case, the difference between the dried sample and the last reswelling sample indicates the total change resulting from K'_F contribution and the mobility effect. Since such processes are very tedious and time

consuming as every swelling step takes a period of 10-14 days, our experiment has been simplified to only one reswelling step, and the K'_F estimation has been taken from the difference between the dried and the reswollen samples.

GENERAL DISCUSSION

It has been found that swelling of the bulk samples imparts three effects (1) the changing of the refractive index of the swollen amorphous phase which creates a change in the form birefringence. (2) irreversible structural changes in the sample which cannot be removed by drying (3) the mobility change in the presence of a solvent in the amorphous phase. The second effect of the irreversible structural change is more prominent in the quenched sample, since this is analogous to the effect of annealing caused by the presence of solvent which enables chains and lamellae to rearrange and makes the structure more perfect, although this occurs to a much lesser extent as compared with the usual process of thermal annealing or isothermal crystallization, about 20° below the melting point.

The annealed sample, with more discrete oriented phase boundaries, gives rise to higher Δ_F and K'_F contribution, which amount to 15-20% at lowelongations,decreasing to 10-15% at high elongations. The quenched samples, however do not have as much such form contribution, which amounts to 5-10% at the elongations investigated. Para-xylene has been chosen and assumed to be the most appropriate solvent for the elimination of form birefringence.

XIII. THE DYNAMIC BIREFRINGENCE OF SUBSTITUTED POLYETHYIENE

It has been shown in this thesis that the strain-optical coefficient determined from the dynamic birefringence technique can be resolved into the crystalline, amorphous and form birefringence contributions. As the last constribution has been evaluated to be very small, the two main contributions are K'_{cr} which is $X_{cr}C'_{cr}\Delta_{cr}$ and K'_{am} which is $(1-X_{cr})C'_{am}\Delta^{o}_{am}$. It is apparent that the value of K' is governed ont only by the magnitude of X_{cr} (percentage of crystallinity), but also by the orientability per unit strain of the crystalline and amorphous regions (C'_{cr} and C'_{am} respectively.)

It is the purpose of this section to make a preliminary survey of the influence of substitutents attached to the polyethylene backbone on the strain-optical coefficient. These may include groups of different polarities and bulkiness. The effect of the concentration of such substituent is also being studied.

The first study in this series involves the incorporation of a small percentage of carbonyl group along the backbone of the ethylene chain in order to investigate the influence of this group on the deformation as well as the alpha-loss process. It has been found by Wilkes and Stein[104] in their infra-red dichroism studies that the carbonyl group orients as much as the crystalline region, which implies that the carbonyl group appears to fit into the crystalline lattice. Chatani[105]

et. al. by their x-ray diffraction studies on low molecular ethylene-carbonyl copolymer also supported such conclusions. Further Phillips in his dielectric dispersion studies, has also found the intensity of the alpha dielectric loss peak which has been assigned to the crystalline region[106-109] increases with increase in CO content. Thus by comparing the dynamic birefringence data of ordinary polyethylene and the CO-substituted polyethylene with varying concentration, some insight about the influence of this substituent on the deformation and the alpha-loss process can be obtained.

QUENCHED CO-CONTAINING SAMPLES

Polyethylene containing 0, 0.5% and 1% carbonyl content samples were obtained through the courtesy of Dr. J.E. Guillet of the university of Toronto, Toronto, Canada, and the molded samples were prepared in the same way as the polyethylene described earlier.

Figures (49), (50) and (51) show the variation of the strain-optical coefficient K' at three different frequencies of 8.64, 1.02 and 0.121 hertz with temperature. It is generally seen that, as compared with pure low density polyethylene, the 0% CO containing copolymer has a higher K' values at the temperatures indicated. Further incorporation of CO seems to lower considerably the value of K' which is very similar to that of ordinary low density polyethylene. Also the alpha-loss temperature seems to fall within the same range of temperature for all the CO containing copolymers as well as polyethylene. Using the method of reduced variables[110],

measurements of K' at three different frequencies (8.64, 1.02 and 0.12 hertz) were made at temperatures from 20 to 100°C at intervals of approximately 10°. Curves of K' versus frequency at each temperature were obtained by replotting the data (a representative plot is shown in Figure 52 for the 0% CO containing polyethylene). The curve determined at any temperature T was then "reduced" to the position it would have occupied at temperature T_o (reference temperature in this case is 50°C) by shifting horizontally by log a_T where a_T is the shift factor $\frac{f \text{ at } T}{f_o \text{ at } T_o}$ A series of experimental measurements at several different temperatures, when each has been reduced to T_o using the appropriate values of a_T, superposed to give a single composite curve representing K' at T_o. Such composite curves have been shown in Figure (58). By plotting the logarithm of the horizontal shift factor versus the reciprocal temperature (1/T), activation energy of about 25 Kcal. per mole was obtained for low density polyethylene in agreement with the values obtained by previous workers[31,32]. The CO-containing compolymers, however, give much lower values of 13-14 Kcal. per mole in all cases. These activation energy values are fairly different from the dielectric activation energies obtained by Phillips in which values of 21-22 Kcal. per mole have been reported by using method of frequency plane maxima. The reason for such lowering of the activation energy in our case is still uncertain.

EFFECT OF ANNEALING

As was observed in the case of polyethylene, annealing usually produces more perfect and ordered spherulites with lower orientability.

Similar observation has been reported by Wilkes[104] for the CO containing copolymers. Figures (53) and (54) show plots of K' and tanα respectively at 1 hertz. One conspicous point here is that the alpha peaks are less marked as compared with those of the quenched, and K' does not fall off as much at higher temperatures. It is to be recalled in the quenched case, a much broader maximum was observed in all the CO-containing polymers than in polyethylene,the annealed samples seem to magnify this observation. It is suggested that the CO group which fits into the crystal lattice may impede the internal motion within the crystals. This might be contradictory to the lower activation energies as reported earlier, but it is to be noted that the calculated activation energies account for the lower temperature α_1 process, while the impeding influence of the carbonyl group affects the higher temperature α_2 process. A complete explanation of this mechanism still awaits confirmatory data from the dielectric , x-ray diffraction and other studies.

BROMINATED, PHOSPHONATED COPOLYMER AND E/VA/VOH TERPOLYMER

The carbonyl group which is comparable in size with the methylene CH_2 unit, has been shown to fit into the crystal lattice. Bulkier groups like the bromine atom and $PO(OH)_2$ are interesting in that they are much bulkier and will most probably be rejected by the crystal lattice and will occupy the interlamellar or non-crystallizable region. The brominated polyethylene was obtained through the courtesy of Dr. Paul Phillips who prepared the copolymer by first purifying the parent polyethylene (used in the earlier work) by reprecipitation from p-xylene to remove

anti-oxidants and other foreign matter present in the commercial product, and bromination was then carried out by dissolving in either trichloroethylene or α-chloronaphthalene at 80°C, then adding bromine and irradiating with a sun lamp. The period of irradiation was varied from one hour up to eight hours. The polymer was then recovered by precipitation at least four times. By chemical analysis, the bromine content of the sample used was found to be 1.7 weight percent.

The phosphonated polyethylene was obtained through the courtesy of Mr. Fred Emerson who prepared the copolymer by chlorophosphonating low density polyethylene by passing oxygen through a solution of the polymer in PCl_3. Hydrolysis of the intermediate poly(phosphoric dichloride) (I) gave the poly (phosphoric acid II)[112].

$$-CH_2-CH_2-CH_2- + PCl_3 + \tfrac{1}{2} O_2 \longrightarrow -CH_2-\underset{\displaystyle POCl_2}{\overset{\displaystyle |}{CH}}-CH_2- + HCl$$

(I)

$$(I) + H_2O \longrightarrow -CH_2-\underset{\displaystyle PO(OH)_2}{\overset{\displaystyle |}{CH}}-CH_2- + 2\ HCl$$

(II)

Chemical analysis of the phosphonated polyethylene shows that the sample contain 1 $PO(OH)_2$ group per 39 carbon atoms.

The E/VA/VOH terpolymer was obtained through the courtesy of

Mr. Roland Tetrault who prepared it by acid hydrolysis of a copolymer of ethylene-vinyl acetate in a toluene-methanol mixture at 66°C[113], according to

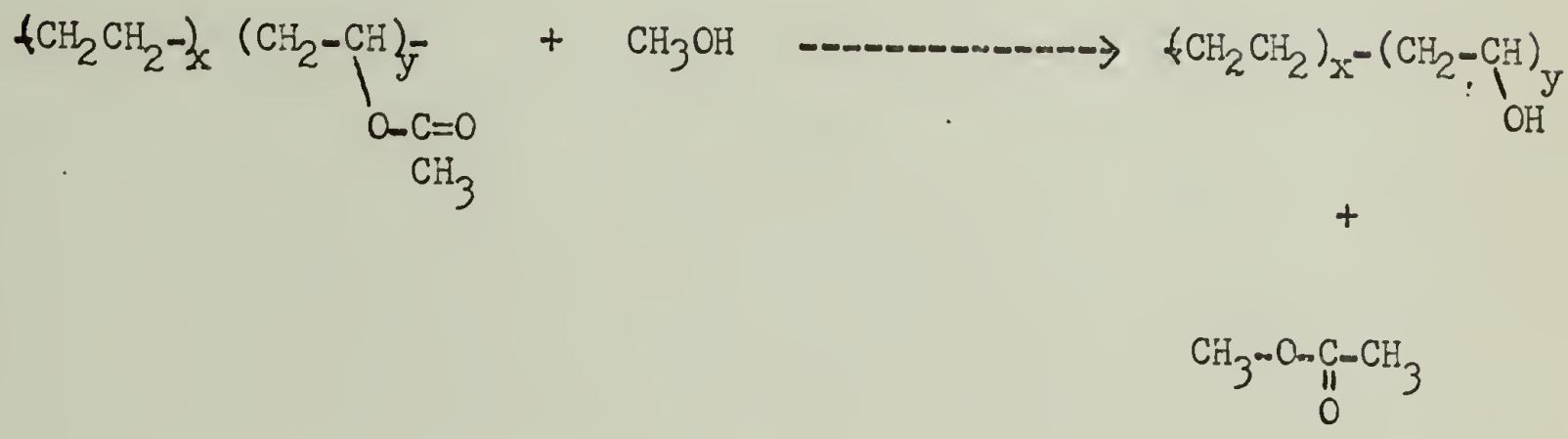

The desired chemical composition was achieved by cooling and neutralizing the reaction mixture after specific reaction times. The hydroxyl content was determined by saponification, the chemical composition of the terpolymer was found to be 75.4% ethylene, 0.45% vinyl acetate, and 24.2% vinyl alcohol (all in mole %).

X-ray evidence[113] indicates that the basic structural unit in this terpolymer is the polyvinyl alcohol unit cell with methylene units present as defects, the percentage of crystallinity has been calculated to be 26.9%.

Determination of crystallinity by x-ray diffraction for the brominated and phosphonated polyethylene samples leads to values of 40 and 20% respectively. A comparison with the value of 54% for the quenched low density polyethylene, shows the lower in percentage of crystallinity in the substituted samples confirms the fact that the substituent perturbs

the crystal lattice and reduces the crystallinity. Phillips[111], in his dielectric and rheo-optical studies of the brominated polyethylenes has suggested that the bromine atoms are incorporated in the folds. Plots of K' at frequencies of 8.64, 1.02 and 0.121 hertz for the substituted polyethylenes are shown in Figures (55-57). It is interesting to find that the brominated and phosphonated samples show a much lower strain-optical coefficient indicative of a smaller contribution from both the crystalline and amorphous regions. The percentage of crystallinity which is lower than polyethylene is understood to give a smaller $X_{cr}K'_{cr}$. The bulky bromine which is believed to occupy the chain fold regions, may also sterically hinder motion of chains in the amorphous phase. These two effect combine and lower the total orientability considerably, thus yielding a much lower K' value. The phosphonated polyethylene which has a much larger $PO(OH)_2$ group as compared with bromine, will produce a more pronounced effect, resulting in the lowest K' value of all of the samples.

The K' values of the E/VA/VOH terpolymer are comparable to those of the brominated copolymer, but are less temperature sensitive. Even at temperature near the quoted melting point (105°C)[113], the strain-optical coefficient does not show any significant decrease, this is most probably due to the fact that a different type of crystal unit cell is involved here as compared with the polyethylene unit cell for the other substituted polyethylenes. Ease of intracrystalline and intercrystalline motions in the α_1 and α_2 processes would be expected to be very different to that in polyethylene. The less temperature dependence in K' would mean

most probably a less ready nature of the two types of intra- and inter-crystalline motions.

The complete master plots of K' versus frequency for all the substituted polyethylenes (Reference temperature 50°C) have been shown in Figure (58). While very little information on the molecular mechanisms can be obtained from these preliminary data, two interesting generalized features can be inferred.

Order in magnitude of K'

0% CO > P.E. ≃ 0.5% CO ≃ 1% CO > E/VA/VOH > Brominated P.E. > Phosphonated P.E.

Frequency dependence

0% CO > P.E. ≃ 0.5% CO ≃ 1% CO > Brominated P.E. > E/VA/VOH > Phosphonated P.E.

XIV. GENERAL DISCUSSION

The total static birefringence of low density polyethylene has been resolved into its three contributions namely; the crystalline, amorphous and form, and the final results are shown in Figure (59). The most remarkable feature of the quenched sample is that the crystalline contribution is always lower than the total birefringence, but has been found to be the main contribution amounting to 70-80% of the total at most elongations. For the annealed sample, up to elongations of 60%, the crystalline contribution to Δ_s is over 100% making the amorphous contribution negative. That is, the amorphous chains are orienting perpendicular to the stretching direction. Similar findings of these sort have been reported for polyethylene[33,37] and polypropylene[94] by other workers. At very high elongations (>50%), when the spherulitic morphology has been transformed to fibrillar morphology, the amorphous region orients parallel to the stretching direction, thus lowering the crystalline contribution to about 80%. The form birefringence, which is a function of the shapes and sizes of the different regions and of the average refractive index difference between the phases, understandably depends upon the morphology as well as the orientation of the phase boundaries. In our case, we have found a higher form contribution in the annealed sample than in the quenched at all elongations. 15-20% contribution was found for the former at low elongations (as compared with 10% in the latter case), and gradually drops down to 10-15% (5-10% in the quenched case) at high elongations.

In the dynamic case, which involves only the reversible processes, the crystalline contribution is comparatively less important. While rotation of crystals around their b-axis has been suggested as the most probable mechanism of orientation at low elongations (~10%) for the quenched sample, it is seen that values of $X_{cr}K'_{cr}$ and $(1-X_{cr})K'_{am}$ are comparable. Thus we believe that reversible motions which involve the alignment of the amorphous chains along the stretching direction due to the splaying apart of the close contact lamellae accounts for the appreciable contribution from the amorphous regions. At elongations higher than 15%, it is likely that the onset of tie-chain tightening makes the rotation around the b-axis less easy. Also tie molecules have reached their limiting extension so that additional amorphous orientation cannot occur. These two effects combine to make a very marked decrease in the total orientability which is reflected in the falling off of the K' values. At this stage, the crystalline contribution passes through a small minimum. At still higher strains (30 to 60% elongations), the spherulitic structure is disrupted and it has been proposed that lamellae break apart into mosiac blocks of crystals, which at higher strains, reconstitute new fibrillar lamellae in which both the chain axes and the lamella axes are oriented parallel to the stretching direction. In this transition region, it is believed that the crystal mobility is greatly enhanced, and the crystalline contribution increases sharply to about 80% of the total at 50% elongation. A general survey of the plots shown on Figure (60) indicates that both $X_{cr}K'_{cr}$ and $(1-X_{cr})K'_{am}$ pass through a maximum at about 15% of strain, after which the latter tapers off to

contribute only 10-15% of the total at 50% elongation. The K'_F contribution is not important and amounts to 5-10% in most cases.

In the annealed sample, at very low elongations (< 10%), the crystalline contribution (i.e. $X_{cr}K'_{cr}$) starts with a value of 30-40% of the total in the initially strained state (~3%), and then decreases to only 10% of the total at 10% elongation. In this region, the more orderly annealed spherulites are broken down into less perfect ones just like those in an unstrained quenched sample. The most probable mechanisms involved here are chain-tilting in the polar region and lamella bending in the equatorial regions of the spherulites. At strains higher than 10%, rotation about the b-axis is believed to occur, and the resulting sample behaves very similarly to the undeformed quenched sample. The maximum observed in $X_{cr}K'_{cr}$ for the quenched sample has been shifted at a higher elongation of 20%, when the onset of tie-chain tightening followed by the transformation of the spherulitic morphology to fibrillar morphology makes the $X_{cr}K'_{cr}$ and $(1-X_{cr})K'_{am}$ versus strain plots appear very much the same as those for the quenched sample. Form birefringence contribution is more important for the annealed sample owing to its having more discrete and oriented phase boundaries. Values of K_F in the region of 10-15% of the total have been found in most cases. A summary of the results has been tabulated in Table III, and the plots of the corresponding contribution are shown in Figure (60) for quenched and (61) for the annealed samples.

In the results of the dynamic birefringence of substituted polyethylene, it has been found that the attachment of substitutents to the

polyethylene backbone has an important influence on the optical properties of the polymer. With groups that can fit into the crystal lattice (such as CO) , it was found that they do not create any decrease in either the percentage of crystallinity or in K'. Bulkier groups like those of bromine and $PO(OH)_2$ which could only occupy chain folds or other non-crystallizable regions decrease the K' by virtue of their lowering effects on the percentage of crystallinity and possibly on the orient-ability per unit strain of the amorphous region.

SUGGESTIONS FOR FUTURE STUDIES

So far we have determined the three contributions to the strain-optical coefficient for the quenched and annealed low density polyethylene. Medium and high density polyethylene samples would be interesting to study because of their higher percentage of crystallinity and more perfect structure. It is expected that in the more crystalline material, inter-crystalline interference will reduce the ability of the crystals to orient, and the amorphous contribution to the total K' would correspondingly be higher. One drawback in such similar type of studies is the non-linear reversible stretching of the polymers in the dynamic birefringence and dynamic x-ray diffraction apparatus. In order to alleviate such difficulty, perhaps the following modification of the experimental conditions can be made.

(1) A smaller dynamic amplitude (example in the order of 0.2 to 0.5%) could be applied to these higher density polyethylene samples, so

that the sample would not slack or break during the vibration cycles. The smaller dynamic amplitude would no doubt create a precision problem in the measurement (especially in the dynamic x-ray diffraction). Longer period of counting (which is feasible in an automatized version of the apparatus) is a possible solution to this problem.

(2) The experiment could also be performed at a higher temperature (e.g. in the region of 40-50°C), so that the enviromental conditions provide a softening effect on the samples, and make them for flexible for vibration.

The above suggested studies would furnish us with the information of the effect of the percentage of crystallinity on the three main contributions of K'.

Also three other types of low density samples could be used for the similar studies, they are;_

(1) Samples which have been annealed at the deformed state: Such samples would be expected to be very different from those which are annealed in the undeformed state and subsequently stretched to the corresponding elongations.

(2) Samples which have been crosslinked below the melting point: It is presumed that such type of samples would have most of the crosslinks in the amorphous phase. Work in this laboratory* has indicated that with small dosage of irradiation, there is very little change in the orientability of the amorphous phase. With higher dosage of irradiation, it is expected

* Ph. D. Thesis work of Mr. Akira Tanaka

that the resulted crosslinks would freeze and lock up most of the amorphous orientation, but such an amount of irradiation would inevitably distort or destroy the crystal lattice.

(3) Samples which have been crosslinked above the melting point: This crosslinking process would provide random crosslinks in the samples. The percentage of crystallinity would prevent most of the crystallization from occuring. The percentage of crystallinity can further be varied by varying the dosage of irradiation, so that both the effect of crystallinity and crosslinking can be studied on the three contributions of K'. It is presumed in the highly crosslinked case, the form contribution would be almost zero since there would not be any distinct phase boundaries in the sample. Also very ordered crystalline region as well as very randomly amorphous region would not be present, and it is expected such samples will have a strucutre of intermediate order.

SUGGESTIONS FOR FURTHER STUDIES ON THE SUBSTITUTED POLYETHYLENES

Perhaps, the future studies on the substituted polyethylenes can be divided into several parts:- (1) the polar influence of the substituents (2) the effect of size of the substituents (3) the concentration effect of the substituents and (4) the location of the substituents in different regions.

(1) Polar Influence of the Substituents: It is well known in organic

chemistry when different groups of varying polarities are attached to a parent compound, many of its physical and chemical properties are affected. This has been mostly explained by the electron-donating and withdrawing effects of the polar substitutents by both the resonance and inductive effect. Analogously, the polyethylene backbone can be pictured as the parent compound and the physcial properties such as the strain-optical coefficient can be studied by varying the polarity of the substituents attached. Such polar groups can be of both electron-donating and electron-withdrawing nature ; examples are methyl group in highly branched and ethylene-propylene copolymer, fluorine group in vinyl fluoride and fluorinated polyethylene, chlorine group in vinyl chloride and chlorinated polyethylene, cyanide group in poly-acrylonitrile, OH group in polyvinyl alcohol, $COOCH_3$ group in polymethacrylate etc. One important point here will be to have the same parent low density polyethylene sample, and the substituent concentration has to be the same for all the substituted polyethylenes.

(2) Effect of Size of the Substituent: This effect could be best studied by choosing substituents with approximately the same polarities but different sizes. Polyacrylonitrile and polyalkylacrylates would be very interesting and convenient samples to study. While CN, COOR have fairly similar polarity, their sizes are very different and can be varied by the proper choice of the alkyl group in COOR. Samples with similar substituent content would furnish us with the effect of soze of such substituents.

(3) Concentration Effect of the Substituents: This would be the similar

kind of study which has been described previously for carbonyl containing polyethylenes. Perhaps a wider range of concentration would furnish us with a better contrast in the results. It is suggested that commercially available different degree chlorinated polyethylenes would be suitable for such type studies.

(4) Location of the Substituent in Different Regions : Such studies would furnish us with the information of the molecular mechanisms involved in different regions of the samples. Thermally oxidized polyethylenes could produce carbonyl group in both the amorphous or crystalline phase depending on the temperature of the oxidation process. Above the melting point, oxidation would occur randomly providing a randomly carbonyl containing sample in both the crystalline and amorphous regions, while that below the melting point would give us samples containing carbonyl groups in the amorphous phase. A different in the K' value will provide us with a clear-cut picture of the assignment of motion and mechanism in both of the phases.

While the dynamic birefringence is a limited tool in that it measures the total orientation of the crystalline, amorphous and the phase boundary regions, more discriminating techniques could be augmented to single out molecular motion in some specific regions. These are:-

(a) X-ray diffraction studies which only look into the orientation of the crystalline region.

(b) Dielectric studies which will provide us with relaxation spectra which can be interpreted on the bases of some molecular relaxation process due to some particular group in the polymer.

(c) Nuclear magnetic resonance studies on substituted polyethylenes containing atoms with nuclear spin. This will provide us with the information of the molecular relaxation process of the substituent.

(d) Dynamic fluorescence polarization studies on inherently fluorescent or fluroescent group attached polymer, so that orientation of the fluorescent group which are representative of a particular region can be studied.

(e) Dynamic infrared dichroism studies on polymers containing well-assigned and non-overlapping peaks would furnish us with information about the orientation of certain function groups which are located in some specific regions.

1. O. Gerngross, K. Horrman and W. Agitz., Z. Physik Chem. B 10, 371 (1930)
2. O. Kratky and H. Mark, Z. Physik. Chem. B 36, 129 (1939)
3. A. Keller in R.H. Doremus, B. W. Roberts and D. Turnbull, "Growth and Perfection of Crystals", Wiley, New York, 1958, pp.499-532
4. R. Eppe, E. W. Fisher and H. A. Stuart, J. Polym. Sci., 34, 721 (1959)
5. H. D. Keith and F. J. Padden, Jr. papers read at American Physical Society meetings at Monterey, Calif. Marach 1961 and Baltimore, Maryland 1962., and at Symposium on Polymer Morphology. Camitle, Dreyfus Laboratory, Research Triangle Inst., July, 1963.
6. F. J. Padden, Jr., and H. D. Keith, J. Appl. Phys.,30, 1479 (1959)
7. J. Mann and L. Rolden-Gonzalez, J. Polym. Sci., 60, 1 (1962)
8. M. B. Rhodes and R. S. Stein, Polymer Letter, 1, 663 (1963)
9. A. Keller, J.Polym. Sci, 39, 151 (1959)
10. F. P. Price, J. Polym. Sci., 39, 139 (1959)
11. H.D. Keith and F. J. Padden, Jr., J. Polym. Sci., 39, 101, 123 (1959)
12. M. Takayanagi, Memoirs of Faculty of Engineering, Kyushu Univ., (Fukuoka, Japan) 23, 41 (1963)
13. R. S. Moore and S. Matsuoka, Abstract of 4th International Congress on Rheology, Brown Univ., Providence, R.I. p.204, August 1963. J. Polym. Sci., C, (No.5), 163 (1964).
14. M. B. Rhodes, D. A. Keedy and R. S. Stein, J. Polym. Sci., 62, S73 (1962)
15. P. Erhardt, K. Sasaguri and R. S. Stein, J. Polym. Sci., C, (No.5) 179 (1964)
16. K. Sasaguri, S. Hoshino and R. S. Stein, J. Appl. Phys., 35, 47 (1964)
17. P. Geil, Polymer Single Crystal, J. Wiley, New York, (1963)

18. R. S. Stein and M. B. Rhodes, J. Appl. Phys., 31, 1873 (1960)

19. I. L. Hay and A. Keller, Kolloid-Z, 204, 43 (1965)

20. K. Kobayashi and T. Nagasawa, J. Polym. Sci., C, No.15, 163 (1967)

21. P. F. Erhardt and R. S. Stein, J. Polym. Sci., B3, 553 (1965)

22. P. F. Erhardt and R. S. Stein, J. Appl. Phys., Applied Polymer Symposia, No.5, 113 (1967)

23. K. Sasaguri, S. Hoshino and R. St. Stein, J. Appl. Phys., 35, 3188 (1964)

24. K. Fujino, H. Kawai, T. Oda and H. Maeda, Proc. Fourth Inter. Congr. Rheol., Interscience, New York, 1965, Part 3, p.501.

25. T. Oda, S. Nomura and H. Kawai, J. Polym. Sci., A3, 1993 (1968)

26. T. Oda, N. Sakaguchi and H. Kawai, J. Polym. Sci, C, No. 15, 223 (1966)

27. S. Iwayanagi and H. Nakane, "Role of the Lamellar Boundary in the Relaxation of Crystalline Polymers" in Preparation.

28. K. Iohara, K. Imada and M. Takayanagi " Thermal Expansion of Lattice Constants of P. E. Single Crystal" in press.

29. R. Hayakawa and Y. Wada, Rep. Prog, Polym. Phys. Japan, 11, 215 (1968)

30. R. S. Stein, S. Onogi, K. Sasaguri and D. A. Keedy, J. Appl. Phys., 34, 80 (1963)

31. S. Onogi, T. Asada, Y. Fukui and T. Fujisawa, J. Polym. Sci., A2, 5, 1067 (1967)

32. A. Takeuchi and R. S. Stein, J. Polym. Sci., A2, 5, 1079 (1967)

33. S. Hoshino, J. Powers, D. G. Legrand, H. Kawai and R. S. Stein, J. Polym. Sci., 58, 185 (1962)

34. O. Weiner, Abhandl, Kgl. Schs. Ges. Wiss. Math-Physik Klasso, 32, 509 (1912)

35. R. S. Stein, J. Polym. Sci., 34, 709 (1959)

36. C. W. Bunn and R. de Daubeny, Trans Faraday Soc., 50, 1173 (1954)

37. R. S. Stein and R. H. Norris, J. Polym. Sci., 21, 381 (1956)

38. S. Onogi, D. A. Keedy and R. S. Stein, J. Polym. Sci., 50, S15 (1961)

39. R. S. Stein and D. A. Keedy, J. Polym. Sci., 57, 801 (1962)

40. D. G. Legrand and P. F. Erhardt, Trans. Soc., Rheol. 6, 301 (1962)

41. R. Yamada, J. Polym. Chem., (Japan), 20, 97 (1963)

42. R. Yamada, C. Hayshi, S. Onogi, and M. Horio, J. Polym. Sci., C5, 123, (1964)., J. Soc. Material Sci., Japan 12, 812, (1963), 13, 117 (1964)

43. B. E. Read, Technique of Polymer Sci., S.C.I. Monograph No. 17, Society of the Chemical Industry, London (1963), p. 198.

44. B. E. Read, Polymer 5, (1) (1964)

45. J. F. Rudd, Polymer Letter 3, 345 (1965)

46. R. Yamada and R. S. Stein, J. Appl. Phys., 36, 3005 (1965)

47. R. D. Andrew, Ind. Eng. Chem., 44, 707 (1952)

48. W. Kuhn, U.Kunzle and A. Preissman, Helv. Chim. Acta., 39, 307, 839 (1947)

49. H. Kawai, T. Itoh, D. A. Keedy and R. S. Stein, J. Polym. Sci.,B2, 1075 (1964)

50.T. Kawaguchi, T. Ito, H. Kawai, D. Keddy and R. S. Stein, ONR report No. 97, Nov., 1967, Polymer Research Inst., U. of Mass.

51. T. Ito, T.Oda, Kawai, T. Kawaguchi, D. A. Keedy and R. S. Stein. The Review of Scientific Instrument., 39, No. 12, 1847-1858, 1968

52. R. S. Stein, J. Polym. Sci., 31, 327 (1958)

53. J. J. Hermans, P. Hermans, D. Vermaas and A. Weidinger, Rec. Trav. Chem. 65, 427 (1946)

54. Z. W. Wilchinsky, J. Appl. Phys., 31, 1969 (1960)

55. K. Sasaguri and R. S. Stein, J. Polym. Sci.,C5, 139 (1964)

56. S. Clough, M. B. Rhodes and R. S. Stein, J. Polym. Sci., C, No. 18, (1967)

57. A. R. Stokes, X-ray Diffraction by Polycrystalline Materials, H. S. Peiser et. al. Eds. (The Institute of Physics, London, 1955) Chapter 17, p.424.

58. C. R. Desper, Ph. D. Dissertation, U. of Mass., Aug. 1966.

59. S. Krimm and A. V. Tobolsky, J. Polym. Sci., 7, 57 (1951)

60. B. E. Read, J. Polym. Sci., Pt.-C, No.5, 87 (1964)

61. S. Clough, J. J. Van Hartsen and R. S. Stein, J. Appl. Phys., 36, 3072 (1965)

62. T. Hashimoto, P. Phillips and R. S. Stein " A 3- dimemsional spherulite deformation model for static and dynamic birefringence" in print.

63. G. Raumann and D. W.Saunders, Proc. Phys. Soc., London, 77, 1028 (1961)

64. I. M. Ward, Applied Material Res. 208 (October), 1964.

65. K. W. Hillier and H. Kolsky, J. P. Lewis, J. Polym. Phys., 20, 227 (1949)

66. Ward, I. M. Proc. Phys. Soc. London, 80, 1176 (1962).

67. H. Nakayayasu, H. Markovitz and D. J. Plazek, Trans. Sco. Rheol. 5, 261 (1961).

68. S. Iwayanagi in "Solid State Physics", Vol. 14, F. Sietz and D. Turnbull, Ed., Academic Press Inc., New York, N. Y. 1963, p.458.

69. M. Takayanagi, Proc. Inter. Congress Rheol., 4th Provdience, Interscience Publisher, New York, 1963, Part 1, 1965

70. M. Takayanagi, J. Polym. Sci., 46, 531 (1960)

71. T. Aremaki, S. Minami, F. Nagatoshi, and M.Takayanagi., Rept. Prog. Polym. Phys. Jap. 7, 237 (1964)

72. T. Hidashima, Rept. Prog, Polym. Phys. Jap. 9, 279 (1966)

73. N. G. McCrum and E. L. Morris, Proc. Roy. Soc. (London), A292, 506 (1966)

74. K. H. Illers, Rheo. Acta 3, 202 (1964)

75. K. M. Sinnott, J.Appl. Phys. 37, 3385 (1966)

76. J. D. Hoffman, G. Williams and E. Passaglia, J. Polym.Sci., C, 14, 173 (1966)

77. C. Nakafuka, K.Minato and T. Takemura, Rept. Prog.Polym.Phys.Jap.11,297 (1968)

78. R.W. Penn, J. Polym. Sci, A2, 4, 595 (1966)

79. M. Takayanagi, T. Matsuo, J. Macromol. Sci.,-Phys. B1 (3), 407 (1967)

80. S. Iwayanagi and H. Nakane, Abstr. Int. Cong. Rheol., Kyoto, 1968, p.40.

81 S. Iwayanagi and H. Nakane, " Role of the Lamellar Boundary in the Relaxation of Crystalline Polymers", in preparation.

82. I. Kimura, A. Tanaka, E.P. Chang, B. Delf and R.S. Stein " Rheo-optical studies of the nature of the alpha-mechanical loss mechanism of polyethylene) in press.

83. K. Iohara, K. Imada and M. Takayanagi " Thermal Expression of Lattice Constants of Polyethylene Single Crystal" in press

84. R. Hayakawa and Y. Wada, Rep. Prog, Polym Physics , Japan 11, 215 (1968)

85. K. Schmieder and K. Wolk. Kolloid-Z., 134, 144 (1953)

86. L. E. Nielsen, J. Appl. Phys., 25, 1209 (1954)

87. Z. H. Stachurski and I. M. Ward, J. Polym. Sci., A-2, 6, 1817 (1968)

88. A. H. Willbourn, Trans Faraday Soc., 54, 717, (1958)

89. K.M. Sinnott, J. Appl. Phys., 37, 3385 (1966)

90. R. S. Stein, S. Krimm, A.V. Tobolsky, Rept. Textile Res. Journal, 1, 1949

91. I. M. Ward , Manuscript on " The Structure of Polymer"

92. I. Kimura, E.P. Chang, A. Tanaka and R.S.Stein, Polymer Preprint, 9 1212, (1968)

93. A. Peterlin, J. Polym. Sci., C, No. 15, 427 (1966)

94. R. J. Samuels, J.Polym. Sci., Pt-A, 3, 1741, (1965)

95. H. Kiho, A. Peterlin and P.H. Geil J. Appl. Phys., 35, 1599 (1964)

96. A. Peterlin, P. Ingram and H. Kiho, Makromol. Chem. 86, 294 (1965)

97. J. Harrison and J. A. Rusnock, J. Appl. Phys. 36, 332, (1965)

98. Private correspondence of S. Onogi to R. S. Stein, December 30, 1969

99. Bunn and Daubeny, Trans Faraday Soc., 1954, 50, 1173

100. R. K. Bullough J. Polym. Sci., 65, 148, (1960) p.517

101. R. S. Stein and F. H. Norris, J. Polymer Sci., 21, 381 (1956)

102. F. A. Bettelheim and R. S. Stein, J. Polymer Sci., 27, 115 (1958)

103. C. W. Bunn, Trans Faraday Soc., 35, 482 (1939)

104. Garth L. Wilkes and Richard S. Stein, ONR technical report No. 118, U. of Mass., July 1969

105. Y. Chatani, and T. Takizawa, J. Polym. Sci., 55, 811 (1961)

106. G. P. Mikhailoo, S. P. Kabin and T. A. Krylova (a) Sov. Phys. Tech. Phys. 2, 1899 (1957), (b) J. Tech. Phys., (U.S.S.R.), 27, 2050 (1957)

107. C. A. F. Tuijnman, Polymer 4, 259 (1968)

108. C. A. F. Tuijnamn, Polymer 4, 315 (1963)

109. H. C. Booij, quoted in McCrum, Read and William "Anelastic and Dielectric Effects in Polymeric Solid", Wiley, London, 1967, p.365

110. J. D. Ferry " Viscoelastic Properties of Polymers", Wiley, 1961.

111. P. J. Phillips and R. S. Stein, ONR Technical report No.124, U. Of Mass., June, 1970.

112. J. P. Schroeder and W. P. Sopchak, J. Polym. Sci., 47, 417 (1960)

113. R. J. Tetrault, W. J. Macknight and Roger S. Porter " Thermal properties of Paritally hydrolysed Ethylene-Vinyl acetate copolymer" in press.

CAPTIONS FOR FIGURES

1. The classical two-phase model of a crystalline polymer.
2. Model by Keller and Fisher and Stuart showing chain zig-zags back and forth within a single crystal.
3. Chain folding and chain re-entry in a single crystal.
4. The Hosemann paracrystalline model.
5. Spherical spherulite deforming to ellipsoidally symmetrical one.
6. Deformation of a spherulite at 6% elongation.
7. Motions of chains and lamella occuring in a deformed spherulite.
8. The Iwayanganagi Model.
9. Optical arrangement in the dynamic birefringence apparatus.
10. Heating and cooling arrangements in the dynamic birefringence apparatus.
11. A diagrammatic sketch of the collimating system.
12. Rotating sector sychronized with the sample stretching.
13. Optical arrangement of the dynamic x-ray diffractometer. (S) film sample (G) goniometer circle (X and X') incident and reflected x-ray beam .
14. A diagrammatic sketch of the dynamic diffractometer.
15. A picture of the photo-switch set consisting of a rotating semi-circular sector disk and a lamp and photo-tubes.
16. Plot of transmission versus retardation.
17. Set of Lissajous figures obtained in a dynamic birefringence measurement. Central Lissajous figure refers ideally to $\delta = \pi/2$. Upper and Lower Lissajous figures are obtained by vertical and horizontal insertion of calibrated retardation plate.
18. Lissajous figure obtained with the analyzing polariod removed.
19. A clock-wise moving Lissajous figure showing positive birefringence-strain phase angle.

47. Strain dependence of static birefringence for bulk, swollen, dried and reswollen quenched samples of low density polyethylene.
48. Strain dependence of K' for bulk, swollen, dried and reswollen quenched samples of low density polyethylene.
49. Temperature dependence of K' at 0.12 hertz for quenched low density polyethylene and 0%, 0.5% and 1% CO containing polyethylene.
50. Temperature dependence of K' at 1 hertz for quenched low density polyethylene and 0%, 0.5% and 1% CO containing polyethylene.
51. Temperature dependence of K' at 8.64 hertzs for quenched low density polyethylene and 0%, 0.5% and 1% CO-containing polyethylene.
52. Strain-optical coefficient of the 0% carbonyl containing polyethylene from 20 to 90°C, plotted logarithmically against frequency at 8 temperatures as indicated.
53. Temperature dependence of K' at 1 hertz for annealed low density polyethylene and 0%, 0.5% and 1% CO-containing polyethylene.
54. Temperature dependence of tanα at 1 hertz for annealed low denisty polyethylene and 0% , 0.5% and 1% CO-containing polyethylene.
55. Temperature . dependence of K' at 0.12 hertz for quenched low density polyethylene and the brominated, phosphonated polyethylene and E/VA./VOH terpolymer,
56. Temperature dependence of K' at 1 hertz for quenched low density polyethylene and the brominated, and phosphated polyethylene and E/VA./VOH terpolymer.

57. Temperature dependence of K' at 0.12 hertz for quenched low density polyethylene and the brominated and phosphonated polyethylene and E/VA/VOH terpolymer.

58. Master curves showing frequency dependence of K' (Reference Temperature 50°C) for quenched low density polyethylene and the brominated and phosphonated polyethylene and E/VA/VOH terpolymer.

59. Strain dependence of static birefringence , crystalline contribution $X_{cr}K_{cr}$ and form contribution Δ_F for quenched and annealed low density polyethylene.

60. Strain dependence of K',crystalline contribution $X_{cr}K'_{cr}$, amorphous contribution $(1-X_{cr})K'_{am}$ and form contribution K'_F for quenched low density polyethylene at 1 hertz.

61. Strain dependence of K',crystalline contribution $X_{cr}K'_{cr}$, amorphous contribution $(1-X_{cr})K'_{am}$ and form contribution K'_F for annealed low density polyethylene at 1 hertz.

Table I. Swelling ratio at an elongation of

Solvent	Refractive Index	10%	20%	30%	40%	50%
Carbon Tetrachloride	1.4607	1.11	1.138	1.14	1.125	1.11
Xylene	1.4980	1.08	1.13	1.128	1.10	1.06
Methyl-benzoate	1.5164	1.034	1.04	1.051	1.061	1.07
Chlorobenzene	1.5250	1.07	1.07	1.077	1.083	1.09
Trichloro-benzene	1.5713	1.212	1.25	1.202	1.193	1.19

Table II, Refractive Index of the swollen amorphous phase at an elongation of

Solvent	Refractive Index	10%	20%	30%	40%	50%
Carbon Tetrachloride	1.4607	1.444	1.4453	1.4454	1.4448	1.444
Xylene	1.4980	1.450	1.455	1.4546	1.452	1.447
Methyl-benzoate	1.5164	1.4455	1.4466	1.4485	1.450	1.4525
Chlorobenzene	1.5250	1.453	1.453	1.510	1.575	1.626
Trichloro-benzene	1.5713	1.486	1.493	1.4905	1.4896	1.485

TABLE III Summary of the Contributions of Static and Dynamic Birefringence

Type of Sample	Quenched			Annealed		
Static Strain	Low ~ 10%	Medium ~30-40%	High > 50%	Low ~ 10%	Medium ~ 30-40%	High > 50%
Δ_{cr}	80-90%	70-75%	60-70%	> 100%	> 100%	~ 80%
				> 100%	> 100%	~ 70%
Δ_{am}	~ 0%*	10-20%*	15-30%*	Negative	Negative	5-10%
				Negative	Negative	20-25%*
Δ_{form}	10%	10%	5-10%	15-20%	10-15%	10-15%
				~ 10%	5-10%	5-10%*
K'_{cr}	40-50%	50%	60-80%	~ 10%	50%	70-80%
K'_{am}	40-55%	40-50%	15-30%	65-70%	35-40%	10-20%
K'_{form}	5-10%	0-5%	5-10%	15-20%	10-15%	10-15%

* Previous Results by Hoshino et. al. J. Polym. Sci. 58, 193 (1962)

Figure 1

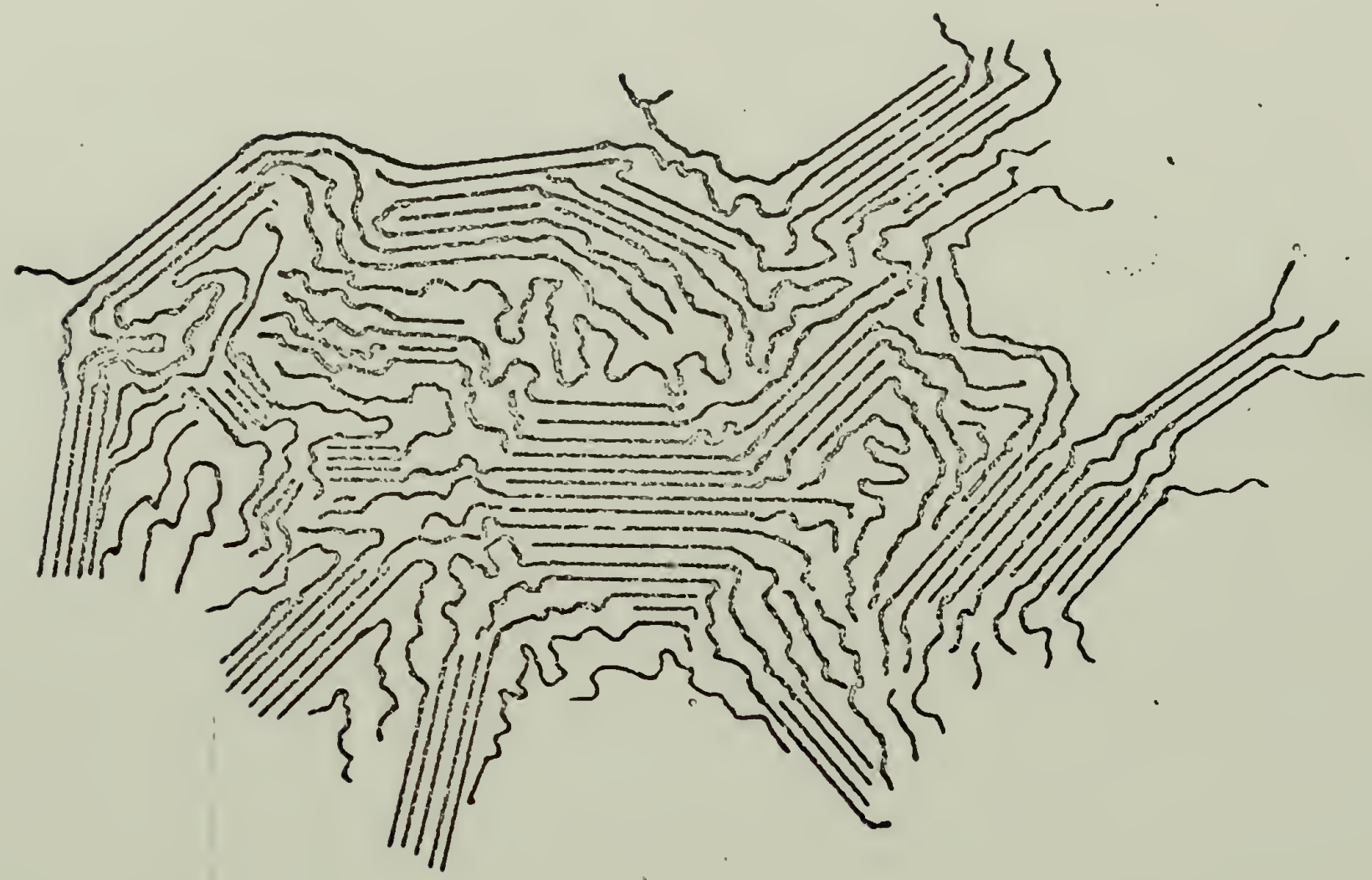

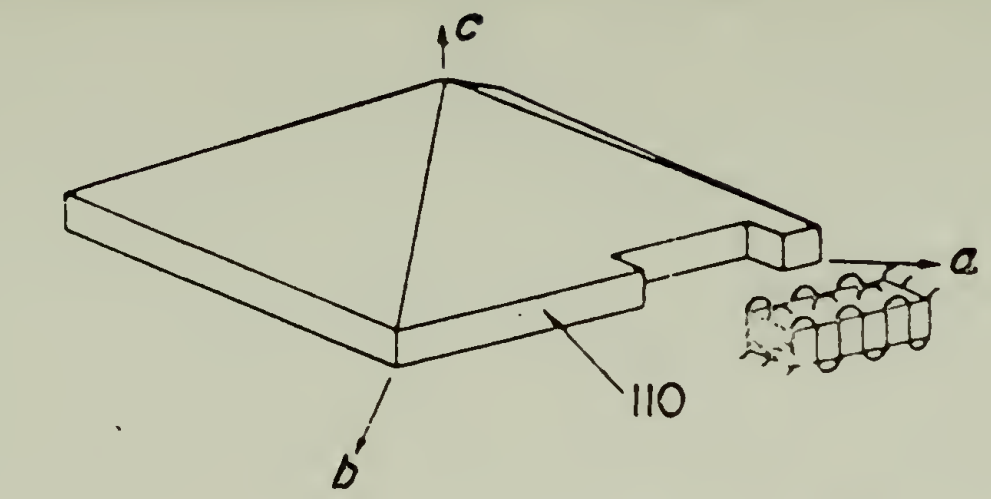

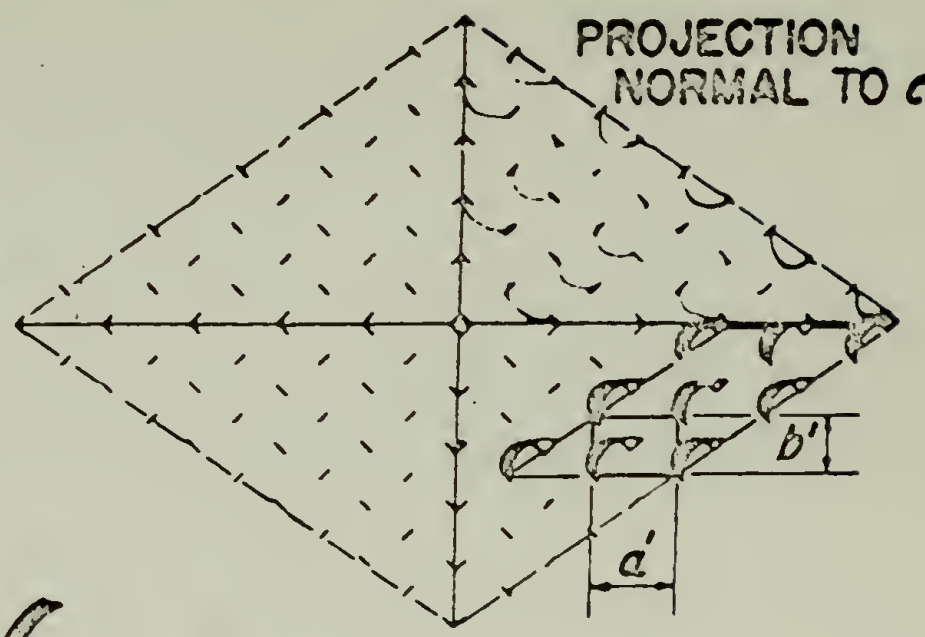

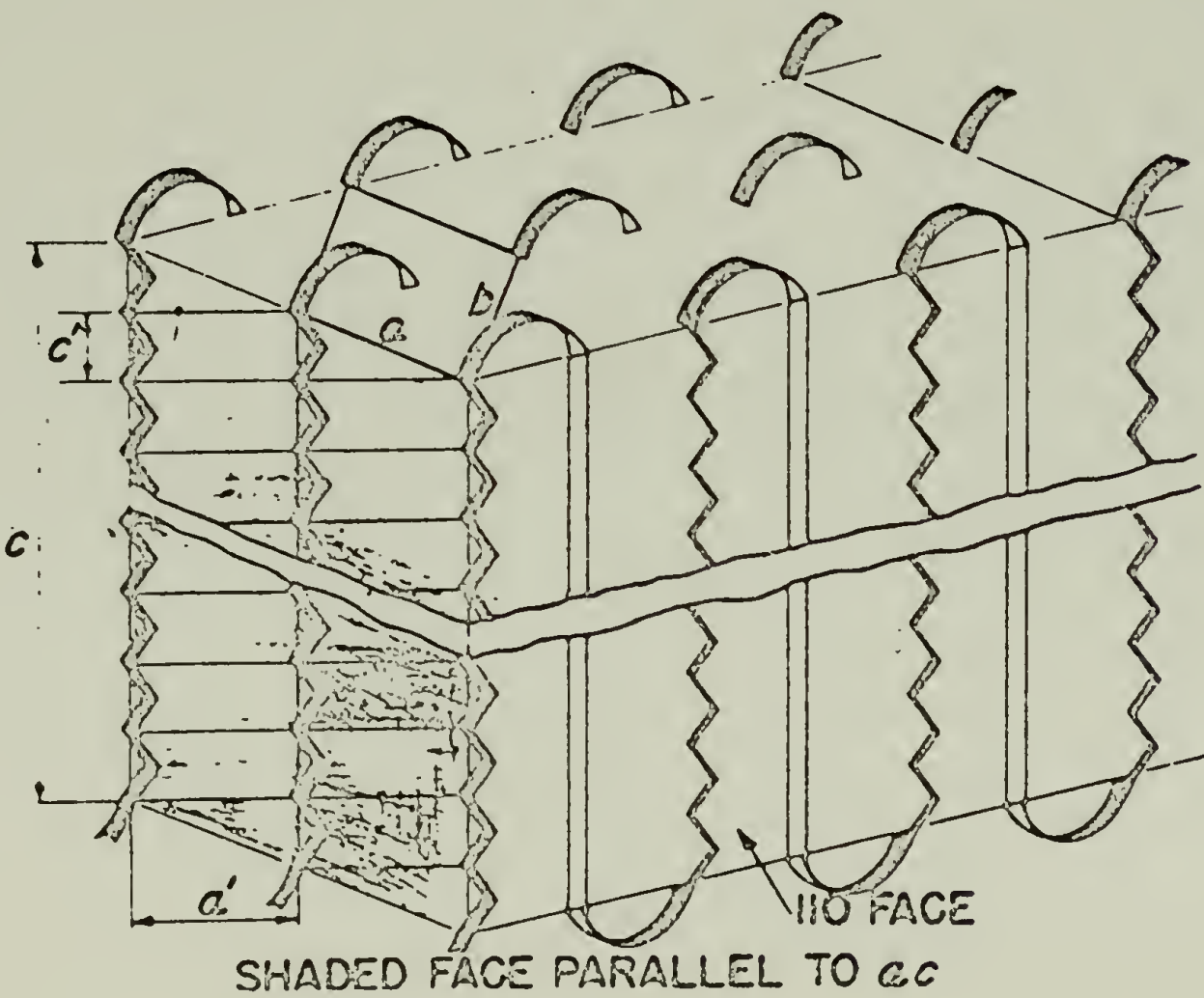

SHADED FACE PARALLEL TO *cc*

ORTHORHOMBIC SUBCELL	
a'	7.42 Å
b'	4.95 Å
c'	2.55 Å

TRICLINIC CELL	
a	7.84 Å
b	5.56 Å
c	~120 Å

Figure 2

(a)

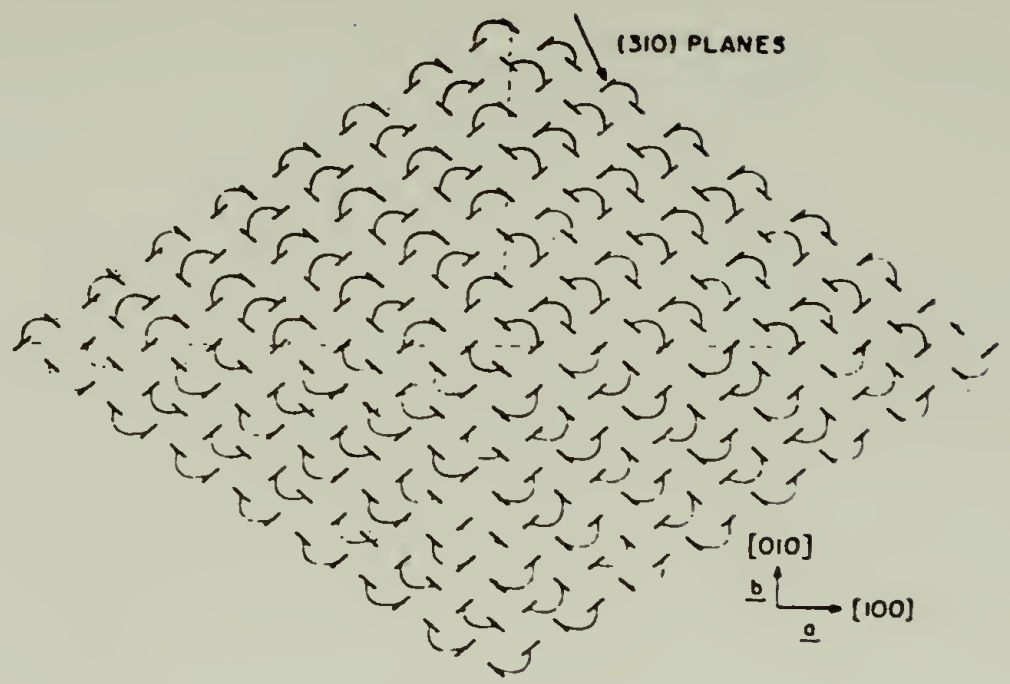

(c)

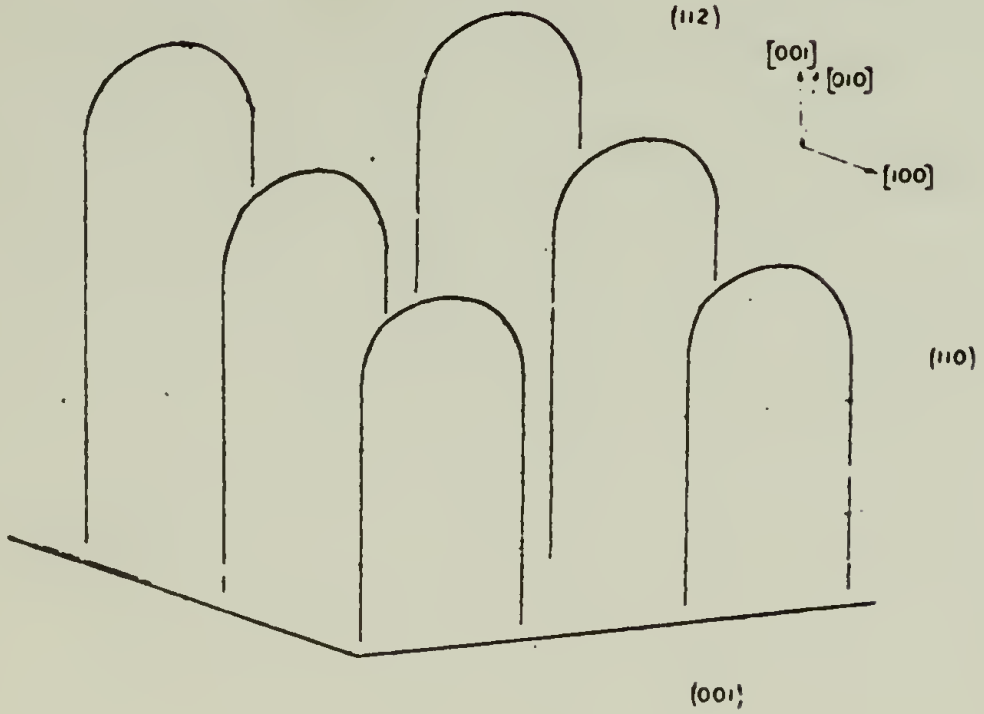

Figure 3

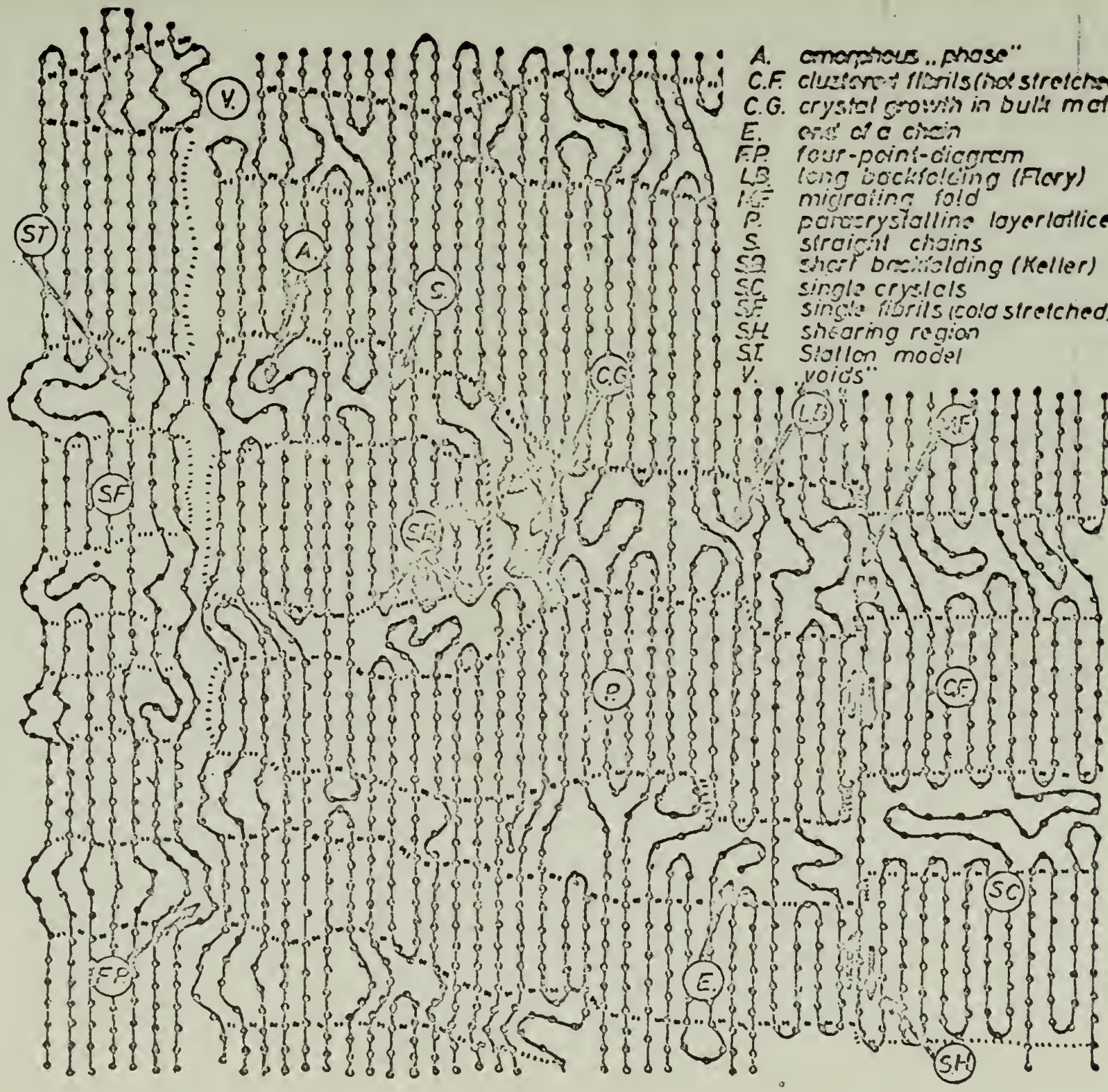
A. amorphous „phase"
C.F. clustered fibrils (hot stretched)
C.G. crystal growth in bulk material
E. end of a chain
F.P. four-point-diagram
L.B. long backfolding (Flory)
M.F. migrating fold
P. paracrystalline layerlattice
S. straight chains
S.B. short backfolding (Keller)
S.C. single crystals
S.F. single fibrils (cold stretched)
SH. shearing region
St. Statton model
V. „voids"
V.
ST
A.
S.
C.G.
L.B.
M.F.
SF
S.B.
P.
C.F.
F.P.
E.
SC
SH

Figure 4

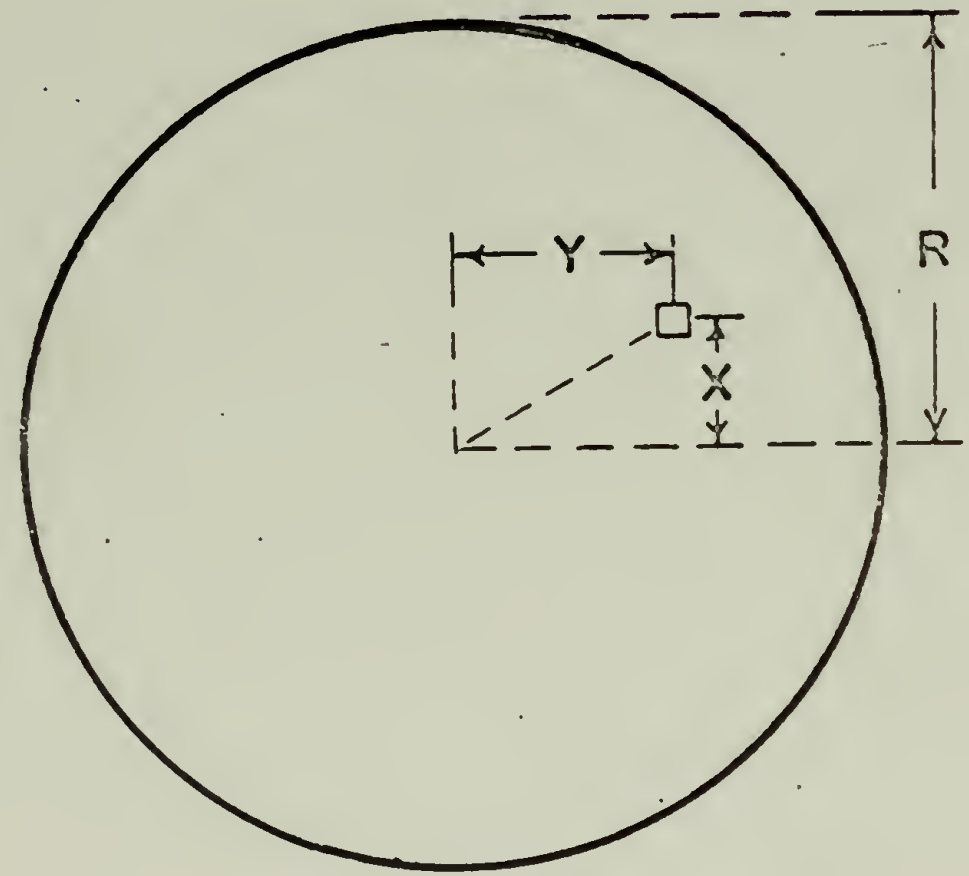

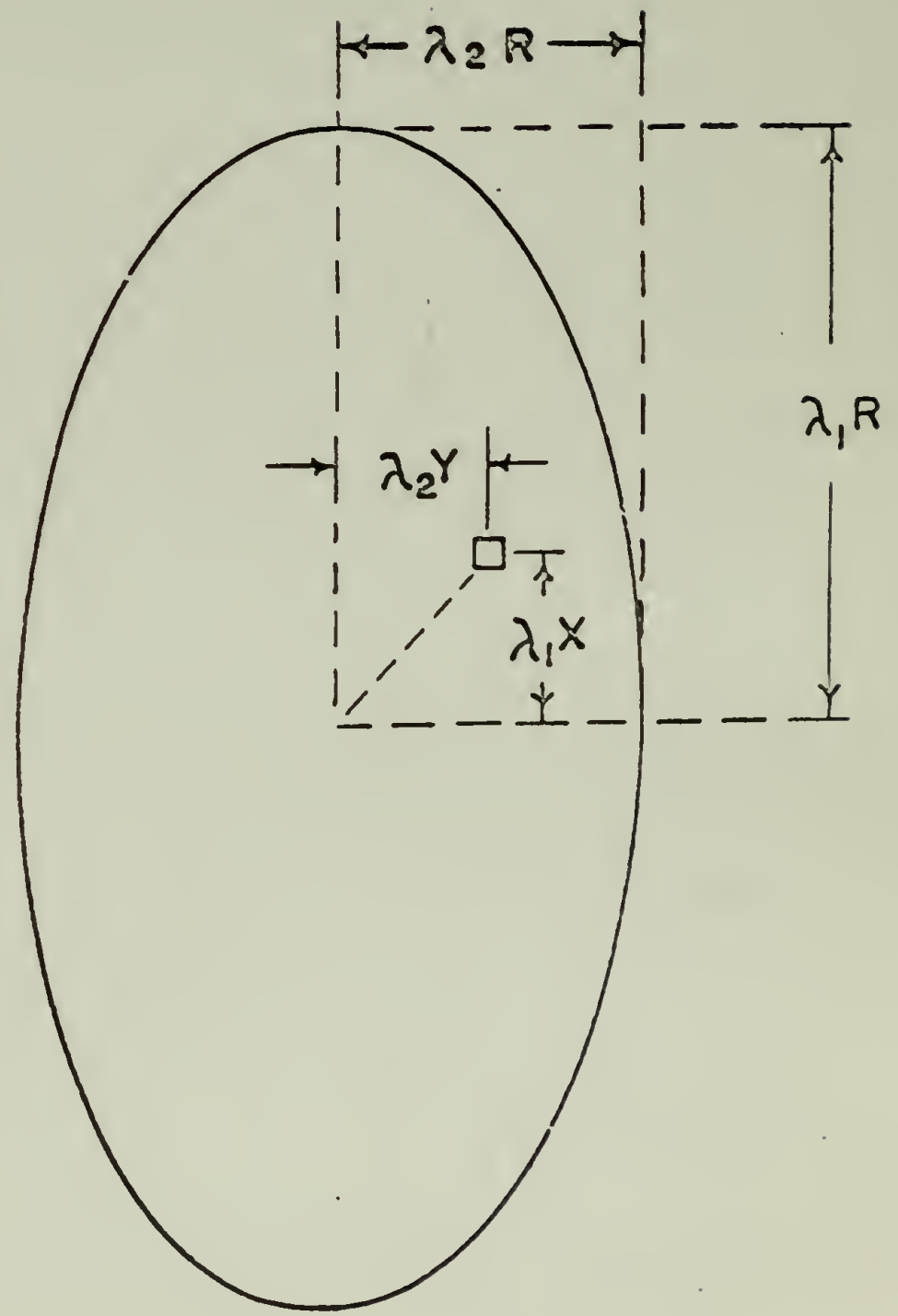

Figure 5

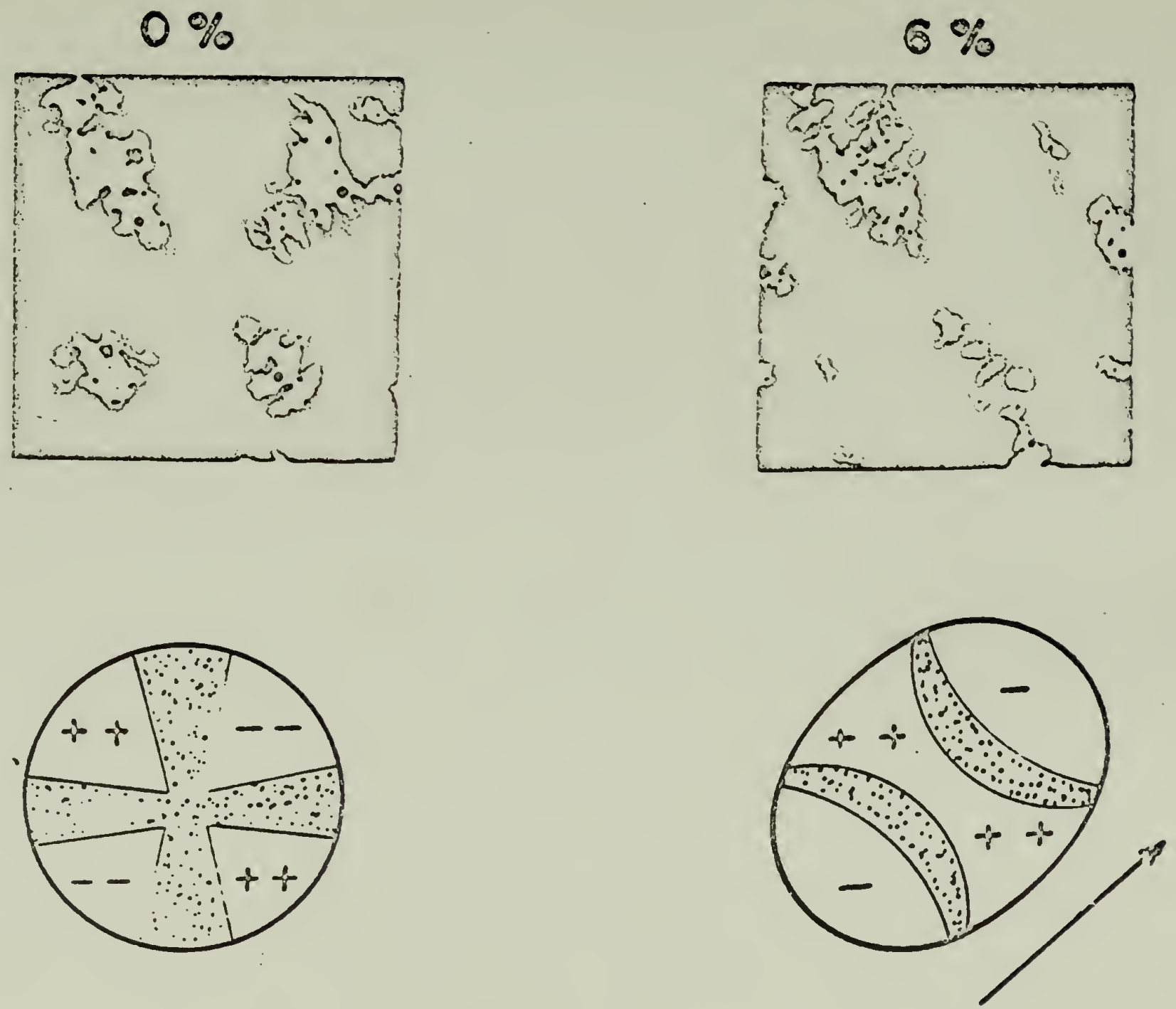

Figure 6

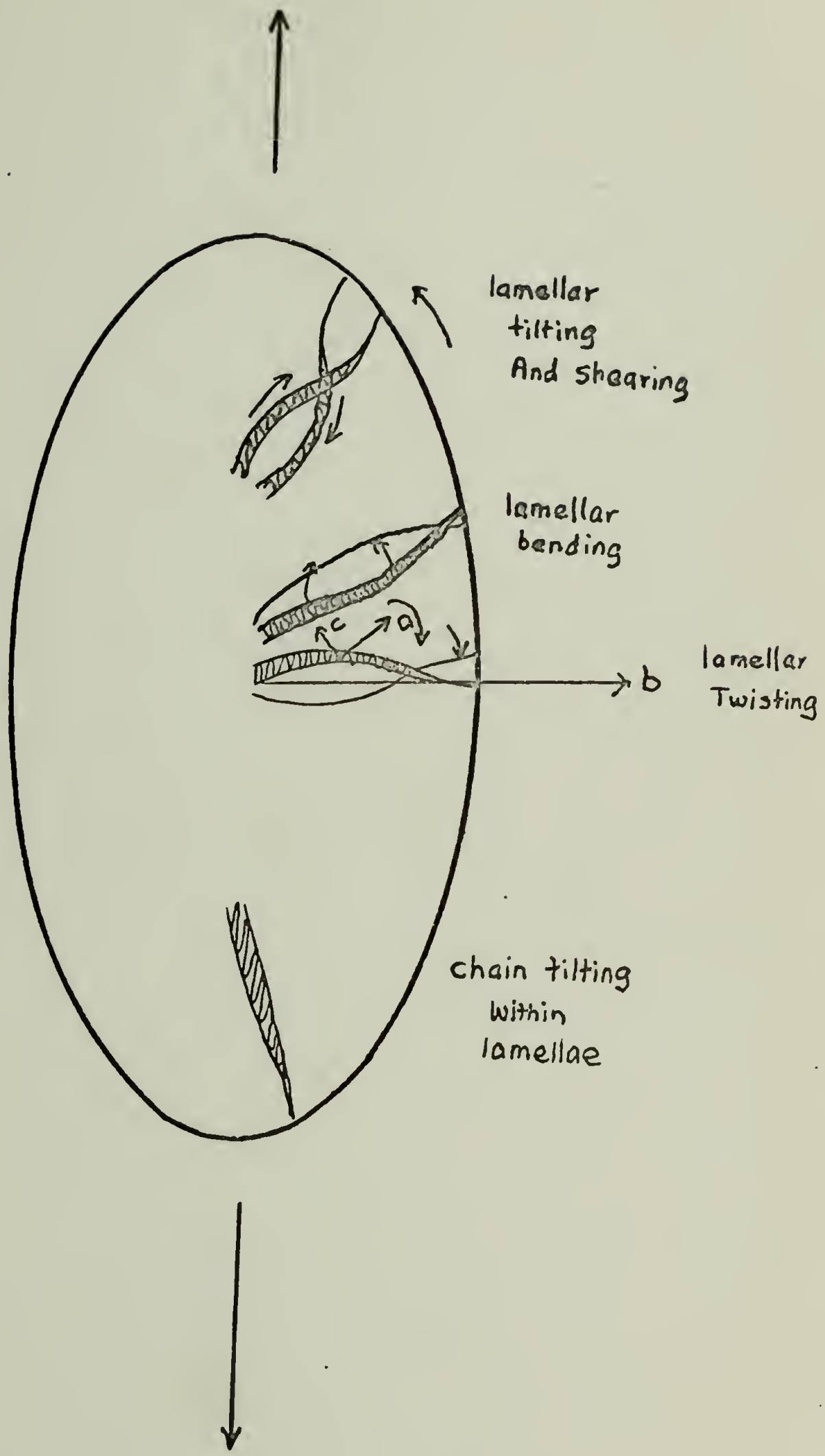
lamellar
tilting
And Shearing
lamellar
bending
c
a
b
lamellar
Twisting
chain tilting
within
lamellae

Figure 7.

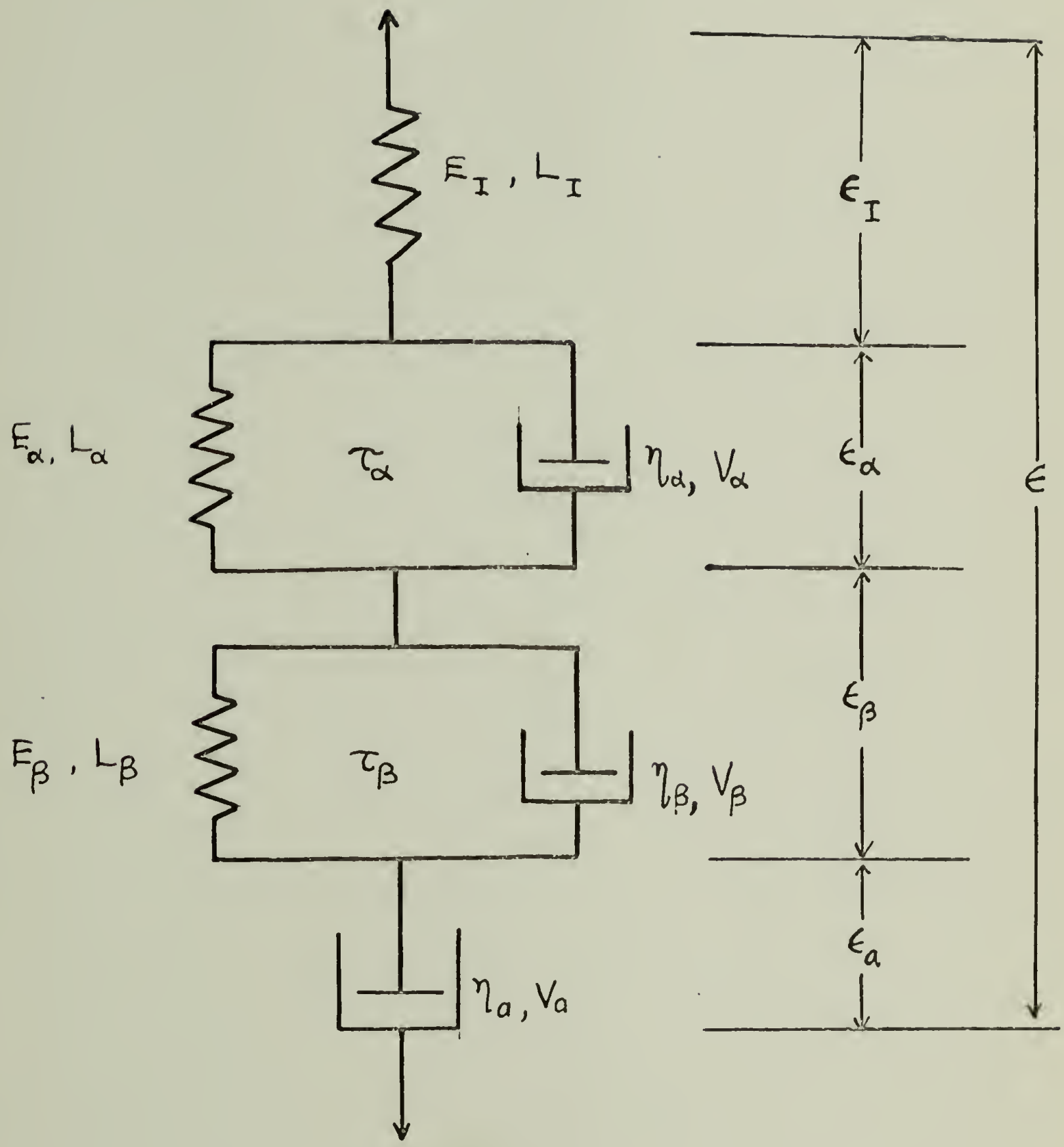

Iwayanagi Model

Figure 8

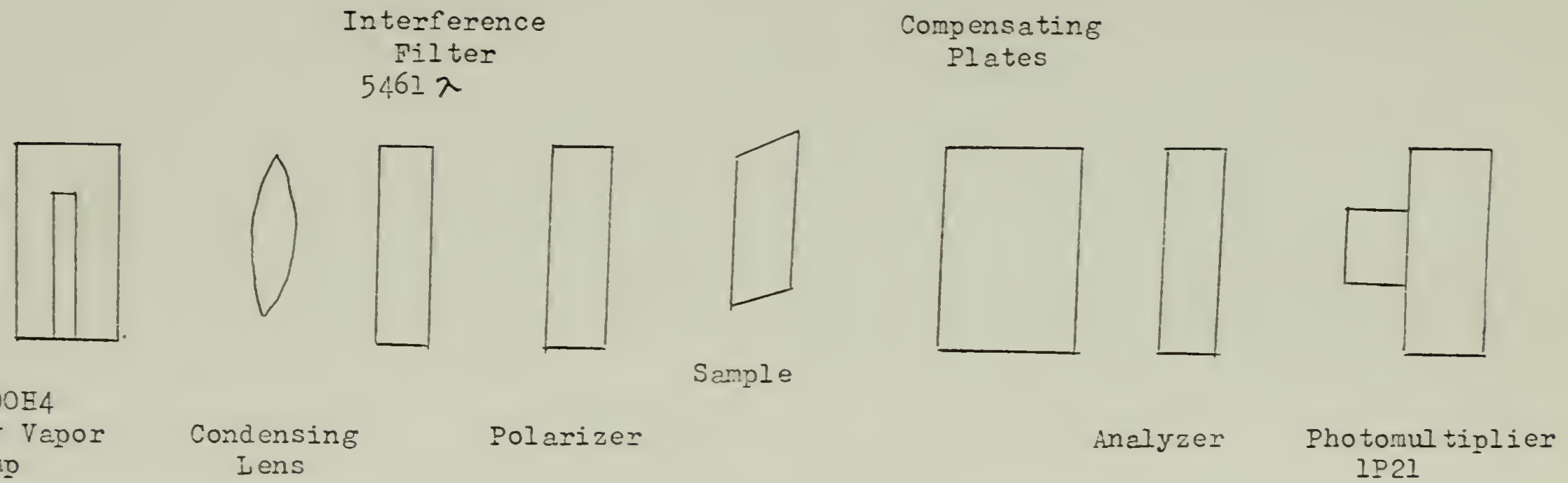
Interference
Filter
5461 λ
Compensating
Plates
Sample
A100E4
Mercury Vapor
Lamp
Condensing
Lens
Polarizer
Analyzer
Photomultiplier
1P21

Figure 9

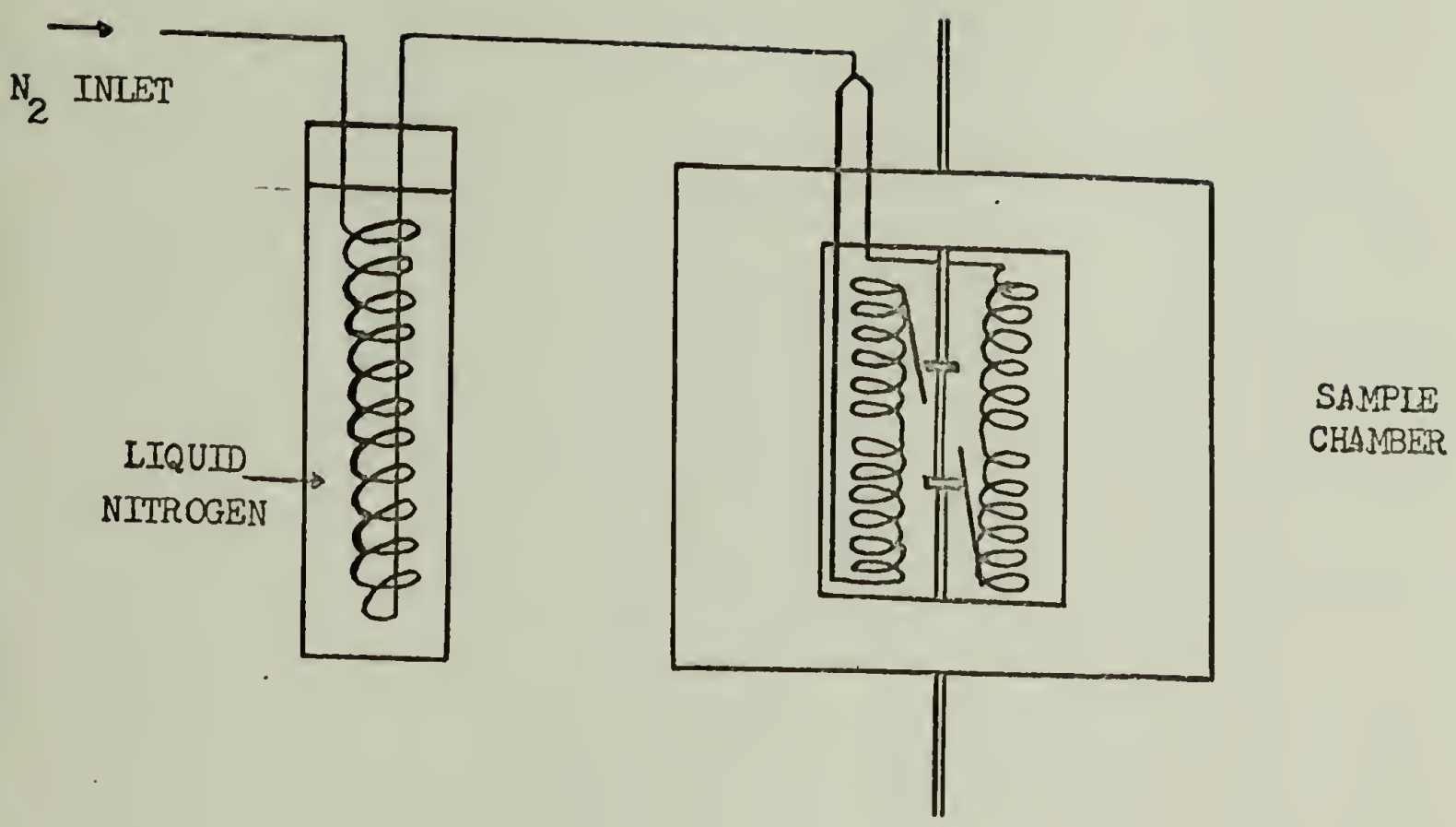
N_2 INLET
LIQUID NITROGEN
SAMPLE CHAMBER

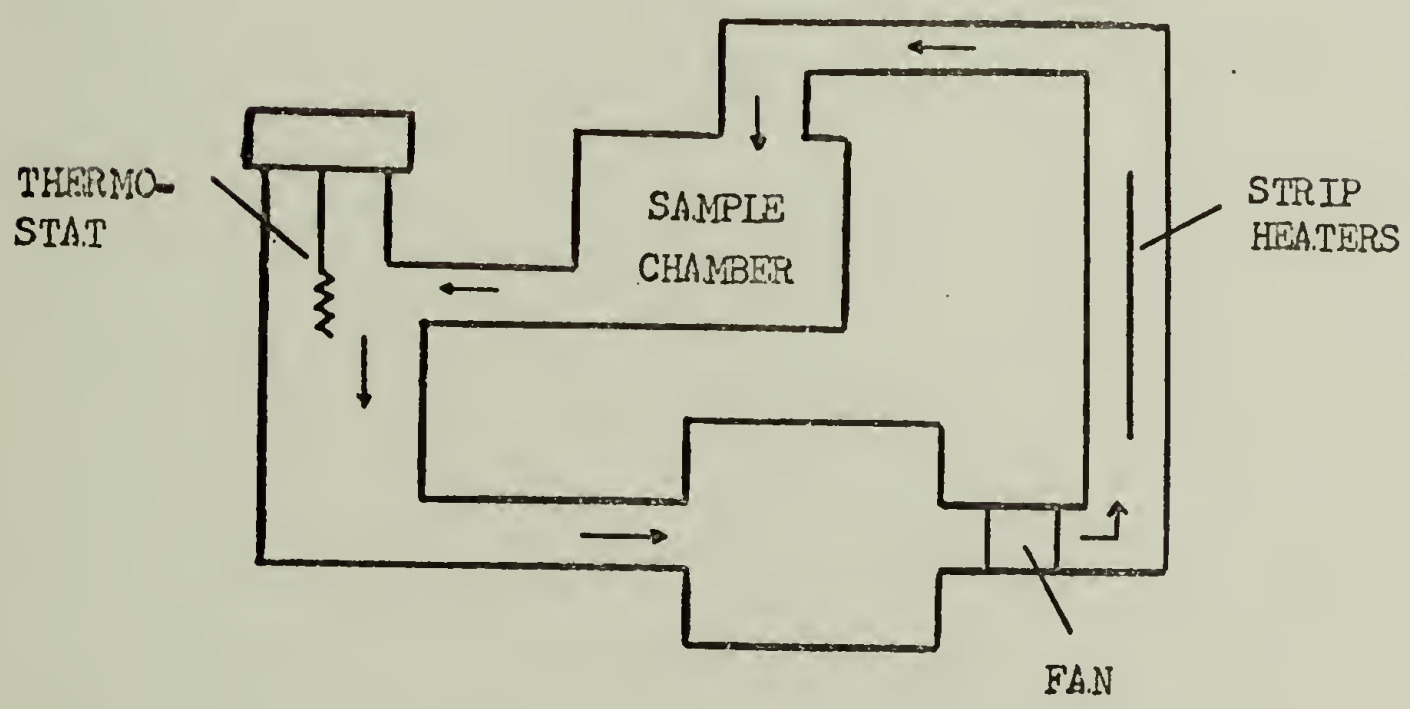
THERMO-STAT
SAMPLE CHAMBER
STRIP HEATERS
FAN

Figure 10.

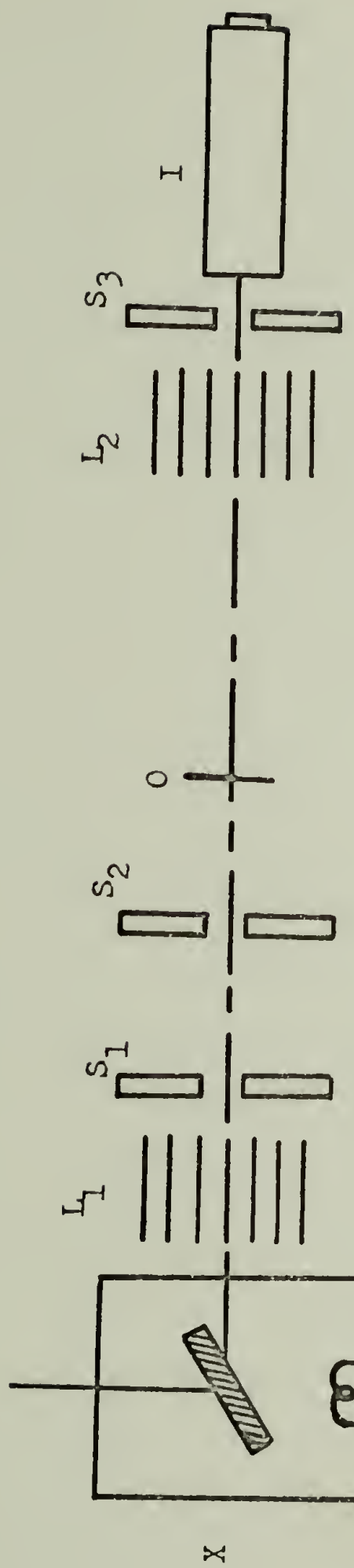

X: X-Ray Tube (EA-75, G.E.)

L_1, L_2: Soller Slits

S_1, S_2, S_3: Slit System

O: Axis of the Goniometer

I: Scintillation Detector

Figure. 11

ANGLE	CHANNEL
$0 \rightarrow \pi$	1
$\pi \rightarrow 2\pi$	4
$\pi/2 \rightarrow 3\pi/2$	2
$-\pi/2 \rightarrow \pi/2$	3

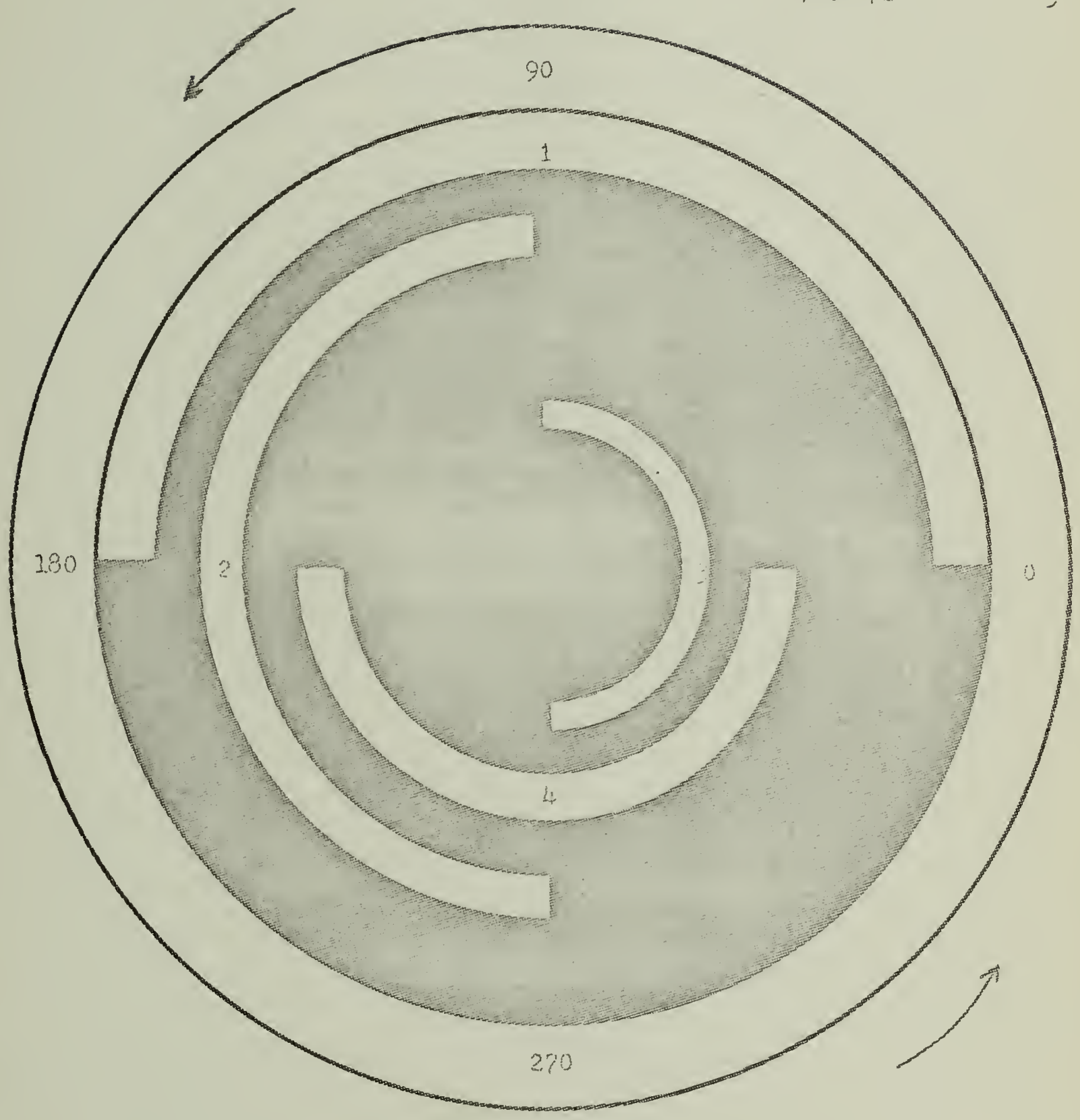

FIGURE 12. ROTATING SECTOR SYCHRONIZED WITH THE SAMPLE STRETCHING

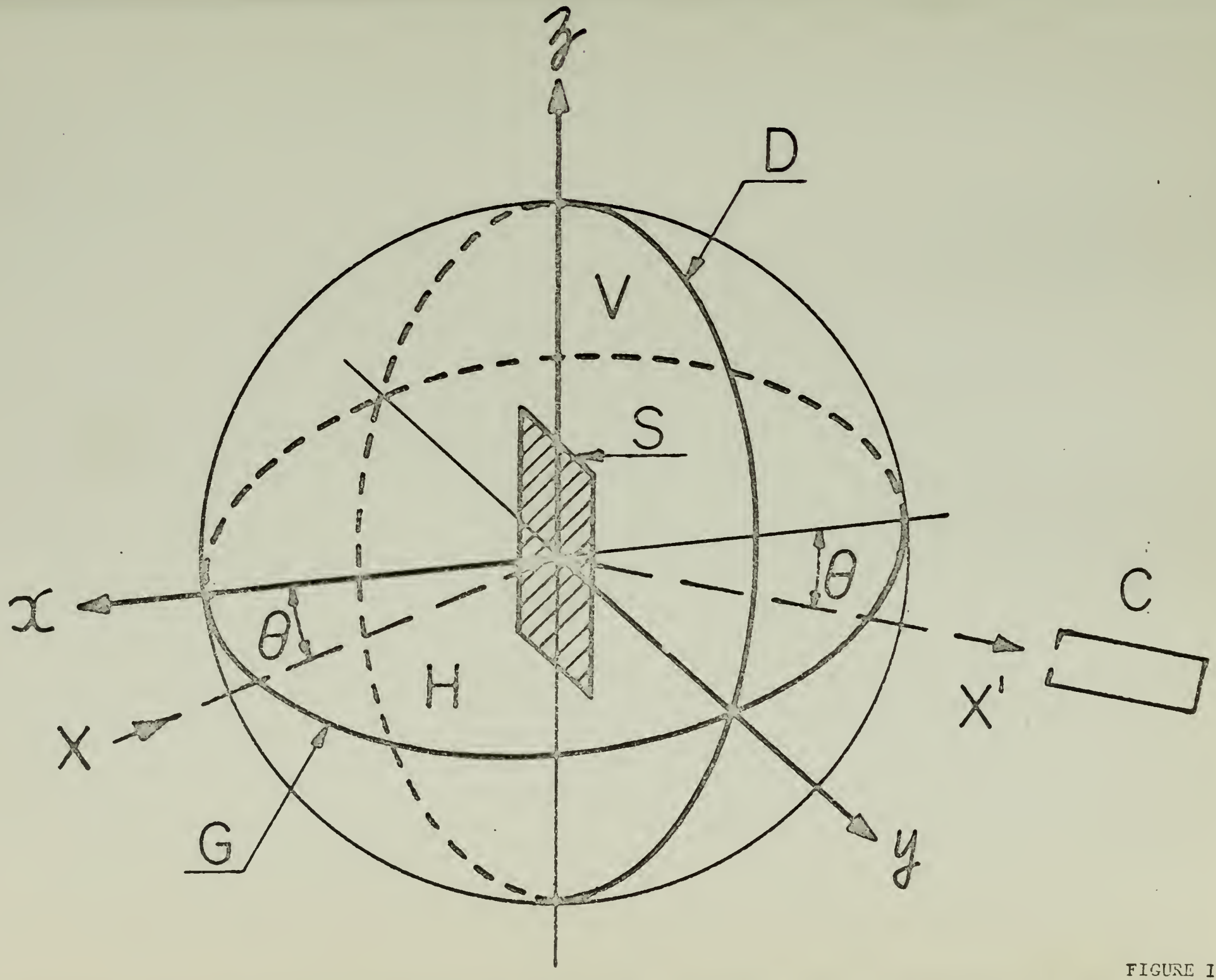

FIGURE 13

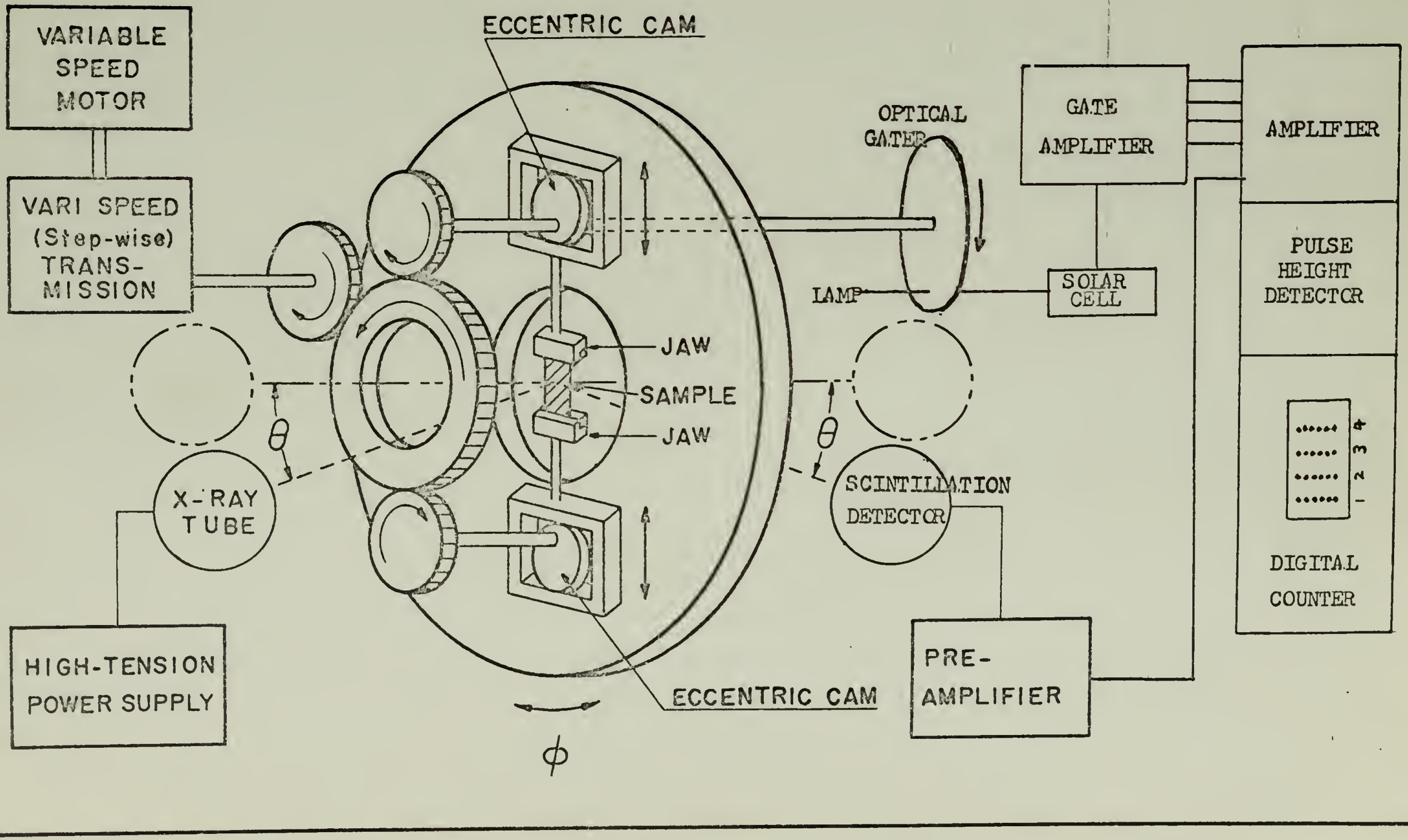
VARIABLE SPEED MOTOR
VARI SPEED (Step-wise) TRANS-MISSION
ECCENTRIC CAM
OPTICAL GATER
GATE AMPLIFIER
AMPLIFIER
PULSE HEIGHT DETECTOR
LAMP
SOLAR CELL
JAW
SAMPLE
JAW
θ
θ
X-RAY TUBE
SCINTILLATION DETECTOR
1 2 3 4
DIGITAL COUNTER
HIGH-TENSION POWER SUPPLY
ECCENTRIC CAM
PRE-AMPLIFIER
φ

FIGURE 14

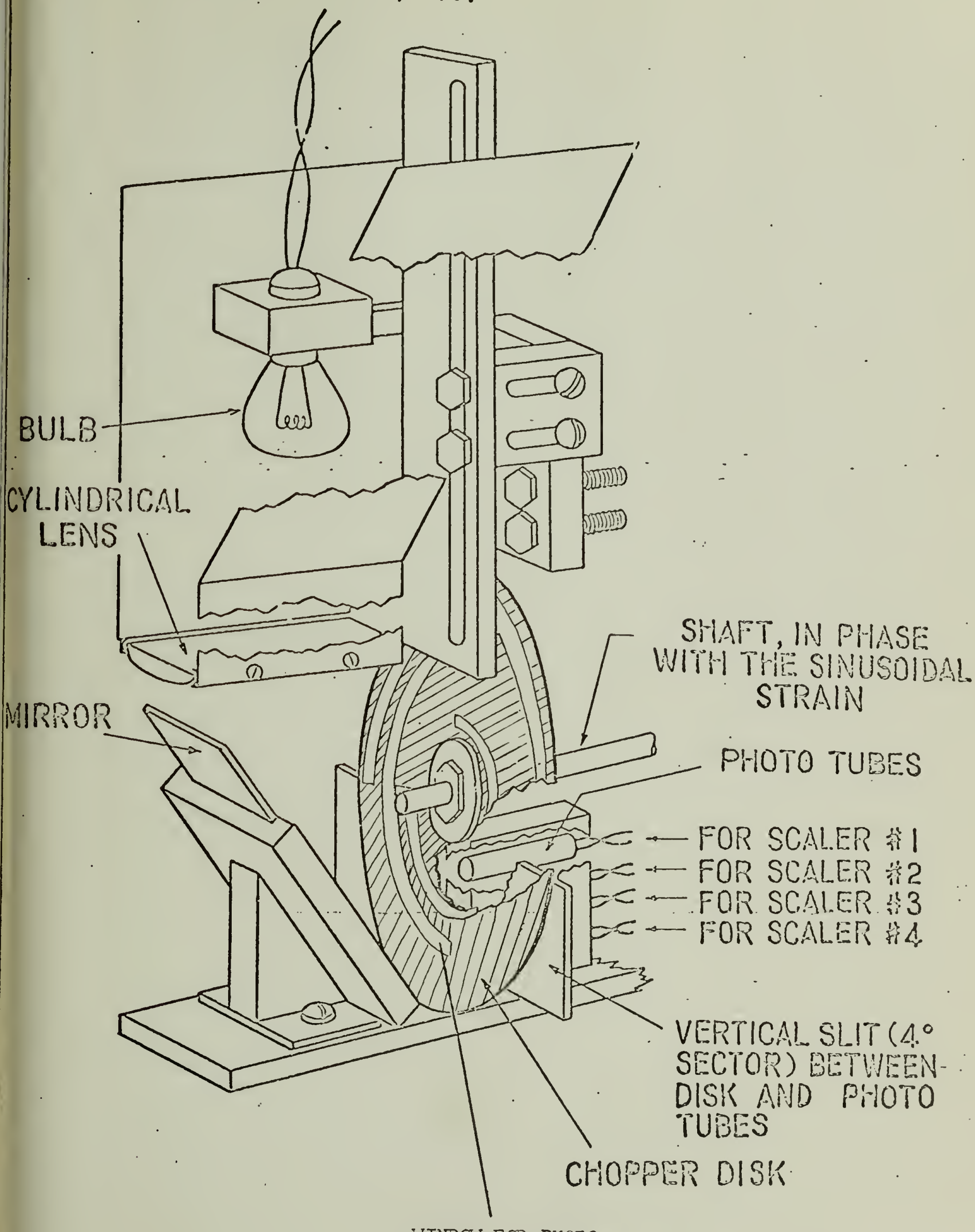
6V, A.C.
BULB
CYLINDRICAL LENS
MIRROR
SHAFT, IN PHASE WITH THE SINUSOIDAL STRAIN
PHOTO TUBES
FOR SCALER #1
FOR SCALER #2
FOR SCALER #3
FOR SCALER #4
VERTICAL SLIT (4° SECTOR) BETWEEN DISK AND PHOTO TUBES
CHOPPER DISK
WINDOW FOR PHOTO-TUBE #2

FIGURE 15

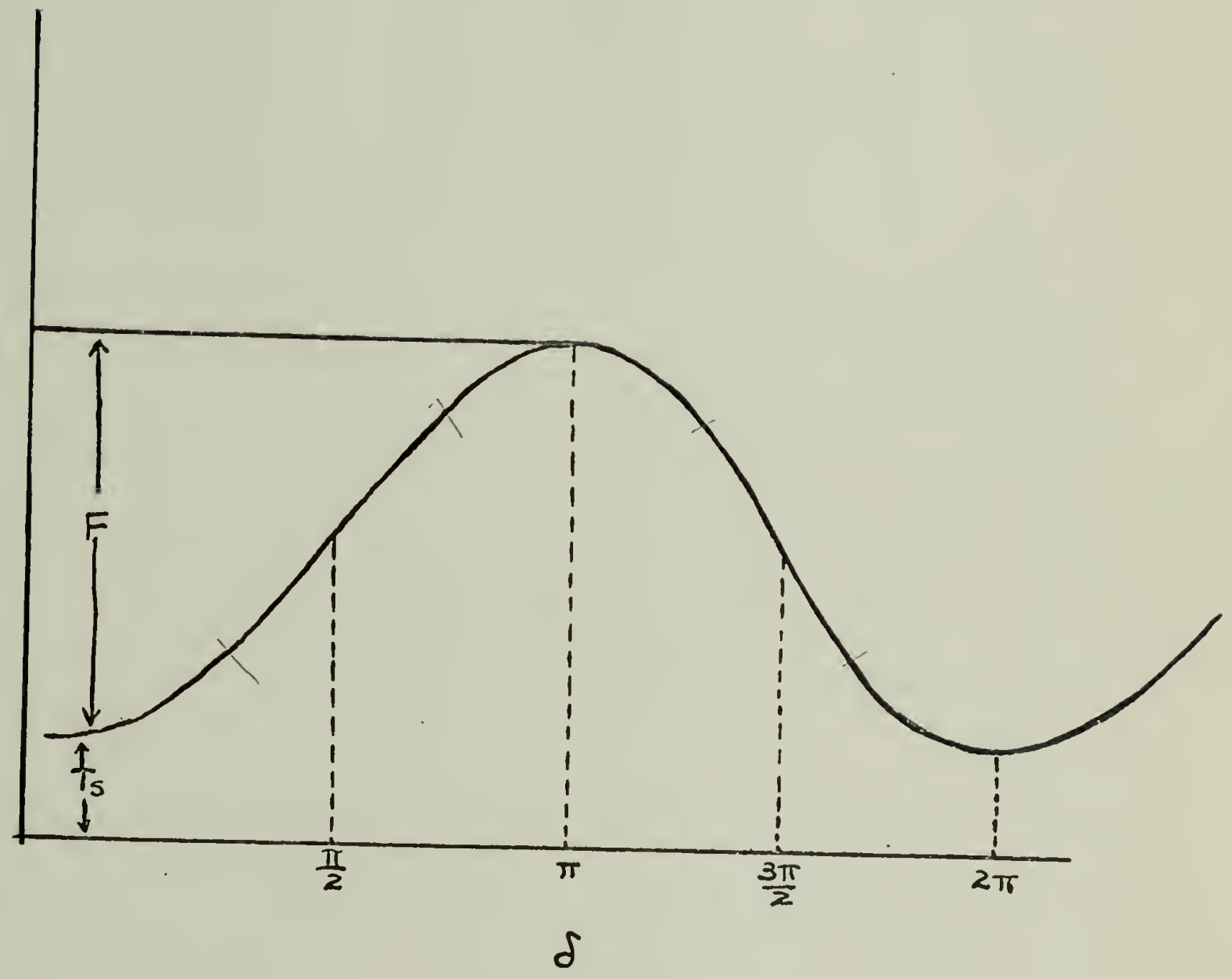

Figure 16

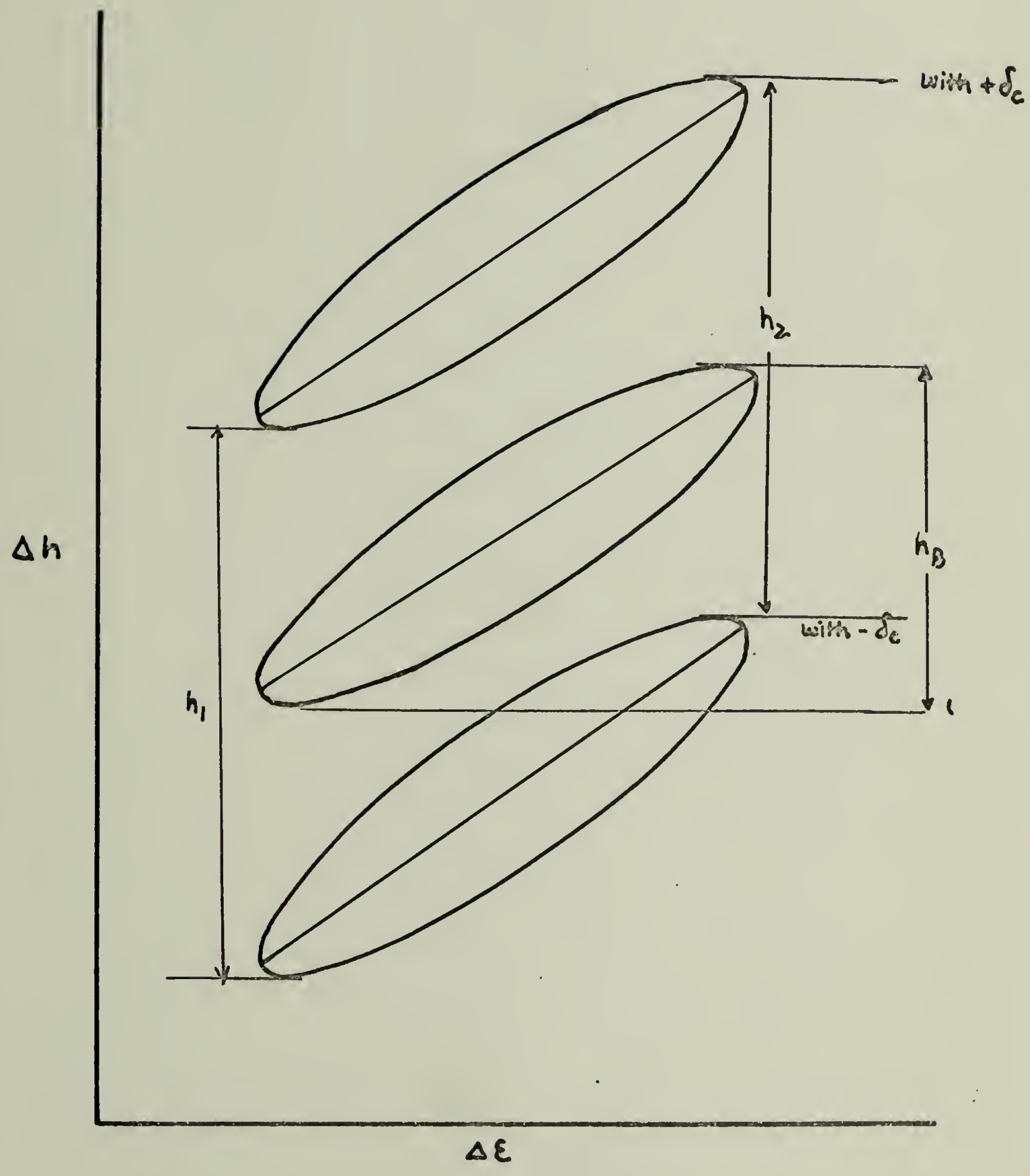

Figure 17.

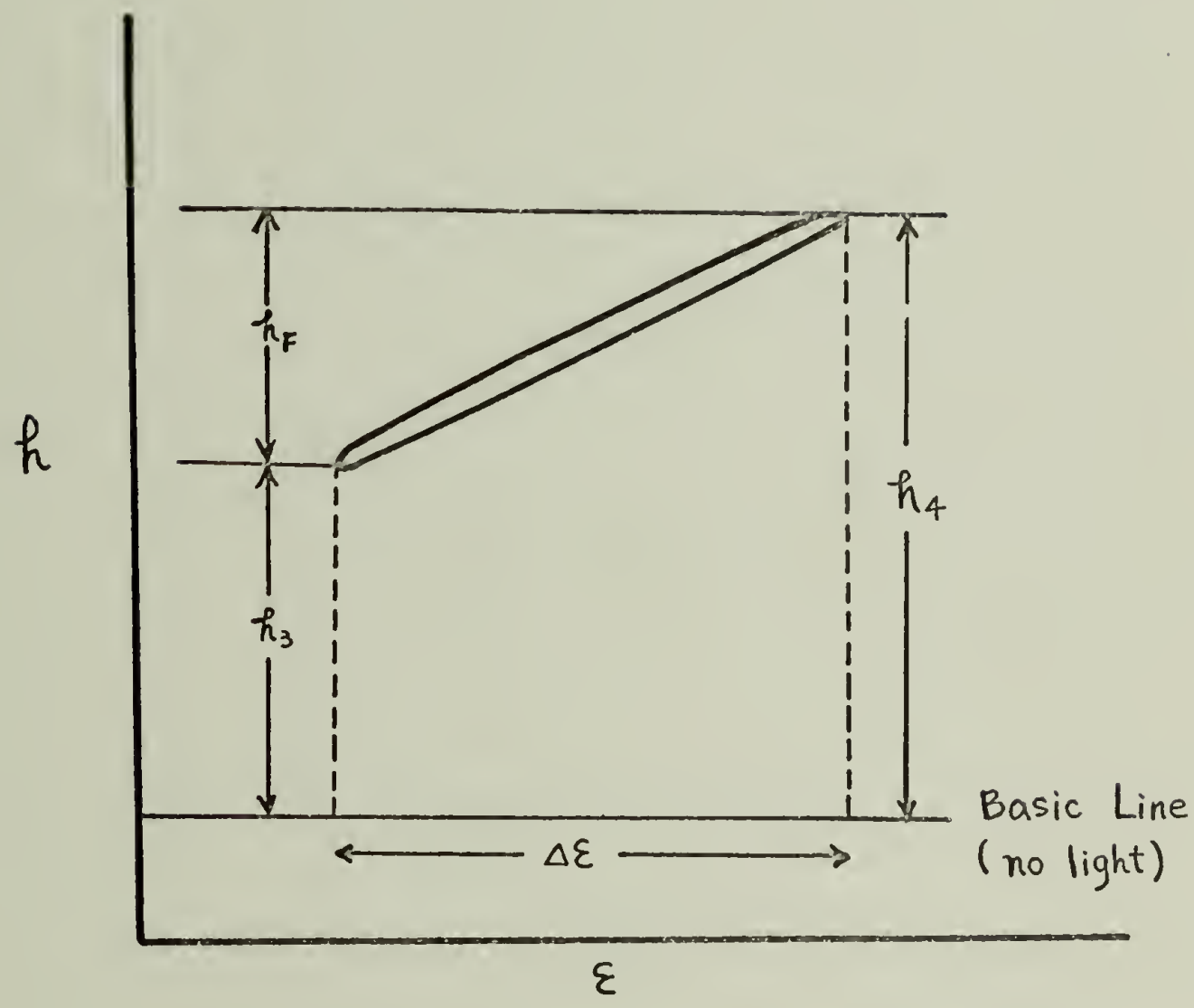

Figure 18

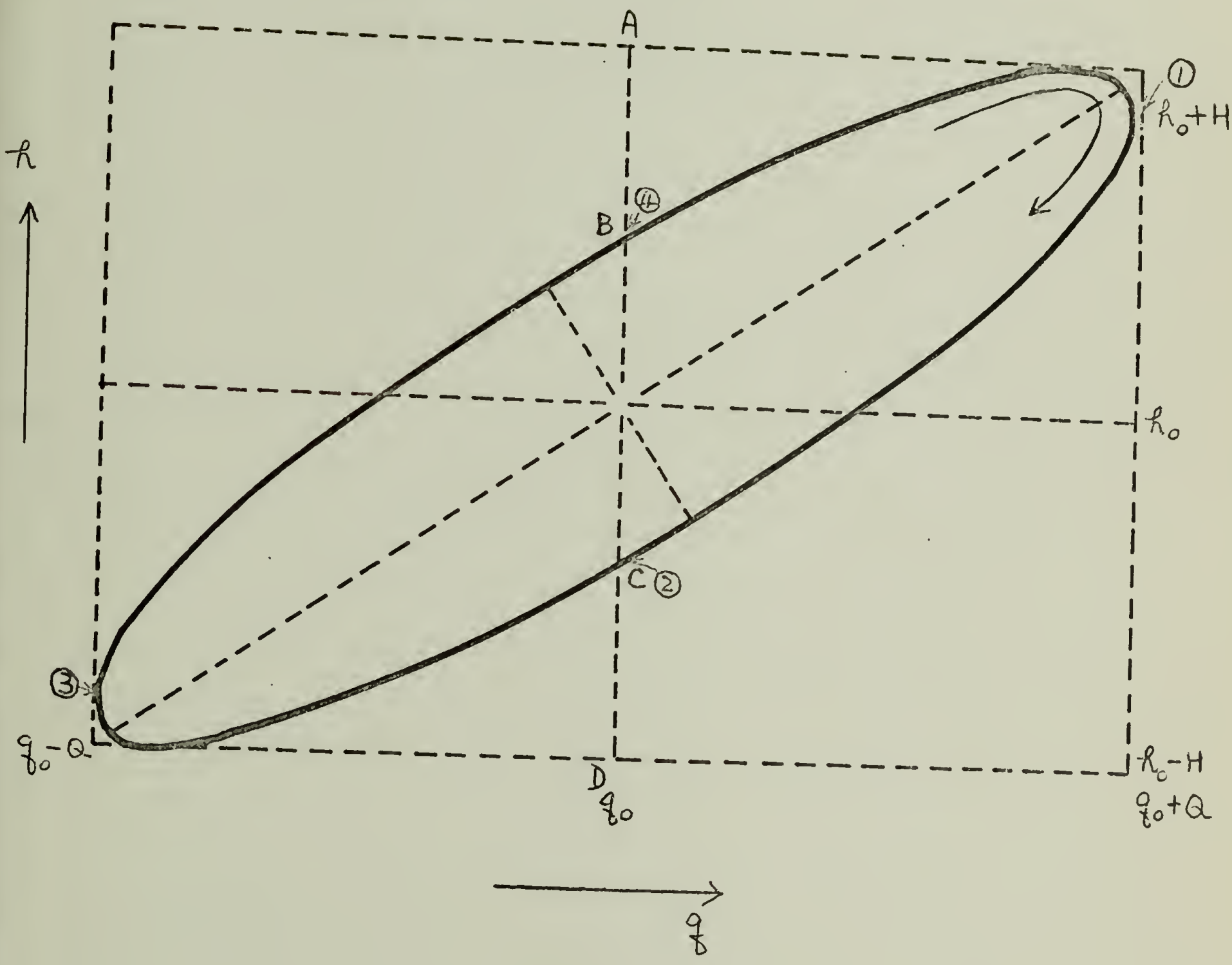

Figure 19

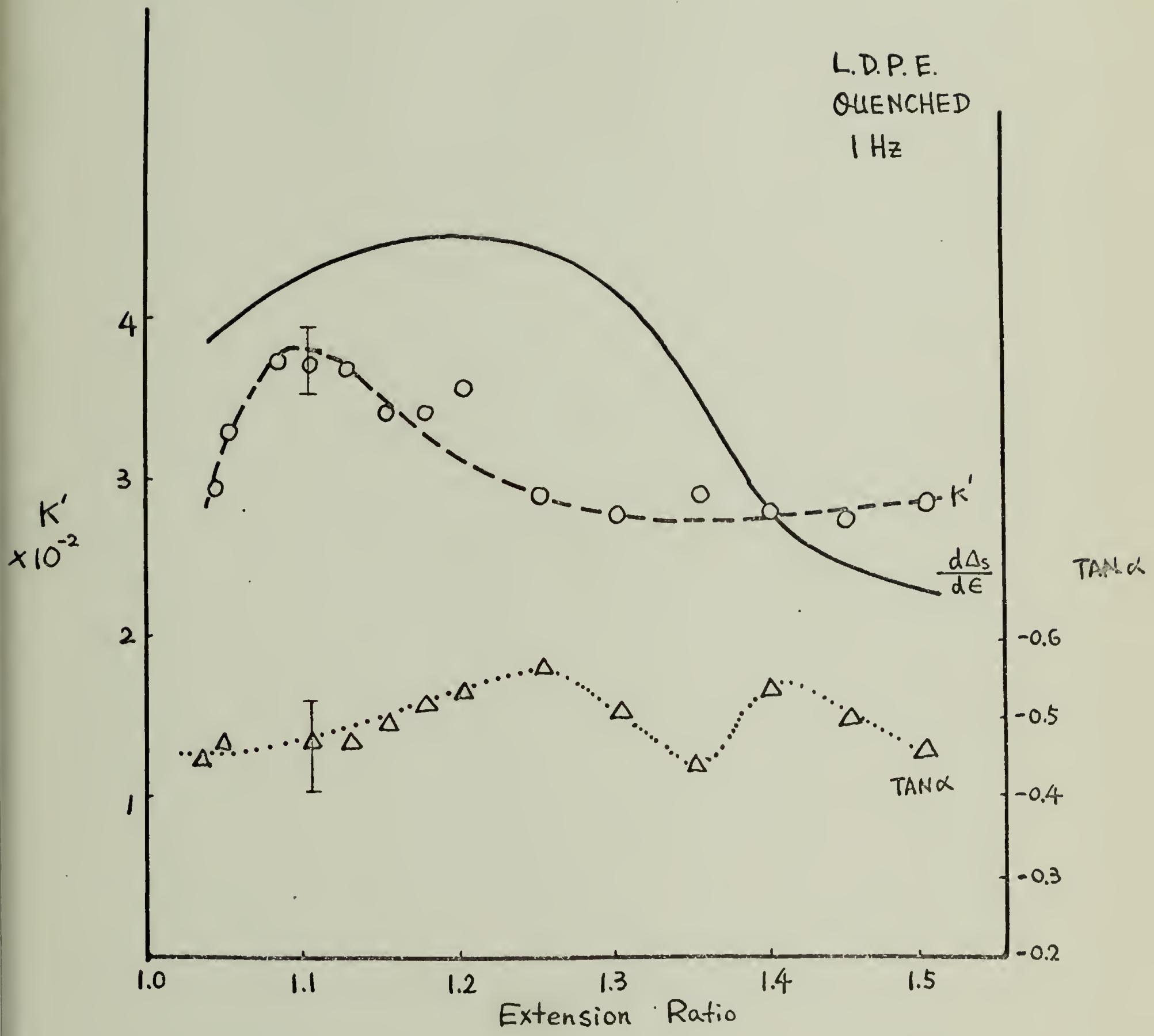
L.D.P.E.
QUENCHED
1 Hz
K'
$\times 10^{-2}$
4
3
2
1
$\frac{d\Delta_s}{d\epsilon}$
K'
TAN α
-0.6
-0.5
-0.4
-0.3
-0.2
TAN α
1.0
1.1
1.2
1.3
1.4
1.5
Extension Ratio

Figure 20

Strain Magnitude	Schematic representation of the Maxwell Model at Stretched State	K	K'	Comparison of K and K' values from expt.
(a) Low (≤10%)	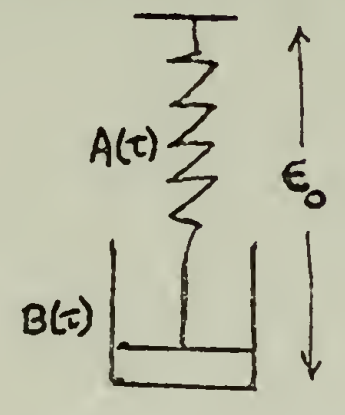	$\epsilon_s = \epsilon_0 e^{-t/\tau}$ $\epsilon_d = 0$ $\Delta = A\epsilon_0 e^{-t/\tau}$ $K = \frac{\Delta}{\epsilon_0} = Ae^{-t/\tau}$ $\simeq A \quad (\tau \to \infty)$	$\epsilon_{vib} = \epsilon e^{i\omega t}$ $\Delta = \Delta_0 e^{i(\omega t - \alpha)}$ $K' = \frac{\Delta}{\epsilon_{vib}} = \frac{\Delta_0}{\epsilon} e^{i\alpha}$ $= \frac{\Delta_0}{\epsilon} \quad (\alpha = 0)$	$K = K'$
(b) Medium (10-40%)		$\epsilon_s = \epsilon_1 e^{-t/\tau}$ $\epsilon_d = \epsilon_1 - \epsilon_s$ $= \epsilon_1(1 - e^{-t/\tau})$ $\Delta = A\epsilon_s + B\epsilon_d$ $K = B + (A-B)e^{-t/\tau}$	$\epsilon_{vib.} = \epsilon e^{i\omega t}$ $\Delta = \Delta_1 e^{i(\omega t - \alpha)}$ $K' = \frac{\Delta_1}{\epsilon} \cos\alpha$	$K > K'$
(c) High (>50%)	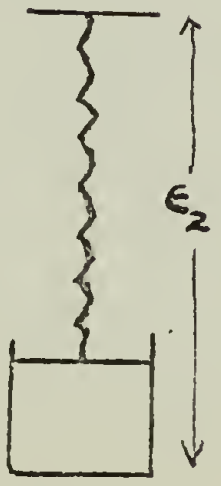	$\epsilon_s = \epsilon_2 e^{-t/\tau}$ $\to 0$ ($\tau \to 0$, high extension of spring) $\epsilon_d = \epsilon_2$ $\Delta = B\epsilon_2$ $K = B$	$\epsilon_{vib.} = \epsilon e^{i\omega t}$ $\Delta = \Delta_2 e^{i(\omega t - \alpha)}$ $K' = \frac{\Delta_2}{\epsilon} \cos\alpha$	$K < K'$

Figure 21

Region	Strain Magnitude	Process measured by K'	K''
1	$\leq 10\%$	Reversible	Reversible
2	10-40%	Rev. + Irrev.	Rev.
3	$> 40\%$	Irrev.	Rev.

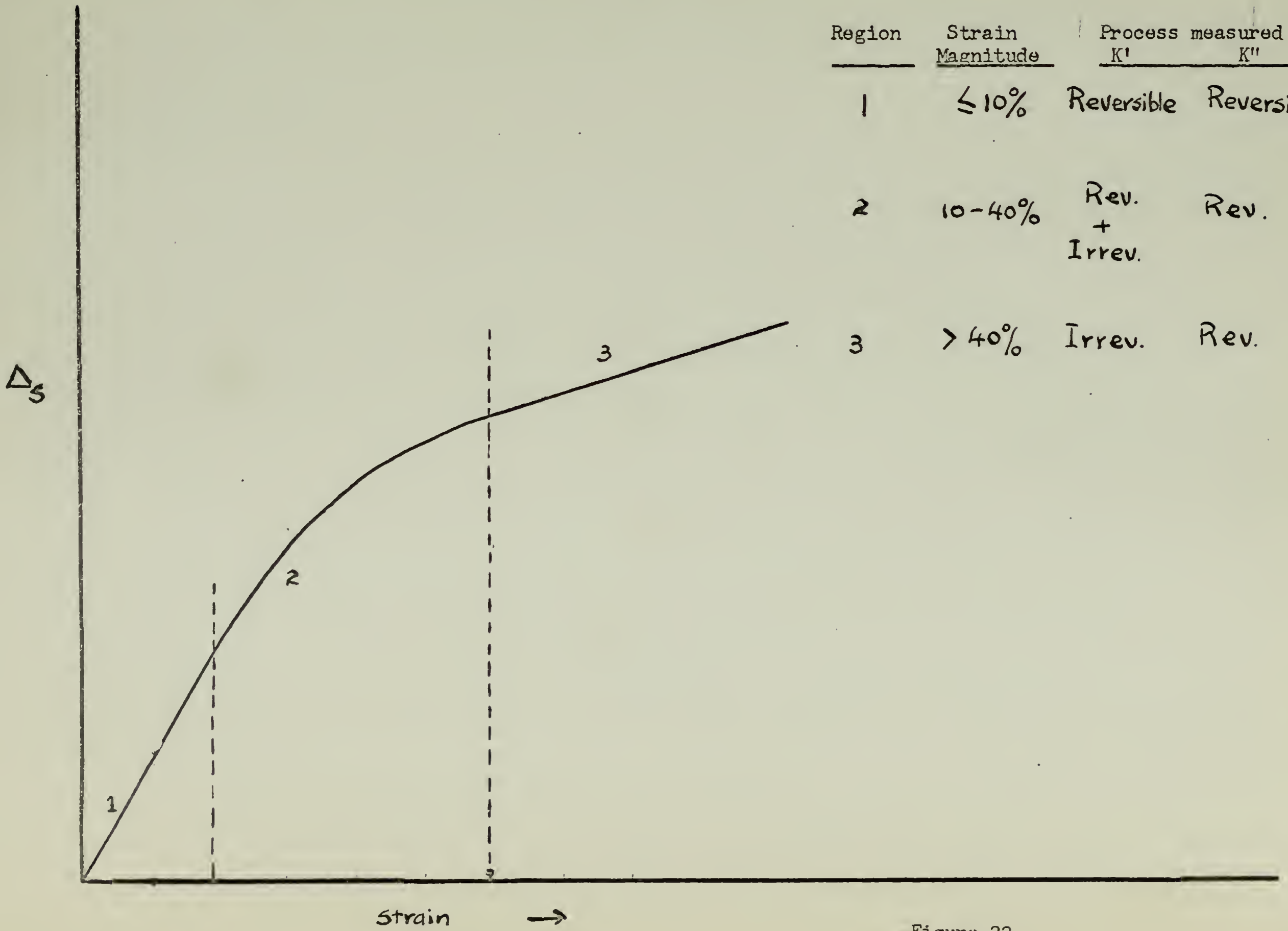

Figure 22

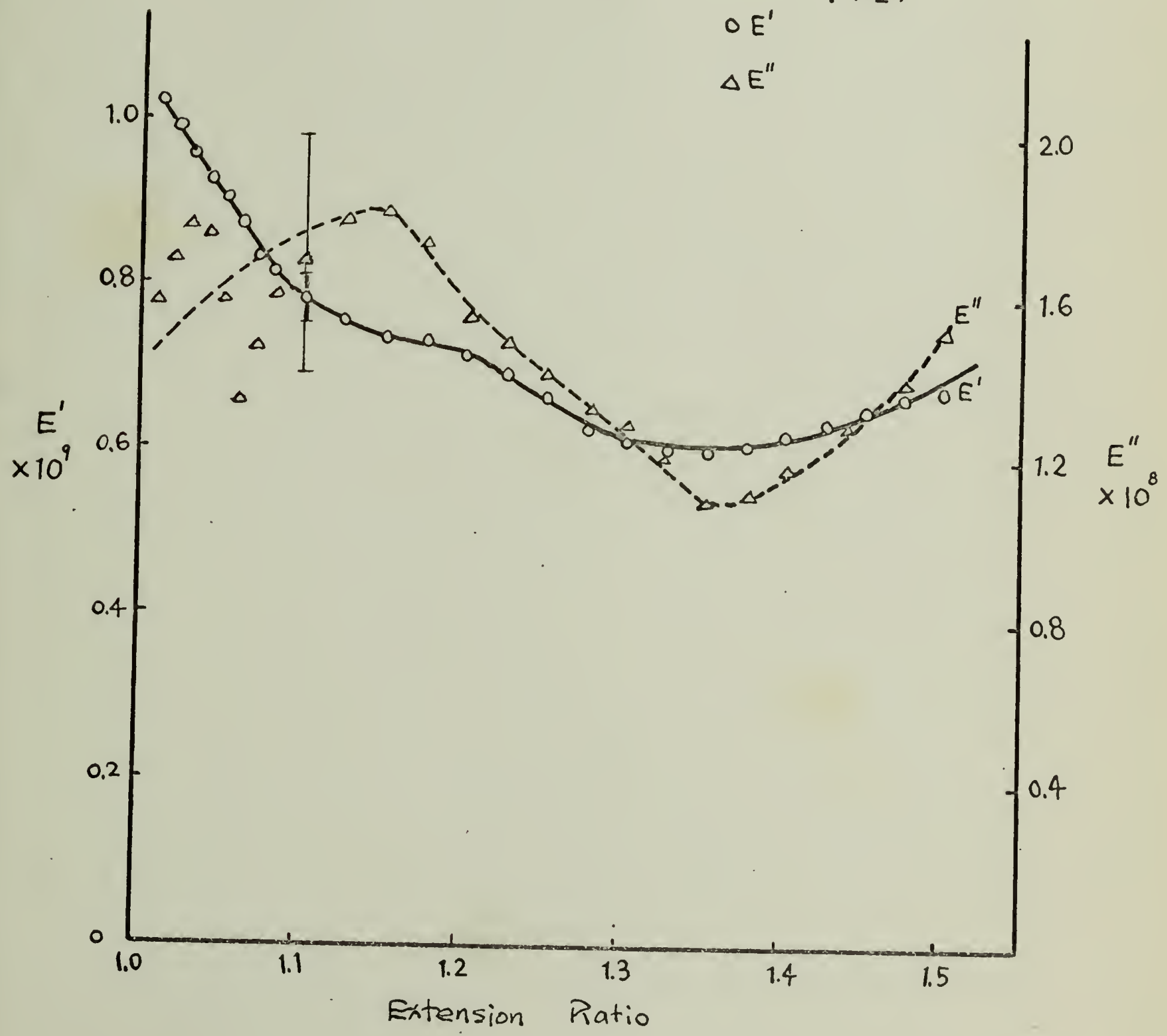
L.D.P.E. (Quenched)
1 Hz.
o E'
Δ E"
E'
x10^9
E"
x10^8
1.0
0.8
0.6
0.4
0.2
0
2.0
1.6
1.2
0.8
0.4
1.0
1.1
1.2
1.3
1.4
1.5
Extension Ratio

Figure 23

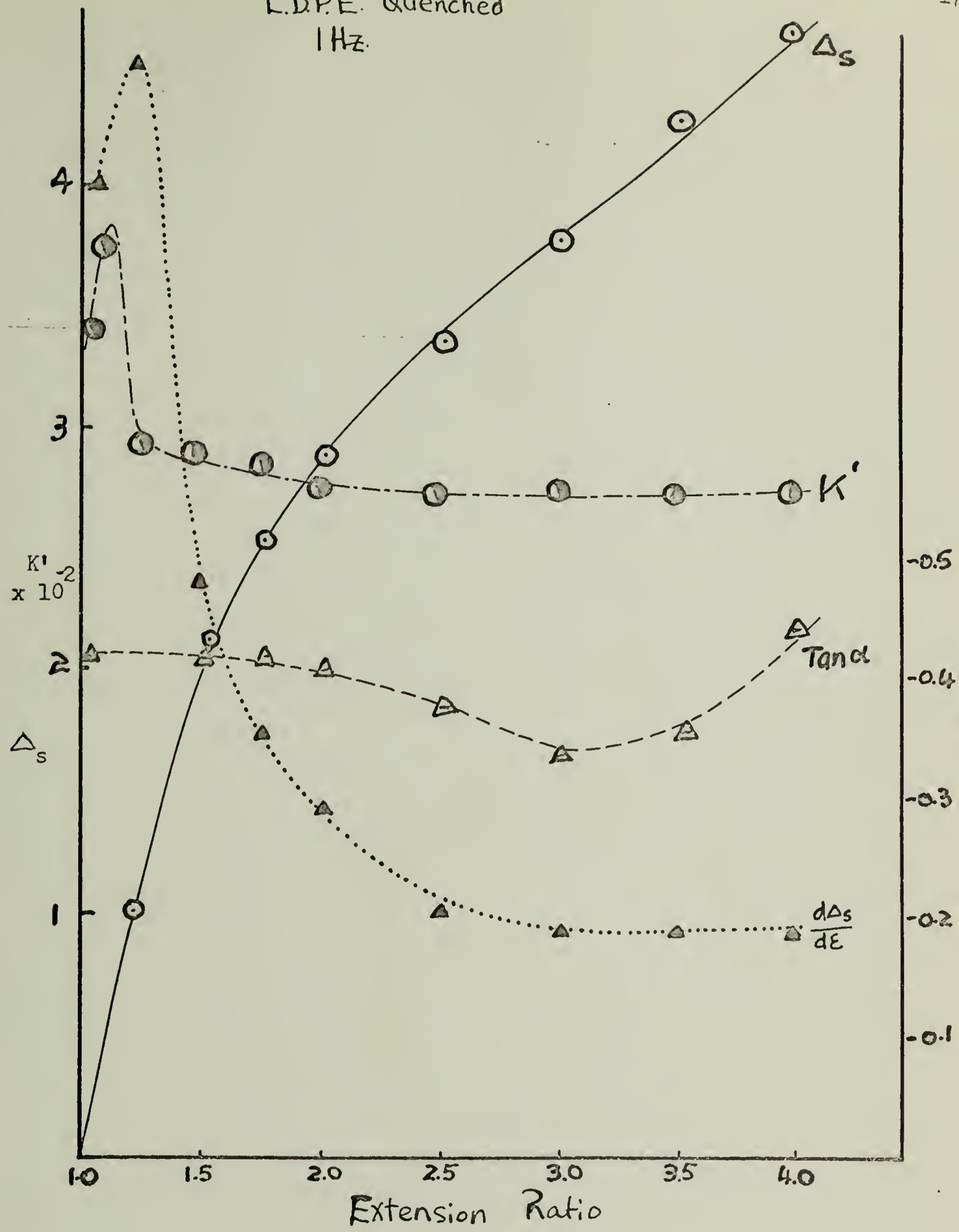
L.D.P.E. Quenched
1 Hz.
Δ_s
K'
Tan α
$\frac{d\Delta_s}{d\varepsilon}$
K' x 10^{-2}
Δ_s
Tan α
4
3
2
1
-0.5
-0.4
-0.3
-0.2
-0.1
1.0
1.5
2.0
2.5
3.0
3.5
4.0
Extension Ratio

Figure 24.

L.D.P.E. (Quenched)
1 Hz

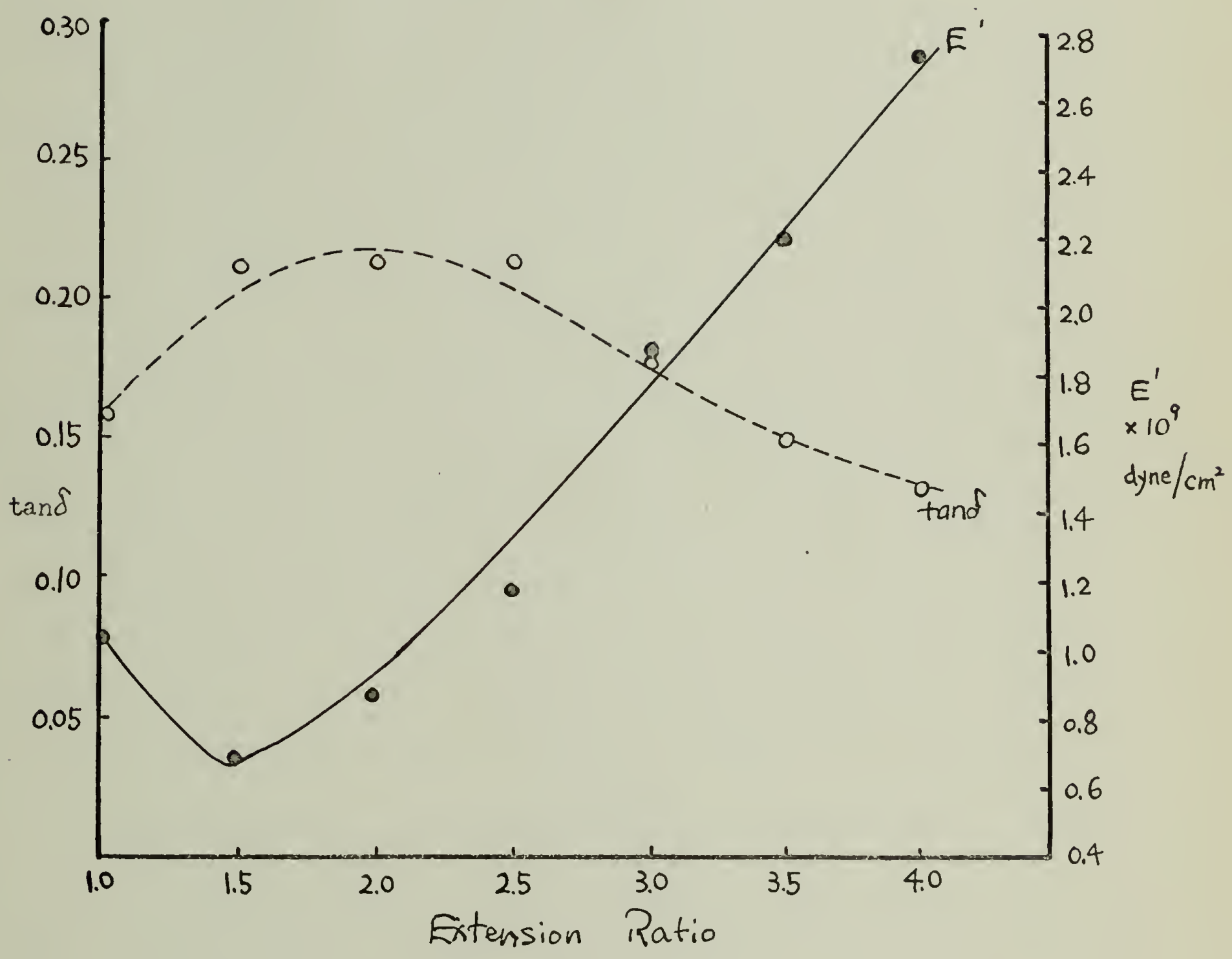

Figure 25.

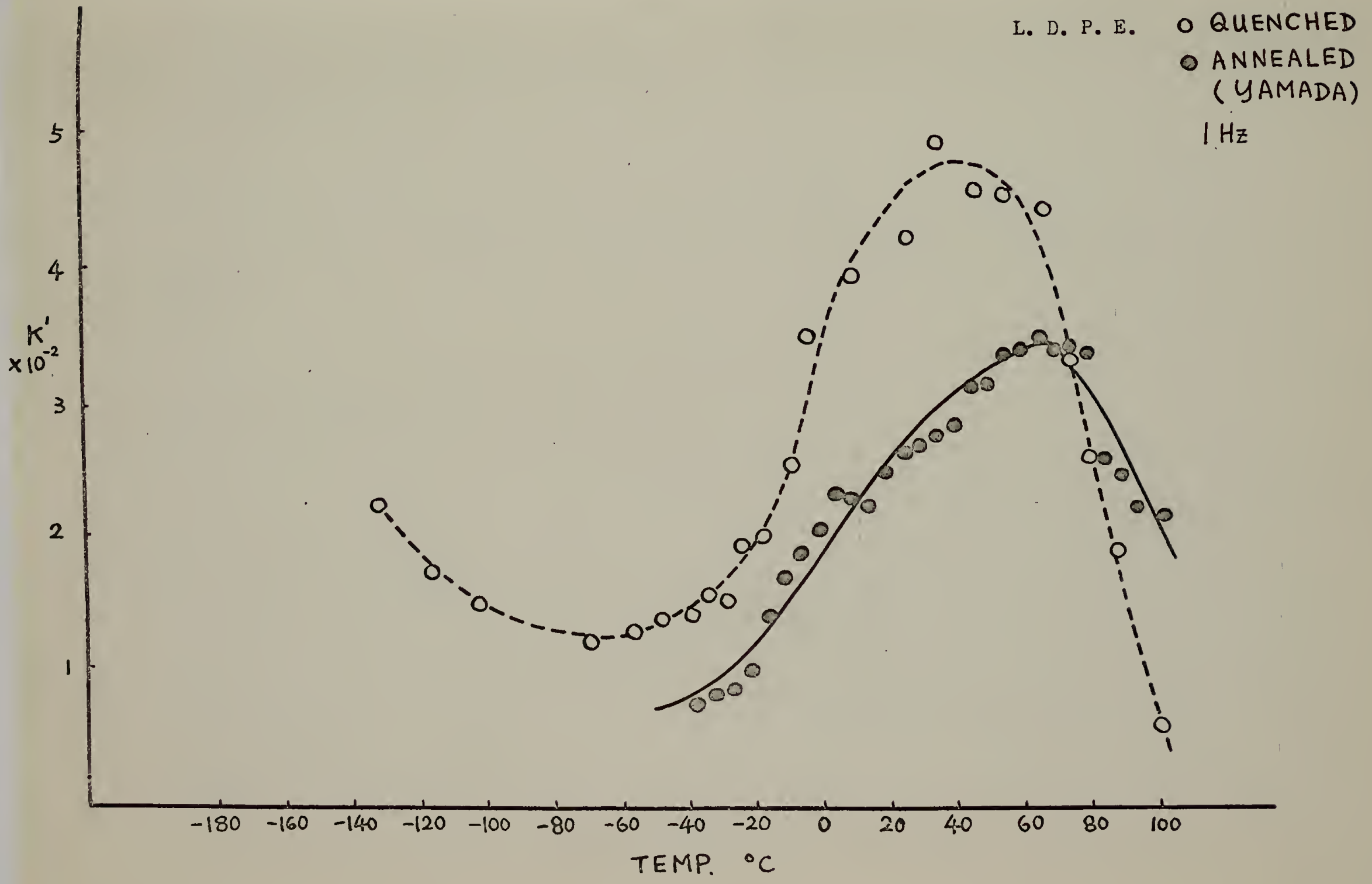
L. D. P. E.
QUENCHED
ANNEALED
(YAMADA)
1 Hz
K'
x10⁻²
5
4
3
2
1
-180
-160
-140
-120
-100
-80
-60
-40
-20
0
20
40
60
80
100
TEMP. °C

Figure 26.

H. D. P. E.

● Annealed
○ Quenched

1 hertz

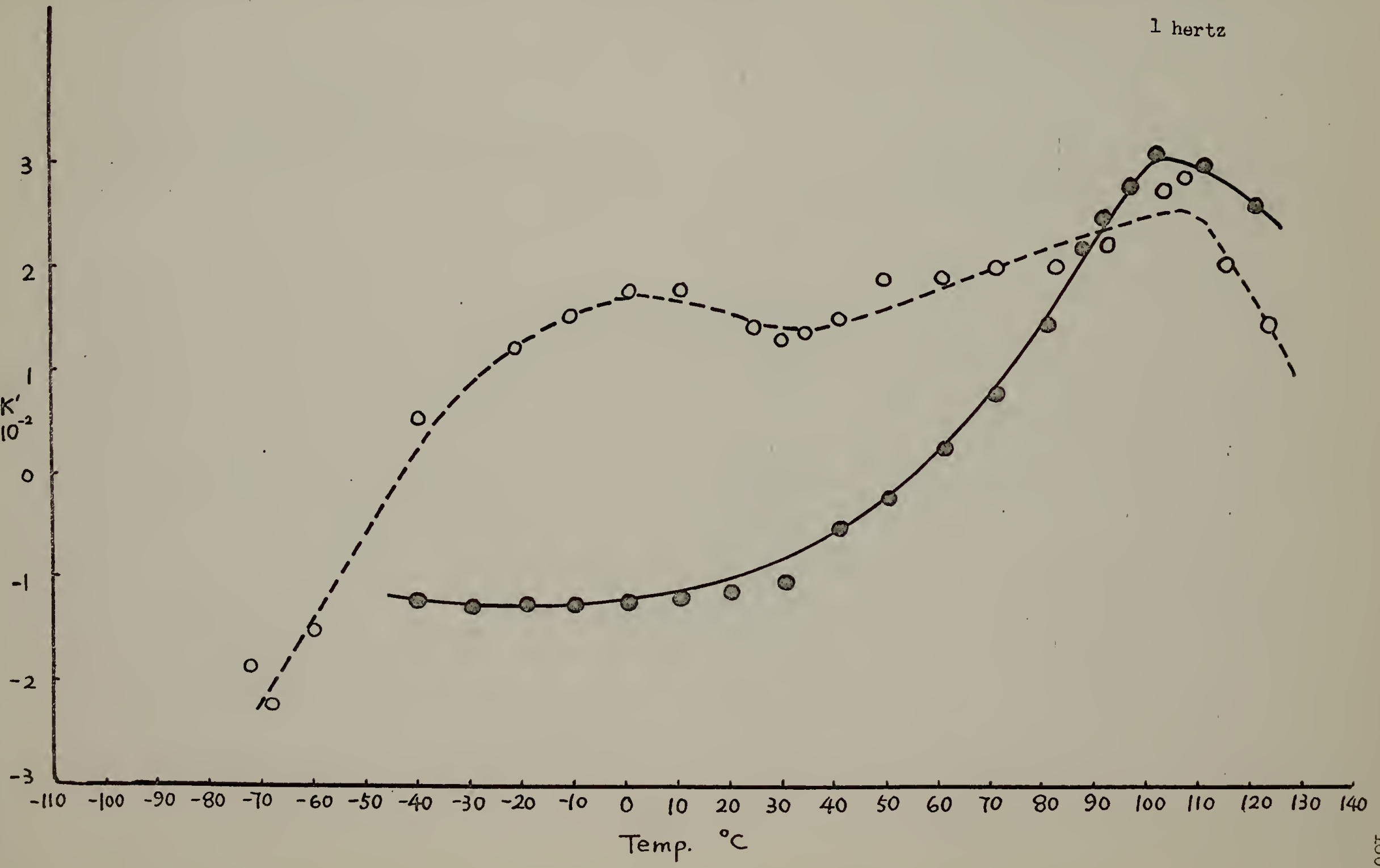

Figure 27.

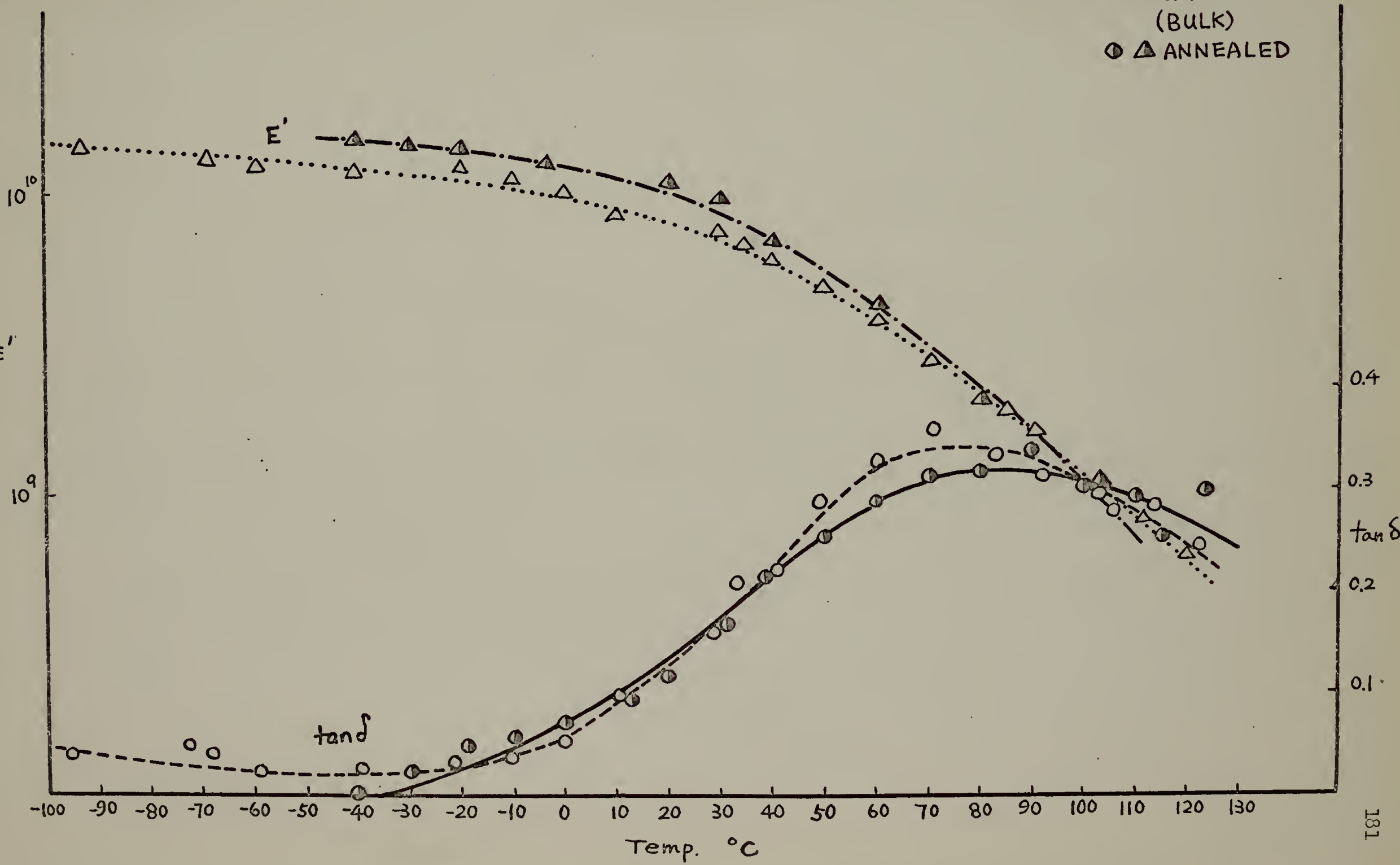
H.D.P.E.
QUENCHED
(BULK)
ANNEALED
E'
10^{10}
10^{9}
tan δ
0.4
0.3
0.2
0.1
-100 -90 -80 -70 -60 -50 -40 -30 -20 -10 0 10 20 30 40 50 60 70 80 90 100 110 120 130
Temp. °C

Figure 28.

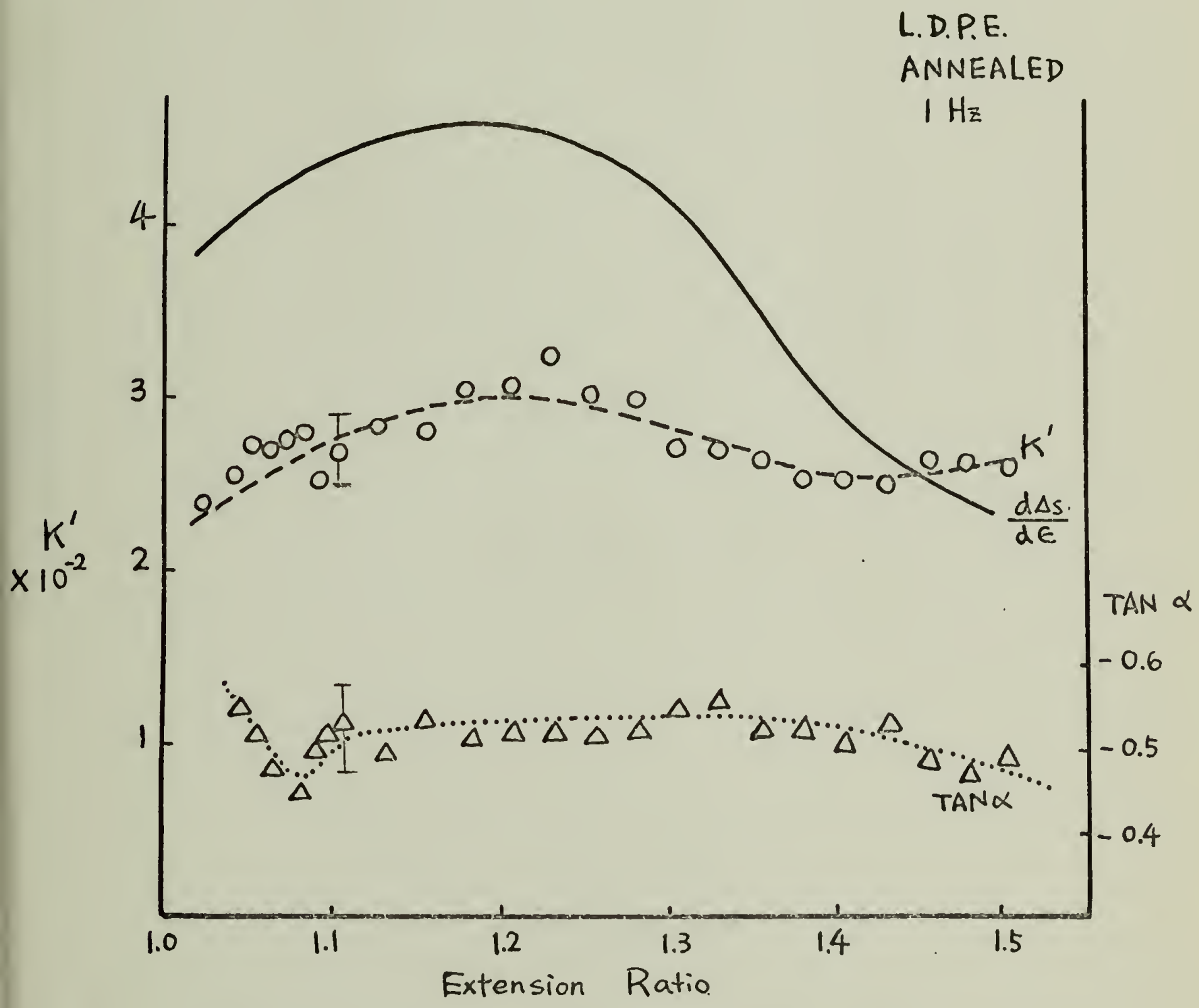
L.D.P.E.
ANNEALED
1 Hz
4
3
2
1
K'
X 10⁻²
K'
dΔs/dε
TAN α
0.6
0.5
0.4
TANα
1.0
1.1
1.2
1.3
1.4
1.5
Extension Ratio

Figure 29.

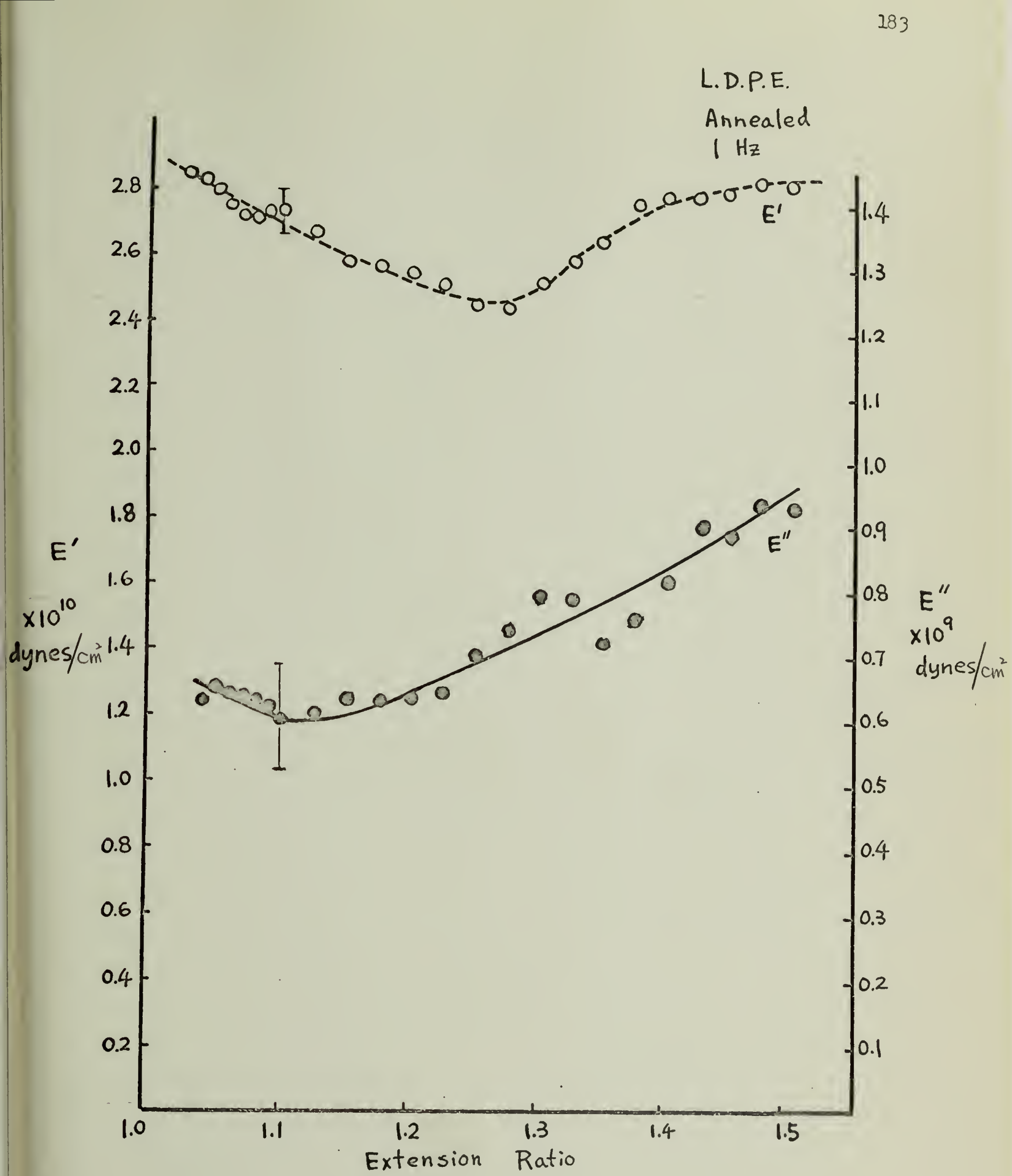
L.D.P.E.
Annealed
1 Hz
E'
E''
E'
x10^10
dynes/cm^2
E''
x10^9
dynes/cm^2
2.8
2.6
2.4
2.2
2.0
1.8
1.6
1.4
1.2
1.0
0.8
0.6
0.4
0.2
1.4
1.3
1.2
1.1
1.0
0.9
0.8
0.7
0.6
0.5
0.4
0.3
0.2
0.1
1.0
1.1
1.2
1.3
1.4
1.5
Extension Ratio

Figure 30.

H.D.P.E.
QUENCHED

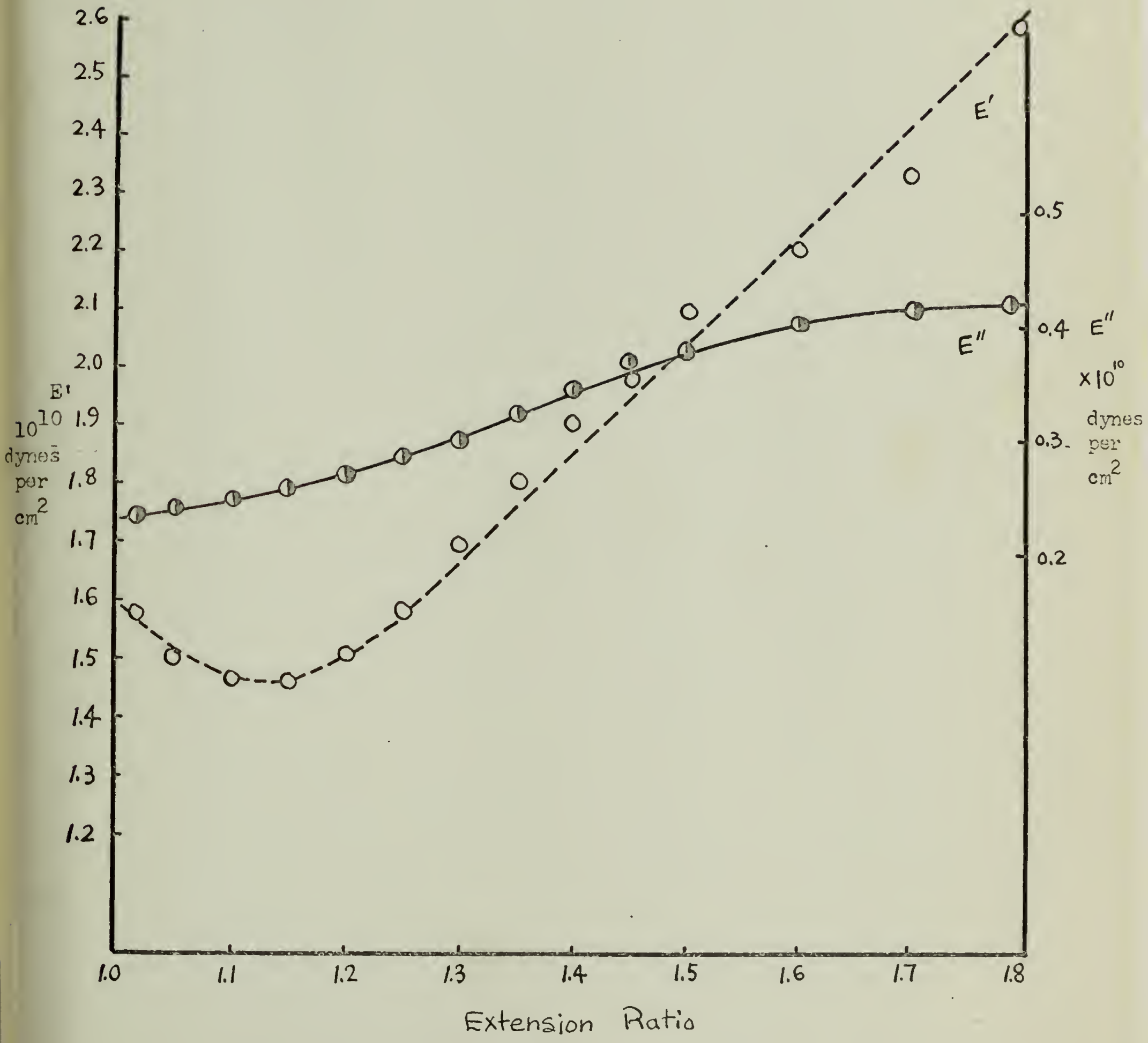

Figure 31.

L.D.P.E.
Quenched.

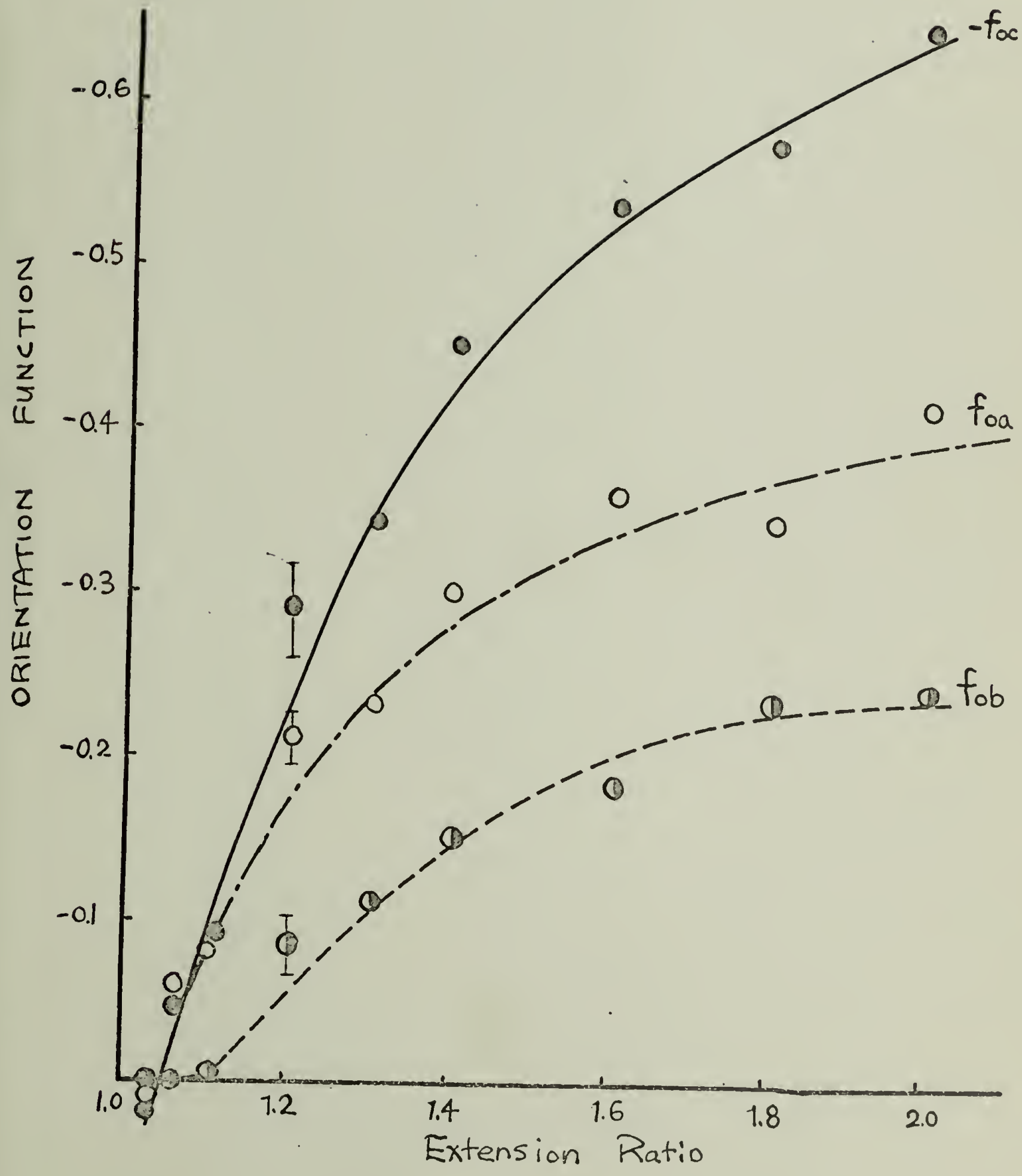

Figure 32.

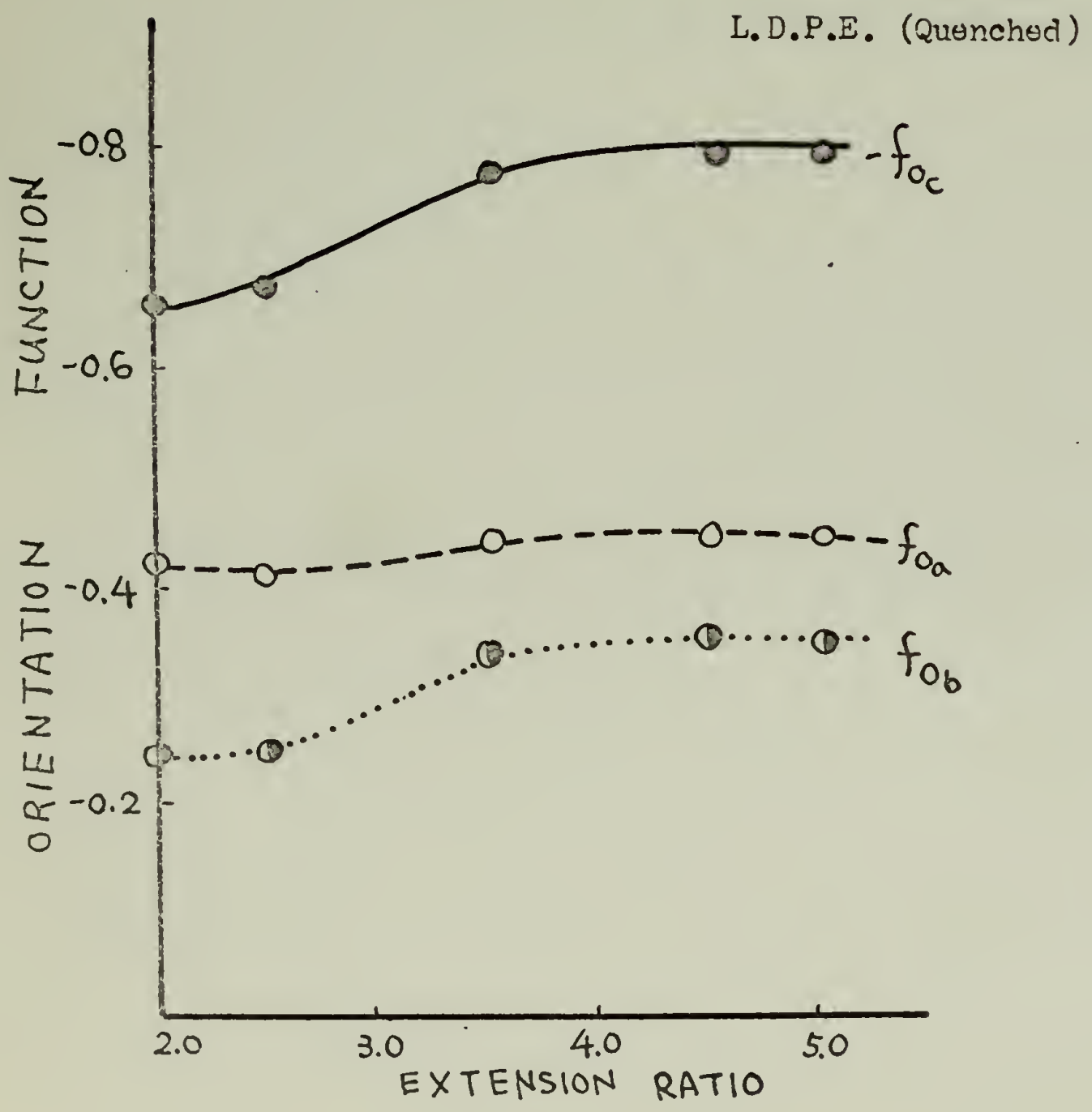
L.D.P.E. (Quenched)
-0.8
-0.6
-0.4
-0.2
FUNCTION
ORIENTATION
$-f_{oc}$
f_{oa}
f_{ob}
2.0
3.0
4.0
5.0
EXTENSION RATIO

(a)

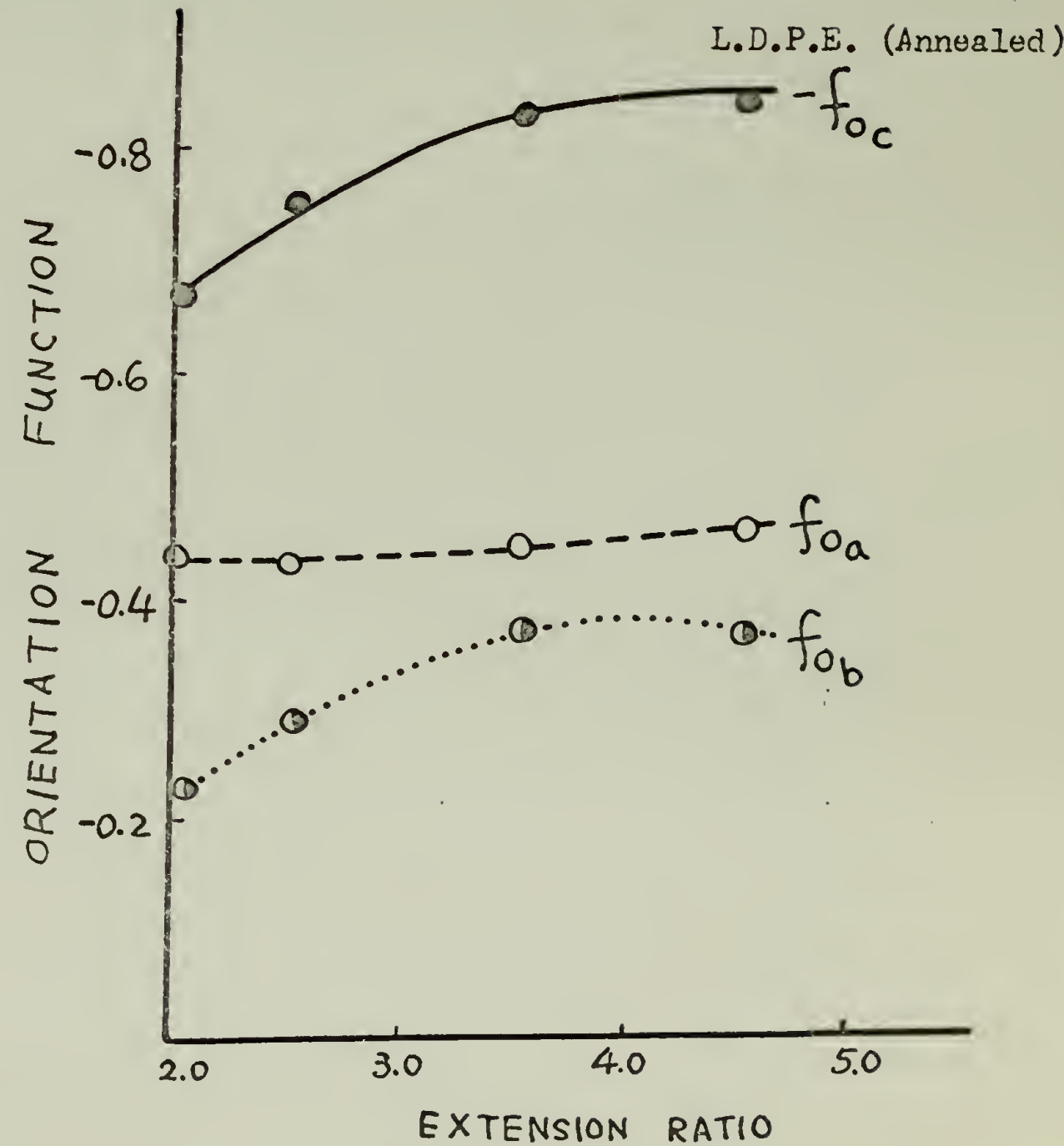
L.D.P.E. (Annealed)
-0.8
-0.6
-0.4
-0.2
FUNCTION
ORIENTATION
$-f_{oc}$
f_{oa}
f_{ob}
2.0
3.0
4.0
5.0
EXTENSION RATIO

(b)

Figure 33.

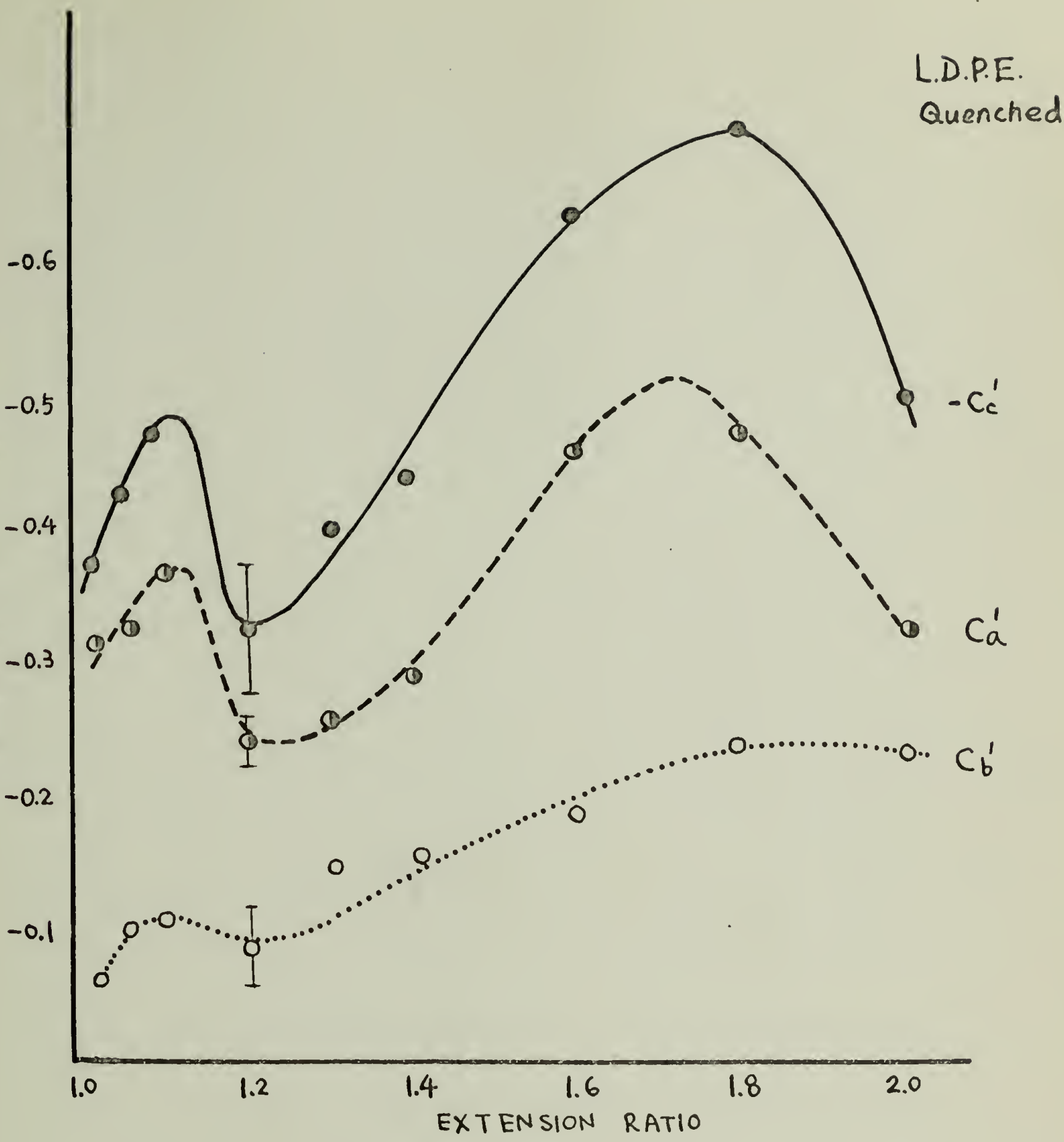
L.D.P.E.
Quenched.
ORIENTATION COMPLIANCE
-0.6
-0.5
-0.4
-0.3
-0.2
-0.1
$-C_c'$
C_a'
C_b'
1.0
1.2
1.4
1.6
1.8
2.0
EXTENSION RATIO

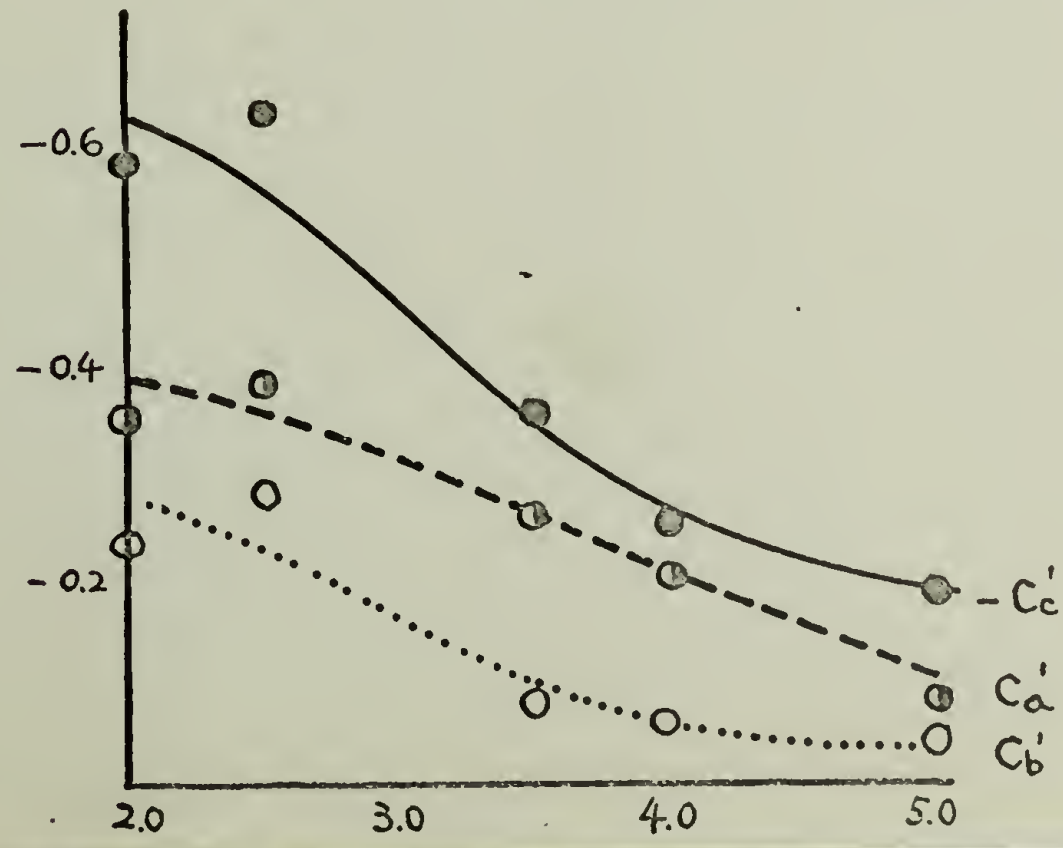
-0.6
-0.4
-0.2
$-C_c'$
C_a'
C_b'
2.0
3.0
4.0
5.0

Figure 34.

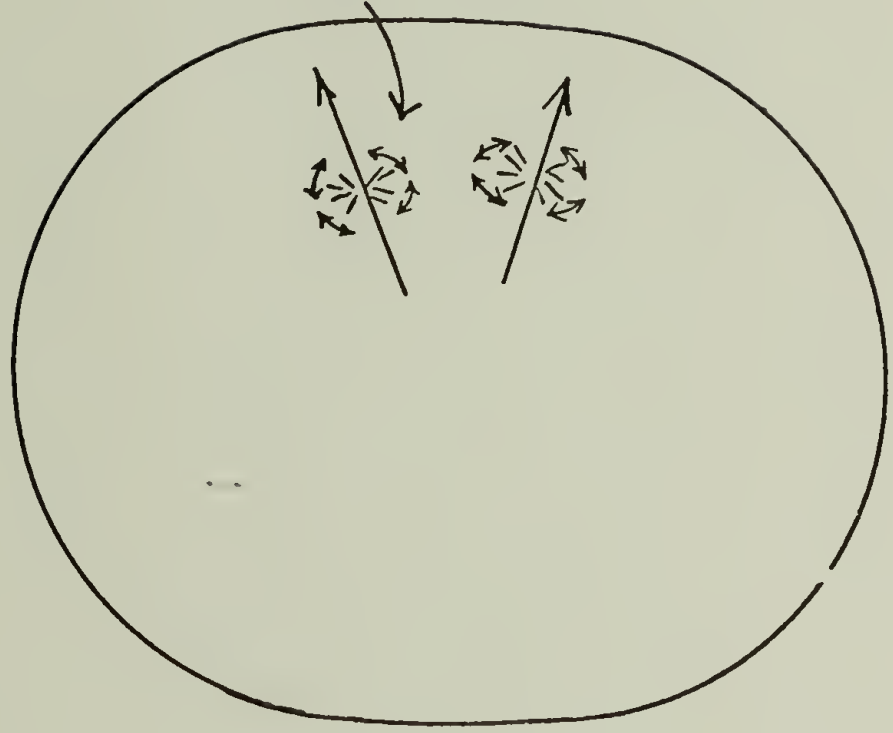

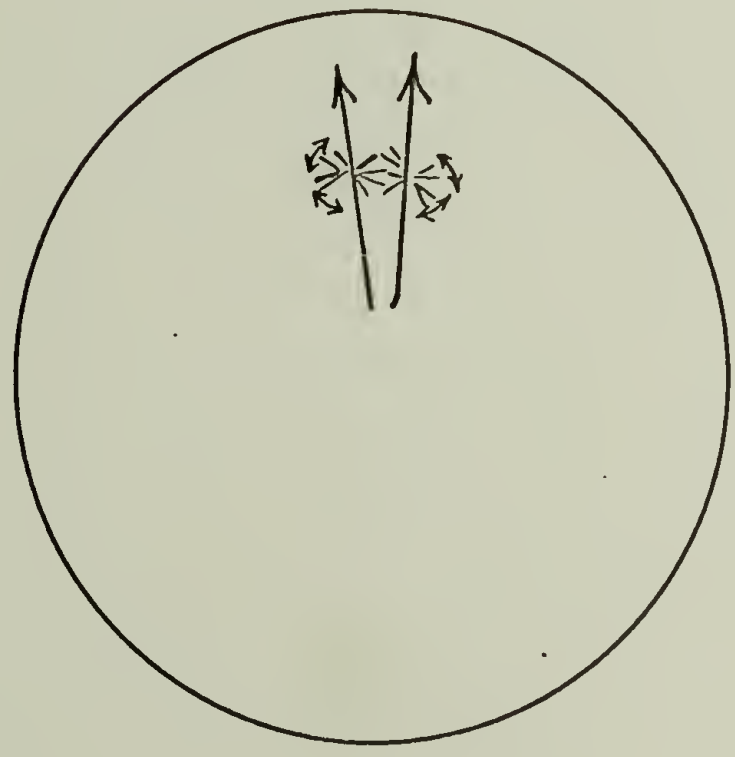

Figure 35.

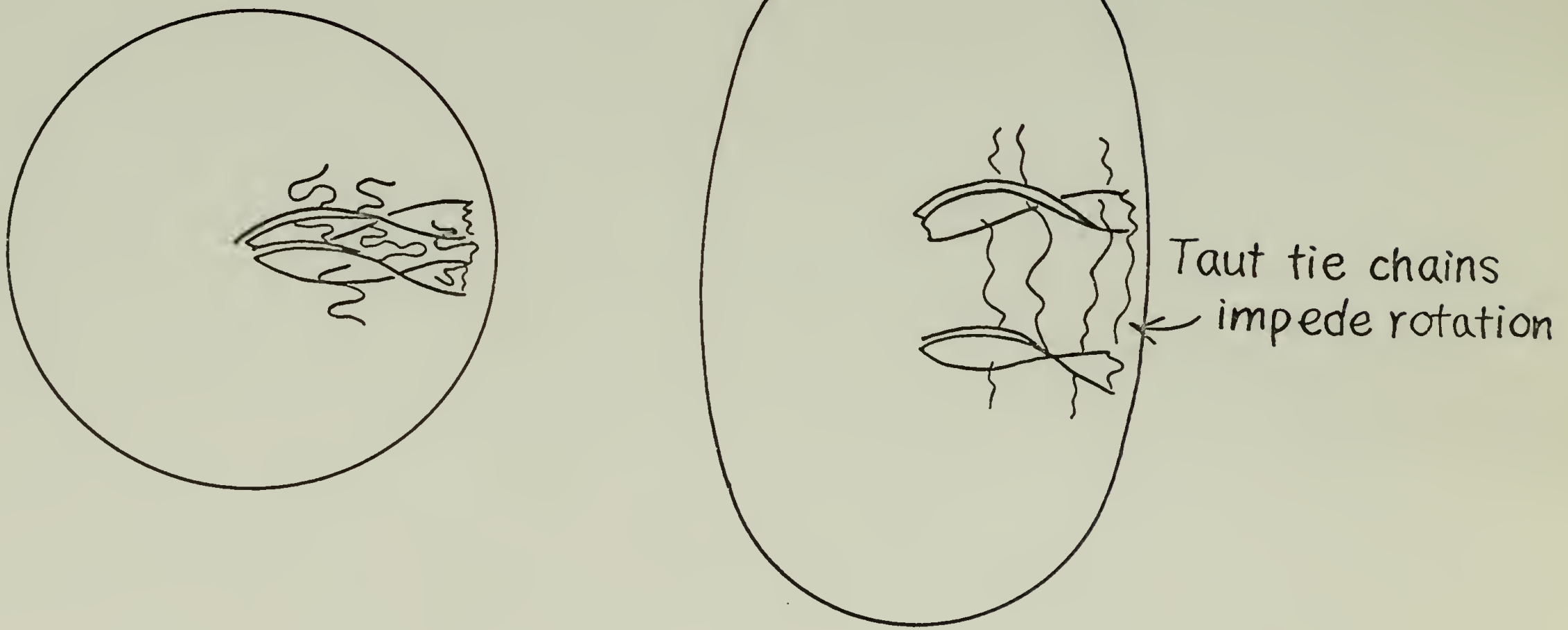

Figure 36.

L.D.P.E.
QUENCHED

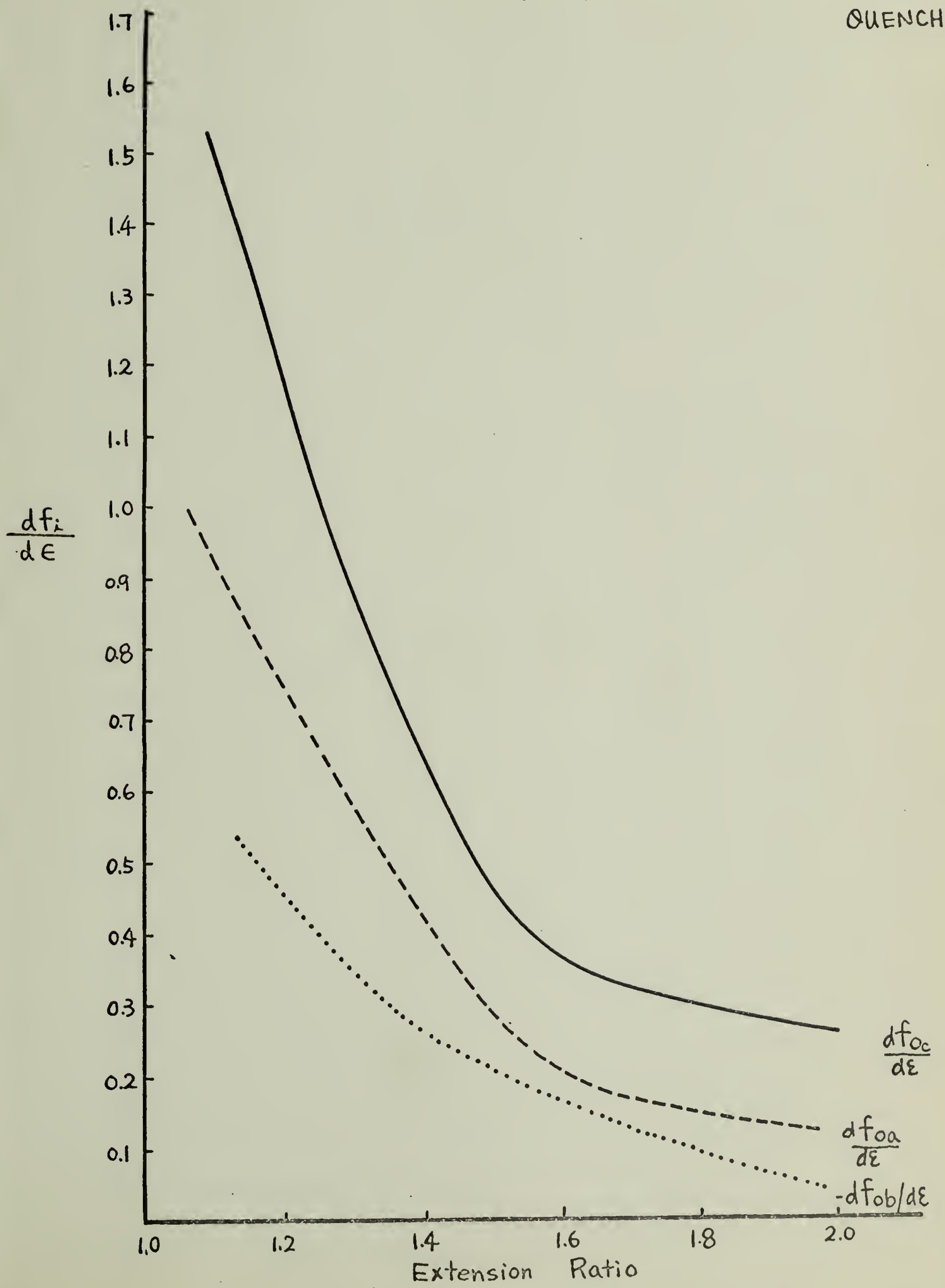

Figure 37.

L.D.P.E.
QUENCHED

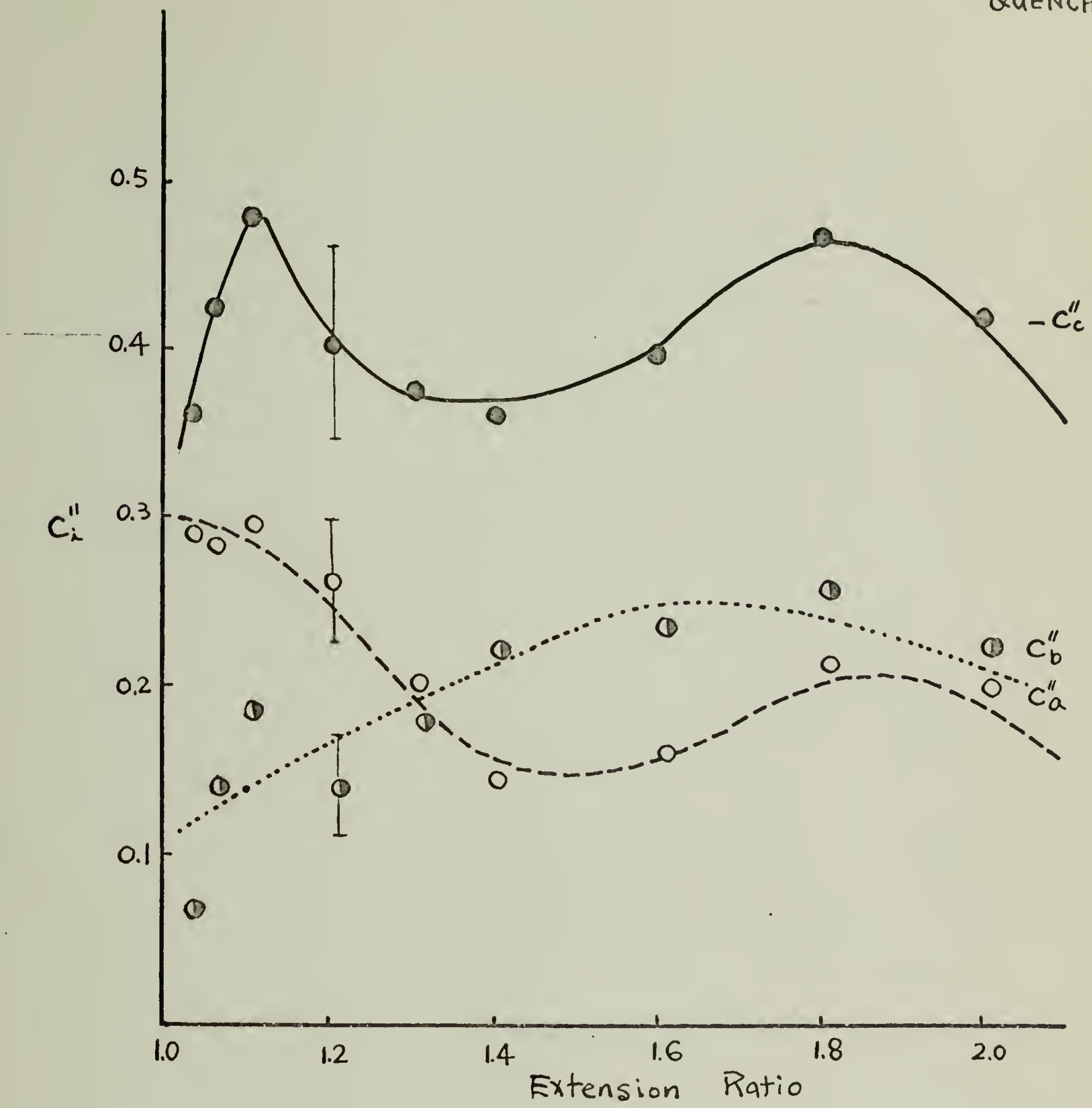

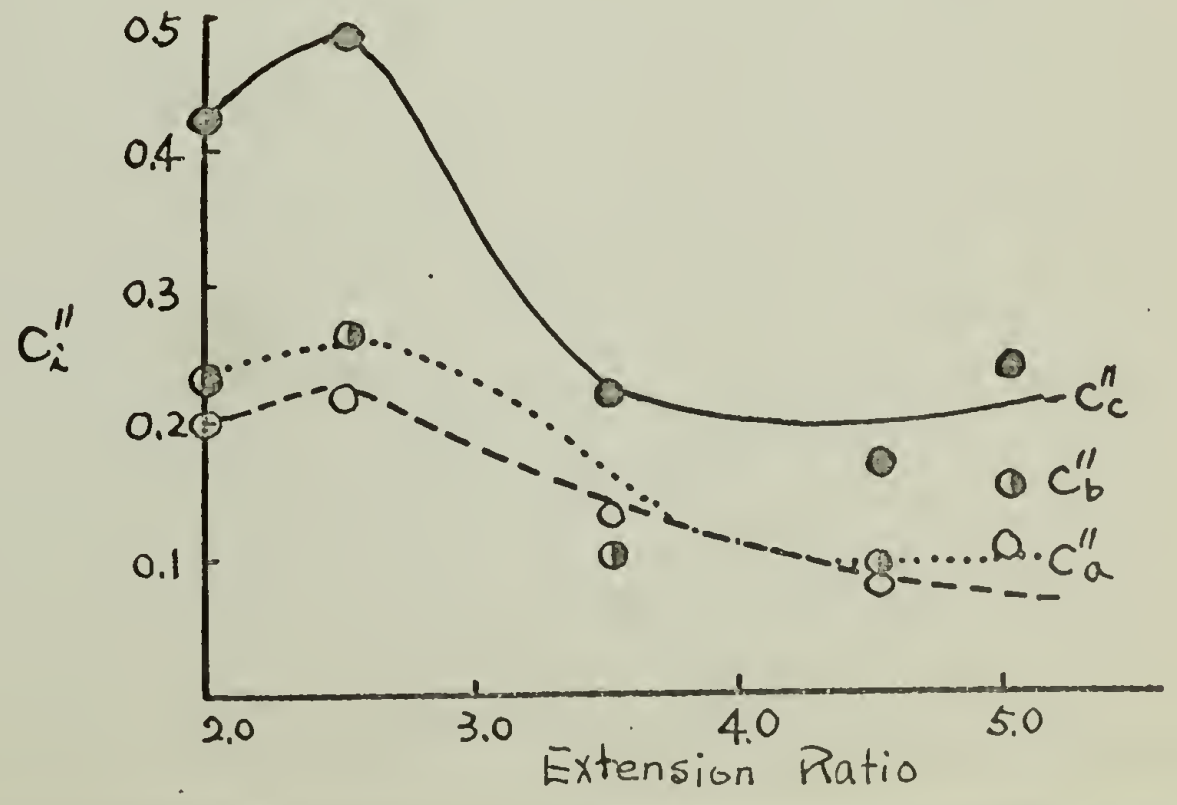

Figure 38.

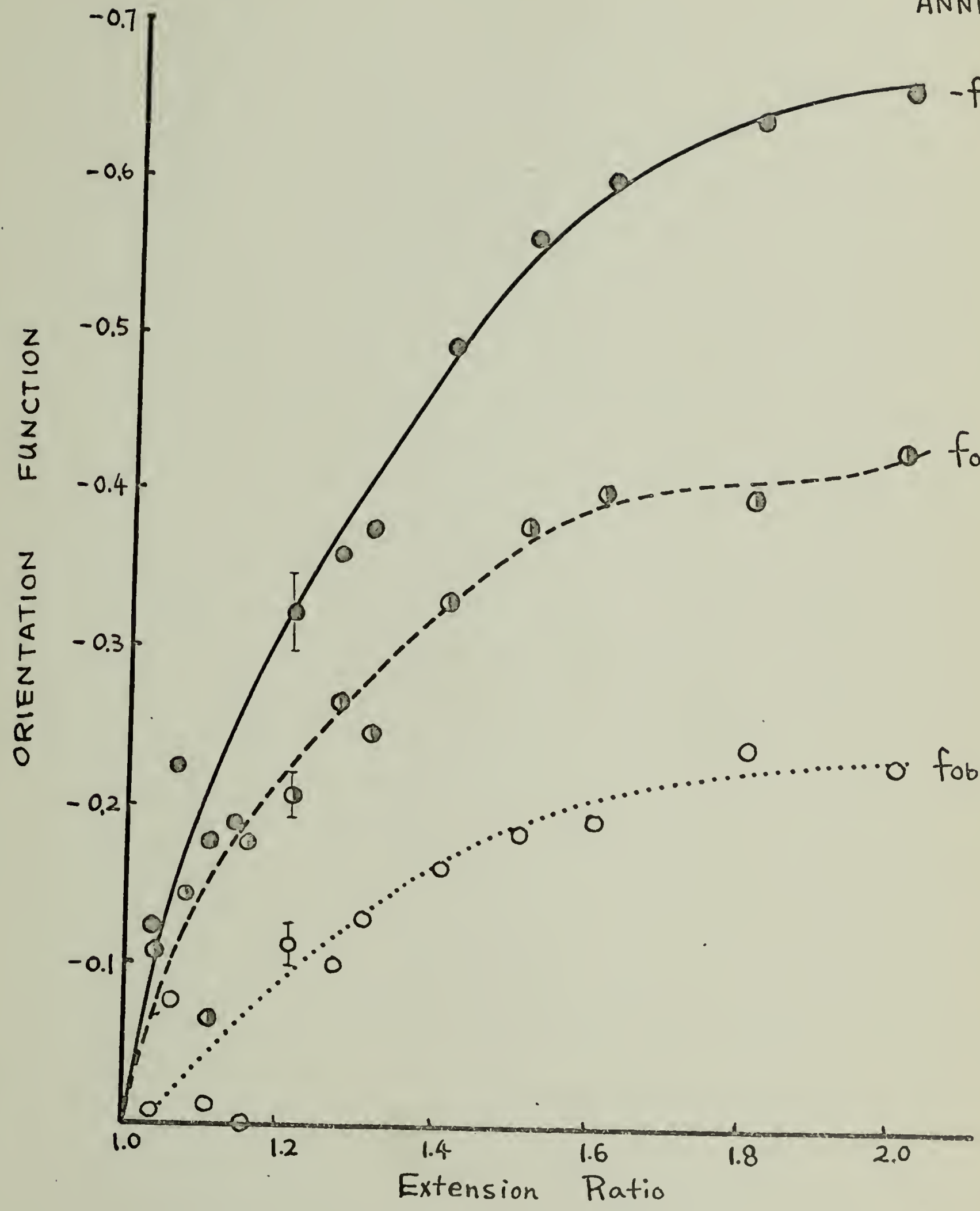
L.D.P.E.
ANNEALED
-0.7
-0.6
-0.5
-0.4
-0.3
-0.2
-0.1
ORIENTATION FUNCTION
-foc
foa
fob
1.0
1.2
1.4
1.6
1.8
2.0
Extension Ratio

Figure 39.

L.D.P.E. ANN.
1 Hz
30°C

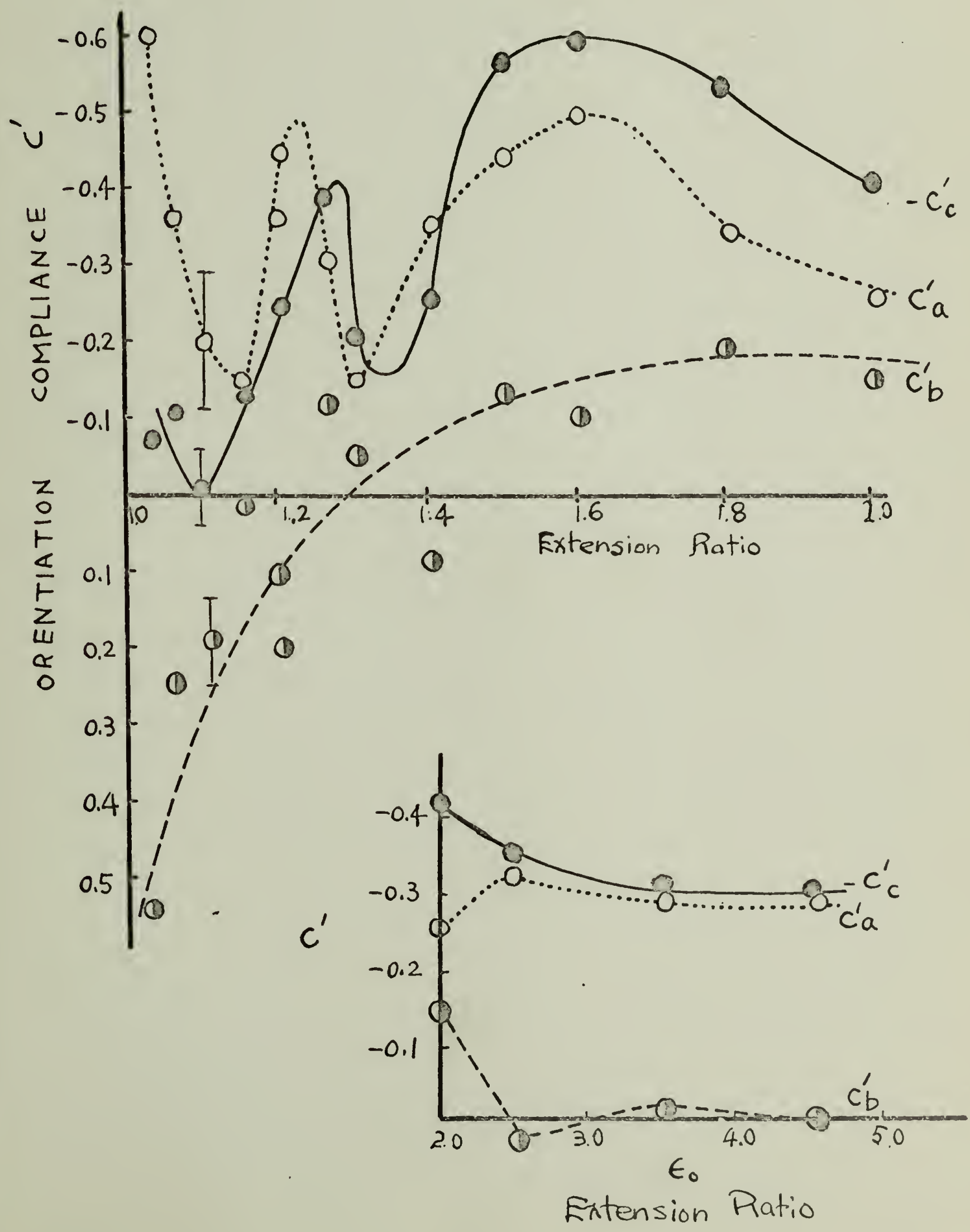

Figure 40.

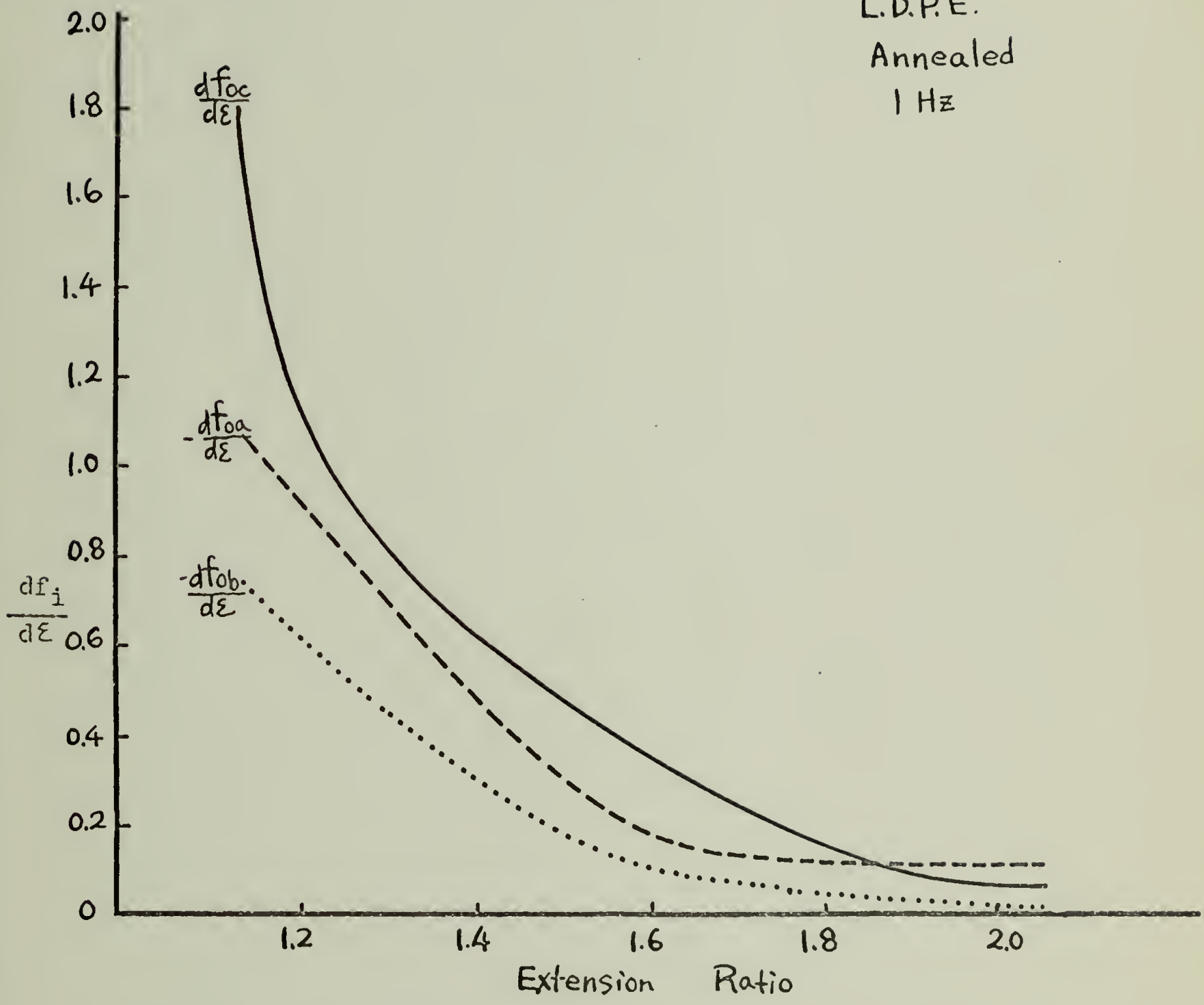
L.D.P.E.
Annealed
1 Hz
2.0
1.8
1.6
1.4
1.2
1.0
0.8
0.6
0.4
0.2
0
$\frac{df_i}{d\varepsilon}$
$\frac{df_{oc}}{d\varepsilon}$
$-\frac{df_{oa}}{d\varepsilon}$
$-\frac{df_{ob}}{d\varepsilon}$
1.2
1.4
1.6
1.8
2.0
Extension Ratio

Figure 41.

L.D.P.E.
ANNEALED
1 Hz.

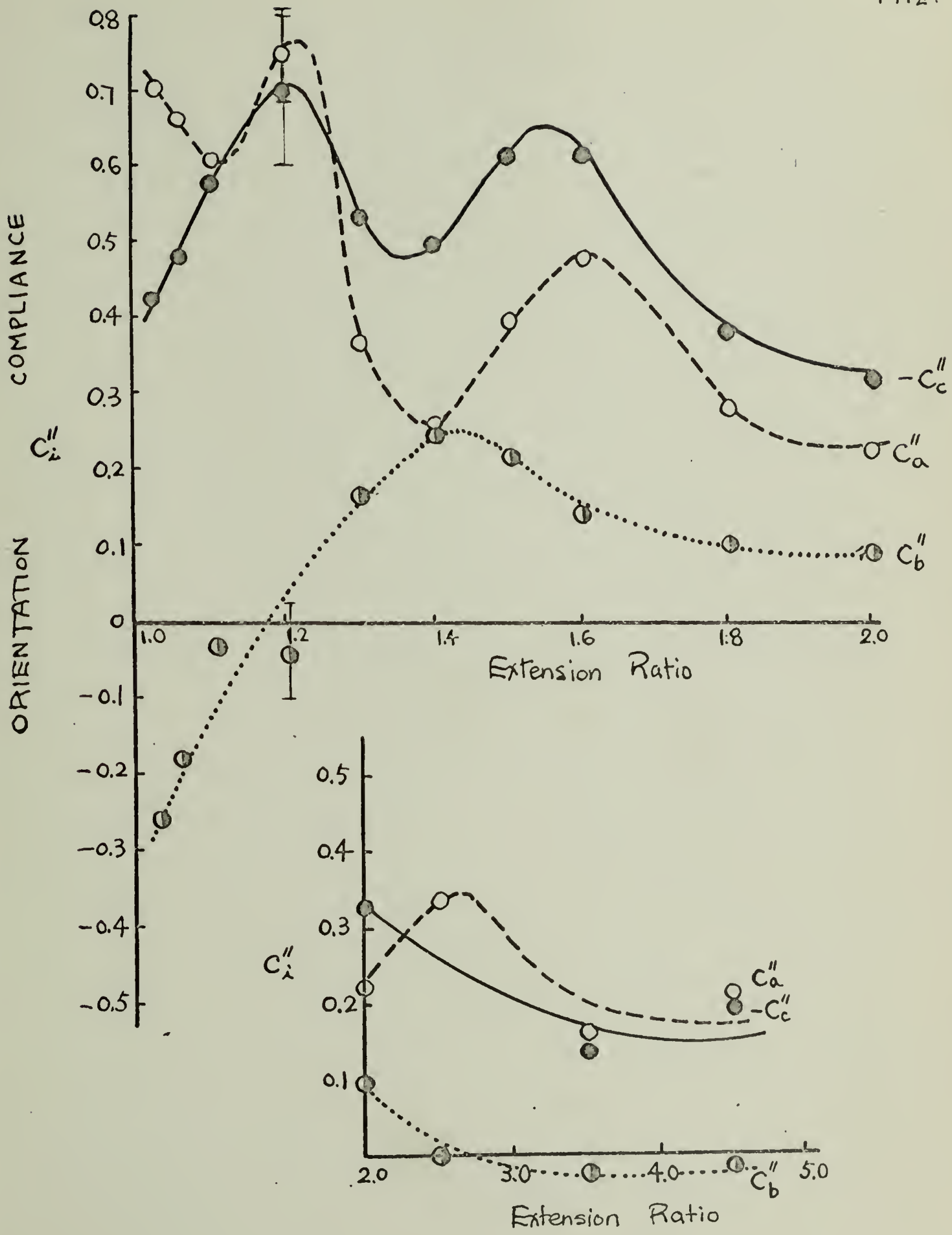

Figure 42.

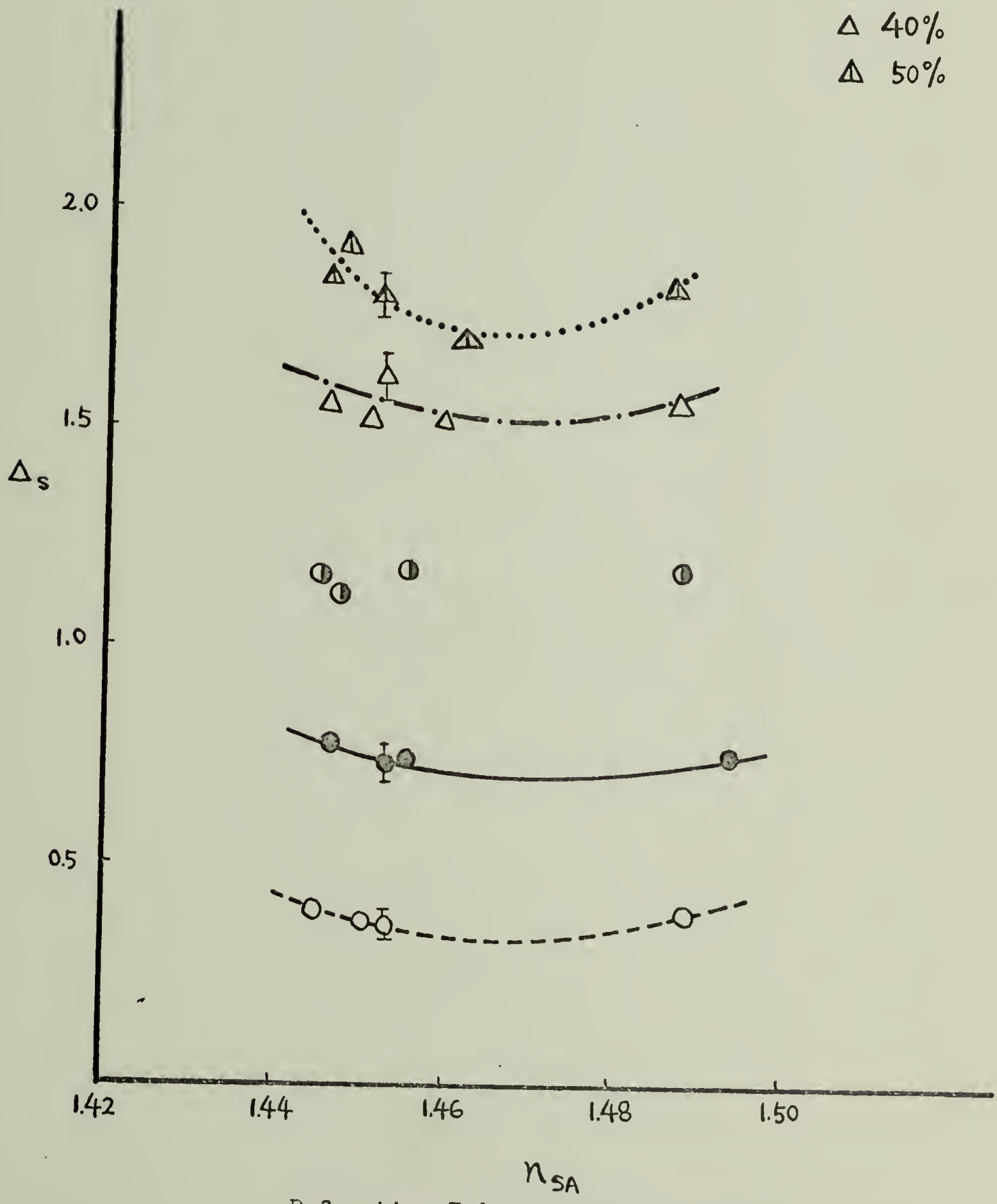
L. D. P. E.
(Annealed)
ELONGATION
10%
20%
30%
40%
50%
2.0
1.5
1.0
0.5
Δs
1.42
1.44
1.46
1.48
1.50
nSA
Refractive Index of Swollen Amorphous Phase

Figure 43.

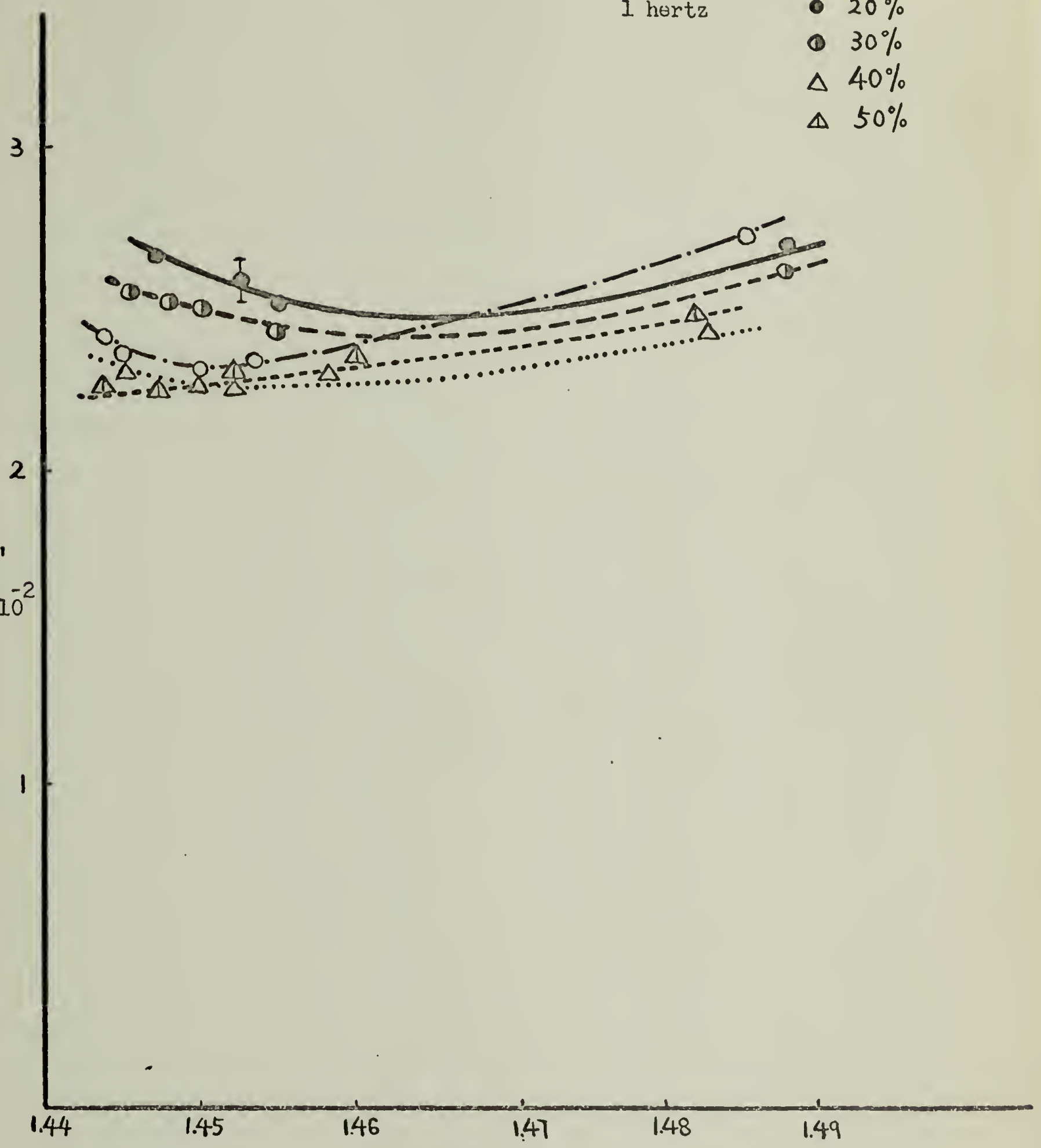
L. D. P. E.
(Annealed)
1 hertz
ELONGATION
10 %
20 %
30 %
40 %
50 %
3
2
1
K'
x 10^-2
1.44
1.45
1.46
1.47
1.48
1.49
n_SA
Refractive Index of Swollen amorphous phase

Figure 44.

L.D.P.E.
ANNEALED

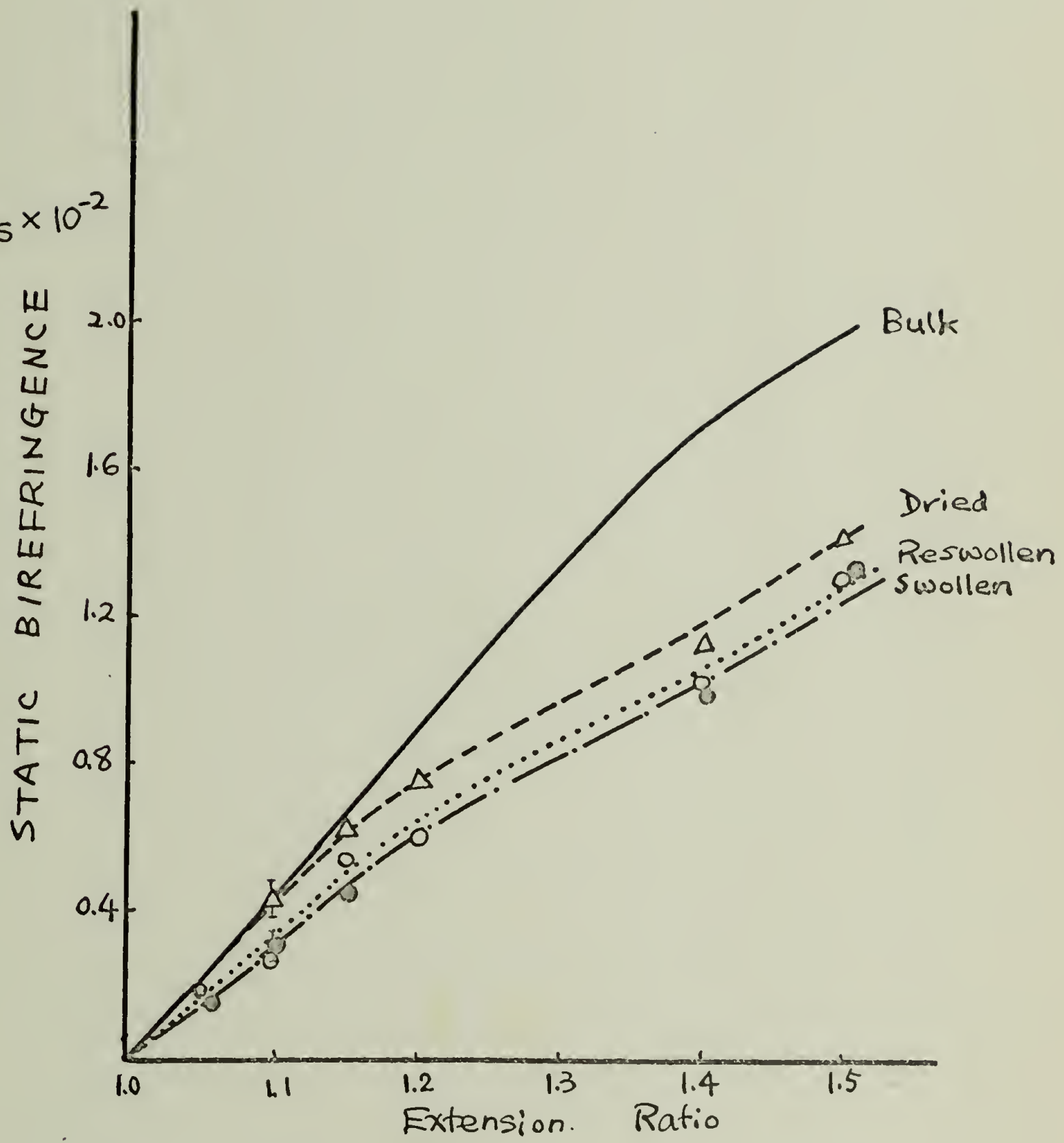

Figure 45.

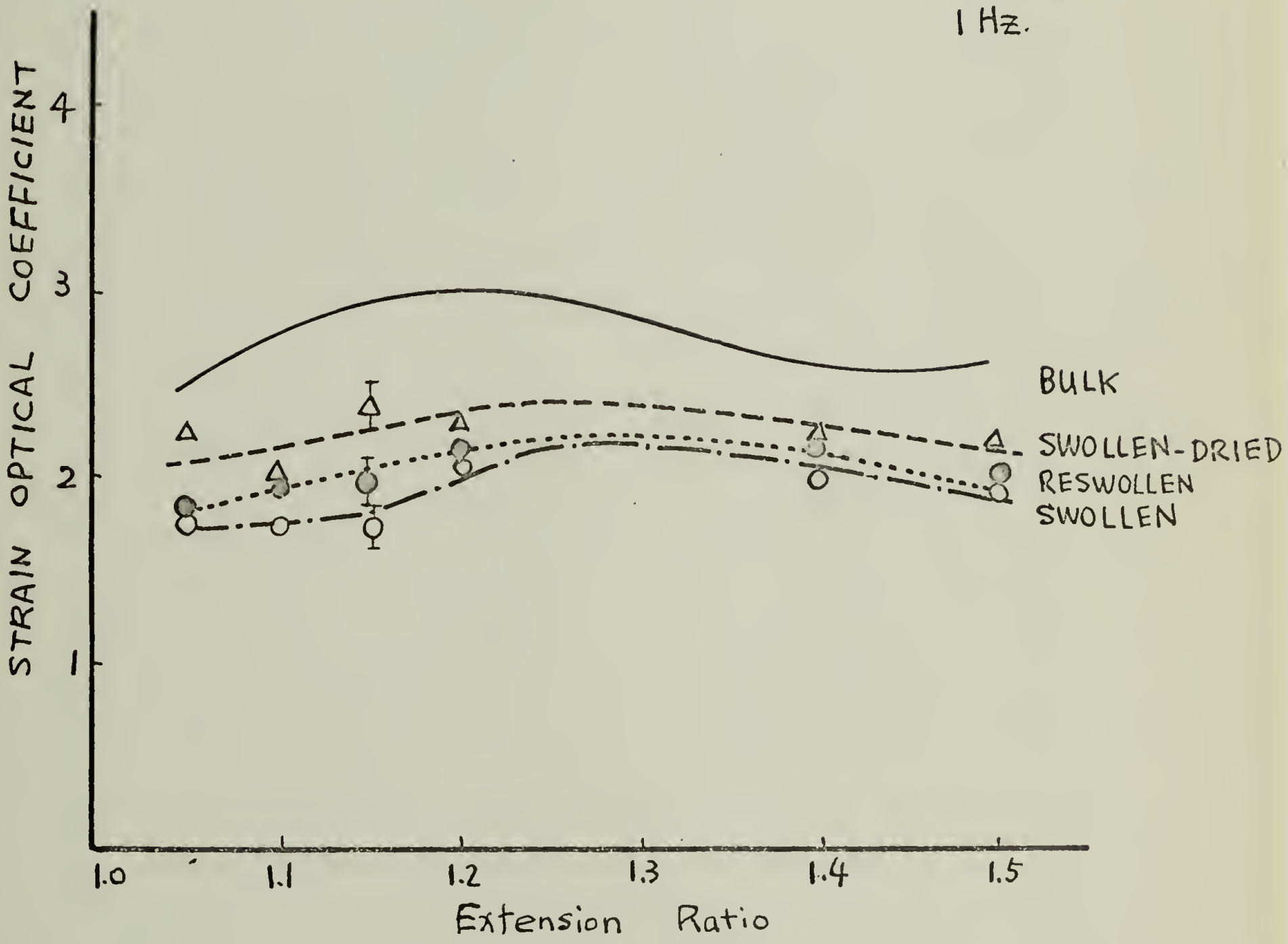
L.D.P.E.
ANN.
1 Hz.
K.
x10⁻²
STRAIN OPTICAL COEFFICIENT
4
3
2
1
BULK
SWOLLEN-DRIED
RESWOLLEN
SWOLLEN
1.0
1.1
1.2
1.3
1.4
1.5
Extension Ratio

Figure 46.

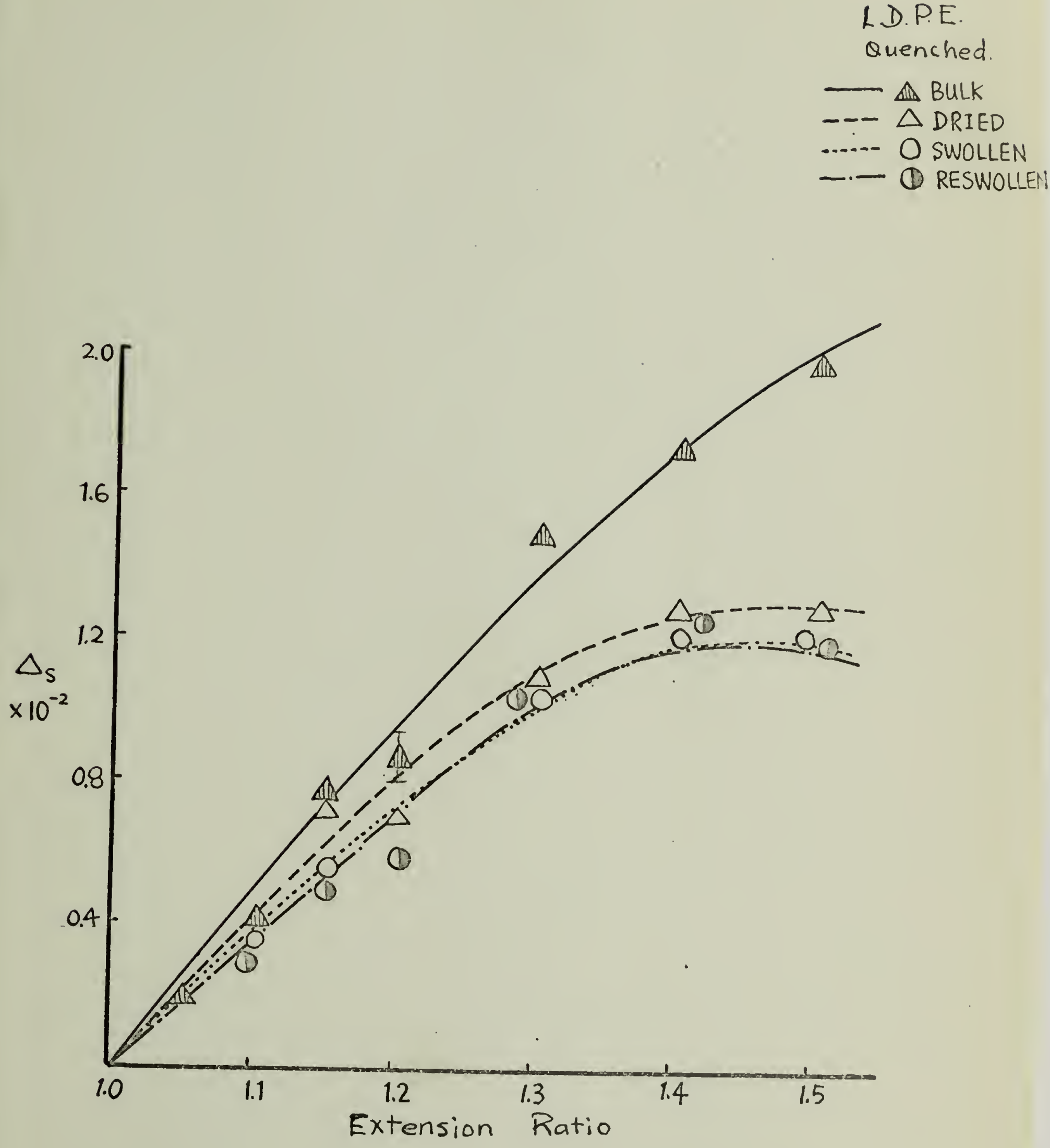
L.D.P.E.
Quenched.
BULK
DRIED
SWOLLEN
RESWOLLEN
2.0
1.6
1.2
0.8
0.4
Δ_s
$\times 10^{-2}$
1.0
1.1
1.2
1.3
1.4
1.5
Extension Ratio

Figure 47.

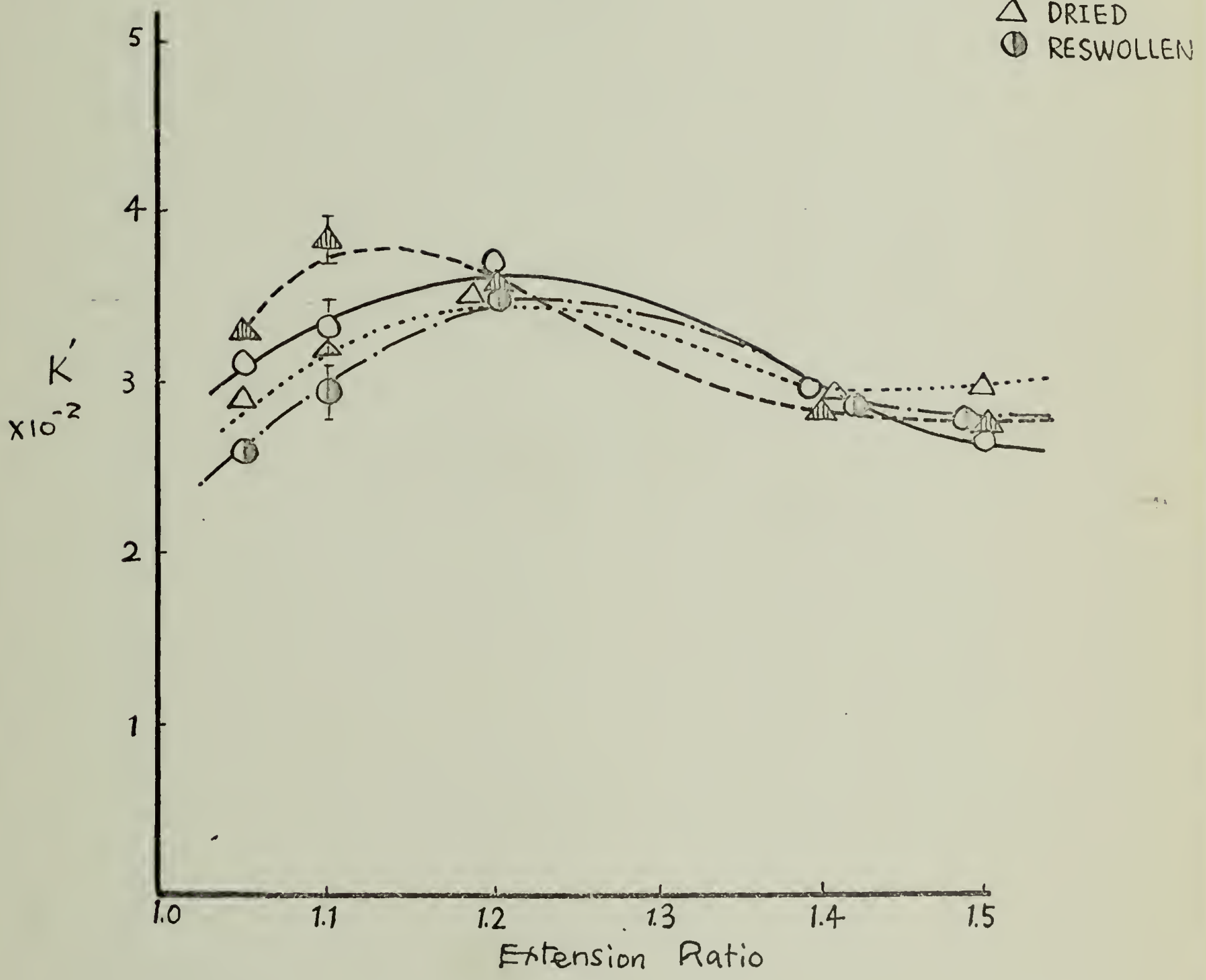
QUENCHED P.E.
1 Hz
BULK
SWOLLEN
DRIED
RESWOLLEN
K'
X10⁻²
5
4
3
2
1
1.0
1.1
1.2
1.3
1.4
1.5
Extension Ratio

Figure 48.

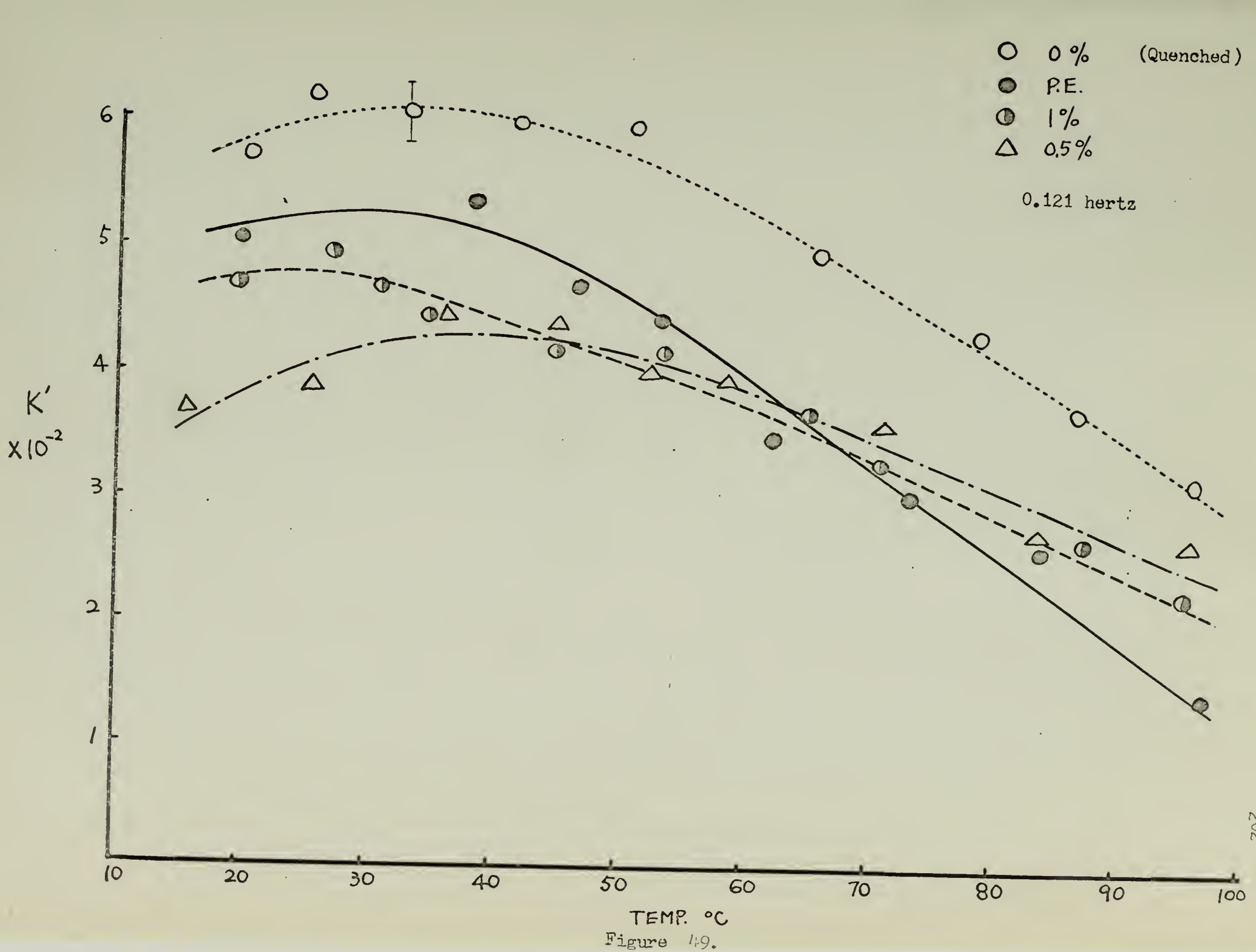
0 %
P.E.
1%
0.5%
(Quenched)
0.121 hertz
K'
X10⁻²
6
5
4
3
2
1
10
20
30
40
50
60
70
80
90
100
TEMP. °C

Figure 49.

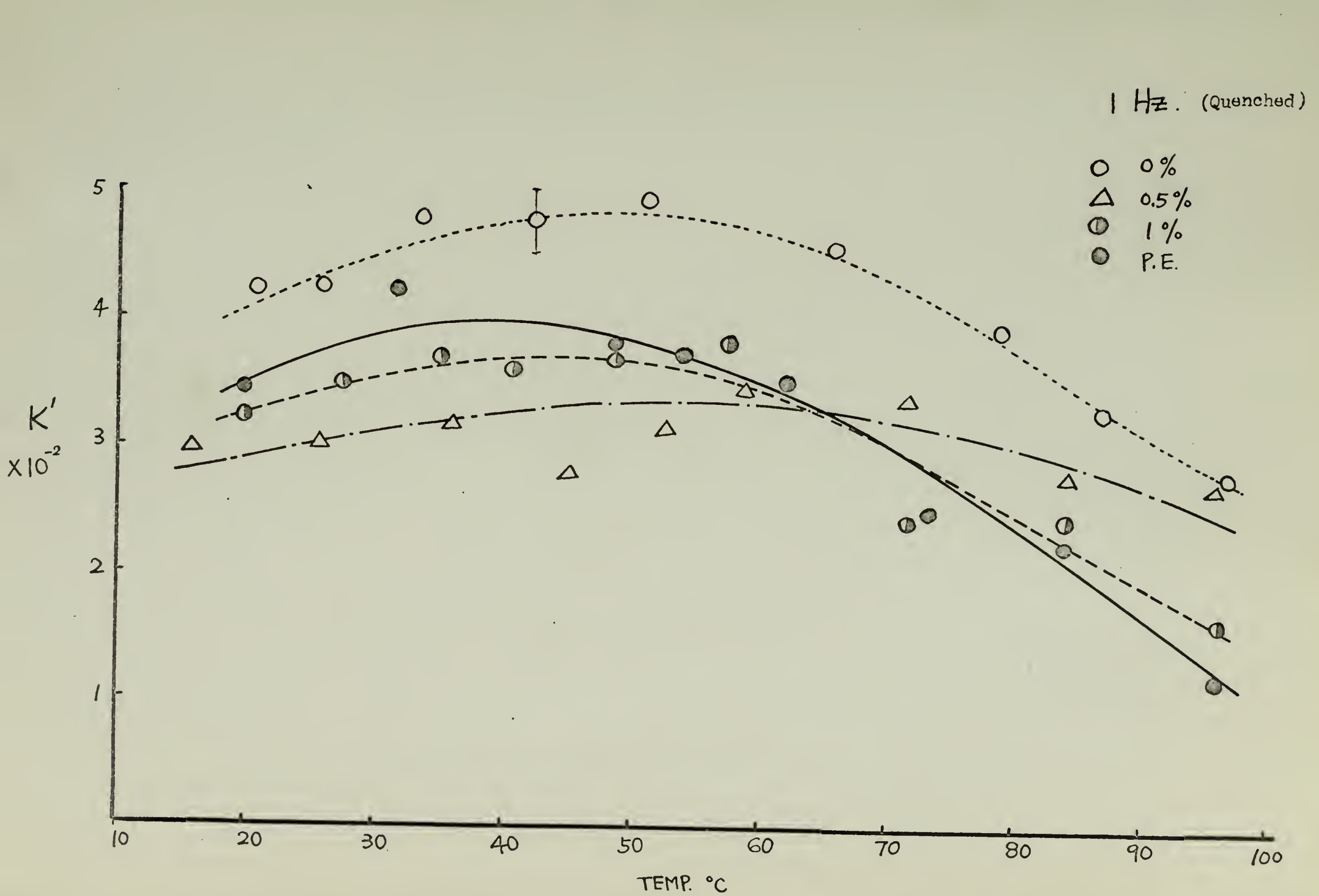
1 Hz. (Quenched)
0 %
0.5 %
1 %
P.E.
K'
X10^-2
5
4
3
2
1
10
20
30
40
50
60
70
80
90
100
TEMP. °C

Figure 50.

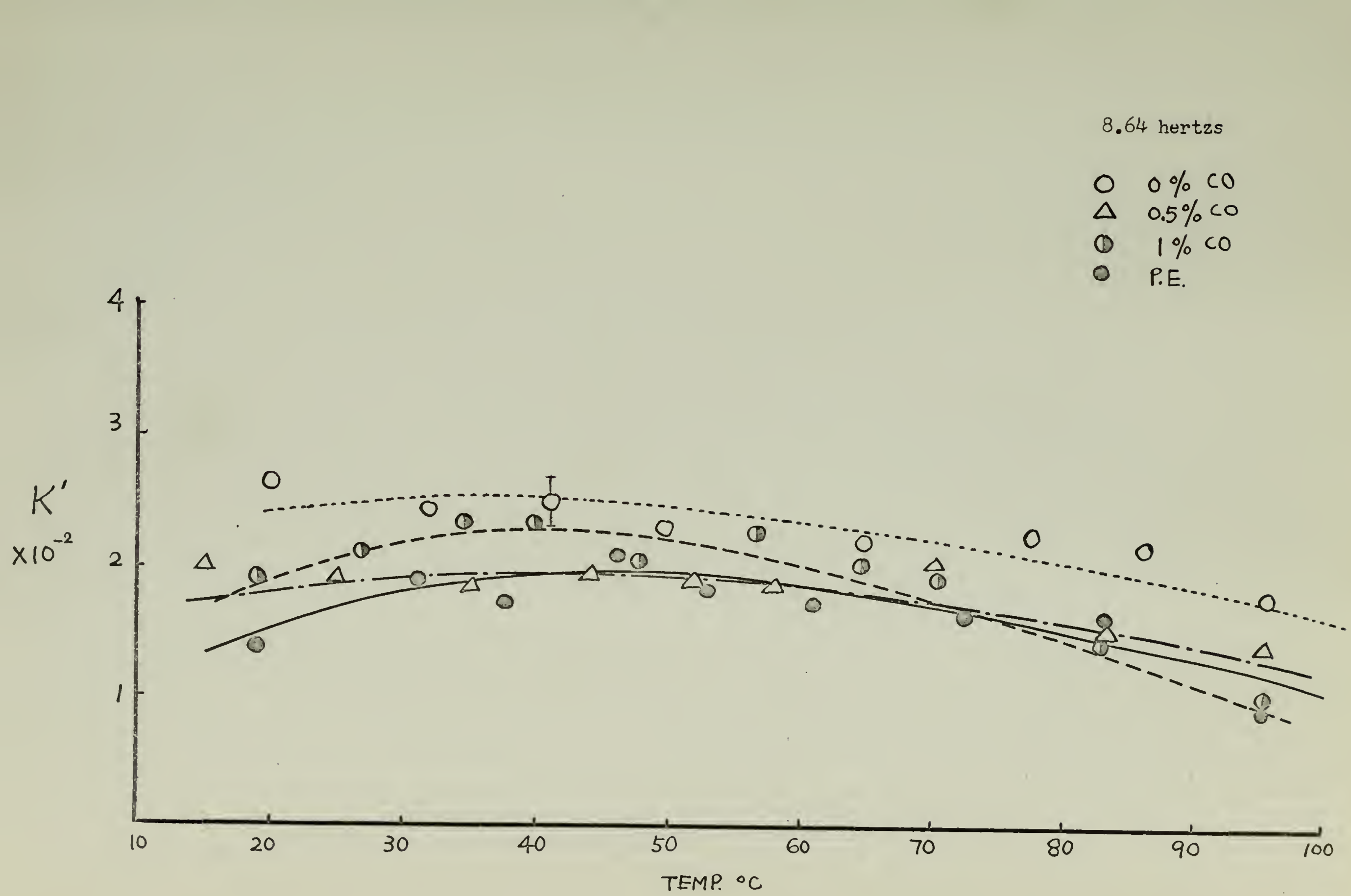
8.64 hertzs
0 % CO
0.5 % CO
1 % CO
P.E.
K'
X10^-2
4
3
2
1
10
20
30
40
50
60
70
80
90
100
TEMP. °C

Figure 51.

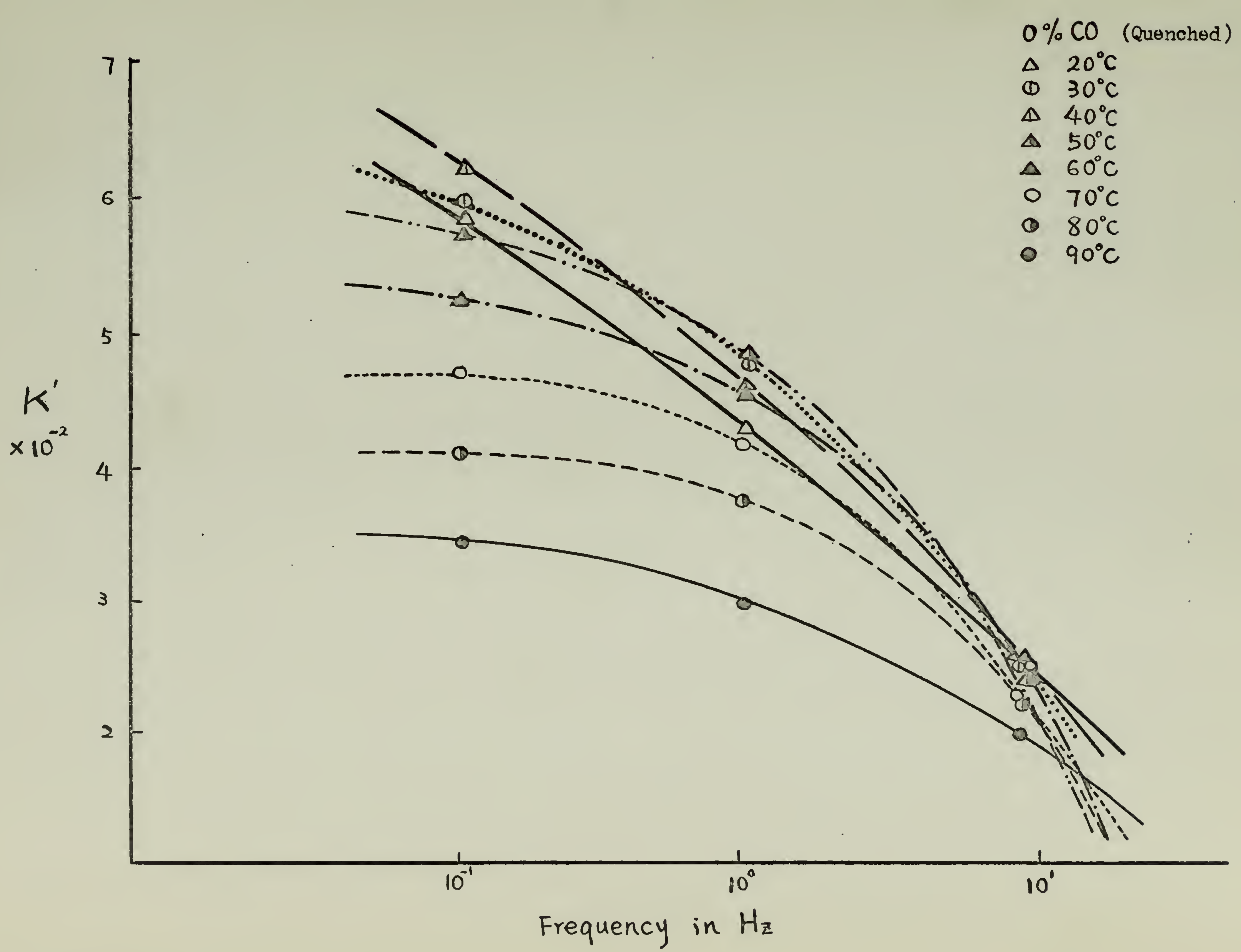
0% CO (Quenched)
20°C
30°C
40°C
50°C
60°C
70°C
80°C
90°C
K'
×10⁻²
7
6
5
4
3
2
10⁻¹
10⁰
10¹
Frequency in Hz

Figure 52.

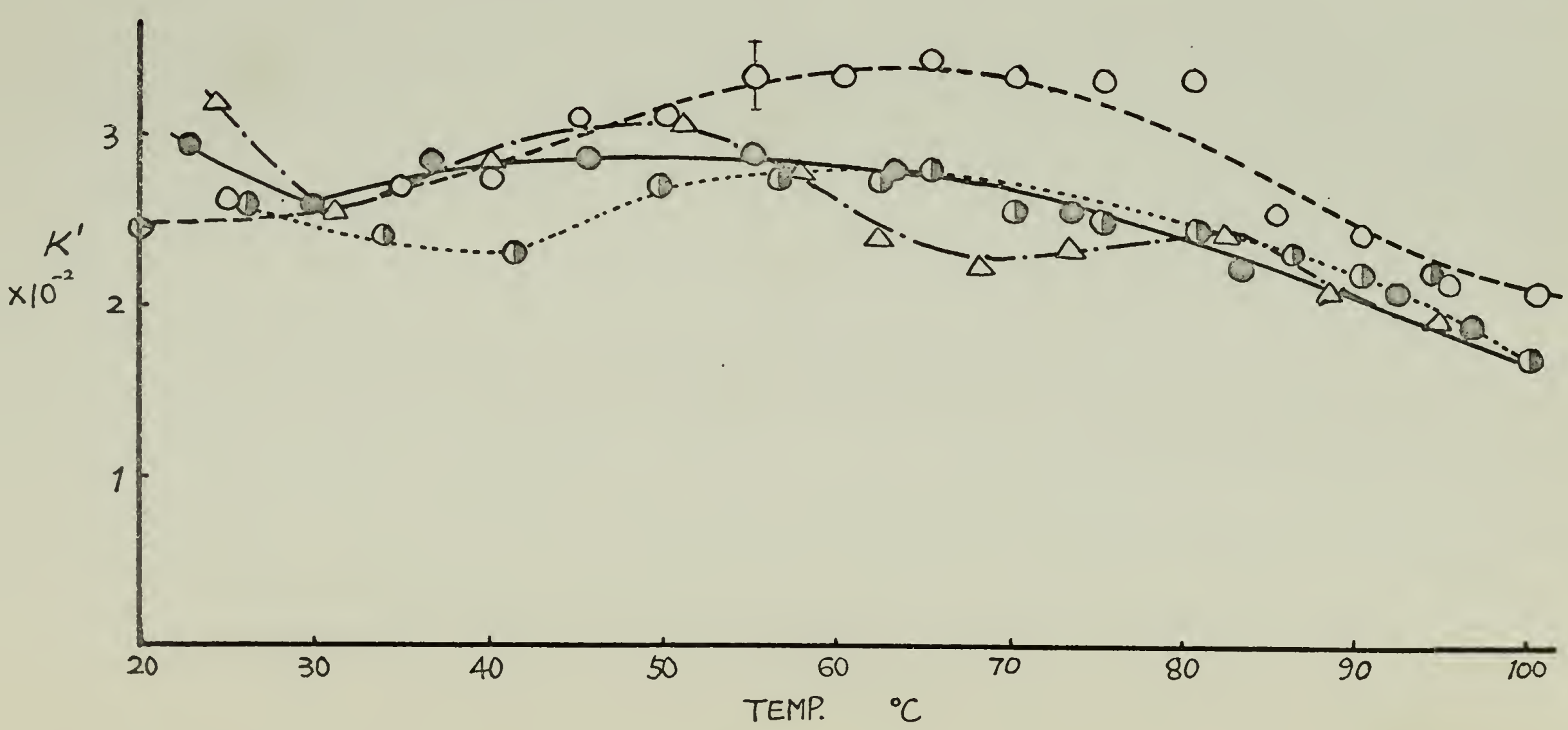
1 Hz.
△ 0% CO
● 0.5% CO
◐ 1.0% CO
○ P.E. (Yamada)
(Annealed)
K'
×10⁻²
3
2
1
20
30
40
50
60
70
80
90
100
TEMP. °C

Figure 53.

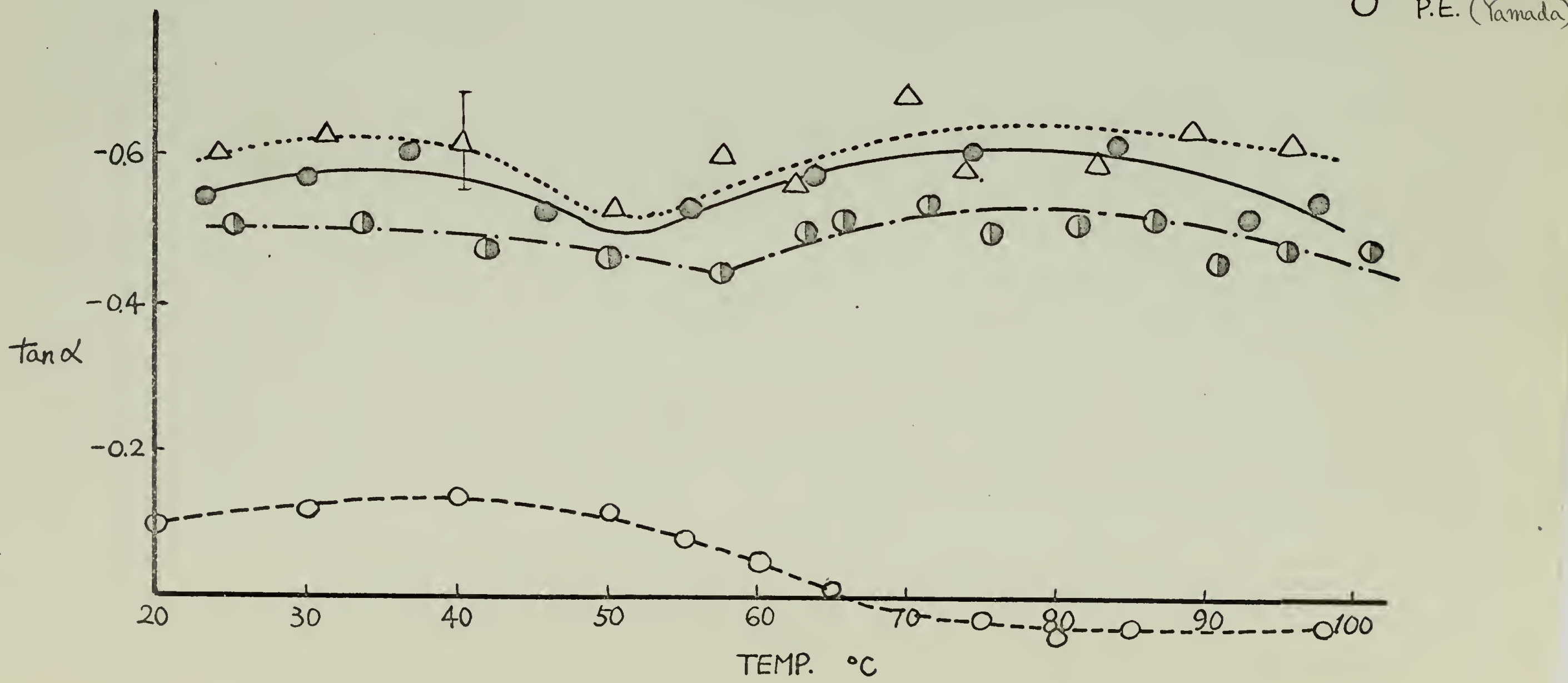
1 Hz.
0 % CO
0.5 % CO
(Annealed) 1.0 % CO
P.E. (Yamada)
-0.6
-0.4
-0.2
tan α
20
30
40
50
60
70
80
90
100
TEMP. °C

Figure 54.

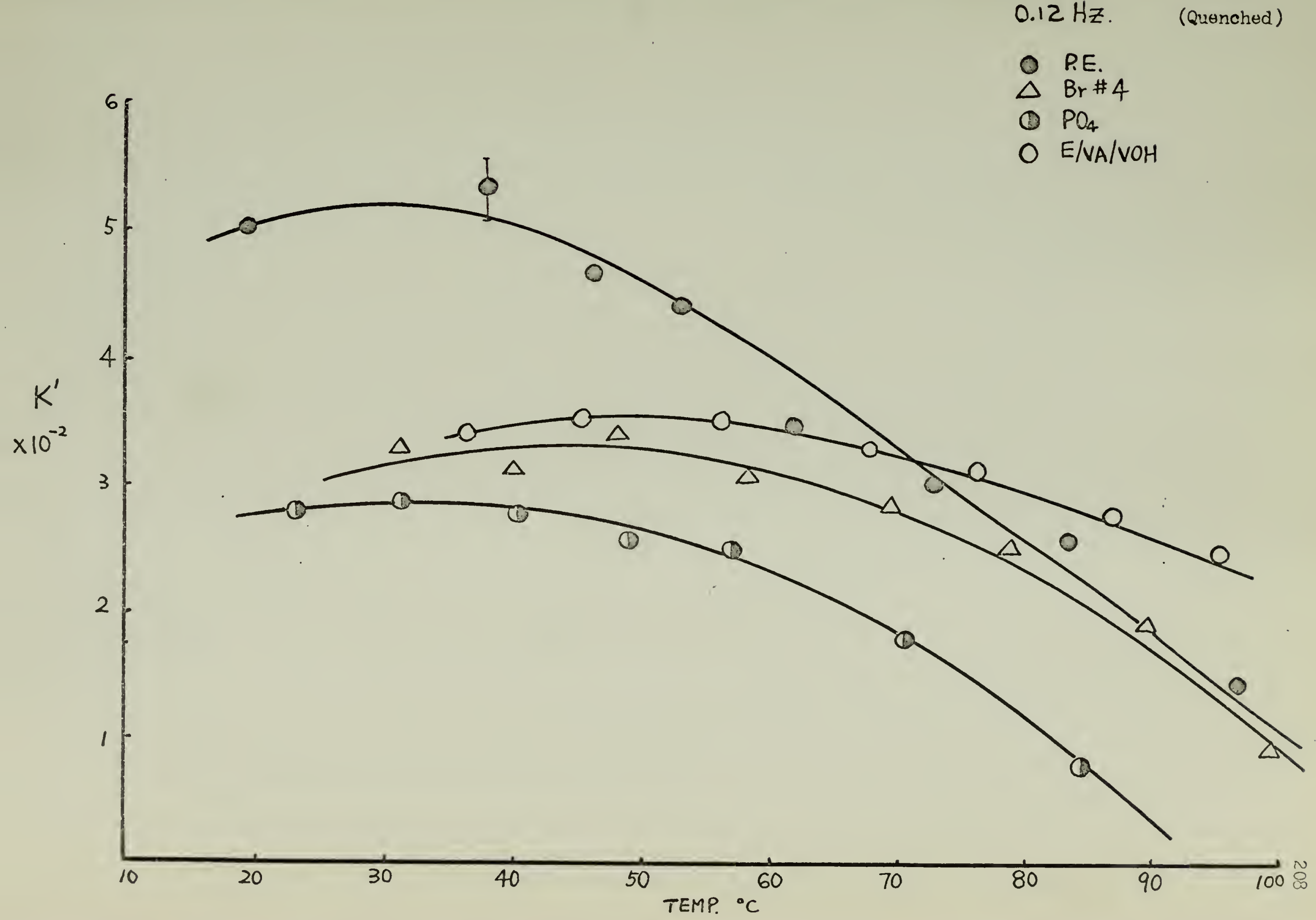
0.12 Hz.
(Quenched)
P.E.
Br #4
PO4
E/VA/VOH
K'
x10-2
6
5
4
3
2
1
10
20
30
40
50
60
70
80
90
100
TEMP. °C
208

Figure 55.

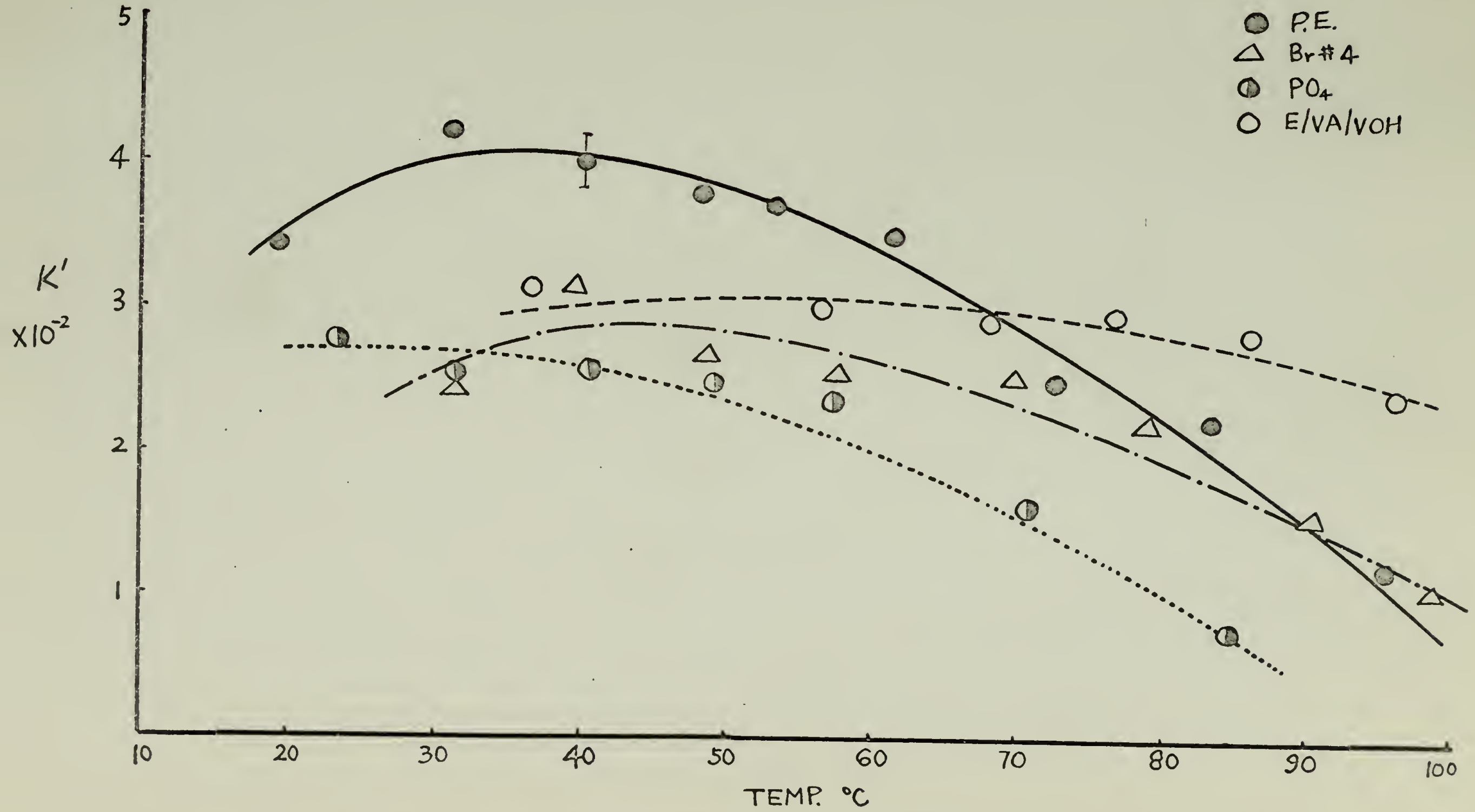
1 Hz. (Quenched)
P.E.
Br#4
PO4
E/VA/VOH
K'
X10-2
5
4
3
2
1
10
20
30
40
50
60
70
80
90
100
TEMP. °C

Figure 56.

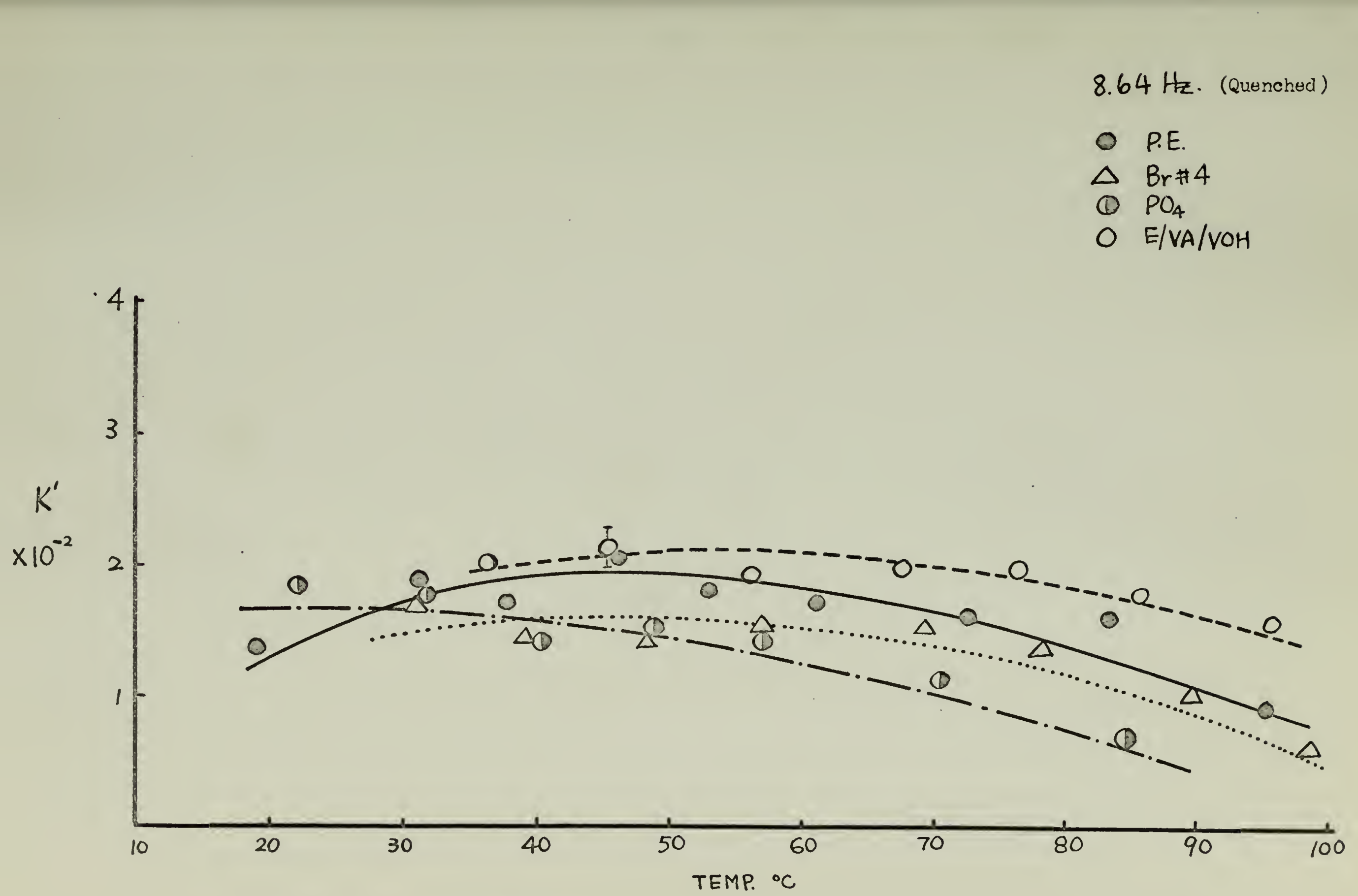
8.64 Hz. (Quenched)
P.E.
Br#4
PO4
E/VA/VOH
K'
X10-2
4
3
2
1
10
20
30
40
50
60
70
80
90
100
TEMP. °C

Figure 57.

(Quenched)

$T_{ref.} = 50°C.$

0% CO

0.5% CO

P.E.

1% CO

E/VA/VOH

Br #4

PO_4

$K' \times 10^{-2}$

6

5

4

3

2

1

10^{-2} 10^{-1} 10^{0} 10^{1} 10^{2}

$a_T \nu$

Figure 58.

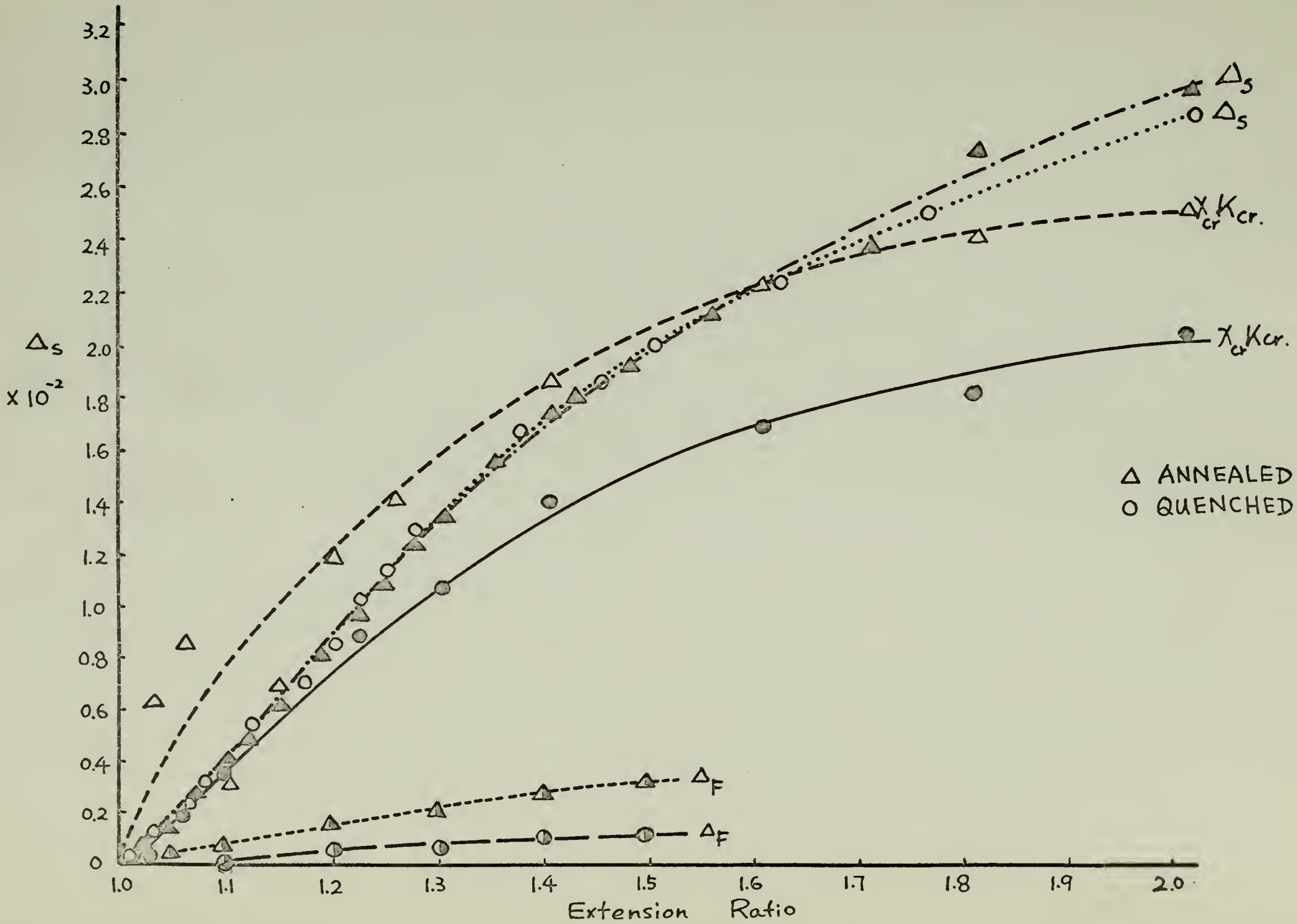
Δ_s $\times 10^{-2}$
3.2
3.0
2.8
2.6
2.4
2.2
2.0
1.8
1.6
1.4
1.2
1.0
0.8
0.6
0.4
0.2
0
Δ_s
Δ_s
$\chi_{cr} K_{cr}$
$\chi_{cr} K_{cr}$
Δ_F
Δ_F
△ ANNEALED
○ QUENCHED
1.0
1.1
1.2
1.3
1.4
1.5
1.6
1.7
1.8
1.9
2.0
Extension Ratio

Figure 59.

L.D.P.E.Q.

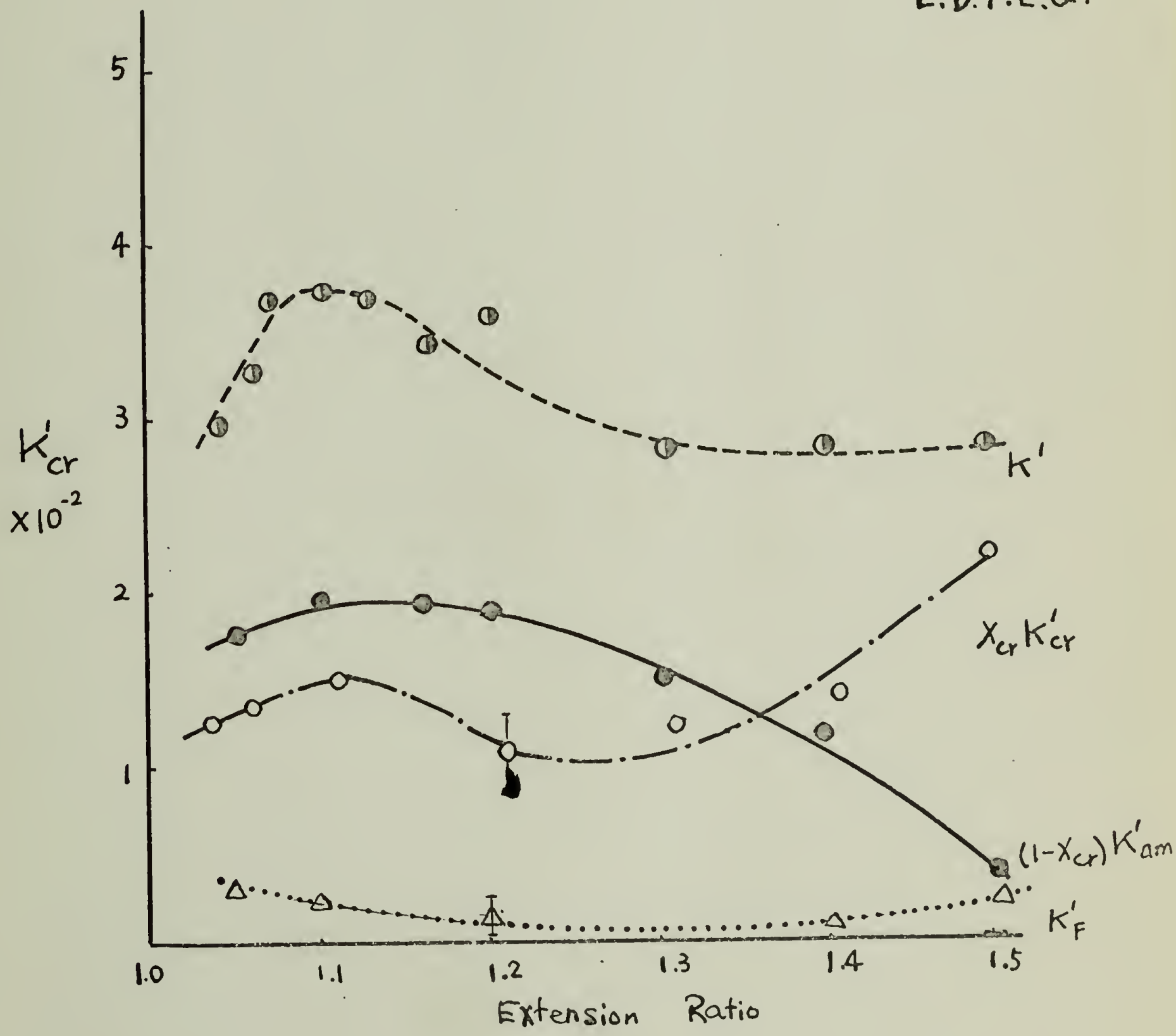

Figure 60.

L.D.P.E. ANN.

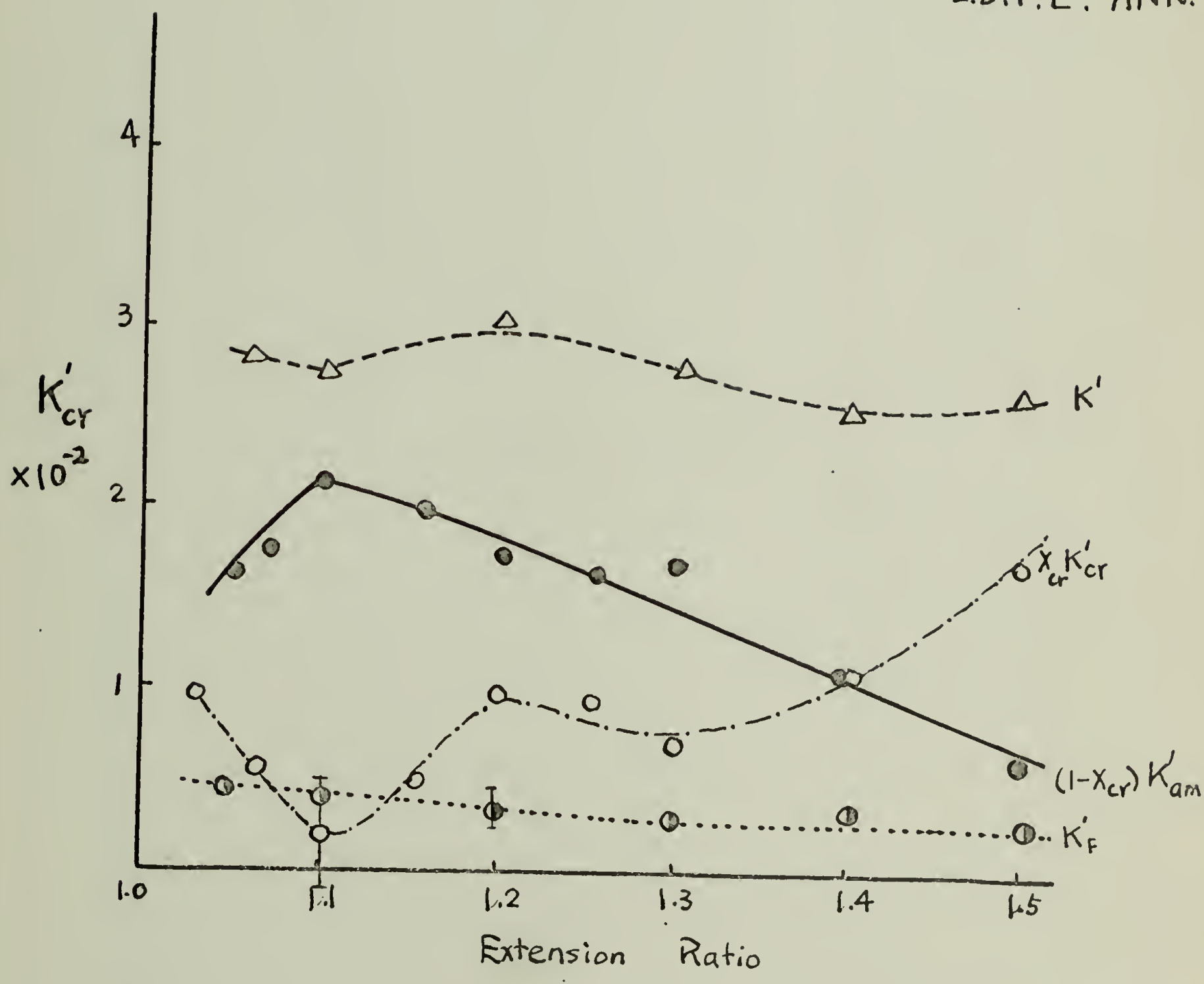

Figure 61.

APPENDIX I

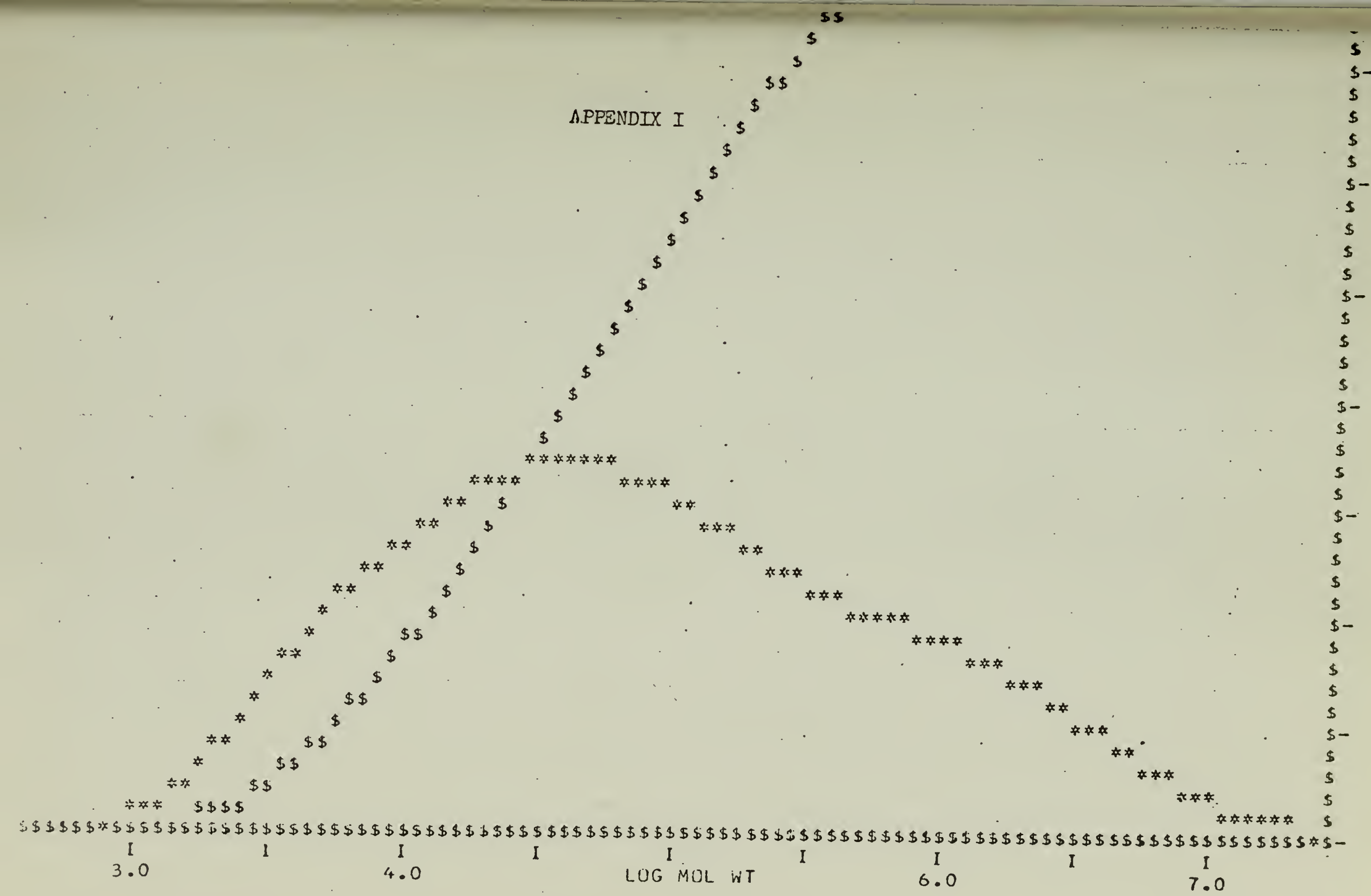

*---GRADE-0910 LOT AA1933 GPC NO.- 4664

CALCULATION OF GEL PERMEATION DATA

RADE-0910 LOT AA1933 DATE-07/06/70 GPC NO.- 4664

4664

OLVENT-TCB TEMP.135C CONC..10 TIME-120S.
OLUMN SET - 69- 8-A COLUMNS-10E7-10E6-10E4-10E3-

XP. ETA	ETA-K	ETA-A	A(0)
0.900	.0004600	0.725	-0.11635D 02

OUNT BEGIN.	COUNT FINISH	BASE BEGIN.	BASE FINISH	CDELTA
20	32	20.9	19.6	0.150

COUNT	HT.	CUM.HT.	MOL.WT.	COR.HT.	LOG MWT
31.87	0.0	0.C	773.	0.0	2.8882
30.87	1.8	0.47	1372.	2.03	3.1375
29.88	6.5	3.14	2719.	6.29	3.4344
28.88	13.9	10.28	5958.	11.84	3.7751
27.89	20.8	22.42	14356.	16.00	4.1570
26.89	26.1	39.23	37545.	18.57	4.5746
25.89	24.3	57.41	104103.	16.45	5.0175
24.90	18.3	72.39	296281.	12.35	5.4717
23.90	14.7	83.95	837195.	10.14	5.9228
22.91	9.8	92.79	2268765.	7.15	6.3558
21.91	4.3	97.76	5711167.	3.46	6.7567
20.91	1.3	99.60	12950323.	1.21	7.1123
19.92	0.0	100.00	25681200.	0.0	7.4096

MN	MW	MZ	MZ+1
16739.	620055.	5810686.	11094650.

SIGMA N	SIGMA W	SIGMA Z	MW/MN
100494.	1794011.	5541070.	37.04

FLAT	SKEW	MZ*MZ+1/MW
-0.637	0.279	103970608.

LAMBDA	CHAIN LGT	ME/100C	CALC. ETA
0.000539	0.0	0.0	0.900

```
000 PROGRAM XRAY
001 RAD(N)=FLOAT(N)/57.2957795142
002 XOF(PHI,XIO)=COS(PHI)*XIO
003 XIF(PHI,XI)=COS(PHI)*SIN(PHI)**2*XI
004 SEC(X)=1./COS(X)
005 FRAD(X)=X/57.2957795142
013 DIMENSION INT(4),DELI1(50,2),DELI2(50,2),XK(50,2),IZERO(50,2)
014 DIMENSION SIGI(50,4,2),SIGT(50,2),X(50,2)
015 DIMENSION ALPHA(4),THETA(2),IINCOH(2),IB(2)
016 TYPE REAL IZERO,IINCOH,IB,MU,LO
20 READ,N
025 PRINT,N
30 READ,(ALPHA(J),J=1,4)
040 READ,MU
050 READ,DO
060 READ,THETA(1),THETA(2)
070 READ,DELAMB
080 READ,XC
090 READ,IINCOH(1),IINCOH(2)
100 READ,IB(1),IB(2)
110 READ,LO
120 DO 130 I=1,N
130 READ,XK(I,1),XK(I,2)
140 DO 150 I=1,N
150 READ,X(I,1),X(I,2)
160 READ,NW1,NW2
170 IF(NW1 .EQ. 3HEND .AND. NW2 .EQ. 5HPARAM)GO TO 370
190 PRINT 190
190 FORMAT(* PARAMETER ERROR. THE PARAMETER TRAILER WAS NOT FOUND.*,
191X /,*THE WRONG NUMBER OF PARAMETERS FOLLOW THE PROGRAM.*)
200 STOP
370 NPLANES=2
380 DO 450 I=1,50
390 DO 450 K=1,NPLANES
410 DO 450 J=1,4
420 SIGI(I,J,K)=0
450 CONTINUE
2000 CONTINUE
2010*              HERE THE INPUT TAPE IS PROCESSED. IT IS ASSUMED
2020*              THAT PALNE 110 WILL BE FIRST ALTERNATING WITH PLANE
2030*              800. THE LAST ENTRY ON THE TAPE (OR THIS CAN BE PUT
2040*              INTO A SEPARATE FILE) WILL BE THE STATEMENT "END".
2050*              THIS WILL INDICATE THE END OF ALL DATA FOR THE RUN.
2060*              IF THE "END STATEMENT" IS FOUND WHERE THE PROGRAM
2070*              IS EXPECTING MORE DATA, A -SYNCHRONIZATION ERROR
2080*              OCCURS AND THE PROGRAM HALTS. A SYNCHRONIZATION
2090*              ERROR ALSO OCCURS WHEN AN END OF FILE IS REACHED.
2100*              THE FORM OF THE "END STATEMENT" WILL BE
2110*
2120*                 END 0 0 0 0
```

```
2130*
2140*                THE ZEROS ARE REQUIRED.                          218
2180 ISTART=0
2190 INCR=10
2200 DO 3000 K=1,2
2205 DO 3000 I=1,N
2206 ISTART=ISTART+INCR
2210 READ,IANGLE,NUMBR
2220 IF(EOF,60)2230,2250
2230 PRINT 2231
2231 FORMAT(* SYNCHRONIZATION ERROR.  END-OF-FILE REACHED BEFORE*,
2232X          * END STATEMENT.*)
2240 STOP
2250 IF(IANGLE .EQ. 3HEND .AND. I .EQ. 1)GO TO 4010
2255 IF(IANGLE .NE. 3HEND)GO TO 2270
2260 PRINT 2261,ISTART
2261 FORMAT(* SYNCHRONIZATION ERROR.  END STATEMENT FOUND IN THE DATA *
2262X      , * AT LINE *,I5)
2265 STOP
2270 IF(IANGLE .EQ. (I-1)*(90/(N-1)))GO TO 2300
2280 PRINT 2290,ISTART,IANGLE,NUMBR
2290 FORMAT(* SYNCHRONIZATION ERROR AT LINE *,I5,*. THE FOLLOWING HEADER
2291X *,/,* WAS NOT AS EXPECTED *,I10,1H,,I10)
2295 STOP
2300 DIMENSION INP(5)
2310 DO 3000 J=1,NUMBR
2315 ISTART=ISTART+INCR
2320 READ,(INP(K),K=1,5)
2330 IF(EOF,60)2230,2340
2340 IF(INP(1) .EQ. 3HEND)GO TO 2260
2350 DO 2360 M=1,4
2360 SIGI(I,M,K)=SIGI(I,M,K)+FLOAT(INP(M+1))
2370 SIGT(I,K)=SIGT(I,K)+(FLOAT(INP(1))/100.)
3000 CONTINUE
3010 GO TO 2200
4010 PRINT 4020
4020 FORMAT(* DATA READ IN OK.*)
4030 DO 4060 K=1,NPLANES
4040 DO 4060 I=1,N
4050 DO 4060 J=1,4
4060 SIGI(I,J,K)=(SIGI(I,J,K)/SIGT(I,K))-IR(K)
4070 PI=3.1415926535.
4080*                NOW CALCULATE THE DELTA I TERMS
4081 PRINT 4082
4082 FORMAT(*-PRINT DELI AND IZERO*)
4083 INPUT,NANS
4084 IF(NANS .NE. 3HYES)GO TO 4090
4085 PRINT 4086
4086 FORMAT(14X,3HANG,9X,5HDELI1,13X,5HDELI2,13X,5HIZERO,
4087X     /,14X,3H---,9X,5H-----,13X,5H-----,13X,5H-----)
4090 DO 4200 K=1,2
4100 DO 4200 I=1,N
4110 DELI1(I,K)=(PI/2.)*(ALPHA(1)*SIGI(I,1,K)-ALPHA(4)*SIGI(I,4,K))
4120 DELI2(I,K)=(PI/2.)*(ALPHA(3)*SIGI(I,3,K) - ALPHA(2)*SIGI(I,2,K))
4130 IZERO(I,K)=(SIGI(I,2,K)+SIGI(I,3,K))*X(I,K)
4135 IZERO(I,K)=IZERO(I,K) * (2./(1.+(COS(2.*FRAD(THETA(K))))**2))
4136C     * (EXP(MU*LO*SEC(FRAD(THETA(K))))/SEC(FRAD(THETA(K))))
```

```
4140 CF=((-DELAMB/(2.*LO))*(1.-MU*DO*SEC(FRAD(THETA(K))))*(IZERO(I,K)+
4141X IINCOH(K)))
4142X +(IR(K)*EXP(-MU*DO*SEC(FRAD(THETA(K))))*MU*SEC(FRAD(THETA(K)))*
4143X DO*DELAMB/(2.*LO))
4145 DELI1(I,K)=DELI1(I,K)-CF
4150 DELI1(I,K)=DELI1(I,K)*(EXP(MU*DO*SEC(FRAD(THETA(K))))/SEC(FRAD(
4151X              THETA(K))))*(2./(1.+(COS(FRAD(2.*THETA(K))))**2))
4160 DELI2(I,K)=DELI2(I,K)*(EXP(MU*DO*SEC(FRAD(THETA(K))))/SEC(FRAD(
4161X              THETA(K))))*(2./(1.+(COS(FRAD(2.*THETA(K))))**2))
4180 IF(NANS.NE.3HYES)GO TO 4200
4190 PRINT ,(I-1)*(90/(N-1)),DELI1(I,K),DELI2(I,K),IZERO(I,K)
4200 CONTINUE
4210*                    COMPUTE THE VALUES OF DELTA I PRIME SUB
4230*                    1C AND DELTA I PRIME SUB 2C.
4240 DIMENSION DIPC(50,2),DIPPC(50,2)
4241 PRINT 4242
4242 FORMAT(*-PRINT DIP*)
4243 INPUT,NANS
4244 IF(NANS .NE. 3HYES)GO TO 4250
4245 PRINT 4246
4246 FORMAT(///,1X,3HANG,4X,5HDIP1C,9X,5HDIP2C,7X,6HDIPP1C,7X,6HDIPP2C,
4247X        /, 1X,3H---,4X,5H-----,9X,5H-----,7X,6H------,7X,6H------)
4250 DO 4300 I=1,N
4260 DIPC(I,1)=(DELI1(I,1)-DELI1(I,2)*YK(I,2))/(1.-XK(I,1)*XK(I,2))
4270 DIPC(I,2)=(DELI1(I,1)*XK(I,1)-DELI1(I,2))/(XK(I,1)*YK(I,2)-1.0)
4280 DIPPC(I,1)=(DELI2(I,1)-DELI2(I,2)*XK(I,2))/(1.-XK(I,1)*XK(I,2))
4290 DIPPC(I,2)=(DELI2(I,1)*XK(I,1)-DELI2(I,2))/(XK(I,1)*XK(I,2)-1.0)
4294 IF(NANS .NE. 3HYES)GO TO 4300
4295 PRINT 4298 ,(I-1)*(90/(N-1)),DIPC(I,1),DIPC(I,2),DIPPC(I,1),
4296X DIPPC(I,2)
4298 FORMAT(1X,I2,1X,4(F12.5,1X))
4300 CONTINUE
4310 DO 4700 K=1,NPLANES
4320 PRINT 4330,K
4330 FORMAT(* EVALUATED INTEGRALS FOR CASE *,I3,1H.)
4340 DIMENSION Y(10),Z(10),X0(2),X1(2),Y0(2),Y1(2),Z0(2),Z1(2)
4345 DIMENSION F0(2),C1(2),C2(2)
4350 DO 4360 I=1,10
4360 Y(I)=X0F(RAD((I-1)*(90/(N-1))),IZERO(I,K))
4370 CALL QSF(10.,Y,Z,10)
4380 PRINT 4385,Z(10)
4383 X0(K)=Z(10)
4385 FORMAT(* X0=*,E14.7)
4390 DO 4400 I=1,N
4400 Y(I)=X1F(RAD((I-1)*(90/(N-1))),IZERO(I,K))
4410 CALL QSF(FLOAT(N),Y,Z,N)
4414 X1(K)=Z(10)
4415 PRINT 4416,Z(N)
4416 FORMAT(* X1=*,E14.7)
4420 DO 4430 I=1,N
4430 Y(I)=X0F(RAD((I-1)*(90/(N-1))),DIPC(I,K))
4435 CALL QSF(FLOAT(N),Y,Z,N)
4436 PRINT 4437,Z(N)
4437 FORMAT(1X,*Y0=*,E14.7)
4438 Y0(K)=Z(10)
4440 DO 4450 I=1,N
4450 Y(I)=X1F(RAD((I-1)*(90/(N-1))),DIPC(I,K))
4455 CALL QSF(FLOAT(N),Y,Z,N)
```

```
4460 PRINT 4465,Z(N)
4463 Y1(K)=Z(10)
4465 FORMAT(* Y1=*,E14.7)
4470 DO 4475 I=1,N
4475 Y(I)=XOF(RAD((I-1)*(90/(N-1))),DIPPC(I,K))
4476 CALL QSF(FLOAT(N),Y,Z,N)
4477 PRINT 4478,Z(N)
4478 FORMAT(1X,*Z0=*,E14.7)
4479 Z0(K)=Z(10)
4480 DO 4490 I=1,N
4490 Y(I)=X1F(RAD((I-1)*(90/(N-1))),DIPPC(I,K))
4494 CALL QSF(FLOAT(N),Y,Z,N)
4495 PRINT 4496,Z(N)
4496 FORMAT(1X,*Z1=*,E14.7)
4497 Z1(K)=Z(10)
4600 F0(K)=(((3.*X1(K)/X0(K))-1.)/2.)
4610 C1(K)=1.5*((Y1(K)/X0(K))-(Y0(K)/X0(K))*(X1(K)/X0(K)))*(L0/DELAMB)
4620 C2(K)=1.5*((Z1(K)/X0(K))-(Z0(K)/X0(K))*(Y1(K)/X0(K)))*(L0/DELAMB)
4630 PRINT 4640,F0(K),C1(K),C2(K)
4640 FORMAT(1X,*F0=*,E14.7,* C1=*,E14.7,* C2=*,E14.7)
4700 CONTINUE
4800 F0B=1.447*F0(1)-0.447*F0(2)
4810 C1B=1.447*C1(1)-0.447*C1(2)
4820 C2B=1.447*C2(1)-0.447*C2(2)
4830 F0C=-(F0(2)+F0B)
4840 C1C=-(C1(2)+C1B)
4850 C2C=-(C2(2)+C2B)
4860 VK1=XC*(-0.0361*C1(2)-0.0809*C1(1))
4870 PRINT4880,F0B,C1B,C2B,F0C,C1C,C2C,VK1
4880 FORMAT(///1X,*F0B=*,E14.7,* C1B=*,E14.7,* C2B=*,E14.7,/,
4881X       1X,*F0C=*,E14.7,* C1C=*,E14.7,* C2C=*,E14.7,/,
4882X       1X,*K1= *,E14.7)
6999 END
7000 SUBROUTINE QSF(H,Y,Z,NDIM)
7010* DESCRIPTION OF PARAMETERS
7020*    H       - THE INCREMENT OF ARGUMENT VALUES.
7030*    Y       - THE INPUT VECTOR OF FUNCTION VALUES.
7040*    Z       - THE RESULTING VECTOR OF INTEGRAL VALUES. Z MAY BE
7050*              IDENTICAL WITH Y.
7060*    NDIM    - THE DIMENSION OF VECTORS X AND Y>
7070*
7100 DIMENSION Z(NDIM),Y(NDIM)
7110 HT=.3333333*H
7120 IF(NDIM-5)7,8,1
7130 1 SUM1=Y(2)+Y(2)
7140 SUM1=SUM1+SUM1
7150 SUM1=HT*(Y(1)+SUM1+Y(3))
7160 AUX1=Y(4)+Y(4)
7170 AUX1=AUX1+AUX1
7180 AUX1=SUM1+HT*(Y(3)+AUX1+Y(5))
7190 AUX2=HT*(Y(1)+3.875*(Y(2)+Y(5))+2.625*(Y(3)+Y(4))+Y(6))
7200 SUM2=Y(5)+Y(5)
7210 SUM2=SUM2+SUM2
7220 SUM2=AUX2-HT*(Y(4)+SUM2+Y(6))
7230 Z(1)=0.
7240 AUX=Y(3)+Y(3)
7250 AUX=AUX+AUX
```

```
7260 Z(2)=SUM2-HT*(Y(2)+AUX+Y(4))
7270 Z(3)=SUM1
7280 Z(4)=SUM2
7290 IF(NDIM-6)5,5,2
7300*                                    INTEGRATION LOOP
7310↑2 DO 4 I=7,NDIM,2
7320    SUM1=AUX1
7330    SUM2=AUX2
7340    AUX1=Y(I-1)+Y(I-1)
7350    AUX1=AUX1+AUX1
7360    AUX1=SUM1+HT*(Y(I-2)+AUX1+Y(I))
7370    Z(I-2)=SUM1
7380    IF(I-NDIM)3,6,6
7390↑3 AUX2=Y(I)+Y(I)
7400    AUX2=AUX2+AUX2
7410    AUX2=SUM2+HT*(Y(I-1)+AUX2+Y(I+1))
7420↑4 Z(I-1)=SUM2
7430↑5 Z(NDIM-1)=AUX1
7440    Z(NDIM)=AUX2
7450    RETURN
7460↑6 Z(NDIM-1)=SUM2
7470    Z(NDIM)=AUX1
7480    RETURN
7490*                                    END OF INTEGRATION LOOP
7500↑7 IF(NDIM-3)12,11,8
7510↑8 SUM2=1.125*HT*(Y(1)+Y(2)+Y(2)+Y(2)+Y(3)+Y(3)+Y(3)+Y(4))
7520    SUM1=Y(2)+Y(2)
7530    SUM1=SUM1+SUM1
7540    SUM1=HT*(Y(1)+SUM1+Y(3))
7550    Z(1)=0.
7560    AUX1=Y(3)+Y(3)
7570    AUX1=AUX1+AUX1
7580    Z(2)=SUM2-HT*(Y(2)+AUX1+Y(4))
7590    IF(NDIM-5)10,9,9
7600↑9 AUX1=Y(4)+Y(4)
7610    AUX1=AUX1+AUX1
7620    Z(5)=SUM1+HT*(Y(3)+AUX1+Y(5))
7630↑10 Z(3)=SUM1
7640    Z(4)=SUM2
7650    RETURN
7660↑11 SUM1=HT*(1.25*Y(1)+Y(2)+Y(2)-.25*Y(3))
7670    SUM2=Y(2)+Y(2)
7680    SUM2=SUM2+SUM2
7690    Z(3)=HT*(Y(1)+SUM2+Y(3))
7700    Z(1)=0.
7710    Z(2)=SUM1
7720↑12 RETURN
7999    END
30000 ENDPROG
```

APPENDIX III -- SAMPLE DATA (FEED IN AND COMPUTATION)

```
010 10  (Total Number of Run)
020 1.00613 1.00272 0.99728 0.99385 (Sector Constants)
030 3.7 (Linear Absorption Coefficient)
040 0.06 (Thickness in cm.)
050 10.5 11.5 ( Theta at 110 and 200 planes)
060 0.04 (Dynamic Amplitude)
070 0.545 (% of Crystallinity)
080 3.7 3.1 (Incoherent Scattering at 110 and 200 Planes)
090 215. 180. (Background Scattering at 110 and 200 Planes)
100 2.6 (Extended Length)
200 0.0785 0.0785 (Dynamic Desmearing Constants at 0 Degree)
210 0.089 0.089                                          10
220 0.0965 0.0965                                        20
230 0.1 0.1                                              30
240 0.1 0.1                                              40
250 0.1 0.1                                              50
260 0.1 0.1                                              60
270 0.1 0.1                                              70
280 0.1 0.1                                              80
290 0.1 0.1                                              90

500 0.735 0.735  (Static Desmearing Constant at 0 Degree)
510 0.78 0.60                                            10
520 0.812 0.54                                           20
530 0.785 0.46                                           30
540 0.71 0.38                                            40
550 0.63 0.30                                            50
560 0.555 0.25                                           60
570 0.495 0.2                                            70
580 0.475 0.2                                            80
590 0.495 0.225                                          90

1000 END PARAM
```

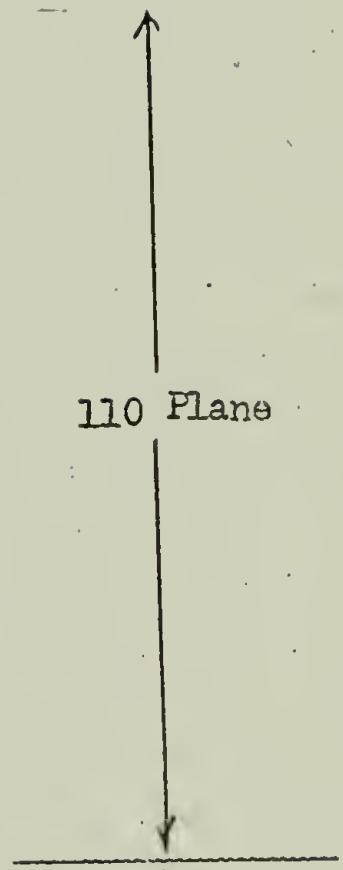
110 Plane
200 plane

	[illegible]	[illegible]	[illegible]	[illegible]
10	[illegible]	[illegible]	[illegible]	[illegible]
20	61.9285[illegible]	2.710071[illegible]	[illegible]	121[illegible].5[illegible]1
30	69.507[illegible]	10.3[illegible]17513		7[illegible]3[illegible].[illegible]9[illegible]5
40	25.[illegible]0940057	33.12757504		5[illegible]42.76[illegible]1[illegible]
50	-15.[illegible]0530[illegible]6	[illegible]4.[illegible]2[illegible]42[illegible]8		3[illegible]4[illegible].[illegible][illegible]5[illegible]
60	-32.96593965	63.04029023		2883.[illegible]234[illegible]6
70	-5[illegible].[illegible]7[illegible]1[illegible]	[illegible]1.7[illegible]0[illegible]6[illegible]8		[illegible]81.7[illegible]5
80	-45.[illegible]2[illegible]6[illegible]0	[illegible]7.[illegible]1[illegible]1[illegible]9		[illegible].[illegible]6[illegible]1[illegible]5
90	-[illegible]0.[illegible]1[illegible]1[illegible]7	[illegible]0.[illegible][illegible]1[illegible]5		[illegible]1[illegible].[illegible]7[illegible]5[illegible]6
0	15.[illegible]3[illegible]0[illegible]0	-1[illegible].[illegible]0[illegible]0[illegible]0		[illegible]67[illegible].13[illegible]1[illegible]
10	12.[illegible]0[illegible]4300	-16.[illegible]8[illegible]51[illegible]8		2196.[illegible]1[illegible]3
20	3.[illegible]4[illegible]1[illegible]6	-10.[illegible]4[illegible]2[illegible]0		1[illegible]40.[illegible]1[illegible]3[illegible]
30	8.1315726[illegible]	10.3[illegible]72081		1[illegible]2.[illegible]6[illegible]735
40	8.[illegible]7[illegible]40[illegible]5[illegible]	17.[illegible]0[illegible]5135		1[illegible]1.[illegible][illegible][illegible]
50	-13.94717250	10.[illegible]8[illegible]8[illegible]7		670.47579[illegible]
60	-24.10231[illegible]	17.[illegible][illegible]1[illegible]		[illegible]2[illegible].[illegible][illegible]7[illegible]
70	-33.[illegible]1[illegible]1034	16.3[illegible][illegible]1[illegible]		3[illegible].[illegible]1[illegible]10
80	-20.22[illegible]362	25.[illegible]1[illegible][illegible][illegible]		331.[illegible]7[illegible]14
90	-18.[illegible]590[illegible]	24.3733[illegible]4		3[illegible].1[illegible][illegible]

PRINT DIP?YES

ANG	DIP1C	DIP2C	DIPP1C	DIPP2C
0	25.12[illegible]3	13.49354	[illegible].[illegible]0455	-20.[illegible]7[illegible]
10	16.03596	17.37[illegible]	12.[illegible]7475	-17.77[illegible]
20	[illegible].13[illegible]9	-2.11[illegible]	[illegible].[illegible]0[illegible]1	-11.[illegible][illegible]
30	[illegible].[illegible]726	[illegible].1[illegible]	11.[illegible]	[illegible].1[illegible]
40	[illegible].[illegible]615	-.[illegible]	[illegible].[illegible]1[illegible]	1[illegible].[illegible]
50	-1[illegible].[illegible]011	-1[illegible].[illegible]	[illegible].[illegible]	[illegible].[illegible]
60	-30.15[illegible]	-[illegible]1.[illegible]	[illegible].[illegible]	11.[illegible]
70	-56.73[illegible]	-27.[illegible]	50.[illegible]	11.[illegible]
80	-43.50516	-15.[illegible]	53.[illegible]	10.[illegible]
90	-50.[illegible]7079	-13.36[illegible]	[illegible].27[illegible]	10.[illegible]

EVALUATED INTEGRALS FOR CASE 1.

X0= .3143[illegible]E+06
X1= .7565957E+05
Y0= .1114725E+04
Y1= -.7333[illegible]E+02
Z0= .1[illegible]E+[illegible]
Z1= .[illegible]E+03
E0= -.[illegible]E+[illegible] C1= -.[illegible]E+[illegible] C2= .[illegible]E+[illegible]

EVALUATED INTEGRALS FOR CASE 2.

X0= .7979[illegible]E+05
X1= .1[illegible]E+05
Y0= -.[illegible]E+[illegible]
Y1= -.[illegible]E+[illegible]
Z0= -.[illegible]E+[illegible]
Z1= .1920069E+03
E0= -.[illegible]E+[illegible] C1= -.[illegible]E+[illegible] C2= .[illegible]E+[illegible]

E0P= -.[illegible]E+[illegible] C1P= -.[illegible]E-[illegible] C2P= .[illegible]E+[illegible]
E00= .[illegible]E+[illegible] C1C= .[illegible]E+[illegible] C2C= -.[illegible]E+[illegible]
X1= .[illegible]E-[illegible]

TIME: [illegible].[illegible] SEC.

```
      PROGRAM MULTIFIT
C     THIS IS A REVISION OF SUBROUTINE RESOLVER
C     REVISED TO ALLOW SIMULTANEOUS PRINTING OF A NUMBER OF TRIAL CURVES
C     REVISED TO ALLOW VARIATION IN STEP IN 2THETA IN COMPUTATION
                  OF THEORETICAL CURVE
C     PRINTOUT OF THE VARIOUS COMPONENT CURVES IS SUPPRESSED
C     LANGUAGE FORTRAN II FOR CDC 3600 PROGRAMMER DESPER
      DIMENSION TM(4), HEADING(10), AO(4), CX(500,10), NDEG(500), NMIN(500)
      DIMENSION DELT(6), THI(6)
      DIMENSION BET(4,10), AEXP(4), C(4,4), FDEG(4). FMIN(4), TMAX(4)
1     READ 106, (HEADING(I), I=1,10)
      IF (EOF, 60) 7,3
3     PRINT 107, (HEADING(I), I=1,10)
      PRINT 112
      DO 40 M=1,500
      DO 40 L=1,10
40    CX(M,L)=0.
      DO 80 L=1,10
      DO 80 I=1,4
80    BET(I,L)=0.
      READ 100, XN
      X=XX
      IF (N*(5-N)) 11,11,12
11    PRINT 110
      STOP
12    READ 100, ((FDEG(I), FMIN(I), AEXP(I), (BET(I,L), L=1,10)), I=1,N)
C     AEXP IS EXPTL INTENSITY, BET IS ESTD LINE BREADTH IN MINUTES
```

Continued next page

```
      READ 100, TLO, ((DELT(K), THI(K)), K=1, 6)
      MINUTES=60.*TLO-DELT(1)
      M=0
      DO 50 K=1, 6
      IF (DELT(K)) 50, 50, 51
51    MDELT=DELT(K)
52    M=M+1
      MINUTES=MINUTES+MDELT
      NDEG(M)=MINUTES/60
      NMIN(M)=MINUTES-60*NDEG(M)
      T=MINUTES
      T=T/60.
      IF (T-THI(K)) 52, 50, 50
50    CONTINUE
      MAXM=M
      DO 30 L=1, 10
      PRINT 108, L
      DO 6 I=1, N
      IF (BET(I, L) 6, 30, 6
6     TMAX(I)=FDEG(I)+FMIN(I)/60.
      DO 2 I=1, N
      DO 8 J=1, N
      R=120.*(TMAX(I)-TMAX(J))/BET(J, L)
8     C(I, J)=1./(1.+R*R)
2     PRINT 101, (C(I, J), J=1, N)
      CALL SIMULEQN (N, AO, AEXP, C)
      PRINT 109
      PRINT 103, ((I, FDEG(I), FMIN(I), AO(I), AEXP(I), BET(I, L))I=1, N)
      DO 60 M=1, MAXM
```

Continued next page

```
      IF (M-500) 61, 61, 60
61    T=60*NDEG(M)+NMIN(M)
      T=T/60.
      DO 5 I=1, N
      R=120.*(T-TMAX(I))/BET(I, L)
      TM(I)=AO(I)/(1.+R*R)
5     CX(M, L)=CX(M, L)+TM(I)
60    CONTINUE
30    CONTINUE
      PRINT 107, (HEADING(I), I=1, 10)
      PRINT 112
      PRINT 105
      PRINT 111,((BET(I, L), I=1, 4), L=1, 10)
      DO 70 M=1, MAXM
70    PRINT 102, NDEG(M), NMIN(M), (CX(M, L), L=1, 10)
      GO TO 1
7     PRINT 104
100   FORMAT (1X, 13F6.4)
101   FORMAT (4(5X, F12.8))
102   FORMAT (1H0, I3, 1X, I3, 7X, 10F12.0)
103   FORMAT (3X, I2, 6X, F3.0, 1X, F3.0, 3X, F9.0, 8X, F9.0, 11X, F4.0)
104   FORMAT (*0END OF CALCULATIONS*)
105   FORMAT (*0CALCULATED RADIAL SCAN CURVES FOR VARIOUS TRIALS*/
     1 * DEG MIN*, 7X, 5X, *TRIAL 1*, 5X, *TRIAL 2, 5X, *TRIAL 3*, 5X, *TRIAL 4*,
     25X, *TRIAL 5*, 5X, *TRIAL 6*, 5X, *TRIAL 7*, 5X, *TRIAL 8*, 5X, *TRIAL 9*,
     34X, *TRIAL 10*)
106   FORMAT (10A8)
107   FORMAT (1H1, 10A8)
```

Continued next page

```
108       FORMAT (*0C MATRIX FOLLOWS FOR TRIAL NUMBER*, I3)
109       FORMAT (* PEAK NO   DEG MIN   RESOLVED INT   EXPERIMENTAL INT   BR
      1EADTH, MIN*)
110       FORMAT (* INTEGER N NOT IN RANGE 1 TO 4, PGM STOPS IN MULTIFIT*)
111       FORMAT (*0LINE BREADTHS *,10(4F3.0))
112       FORMAT (*0CALCULATIONS BASED ON LORENTZIAN TYPE FUNCTIONS*)
          END MULTIFIT
```

INPUT DATA FORMAT FOR MULTIFIT

Column numbers:

1	2-7	8-13	14-19	20-25	26-31	32-37	38-43	44-49	50-55	56-61	62-67	68-73	74-79
PUNCH IDENTIFYING COMMENTS IN COLUMNS 1-80 OF THE FIRST DATA CARD													
XN													
FDEG	FMIN	AEXP	BET	BET	BET	BET	BET	BET	BET	BET	BET	BET	
(A total of XN cards of the above type, one for each peak, Up to four peaks allowed.)													
TLO	DELT	THI	DELT	THI	DELT	THI	DELT	THI	DELT	THI	DELT	THI	

Example:

MULTIFIT RUN NUMBER 1 - QUENCHED LOW DENSITY P.E. - 20% STRAIN

3.												
19.	0	2510.	360.	360.	360.	360.	360.	380.	380.	380.	380.	380.
21.	0	7410	10.	15.	20.	25.	30.	10.	15.	20.	25.	30.
23.	0.	1910.	10.	15.	20.	25.	30.	10.	15.	20.	25.	30.
15.	30.	20.	10.	21.	5.	21.6	20.	23.5	5	24.	20.	25.